UNIVERSITY OF CALIFORNIA
SANTA CRUZ

SEARCHING FOR BEYOND STANDARD MODEL PHYSICS AT LOW AND HIGH ENERGY EXPERIMENTS

A dissertation submitted in partial satisfaction of the
requirements for the degree of

DOCTOR OF PHILOSOPHY

in

PHYSICS

by

Douglas Tuckler

September 2020

The Dissertation of Douglas Tuckler
is approved:

Stefano Profumo, Chair

Stefania Gori

Wolfgang Altmannshofer

Quentin Williams
Interim Vice Provost and Dean of Graduate Studies

Table of Contents

List of Figures

List of Tables

Abstract

Searching for Beyond Standard Model physics at Low and High Energy experiments

by

Douglas Tuckler

The Standard Model (SM) of particles physics is an extremely successful theory of particles and their interactions. However, it has become clear that the SM is an incomplete description of our Universe and that new physics beyond the SM (BSM) is needed to answer many of its open questions. In this talk we will discuss two open questions.

In the first part, we will present a model that can address the SM flavor puzzle. The hierarchical pattern in quark masses and mixings can be explained by assuming that the SM Higgs only generates mass for the 3rd generation fermions, while an additional source of electroweak symmetry breaking generates mass for the 1st and 2nd generations. Such a scenario can be realized in a "flavorful" two Higgs doublet model (2HDM). The characteristic Higgs collider signatures of this setup differ significantly from well-studied 2HDMs with natural flavor conservation. The presence of large SM Higgs flavor violating couplings can lead to enhanced rare top quark decays. We will also discuss some possible UV completions of this scenario.

In the second part, we will discuss a vector leptoquark scenario that can address the lepton flavor universality anomalies observed by the LHCb collaboration in B meson decays. We will show that a vector leptoquark solution of the B-anomalies can also alleviate discrepancies between the SM predictions and the experimental values of the electron and muon anomalous magnetic moments. In addition, leptoquark models generically yield new sources of CP violation that induce electric and magnetic dipole moments of elementary particles. We will show

that present and future electron and neutron EDM experiments set interesting constraints on the CP violating phases of the leptoquark couplings.

This thesis is dedicated to my family whose love and support has made it possible for me to pursue a career in physics. I can't thank you enough.

Acknowledgments

The work presented in this thesis would not have been possible without the help and support of the many people I have had the wonderful opportunity of meeting.

I would like to first give thanks to all of my collaborators for the opportunity to work with you: Wolfgang Altmannshofer, Josh Eby, Stefania Gori, Brian Maddock, Mario, Martone, H. Patel, Stefano Profumo, and Dean J. Robinson. Working with all of you has been a pleasure and you have all taught me so much.

Thank you to all the the friends I have made at the University of Cincinnati, UC Santa Cruz, and Fermilab. I always enjoyed our discussions about physics and non-physic topics. You have all been important in my professional and personal growth. A special thanks to two dear friends Josh Eby and Brian Maddock who have been instrumental in my success in graduate school and in life.

Thanks to Sarah Dill at the University of Cincinnati and Ben Miller at UC Santa Cruz for making graduate school life more manageable, and making sure that I was always in good mental health. I really appreciate your support.

I would also like to give thanks to Wolfgang Altmannshofer who I consider to be a second advisor. Thank for for all the helpful discussions and help you have given me throughout the years, and for the wonderful opportunities to work with you.

Thanks to L.C.R. Wijewardhana who reached out to me after I finished undergraduate school and gave me the wonderful opportunity to attend graduate school at the University of Cincinnati. I am forever indebted to you for giving me a chance to prove myself, and for mentoring me during my time in Cincinnati

Finally, I would like to give a big thanks to my advisor and mentor Stefania Gori for giving me the opportunity to work with her and for all the support she has given me through out the years. It has been wonderful working with you and

I am grateful for all your help and guidance and for setting me up for success in the future. I could not have asked for a better advisor. Thank you so much for everything.

Part I

The Standard Model

Chapter 1

Introduction

We are currently in a very exciting time in particle physics. The discovery of the Higgs boson in 2012 at the Large Hadron Collider (LHC) [6, 7] has confirmed a nearly 60 year old theory of electroweak symmetry breaking [8–10] and extolled years of experimental effort. This discovery has proven that the Standard Model of particle physics is an extremely successful theory of fundamental particles and their interactions. Other correct predictions of the SM include the existence of fundamental particles, such as the electroweak gauge bosons, the top and charm quark, gluons, and the tau neutrino, particles that were subsequently discovered by experimental collaborations [11–22]; and a very precise prediction of the anomalous magnetic moment of the electron that agrees with experiment to less than one part per billion [23–25].

Despite its success, various experimental observations indicate the existence of physical phenomena that the SM can not explain. Among these are the hierarchy problem, the existence of dark matter (DM), the origin of the matter-antimatter asymmetry in the universe, the hierarchical flavor structure of particles masses (i.e the SM flavor puzzle), and the origin of neutrino-masses. Perhaps the most fundamental issue of the SM is that it does not contain a description of gravity in

terms of a renormalizable quantum field theory. While this is not an exhaustive list, these open problems indicate that the SM should be thought of as a low-energy effective theory of some more fundamental theory, and that answering these questions requires the presence of new physics beyond the SM (BSM).

In addition to these fundamental issues, there are various experimental "anomalies" that are in tension with SM predictions. Among these are the discrepancy between the SM prediction and the measured value of the anomalous magnetic moment of the muon a_μ, and the apparent violation of lepton flavor universality observed in semi-leptonic decays of B mesons. These experimental results are in tension with the SM at $\sim 3-4\sigma$ level and, while upcoming results from the Muon $g-2$ experiment and B factories will shed light on these anomalies, the current discrepancies could be a hint of BSM physics.

In this thesis we will explore BSM explanations for two of the issues mentioned above. In Part II we will focus on addressing the SM flavor puzzle and identifying the origin of mass for the first two generations of SM fermions. In particular, we will study the phenomenological consequences of an additional source of electroweak symmetry breaking that generates mass exclusively for the first and second generations. In Part III we will explore a leptoquark solution to the anomalies observed in tests of LFU, and how such a solution can also address the discrepancy in the anomalous magnetic moment of the muon.

To motivate these two BSM scenarios, we will first briefly discuss the experimental challenges that lead to a lack of knowledge of the SM Higgs couplings to light fermions in Sec. 1.3. In Sec. 1.4 we discuss some aspects of LFU and the experimental status of the B anomalies.

SM Field	$SU(3)_C$	$SU(2)_L$	$U(1)_Y$
G^a_μ	**8**	**1**	0
W^a_μ	**1**	**3**	0
B_μ	**1**	**1**	0
$Q_L = (u_L, d_L)^T$	**3**	**2**	$+1/6$
$L_L = (\nu_L, \ell_L)^T$	**1**	**2**	$-1/2$
u_R	**3**	**1**	$+2/3$
d_R	**3**	**1**	$-1/3$
e_R	**1**	**1**	-1
h	**1**	**2**	$+1/2$

Table 1.1: Field content of the SM and their $SU(3)_C \times SU(2)_L \times U(1)_Y$ charge assignments.

1.1 Particle Content of the Standard Model

The interactions of fundamental particles of the SM is described by the gauge group $SU(3)_C \times SU(2)_L \times U(1)_Y$, where $SU(3)_C$ describes the strong interactions between quarks and gluons (i.e Quantum Chromodynamics (QCD)), and $SU(2)_L \times U(1)_Y$ denotes electroweak interactions of SM particles. The subscript "C" in $SU(3)_C$ denotes the color charge associated with the strong interactions, the "L" in $SU(2)_L$ indicates the left-handed chiral structure of electroweak interactions, and the subscript "Y" in $U(1)_Y$ is weak hypercharge.

The strong interactions are mediated by eight massless gluons G^a_μ $(a = 1, \ldots, 8)$ that are in the adjoint representation of $SU(3)_C$, while the electroweak interactions are mediated by the $SU(2)_L$ triplet gauge field W^a_μ $(a = 1, 2, 3)$ and the $U(1)_Y$ gauge field B_μ. After electroweak symmetry breaking (EWSB) the weak gauge bosons mix to give three physical mass eigenstates, namely, the massive vector bosons $W^\pm, Z$ and the massless photon γ.

In addition to the gauge bosons mentioned above, the SM contains three gen-

erations of fermions – the quarks and leptons. Quarks are spin-1/2 particles that participate in the strong and electroweak interactions, while leptons only participate in the electroweak interactions (i.e. they do not have color charge). SM fermions are present in left- and right-handed types that are treated differently by the chiral structure of the weak interactions. Left-handed particles fermions transform as doublets under $SU(2)_L$ while right-handed fermions are singlets under $SU(2)_L$ transformations.

The prediction and discovery of the $W^{\pm}$ and Z bosons is one of the great achievements of the SM. The fact that they mediate short range forces indicates that they must have relatively large masses. However, gauge invariance implies that mass terms for gauge bosons and fermions of the form

$$\mathcal{L} \supset \frac{1}{2} m_B^2 B_\mu B^\mu - m\bar{\psi}\psi, \tag{1.1}$$

where ψ is a SM fermions, are prohibited and can not be inserted by hand into the Lagrangian of the SM. Therefore, gauge invariance implies that all gauge bosons and fermions are massless. However, non-zero masses for the $W^{\pm}, Z$ bosons and SM fermions have been measured experimentally[1] and an additional theoretical ingredient is needed to explain this observation. Preservation of gauge invariance can be achieved by introducing a single scalar field Φ charged under $SU(2)_L \times U(1)_Y$ that acquires a vacuum expectation value (VEV). The VEV of the scalar field leads to spontaneous symmetry breaking that dynamically generates masses for *both* gauge bosons and fermions. The scalar field Φ is called the *Higgs field* and, after EWSB, gives rise to a massive scalar particle h i.e. the Higgs boson.

The field content of the SM and their charge assignments under the SM gauge

[1] Except the top quark, the masses of quarks have not been measured experimentally and are determined using lattice QCD methods.

group is given in Tab. 1.1, where the SM fields are written in the gauge eigenstate basis. The $SU(3)_C$, $SU(2)_L$, and $U(1)_Y$ gauge bosons are represented by G^a_μ, W^a_μ, and B_μ, respectively. The left-handed quark and lepton doublets are denoted by Q_L and L_L, while the right-handed $SU(2)_L$ singlet up quarks, down quarks, and leptons are denoted by u_R, d_R, and e_R, respectively. Note that there are three flavors of each quark and lepton field; the flavor indices are suppressed in Tab. 1.1.

Interactions between SM particles are described by the most general renormalizable Lagrangian that is consistent with the symmetries of the SM. The SM Lagrangian can be divided into three parts

$$\mathcal{L}_{\text{SM}} = \mathcal{L}_{\text{kinetic}} + \mathcal{L}_{\text{Higgs}} + \mathcal{L}_{\text{Yukawa}} \tag{1.2}$$

where $\mathcal{L}_{\text{kinetic}}$ encodes the gauge interactions of SM particles and is given by

$$\mathcal{L}_{\text{kinetic}} = -\frac{1}{4}G^a_{\mu\nu}G^{a\mu\nu} - \frac{1}{4}W^a_{\mu\nu}W^{a\mu\nu} - \frac{1}{4}B_{\mu\nu}B^{\mu\nu} + \sum_i \bar{\psi}_i i\not{D}\psi_i, \tag{1.3}$$

where the gauge field strength tensors are

$$G^a_{\mu\nu} = \partial_\mu G^a_\nu - \partial_\nu G^a_\mu + g_s f^{abc} G^b_\mu G^c_\nu \tag{1.4}$$

$$W^a_{\mu\nu} = \partial_\mu W^a_\nu - \partial_\nu W^a_\mu + g_2 \epsilon^{abc} W^b_\mu W^c_\nu \tag{1.5}$$

$$B_{\mu\nu} = \partial_\mu B_\nu - \partial_\nu B_\mu, \tag{1.6}$$

with g_s, g_2, g_1 being the $SU(3)_C$, $SU(2)_L$, and $U(1)_Y$ gauge couplings, respectively. ψ_i is a SM fermion field with $i = 1, 2, 3$ denoting the flavor (or generation) of the fermion and $\not{D} = \gamma^\mu D_\mu$ is the covariant derivative

$$D_\mu = \partial_\mu - ig_1 B_\mu Y - \frac{1}{2} i g_2 \sigma_a W^a_\mu - i g_s t_a G^a_\mu \tag{1.7}$$

The second term in Eq. (1.2) $\mathcal{L}_{\text{Higgs}}$ describes gauge and self-interactions of the SM Higgs boson and is given by

$$\mathcal{L}_{\text{Higgs}} = (D_\mu \Phi)^\dagger D^\mu \Phi - V(\Phi) \tag{1.8}$$

where $V(\Phi)$ is the Higgs potential. Note that the covariant derivative for the Higgs field Φ does not contain the last term in Eq. (1.7) since the Higgs does not have color charge.

Finally, $\mathcal{L}_{\text{Yukawa}}$ describes the interactions of the Higgs boson with SM fermions and is given by

$$-\mathcal{L}_{\text{Yukawa}} \;=\; \sum_{i,j} \left(y^u_{ij} (\overline{Q}^i_L u^j_R) \tilde{\Phi} + y^d_{ij} (\overline{Q}^i_L d^j_R) \Phi + y^e_{ij} (\overline{L}^i_L e^j_R) \Phi \right) \;+ \text{h.c.} \;, \tag{1.9}$$

where $\tilde{\Phi} = i\sigma_2 \Phi^*$, $y^{u,d,e}$ are 3×3 Yukawa coupling matrices, and $i, j = 1, 2, 3$ are flavor indices.

The Higgs and Yukawa Lagrangians are perhaps the most important parts of the SM and it is worth spending some time discussing the Higgs mechanism and electroweak symmetry breaking.

1.2 The Higgs Mechanism and Gauge Boson Masses

The most general renormalizable scalar potential of the SM Higgs is given by

$$V(\Phi) = -\mu^2 \Phi^\dagger \Phi + \lambda (\Phi^\dagger \Phi)^2. \tag{1.10}$$

We can analyze the vacuum of the Higgs potential by considering the possible signs of $-\mu^2$ and λ.

1. For $-\mu^2 < 0,\ \lambda < 0$, the potential is unbounded from below and there is no stable vacuum state.

2. For $-\mu^2 > 0,\ \lambda > 0$ the potential has a minimum at $\Phi = 0$ and the electroweak symmetry of the SM is unbroken. In this case the $W^{\pm}$ and Z bosons would remain massless.

3. For $-\mu^2 < 0,\ \lambda > 0$ the potential has a minimum at $\Phi \neq 0$ and electroweak symmetry is broken via $SU(2)_L \times U(1)_Y \to U(1)_{\rm EM}$, leaving electromagnetism unbroken. It is this case that is responsible for generating mass for the weak gauge bosons and the SM fermions, but leaves the photon massless.

The SM Higgs field Φ is an $SU(2)_L$ complex scalar field with four degree of freedom and can be decomposed as

$$\Phi = \frac{1}{\sqrt{2}} \begin{pmatrix} \phi_1 + i\phi_2 \\ \phi_3 + i\phi_4 \end{pmatrix} \to \begin{pmatrix} 0 \\ \frac{1}{\sqrt{2}}(v+h) \end{pmatrix}, \tag{1.11}$$

where in the last step we perform a gauge transformation (unitary gauge) that removes the fields $\phi_{1,2,4}$ from the Lagrangian so that we are left with one massive field ϕ_3 that is expanded about the minimum of the Higgs potential so that $\phi_3 = v + h$. The massless fields $\phi_{1,2,4}$ are "eaten" by the the electroweak gauge bosons and their masses will be generated. The mass terms for the $W^{\pm}$ and Z bosons can be read by expanding the first term in Eq. (1.8), after which we find

$$M_W = g_2 v/2\ ,\ M_Z = v\sqrt{g_1^2 + g_2^2}/2. \tag{1.12}$$

The VEV of the SM Higgs has given mass to the electroweak gauge bosons in a dynamical way that preserves gauge invariance! The measured values of the $W^{\pm}, Z$ boson masses are $M_W = 80.379 \pm 0.0012$ GeV and $M_Z = 91.187 \pm 0.0021$

GeV [26]. Given the measured value of the M_W and the gauge coupling g_2, the VEV of the Higgs can be determined to be $v = 246$ GeV. In addition, to the weak gauge bosons, EWSB gives rise to an additional massive particle – the Higgs boson h – with a measured mass of $m_h = 125.10 \pm 0.14$ GeV.

1.3 The Origin of Fermion Masses

If we omit for the moment the Yukawa Lagrangian of Eq. (1.9) we see that the SM has a relatively simple description in terms of a small set of parameters: the gauge couplings g_s, g_1, g_2, the SM Higgs mass m_h, and the Higgs VEV v. The Yukawa Lagrangian, on the other hand, is responsible for much of the complicated and interesting structure of the SM.

The mechanism that is responsible for generating the weak gauge boson masses is also responsible for giving mass to the SM fermions. If we expand Eq.(1.9) in the unitary gauge we find that the mass terms of the SM fermions are given by

$$-\mathcal{L}_{\text{Yukawa}} \supset \bar{u}_L^i \mathcal{M}_{ij}^u u_R^j + \bar{d}_L^i \mathcal{M}_{ij}^d d_R^j + \bar{\ell}_L^i \mathcal{M}_{ij}^\ell e_R^j \tag{1.13}$$

where $M_{ij}^f = v\, y_{ij}^f/\sqrt{2},\ (f = u, d, \ell)$ are fermion mass matrices that are, in general, complex 3×3 matrices. The fermion mass matrices can be simultaneously diagonalized by independent bi-unitary transformations that rotate the flavor eigenstates into the physical mass eigenstates

$$\mathcal{M}_{diag}^u = U_{u_L}^\dagger \mathcal{M}_{ij}^u U_{u_R} = \begin{pmatrix} m_u & & \\ & m_c & \\ & & m_t \end{pmatrix}, \tag{1.14}$$

$$\mathcal{M}^d_{diag} = U^\dagger_{d_L} \mathcal{M}^d U_{d_R} = \begin{pmatrix} m_d & & \\ & m_s & \\ & & m_b \end{pmatrix}, \tag{1.15}$$

$$\mathcal{M}^\ell_{diag} = U^\dagger_{e_L} \mathcal{M}^\ell U_{e_R} = \begin{pmatrix} m_e & & \\ & m_\mu & \\ & & m_\tau \end{pmatrix}. \tag{1.16}$$

An interesting consequence of diagonalizing the up and down quark mass matrices is that they do not leave the charged weak current interactions invariant. This is a result of the up and down quark mass matrices being diagonalized by different unitary transformations. In particular, we find that the $W^\pm$ boson interactions with quarks transform as

$$-\frac{g_2}{2}\gamma^\mu \overline{Q}_L \gamma^\mu W^a_\mu \sigma_a Q_L \xrightarrow[\text{basis}]{\text{mass}} -\frac{g_2}{2}\bar{u}^i_L \gamma_\mu W^\pm V^{ij}_{CKM} d^j_L, \tag{1.17}$$

where the Cabbibo-Kobayashi-Maskawa (CKM) matrix V_{CKM} is a 3×3 unitary matrix defined as

$$V_{CKM} = U^\dagger_{u_L} U_{d_L}. \tag{1.18}$$

The mismatch that appears in the up and down quarks when transforming from the flavor to the mass eigenstate basis gives rise to tree-level flavor changing couplings of the $W^\pm$ boson. This allows for the presence of flavor changing neutral currents (FCNCs) that occur at the one-loop level.

We see that the fermion sector is described is described by 13 free parameters: 10 in the quark sector (the 6 quark masses and 4 parameters of the CKM matrix), and 3 in the lepton sector (the 3 lepton masses).[2] These parameters are

[2]We assume that neutrino are massless and that there are no right-handed neutrinos in the lepton sector.

arbitrary: their values are not predicted by the SM and can only be determined from experimental measurements. The values of the fermion masses have been determined to be [26]

$$\begin{aligned} &m_u \simeq 2.2 \times 10^{-3} \text{ GeV} \ , \ m_c \simeq \ 1.27 \text{ GeV} \ , \ m_t \simeq 173 \text{ GeV} \\ &m_d \simeq \ 4.7 \times 10^{-3} \text{ GeV} \ , \ m_s \simeq 0.092 \text{ GeV} \ , \ m_b \simeq 4.18 \text{ GeV} \\ &m_e \simeq 5.1 \times 10^{-4} \text{ GeV} \ , \ m_\mu, \simeq 0.105 \text{ GeV} \ , \ m_\tau \simeq 1.776 \text{ GeV} \end{aligned} \tag{1.19}$$

The values of the CKM matrix have been experimentally measured from various quark flavor transitions and are given by [27]

$$\begin{aligned} &|V_{ud}| \simeq 0.97 \ , \ |V_{us}| \simeq 0.23 \ , \ |V_{ub}| \simeq 3.7 \times 10^{-3} \\ &|V_{cd}| \simeq 0.23 \ , \ |V_{cs}| \simeq 0.97 \ , \ |V_{cb}| \simeq 0.042 \\ &|V_{td}| \simeq 8.7 \times 10^{-3} \ , \ |V_{ts}| \simeq 0.041 \ , \ |V_{tb}| \simeq 1.0 \end{aligned} \tag{1.20}$$

$$\tag{1.21}$$

Already we can observe an interesting pattern in the values of the fermion masses and the elements of the CKM matrix: there is a large difference between the masses of the fermions and the elements of the CKM matrix. For example, taking ratios of the masses of the first and third generations we find

$$\frac{m_t}{m_u} \sim 10^5 \ , \ \frac{m_b}{m_d} \sim 10^3 \ , \ \frac{m_\tau}{m_e} \sim 10^3. \tag{1.22}$$

In general we see that $m_3 \gg m_2 \gg m_1$ (where 1,2,3 denote the fermion generation). In addition, the off-diagonal elements of the CKM matrix are much smaller then the diagonal elements. The hierarchical structure observed in the fermion masses and in the CKM matrix is a long-standing problem known as the *SM flavor*

puzzle.

The hierarchy in the fermion masses can be translated into a hierarchy in the Yukawa couplings of the Higgs bosons. The Yukawa interactions in Eq. (1.9) also gives rise to Higgs interactions with fermions of the form $y_f h\bar{f}f$ where $y_f = \sqrt{2}m_f/v$. The Yukawa couplings are determined once the the fermion masses and Higgs VEV are measured. The SM flavor puzzle in then translated into a question of why the Higgs couplings to first and second generation fermions are so small compared to its couplings to the third generation fermions.

This question can also be framed from an experimental point of view. The LHC measurements of Higgs rates [28–30] show an overall good agreement with Standard Model (SM) predictions. By now it is established that the couplings of the Higgs to the weak gauge bosons are SM-like to a good approximation. This implies that the main origin of the weak gauge bosons' mass is the vacuum expectation value (vev) of the 125 GeV Higgs boson. Also the masses of the top quark, the bottom quark and the tau lepton appear to be largely due to the 125 GeV Higgs, as indicated by the measured values of Higgs couplings to the third generation fermions [31–36]. In the lepton sector, ATLAS and CMS have recently measured the Higgs coupling to muons at the 2σ and 3σ level, respectively, by observing the $h \to \mu^+\mu^-$ decay [37, 38].

However, little is known about the origin of the masses of the remaingin first and second generation fermions. Direct measurements of the Higgs couplings to these fermions are challenging.The Higgs coupling to electrons is tiny and the $h \to e^+e^-$ rate in the SM is far beyond the experimental reach of the LHC. Sensitivities to the Higgs electron coupling not far above the SM might be reached at future e^+e^- colliders running on the Higgs pole [39, 40]. In the quark sector, various ideas have been explored to determine the coupling of the Higgs to charm quarks.

Those include the measurement of the exclusive $h \to J/\psi\gamma$ decay rate [41–44], inclusive $h \to c\bar{c}$ measurements using charm-tagging techniques [43, 45, 46], and Higgs production in association with charm quarks [47]. The rates of the exclusive Higgs decays $h \to \phi\gamma$, $h \to \rho\gamma$, and $h \to \omega\gamma$ are sensitive to the Higgs couplings to strange, down, and up quarks [48, 49]. Also the Higgs p_T distribution [50–52] and the $W^{\pm}h$ charge asymmetry [53] have sensitivity to the light quark couplings.

While inclusive $h \to c\bar{c}$ measurements might reach SM sensitivities at a future 100 TeV collider [43] and will be quite precisely determined at future e^+e^- colliders [54], the Higgs couplings to strange, down, and up quarks remain out of direct experimental reach in the foreseeable future, unless they are enhanced by orders of magnitude, if compared to SM expectations.

Given the limited sensitivities of the direct measurements of the Higgs couplings to the light generations, we develop complementary strategies to identify the origin of the masses of first and second generation in Part II of this thesis. Motivated by our limited knowledge of the Higgs couplings to first two generation fermions, we analyze the collider phenomenology of a class of two Higgs doublet models (2HDMs) with a non-standard Yukawa sector. One Higgs doublet is mainly responsible for the masses of the weak gauge bosons and the third generation fermions, while the second Higgs doublet provides mass for the lighter fermion generations. The characteristic collider signatures of this setup differ significantly from well-studied 2HDMs with natural flavor conservation, flavor alignment, or minimal flavor violation. New production mechanisms for the heavy scalar, pseudoscalar, and charged Higgs involving second generation quarks can become dominant. The most interesting decay modes include $H/A \to cc, tc, \mu\mu, \tau\mu$ and $H^{\pm} \to cb, cs, \mu\nu$. Searches for low mass di-muon resonances are currently among the best probes of the heavy Higgs bosons in this setup.

1.4 Lepton Flavor Universality

In the SM the electroweak gauge bosons $W^{\pm}, Z, \gamma$ couple to all three lepton generations in the same way, up to differences in the lepton masses. This aspect of the electroweak interactinos is known as lepton flavor universality (LFU). Ratios of the partial widths of $Z \to \ell^+\ell^-$ ($\ell = e, \mu, \tau$) have been observed to be equal to unity (up to phase space differences) giving good agreement with LFU [55, 56]. In addtion, measurements of $W^{\pm}$ decay to lepton and neutrinos are in good agreement with LFU [56–59].

Semi-leptonic decays of B mesons provide an ideal laboratory for testing LFU. Over the past several years, multiple B-physics experiments, including BaBar, LHCb, and Belle, have reported anomalies in decays associated with the $b \to c\ell\nu$ and $b \to s\ell\ell$ transitions. Violations of lepton flavor universality, known to be theoretically clean probes of New Physics (NP), are of particular interest. In the Standard Model (SM) LFU is only broken by the lepton masses. Hints for additional sources of LFU violation have been observed in the ratios of branching ratios of flavor-changing charged current and neutral current decays of B mesons, R_D, R_{D^*}, R_K, and R_{K^*},

$$R_{D^{(*)}} = \frac{\mathrm{BR}(B \to D^{(*)}\tau\nu)}{\mathrm{BR}(B \to D^{(*)}\ell\nu)}\,, \qquad R_{K^{(*)}} = \frac{\mathrm{BR}(B \to K^{(*)}\mu^+\mu^-)}{\mathrm{BR}(B \to K^{(*)}e^+e^-)}\,. \tag{1.23}$$

The experimental world averages of R_D and R_{D^*} from the heavy flavor averaging group (HFLAV) are based on measurements from BaBar [60], Belle [61–63], and LHCb [64, 65], and read [66]

$$R_D = 0.340 \pm 0.027 \pm 0.013\,, \qquad R_{D^*} = 0.295 \pm 0.011 \pm 0.008\,, \tag{1.24}$$

with an error correlation of $\rho = -38\%$. The corresponding SM predictions are

known with high precision [67–69]. The values adopted by HFLAV are [66]

$$R_D^{\rm SM} = 0.299 \pm 0.003\,, \qquad R_{D^*}^{\rm SM} = 0.258 \pm 0.005\,. \tag{1.25}$$

The combined discrepancy between the SM prediction and experimental world averages of R_D and R_{D^*} is at the 3.1σ level.

The most precise measurement to date of the LFU ratio R_K has been performed by LHCb [70]

$$R_K = 0.846^{+0.060+0.016}_{-0.054-0.014}\,, \qquad \text{for} \quad 1.1\,\text{GeV}^2 < q^2 < 6\,\text{GeV}^2\,, \tag{1.26}$$

with q^2 being the dilepton invariant mass squared. The SM predicts $R_K^{\rm SM} \simeq 1$ with theoretical uncertainties well below the current experimental ones [71]. The above experimental value is closer to the SM prediction than the Run-1 result [72]. However, the reduced experimental uncertainties still imply a tension between theory and experiment of 2.5σ.

The most precise measurement of R_{K^*} is from a Run-1 LHCb analysis [73] that finds

$$R_{K^*} = \begin{cases} 0.66^{+0.11}_{-0.07} \pm 0.03\,, & \text{for } 0.045\,\text{GeV}^2 < q^2 < 1.1\,\text{GeV}^2\,, \\ 0.69^{+0.11}_{-0.07} \pm 0.05\,, & \text{for } 1.1\,\text{GeV}^2 < q^2 < 6\,\text{GeV}^2\,. \end{cases} \tag{1.27}$$

The result for both q^2 bins are in tension with the SM prediction [71], $R_{K^*}^{\rm SM} \simeq 1$,

by $\sim 2.5\sigma$ each. Recent measurements of R_{K^*} and R_K by Belle [74, 75][3]

$$R_{K^*} = \begin{cases} 0.90^{+0.27}_{-0.21} \pm 0.10\,, & \text{for } 0.1\,\text{GeV}^2 < q^2 < 8\,\text{GeV}^2\,, \\ 1.18^{+0.52}_{-0.32} \pm 0.10\,, & \text{for } 15\,\text{GeV}^2 < q^2 < 19\,\text{GeV}^2\,, \end{cases} \tag{1.28}$$

$$R_K = \begin{cases} 0.98^{+0.27}_{-0.23} \pm 0.06\,, & \text{for } 1\,\text{GeV}^2 < q^2 < 6\,\text{GeV}^2\,, \\ 1.11^{+0.29}_{-0.26} \pm 0.07\,, & \text{for } 14.18\,\text{GeV}^2 < q^2\,, \end{cases} \tag{1.29}$$

are compatible with both the SM prediction and the LHCb results. Several papers have re-analyzed the status of the B anomalies in light of the latest experimental updates, and found preference for new physics with high significance [76–82]. A review of new physics explanations of these anomalies can be found in [83].

In Ch. 5 we present a vector leptoquark scenario that can address the LFU anomalies in decays associated with the $b \to c\ell\nu$ and $b \to s\ell\ell$ transitions. Independent of the anomalies, leptoquarks generically yield new sources of CP violation that can induce electric and magnetic dipole moments of elementary particles. In light of upcoming low-energy experiments with much greater sensitivity to electric and magnetic dipole moments of elementary particles, it is interesting to ask whether solutions to the flavor anomalies may also be associated with sizable CP violating complex phases that may be probed by these experiments.

[3] Here we quote the isospin average of $B^0 \to K^{(*)0}\ell^+\ell^-$ and $B^\pm \to K^{(*)\pm}\ell^+\ell^-$ decays.

Part II

Theory and Phenomenology of Flavorful Two Higgs Doublet Models

Introduction

This Part of the thesis in aimed at addressing the SM flavor puzzle i.e. the question of why the fermion masses and the CKM matrix exhibit a hierarchical structure. Other ways to phrase this question are: (1) why does the SM Higgs boson have very tiny couplings to first and second generation fermions, while its couplings to third generation fermions are $\sim \mathcal{O}(1)$? or (2) is the VEV of the SM Higgs boson the source of mass generation for the first and second generations of fermions?

The SM flavor puzzle can be partially addressed by introducing an additional source of EWSB that is responsible for generating mass for the first and second generation fermions, as proposed in [84] (see also [85–88]). Arguably the simplest realization of this scenario is a Two Higgs Doublet Model (2HDM), in which one Higgs doublet (approximately identified as the 125 GeV Higgs boson) couples mainly to the third generation, while the second Higgs doublet couples mainly to the first and second generations. The observed pattern of quark masses and mixing can be obtained by asserting suitable textures for the quark mass matrices, leading to a "flavorful" Two Higgs Doublet Model (F2HDM).

We begin in Ch. 2 by first motivating the F2HDM from experimental measurements of SM Higgs rates and couplings, after which we introduce the model and Yukawa textures that are able to partially address the SM flavor puzzle. We also discuss in detail the collider phenomenology predicted by the model that can lead

to very distinct and unique collider signatures that are not traditionally searched for at the LHC. In Ch. 3 we provide an ultra-violet (UV) realization of the Yukawa textures presented in Ch. 2 and discuss low-energy flavor constraints. Finally, we discuss additional probes of F2HDMs in Ch. 4 focusing in particular on the rare top quark decays $t \to hq$, where h is the SM higgs boson and $q = u, c$, is a light up-type quark.

Chapter 2

Collider Signatures of Flavorful Two Higgs Doublet Models

2.1 Introduction

The LHC collaborations have established with Run I data that the 125 GeV Higgs boson has Standard Model (SM)-like properties [30]. In particular, the couplings of the Higgs boson to the electroweak gauge bosons have been measured with an uncertainty of 10% at the 1σ level, combining results from ATLAS and CMS [30]. The Higgs coupling to τ leptons has been measured at the 15% level [30], and, assuming no significant contribution of new degrees of freedom to the gluon fusion Higgs production cross section, the Higgs coupling to top quarks has been found to be SM-like with approximately 15% uncertainty [30]. More recently, analyses of ~ 36 fb^{-1} of Run II LHC data have provided evidence for the decay of the Higgs boson into a pair of b quarks with a branching fraction consistent with the SM expectation [89, 90]. Taken together, these results imply that the main origin of the masses of the weak gauge bosons and third generation

fermions is the vacuum expectation value (vev) of the 125 GeV SM-like Higgs.

However, it is not known whether the vacuum of the SM Higgs field is (solely) responsible for the generation of all the elementary fermion masses. So far, the $h \to \mu\mu$ branching fraction is bounded by a factor of ~ 2.6 above the SM prediction [91,92]. With 300 fb^{-1} of data, the SM partial width for this decay mode will be accessible at LHC, and it could be measured with a precision of $\sim 8\%$ at the High-Luminosity LHC (HL-LHC) [93–95]. The $h \to c\bar{c}$ rate is more difficult to access at the LHC. At present, the most stringent bound arises from the ATLAS search for $Zh, h \to c\bar{c}$, exploiting new c-tagging techniques, and only probes the branching fraction down to ~ 110 times the SM expectation [96]. Studies of future prospects for the HL-LHC have shown that LHCb may be able to set a stronger bound on the $hc\bar{c}$ coupling, at the level of ~ 4 times the SM expectation [97]. The charm coupling may be determined more precisely at future colliders, such as e^+e^- machines [98], as well as proton-electron colliders [99]. Finally, because of their tiny values, the SM Higgs couplings to the other light quarks, as well as the electron, are even more challenging to measure and will likely remain out of reach for the foreseeable future [39, 43, 50–53, 100–103]. Signals that would provide immediate evidence for a beyond SM Higgs sector, such as $h \to \tau\mu$ and $t \to ch$, have branching fractions that are constrained to be less than few $\times\ 10^{-3}$ [104–107].

At the same time, the origin of the large hierarchies in the SM fermion masses, as well as the hierarchical structure of the CKM quark mixing matrix, is a long-standing open question: the SM flavor puzzle. In this chapter we study the possibility that the origin of the first and second generation fermion masses is *not* the 125 GeV Higgs but an additional source of electro-weak symmetry breaking as proposed in [84] (see also [85–88]) and study the implications. Arguably the simplest realization of such a setup is a two Higgs doublet model (2HDM) where

one doublet (that we approximately identify as the 125 GeV Higgs) couples mainly to the third generation, while a second doublet couples mainly to the first and second generation. One motivation, with regards to fermion mass generation, is a reduction of the Yukawa coupling hierarchy between the third and the lighter generations via a Higgs vev hierarchy.

In such a framework we expect distinct phenomenological implications at low and high energy experiments. A generic prediction are flavor-violating couplings of the 125 GeV Higgs [84–86] which could explain the small hint for the lepton flavor-violating Higgs decay $h \to \tau\mu$ at CMS [108]. Other signatures include rare lepton flavor-violating B meson decays like $B \to K^{(*)}\tau\mu$ with branching ratios as large as 10^{-7} and the rare top decay $t \to ch$ with branching ratios as large as 10^{-3} [84].

We determine the characteristic collider signatures of the second Higgs doublet. We find that novel production mechanisms involving second generation quarks can become dominant for moderate and large $\tan\beta$. The largest production mode of the neutral Higgs bosons is production from a $c\bar{c}$ initial state. The charged Higgs bosons are dominantly produced from a cs initial state. The most interesting decay modes include $H/A \to cc, tc, \mu\mu, \tau\mu$ and $H^{\pm} \to cb, cs, \mu\nu$. Our work provides continued motivation to search for low mass di-muon resonances and low mass di-jet resonances. Searches for di-muon resonances are currently the best probes of the considered setup, while searches for di-jet resonances have sensitivities similar to the "traditional" di-tau searches for additional neutral Higgs bosons.

The chapter is organized as follows. In Sec. 2.2 we discuss aspects of the proposed 2HDM framework that are relevant for our analysis, focusing in particular on the couplings of the heavy Higgs bosons. In Sec. 2.3 the modifications to the properties of the 125 GeV Higgs are analysed and confronted with Higgs coupling

measurements at the LHC. In Sec. 2.4, we discuss the collider phenomenology of the heavy neutral Higgs bosons and identify distinct features in production and decay modes. The production and decay modes of the charged Higgs are discussed in Sec. 2.5. In Sec. 2.6 we discuss the constraints that can be derived using current searches for heavy Higgs bosons and show predictions for novel collider signatures. We conclude in Sec. 3.5.

2.2 Two Flavorful Higgs Doublets

The considered setup is a 2HDM in which one Higgs doublet is mainly responsible for the mass of the third generation of SM fermions, while the second Higgs doublet gives masses mainly to the first and second generations. We start by briefly reviewing generic 2HDMs (see e.g. [109,110]) in Sec. 2.2.1. In Sec. 2.2.2 we discuss the specific Yukawa textures of our model and the resulting heavy Higgs couplings.

2.2.1 Generic Two Higgs Doublet Models

The two Higgs doublets with hypercharge $+1/2$ are denoted Φ and Φ' and decompose as

$$\Phi = \begin{pmatrix} \phi^+ \\ \frac{1}{\sqrt{2}}(v + \phi + ia) \end{pmatrix} , \quad \Phi' = \begin{pmatrix} \phi'^+ \\ \frac{1}{\sqrt{2}}(v' + \phi' + ia') \end{pmatrix} , \tag{2.1}$$

where $v^2 + v'^2 = v_W^2 = (246\text{ GeV})^2$ is the SM Higgs vacuum expectation value (vev) squared and the ratio of Higgs vevs is $\tan\beta = t_\beta = v/v'$. Note that in generic two Higgs doublet models, the Higgs fields Φ and Φ' can be transformed into each other, and the ratio of Higgs vevs is therefore a basis dependent quantity [**?**].

For simplicity we will not consider CP violation in the Higgs sector.[1] In this case, after electroweak symmetry breaking, the components of Φ and Φ' mix in the following way to form mass eigenstates

$$\begin{pmatrix} \phi^+ \\ \phi'^+ \end{pmatrix} = \begin{pmatrix} s_\beta & -c_\beta \\ c_\beta & s_\beta \end{pmatrix} \begin{pmatrix} G^+ \\ H^+ \end{pmatrix} , \tag{2.2}$$

$$\begin{pmatrix} a \\ a' \end{pmatrix} = \begin{pmatrix} s_\beta & -c_\beta \\ c_\beta & s_\beta \end{pmatrix} \begin{pmatrix} G^0 \\ A \end{pmatrix} , \tag{2.3}$$

$$\begin{pmatrix} \phi \\ \phi' \end{pmatrix} = \begin{pmatrix} c_\alpha & s_\alpha \\ -s_\alpha & c_\alpha \end{pmatrix} \begin{pmatrix} h \\ H \end{pmatrix} , \tag{2.4}$$

with $c_x \equiv \cos x$, $s_x \equiv \sin x$ for $x = \alpha, \beta$. The three states G^0, $G^\pm$ provide the longitudinal components of the Z and $W^\pm$ gauge bosons. The remaining physical states consist of two CP-even scalars h and H, one CP-odd scalar A, and the charged Higgs $H^\pm$. We will identify h with the SM-like Higgs with a mass of $m_h \simeq 125$ GeV. The heavy Higgs bosons H, A, and $H^\pm$ are approximately degenerate in the decoupling limit, $m_H \simeq m_A \simeq m_{H^\pm}$, with mass splittings of $\mathcal{O}(v_W^2/m_A^2)$. In the decoupling limit, the mixing angle α is strongly related to β with $\alpha = \beta - \frac{\pi}{2} + \mathcal{O}(v_W^2/m_A^2)$.

Turning to the interactions of the two Higgs doublets with the SM fermions, the most general Yukawa Lagrangian can be written as

$$\begin{aligned} -\mathcal{L}_Y &= \sum_{i,j} \Big(\lambda^u_{ij} (\bar{q}_i u_j) \tilde{\Phi} + \lambda'^u_{ij} (\bar{q}_i u_j) \tilde{\Phi}' + \lambda^d_{ij} (\bar{q}_i d_j) \Phi + \lambda'^d_{ij} (\bar{q}_i d_j) \Phi' \\ &\qquad + \lambda^e_{ij} (\bar{\ell}_i e_j) \Phi + \lambda'^\ell_{ij} (\bar{\ell}_i e_j) \Phi' \Big) + \text{h.c.} , \end{aligned} \tag{2.5}$$

[1] Note that the Yukawa couplings of the Higgs bosons to quarks necessarily contain complex parameters to reproduce the phase in the CKM matrix and will lead to CP violation in the Higgs potential at the loop level. However, such effects are generically small and will be neglected here.

where $\tilde{\Phi}^{(\prime)} = i\sigma_2(\Phi^{(\prime)})^*$. The q_i, ℓ_i are the three generations of left-handed quark and lepton doublets, and the u_i, d_i, e_i are the right-handed up quark, down quark, and charged lepton singlets. (A discussion of neutrino masses and mixing is beyond the scope of this work.) In all generality, the mass matrices of the charged SM fermions receive contributions from both Higgs doublets. In the fermion mass eigenstate basis we use the notation

$$m^{(\prime)u}_{qq'} = \frac{v^{(\prime)}}{\sqrt{2}}\langle q_L|\lambda^{(\prime)u}|q'_R\rangle \ , \qquad \text{for } q, q' \in \{u, c, t\} \ , \tag{2.6}$$

$$m^{(\prime)d}_{qq'} = \frac{v^{(\prime)}}{\sqrt{2}}\langle q_L|\lambda^{(\prime)d}|q'_R\rangle \ , \qquad \text{for } q, q' \in \{d, s, b\} \ , \tag{2.7}$$

$$m^{(\prime)}_{\ell\ell'} = \frac{v^{(\prime)}}{\sqrt{2}}\langle \ell_L|\lambda^{(\prime)\ell}|\ell'_R\rangle \ , \qquad \text{for } \ell, \ell' \in \{e, \mu, \tau\} \ . \tag{2.8}$$

Notice that in the mass basis the matrices $m^{(\prime)}_{xx'}$, with $x = q, \ell$, are not diagonal. The couplings of the physical neutral Higgs bosons to the fermions can be parameterized as

$$\begin{aligned}
\mathcal{L} \ \supset \ & -\sum_{i,j}(\bar{u}_i P_R u_j)\left(h(Y^u_h)_{ij} + H(Y^u_H)_{ij} + iA(Y^u_A)_{ij}\right) \\
& -\sum_{i,j}(\bar{d}_i P_R d_j)\left(h(Y^d_h)_{ij} + H(Y^d_H)_{ij} + iA(Y^d_A)_{ij}\right) \\
& -\sum_{i,j}(\bar{\ell}_i P_R \ell_j)\left(h(Y^\ell_h)_{ij} + H(Y^\ell_H)_{ij} + iA(Y^\ell_A)_{ij}\right) \\
& +\text{h.c.} \ .
\end{aligned} \tag{2.9}$$

In the fermion mass eigenstate basis we find for the flavor-diagonal Higgs couplings

$$Y^h_\ell \ \equiv \ \langle \ell_L|Y^\ell_h|\ell_R\rangle = \frac{m_\ell}{v_W}\left(\frac{c_\alpha}{s_\beta} - \frac{m'_{\ell\ell}}{m_\ell}\frac{c_{\beta-\alpha}}{s_\beta c_\beta}\right) \ , \tag{2.10}$$

$$Y^H_\ell \ \equiv \ \langle \ell_L|Y^\ell_H|\ell_R\rangle = \frac{m_\ell}{v_W}\left(\frac{s_\alpha}{s_\beta} + \frac{m'_{\ell\ell}}{m_\ell}\frac{s_{\beta-\alpha}}{s_\beta c_\beta}\right) \ , \tag{2.11}$$

$$Y_\ell^A \equiv \langle \ell_L | Y_A^\ell | \ell_R \rangle = \frac{m_\ell}{v_W} \left(\frac{1}{t_\beta} - \frac{m'_{\ell\ell}}{m_\ell} \frac{1}{s_\beta c_\beta} \right) , \tag{2.12}$$

for $\ell = e, \mu, \tau$, and analogous for the quark couplings. m_ℓ are the mass eigenvalues that is, from (2.8), $m_\ell = m_{\ell\ell} + m'_{\ell\ell}$. For the flavor-violating Higgs couplings we obtain

$$Y_{\ell\ell'}^h \equiv \langle \ell_L | Y_h^\ell | \ell'_R \rangle = -\frac{m'_{\ell\ell'}}{v_W} \frac{c_{\beta-\alpha}}{s_\beta c_\beta} , \tag{2.13}$$

$$Y_{\ell\ell'}^H \equiv \langle \ell_L | Y_H^\ell | \ell'_R \rangle = +\frac{m'_{\ell\ell'}}{v_W} \frac{s_{\beta-\alpha}}{s_\beta c_\beta} , \tag{2.14}$$

$$Y_{\ell\ell'}^A \equiv \langle \ell_L | Y_A^\ell | \ell'_R \rangle = -\frac{m'_{\ell\ell'}}{v_W} \frac{1}{s_\beta c_\beta} , \tag{2.15}$$

for $\ell \neq \ell'$ and $\ell, \ell' = e, \mu, \tau$. Analogous expressions hold for the flavor-violating quark couplings.

We write the couplings of the charged Higgs bosons to the fermions as

$$\begin{aligned} \mathcal{L} \supset & -\sqrt{2} \sum_{i,j} \Big((\bar{d}_i P_R u_j) H^-(Y_\pm^u)_{ij} + (\bar{u}_i P_R d_j) H^+(Y_\pm^d)_{ij} \\ & + (\bar{\nu}_i P_R \ell_j) H^+(Y_\pm^\ell)_{ij} \Big) + \text{h.c.} . \end{aligned} \tag{2.16}$$

In the fermion mass eigenstate basis we find for the couplings to quarks

$$Y_{qq'}^\pm \equiv \langle q_L | Y_\pm^d | q'_R \rangle \frac{m_{q'}}{v_W} \left(\frac{V_{qq'}}{t_\beta} - \sum_{x=d,s,b} \frac{m'_{xq'}}{m_{q'}} \frac{V_{qx}}{s_\beta c_\beta} \right) , \tag{2.17}$$

for $q \in \{u, c, t\}$ and $q' \in \{d, s, b\}$, and

$$Y_{qq'}^\pm \equiv \langle q_L | Y_\pm^u | q'_R \rangle = \frac{m_{q'}}{v_W} \left(\frac{V_{q'q}^*}{t_\beta} - \sum_{x=u,c,t} \frac{m'_{xq'}}{m_{q'}} \frac{V_{xq}^*}{s_\beta c_\beta} \right) ,$$

for $q \in \{d, s, b\}$ and $q' \in \{u, c, t\}$. In the above expressions, V is the CKM matrix.

In the lepton sector, we neglect neutrino mixing as it is of no relevance for our considerations. We find

$$Y_\ell^\pm \equiv \langle \nu_\ell | Y_\pm^\ell | \ell_R \rangle = \frac{m_\ell}{v_W} \left(\frac{1}{t_\beta} - \frac{m'_{\ell\ell}}{m_\ell} \frac{1}{s_\beta c_\beta} \right) \ . \tag{2.18}$$

The physical couplings of the Higgs bosons to the fermions are completely determined by the two angles α and β, the mass matrices m' in the fermion mass eigenstate basis, and the known masses of the SM fermions, as well as CKM elements. Note that none of the expressions above assumes a specific Yukawa texture. The expressions hold in any 2HDM.

2.2.2 Yukawa Textures

Our setup imposes that the Yukawa couplings of Φ are rank 1 and that they provide mass only to one generation of fermions, that will become the dominant component of the third generation. This assumption singles out a Higgs basis and renders the ratio of Higgs vevs, $\tan\beta$, well defined and physical.

We start with a discussion of the lepton sector. In the flavor basis where the Φ lepton Yukawa is diagonal, we consider the following Yukawa texture

$$\lambda^\ell \sim \frac{\sqrt{2}}{v} \begin{pmatrix} 0 & 0 & 0 \\ 0 & 0 & 0 \\ 0 & 0 & m_\tau \end{pmatrix} \ , \ \lambda'^\ell \sim \frac{\sqrt{2}}{v'} \begin{pmatrix} m_e & m_e & m_e \\ m_e & m_\mu & m_\mu \\ m_e & m_\mu & m_\mu \end{pmatrix} \ . \tag{2.19}$$

This texture gives the observed lepton masses, and it can naturally explain the hierarchy between second and third generation lepton masses, if $v' \ll v$, or equivalently $\tan\beta \gg 1$. Next we rotate into the mass eigenstate basis. Expanding in

m_μ/m_τ and m_e/m_μ we find

$$
\begin{aligned}
m'_{ee} &= m_e + \mathcal{O}(m_e^2/m_\tau)\,, && (2.20)\\
m'_{\mu\mu} &= m_\mu + \mathcal{O}(m_\mu^2/m_\tau)\,, && (2.21)\\
m'_{\tau\tau} &= \mathcal{O}(m_\mu)\ , && (2.22)\\
m'_{e\mu} &= \mathcal{O}(m_e m_\mu/m_\tau)\,,\ m'_{\mu e} = \mathcal{O}(m_e m_\mu/m_\tau)\,, && (2.23)\\
m'_{e\tau} &= \mathcal{O}(m_e)\,, \qquad m'_{\tau e} = \mathcal{O}(m_e)\,, && (2.24)\\
m'_{\mu\tau} &= \mathcal{O}(m_\mu)\,, \qquad m'_{\tau\mu} = \mathcal{O}(m_\mu)\,. && (2.25)
\end{aligned}
$$

The diagonal entries for the first and second generation are to a good approximation determined by the corresponding observed lepton masses. Note that $e-\mu$ mixing is not given by an entry of $\mathcal{O}(m_e)$ as one could naïvely expect, but is additionally suppressed. The reason for this suppression is a global $U(2)_\ell \times U(2)_e$ flavor symmetry acting on the first two generation of leptons that is only broken by a single Yukawa coupling λ'^ℓ. This suppression of $e-\mu$ mixing is sufficient to avoid the stringent constraints from flavor-violating low energy transitions like $\mu \to e\gamma$ or $\mu \to e$ conversion.

It seems natural to assume analogous Yukawa textures also in the quark sector. However, in addition to reproducing quark masses, the quark Yukawas also have to conform with the observed values of the CKM quark mixing matrix. Given that the hierarchies in the down-quark masses and the hierarchies among CKM elements are comparable, while the hierarchies in the up-quark masses are considerably larger, we will assume that the quark mixing is mainly generated from the down Yukawas.

The up sector can then be chosen in a way completely analogous to the lepton sector. The expressions (2.19)-(2.25) hold with the replacements $e \to u$, $\mu \to c$,

and $\tau \to t$. The strongly suppressed $u - c$ mixing guarantees that constraints from neutral D meson oscillations are easily avoided in this setup [**?**].

A down-quark Yukawa texture that naturally leads to the observed down-quark masses and CKM mixing angles reads

$$\lambda^d \sim \frac{\sqrt{2}}{v} \begin{pmatrix} 0 & 0 & 0 \\ 0 & 0 & 0 \\ 0 & 0 & m_b \end{pmatrix} , \; \lambda'^d \sim \frac{\sqrt{2}}{v'} \begin{pmatrix} m_d & \lambda m_s & \lambda^3 m_b \\ m_d & m_s & \lambda^2 m_b \\ m_d & m_s & m_s \end{pmatrix} , \tag{2.26}$$

with the Cabibbo angle $\lambda \simeq 0.23$. To a reasonable approximation one has $\lambda^2 m_b \sim m_s$, while $\lambda^3 m_b$ and λm_s are a factor of few larger than m_d. We consider this small missmatch acceptable at the level of Yukawa textures.

Rotating into the mass eigenstate basis we find

$$\begin{aligned}
m'_{dd} &= m_d + \mathcal{O}(m_s \lambda^4) , && (2.27)\\
m'_{ss} &= m_s + \mathcal{O}(m_s \lambda^2) , && (2.28)\\
m'_{bb} &= \mathcal{O}(m_s) \; , && (2.29)\\
m'_{ds} &= \mathcal{O}(m_s \lambda^3) , \quad m'_{sd} = \mathcal{O}(m_d \lambda^2) , && (2.30)\\
m'_{db} &\simeq -m_b V^*_{td} , \quad m'_{bd} = \mathcal{O}(m_d) , && (2.31)\\
m'_{sb} &\simeq -m_b V^*_{ts} , \quad m'_{bs} = \mathcal{O}(m_s) . && (2.32)
\end{aligned}$$

Note that the m'_{db} and m'_{sb} parameters are approximately fixed by the requirement to quantitatively reproduce the CKM mixing matix. The fact that $d - s$ mixing is suppressed, and at most of order $m_s \lambda^3$, eases constraints from neutral Kaon oscillations. Nevertheless, Kaon, B_d, and B_s meson oscillations do put constraints on the size of the m'_{sd} m'_{bd}, and m'_{bs} parameters and on $\tan\beta$ depending on the heavy Higgs masses. The flavor-violating entries in the down sector have only

a relevant impact on the production of the heavy Higgses in association with b-quarks (see Sec. 2.4 below). In order to avoid the constraints from meson oscillations, one could use the following λ'^d Yukawa coupling

$$\lambda'^d \simeq \frac{\sqrt{2}}{v'} \begin{pmatrix} m_d & \lambda m_s & \lambda^3 m_b \\ 0 & m_s & \lambda^2 m_b \\ 0 & 0 & m_s \end{pmatrix}, \tag{2.33}$$

which would lead to a production cross section of the heavy Higgses in association with b-quarks that is approximately a factor of 2 smaller compared to the texture in Eq. (2.26). In the following we will stick to the texture in Eq. (2.26), keeping in mind that meson mixing might constrain the production of the heavy Higgses in association with b-quarks to be as much as a factor 2 smaller than what shown in the plots of Fig. 2.5.

We now combine the Yukawa textures specified above with the generic expressions for heavy Higgs couplings discussed in Sec. 2.2.1. For the flavor-diagonal heavy Higgs couplings to taus we find

$$\kappa_\tau^H = \frac{Y_\tau^H}{Y_\tau^{\rm SM}} = \frac{1}{t_\beta}\frac{s_\alpha}{c_\beta} + \mathcal{O}\left(\frac{m_\mu}{m_\tau}\right) \times \frac{t_\beta}{s_\beta^2} s_{\beta-\alpha}\,, \tag{2.34}$$

$$\kappa_\tau^A = \frac{Y_\tau^A}{Y_\tau^{\rm SM}} = \frac{1}{t_\beta} + \mathcal{O}\left(\frac{m_\mu}{m_\tau}\right) \times \frac{t_\beta}{s_\beta^2}\,, \tag{2.35}$$

$$\kappa_\tau^\pm = \frac{Y_{\nu_\tau\tau}^\pm}{Y_\tau^{\rm SM}} = \frac{1}{t_\beta} + \mathcal{O}\left(\frac{m_\mu}{m_\tau}\right) \times \frac{t_\beta}{s_\beta^2}\,, \tag{2.36}$$

and analogous expressions hold for the couplings to third generation quarks. The leading terms in these couplings are suppressed for moderate and large $\tan\beta$ with respect to the SM Higgs couplings. The corrections that are suppressed by the ratio of second to third generation masses are proportional to $\tan\beta$ and can actually dominate in the large $\tan\beta$ regime.

For the couplings to muons, the second term in (2.10)-(2.12) is no longer subdominant. From (2.21), $m'_{\mu\mu}/m_\mu = 1 + \mathcal{O}(m_\mu/m_\tau)$, so we find

$$\kappa_\mu^H = \frac{Y_\mu^H}{Y_\mu^{\rm SM}} = t_\beta \frac{c_\alpha}{s_\beta} + \mathcal{O}\left(\frac{m_\mu}{m_\tau}\right) \times \frac{t_\beta}{s_\beta^2} s_{\beta-\alpha}\,, \tag{2.37}$$

$$\kappa_\mu^A = \frac{Y_\mu^A}{Y_\mu^{\rm SM}} = -t_\beta + \mathcal{O}\left(\frac{m_\mu}{m_\tau}\right) \times \frac{t_\beta}{s_\beta^2}\,, \tag{2.38}$$

$$\kappa_\mu^\pm = \frac{Y_{\nu_\mu\mu}^\pm}{Y_\mu^{\rm SM}} = -t_\beta + \mathcal{O}\left(\frac{m_\mu}{m_\tau}\right) \times \frac{t_\beta}{s_\beta^2}\,. \tag{2.39}$$

Analogous expressions hold for the second generation quark couplings and for the couplings to first generation fermions. Note the enhancement of these couplings by $\tan\beta$. Flavor off-diagonal couplings of the heavy Higgses between second and third generation are generically of the same order as the corresponding flavor-diagonal couplings to the second generation. In the lepton sector we have for example

$$\kappa_{\mu\tau}^H = \frac{Y_{\mu\tau}^H}{Y_\tau^{\rm SM}} = \mathcal{O}\left(\frac{m_\mu}{m_\tau}\right) \times \frac{t_\beta}{s_\beta^2} s_{\beta-\alpha}\,, \tag{2.40}$$

$$\kappa_{\mu\tau}^A = \frac{Y_{\mu\tau}^A}{Y_\tau^{\rm SM}} = \mathcal{O}\left(\frac{m_\mu}{m_\tau}\right) \times \frac{t_\beta}{s_\beta^2}\,. \tag{2.41}$$

Analogous expressions hold for the flavor-violating couplings involving the second and third generation of quarks. Flavor-violating couplings of the charged Higgs to quarks contain additional terms that are proportional to small CKM elements. For example

$$\kappa_{st}^\pm = \frac{Y_{st}^\pm}{Y_t^{\rm SM}} \simeq \frac{V_{ts}}{t_\beta} + \mathcal{O}\left(\frac{m_c}{m_t}\right) \times \frac{t_\beta}{s_\beta^2}\,. \tag{2.42}$$

Given these couplings, the collider phenomenology of the heavy Higgs bosons in our model can be markedly different, if compared to less flavorful 2HDM se-

tups that have been studied extensively in the literature [111–125].[2] In contrast to models with natural flavor conservation [133], flavor alignment [113, 134] or minimal flavor violation [135, 136], the couplings of the heavy Higgses to fermions are not proportional to the fermion masses. For moderate and large values of $\tan\beta$, the couplings to the third generation fermions are suppressed, while the couplings to the second and first generation are enhanced, if compared to the couplings of the SM Higgs. Therefore, the branching ratios do not have to be dominated by decays to third generation (top, bottom, tau), and we expect sizable branching ratios involving charm quarks and muons. Moreover, new non-standard production modes for the heavy Higgs bosons involving light quark generations can become relevant.

Before discussing the corresponding heavy Higgs collider phenomenology in detail in Secs. 2.4, 2.5, and 2.6, we briefly outline the modified properties of the 125 GeV Higgs and the implied constraints on the parameter space.

2.3 Properties of the SM-like Higgs

In our model, the couplings of the light Higgs to SM particles are generically modified. The existing measurements of the Higgs rates at the LHC depend crucially on the Higgs couplings to vector bosons and to the third generation fermions. For the couplings of the light Higgs boson to third generation fermions we find

$$\kappa_t \equiv \frac{Y_t}{Y_t^{\rm SM}} = \frac{c_\alpha}{s_\beta} + \mathcal{O}\left(\frac{m_c}{m_t}\right) \times \frac{t_\beta}{s_\beta^2} c_{\beta-\alpha} \,, \tag{2.43}$$

$$\kappa_b \equiv \frac{Y_b}{Y_b^{\rm SM}} = \frac{c_\alpha}{s_\beta} + \mathcal{O}\left(\frac{m_s}{m_b}\right) \times \frac{t_\beta}{s_\beta^2} c_{\beta-\alpha} \,, \tag{2.44}$$

[2] See also [**?**, 126–132] for studies of interesting 2HDM setups with new sources of flavor violation.

$$\kappa_\tau \equiv \frac{Y_\tau}{Y_\tau^{\rm SM}} = \frac{c_\alpha}{s_\beta} + \mathcal{O}\left(\frac{m_\mu}{m_\tau}\right) \times \frac{t_\beta}{s_\beta^2} c_{\beta-\alpha} \ . \tag{2.45}$$

Note that the bulk of the correction with respect to the SM prediction is universal for the top, the bottom and the tau (c_α/s_β), and are the same as in a 2HDM type I. The higher order terms are suppressed by small fermion mass ratios and can have order one CP violating phases. They can become relevant in the large $\tan\beta$ regime.

As in any other 2HDM, the reduced couplings of the light Higgs to the weak gauge bosons are given by

$$\kappa_W = \kappa_Z \equiv \kappa_V = s_{\beta-\alpha} \ . \tag{2.46}$$

The couplings of the Higgs to the lighter fermion generations are also modified. The expressions for the second generation read

$$\kappa_\mu \equiv \frac{Y_\mu}{Y_\mu^{\rm SM}} = -\frac{s_\alpha}{c_\beta} + \mathcal{O}\left(\frac{m_\mu}{m_\tau}\right) \times \frac{t_\beta}{s_\beta^2} c_{\beta-\alpha} \ , \tag{2.47}$$

$$\kappa_c \equiv \frac{Y_c}{Y_c^{\rm SM}} = -\frac{s_\alpha}{c_\beta} + \mathcal{O}\left(\frac{m_c}{m_t}\right) \times \frac{t_\beta}{s_\beta^2} c_{\beta-\alpha} \ , \tag{2.48}$$

$$\kappa_s \equiv \frac{Y_s}{Y_s^{\rm SM}} = -\frac{s_\alpha}{c_\beta} + \mathcal{O}\left(\frac{m_s}{m_b}\right) \times \frac{t_\beta}{s_\beta^2} c_{\beta-\alpha} \ . \tag{2.49}$$

Analogous expressions hold for the first generation, with second generation masses replaced by first generation masses. The couplings to the first and second generation depend in a different way on α and β as compared to the couplings of the third generation. This is a distinct feature of our framework in comparison to 2HDMs with natural flavor conservation [133] or flavor alignment [113,134], which predict modifications of the couplings that are universal across the generations. The corrections to the couplings for all first and second generation fermions are

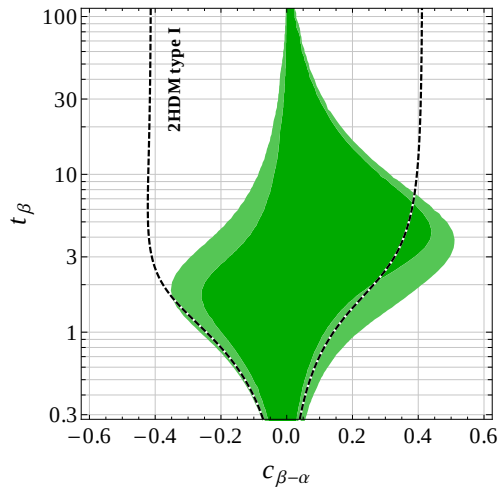

Figure 2.1: Allowed region in the $\cos(\beta-\alpha)$ vs. $\tan\beta$ plane from measurements of the 125 GeV Higgs rates at the LHC. The dark green and light green regions correspond to the 1σ and 2σ allowed regions, allowing the $\mathcal{O}(m_{\rm 2nd}/m_{\rm 3rd})$ terms in the relevant Higgs couplings to float between $-3m_{\rm 2nd}/m_{\rm 3rd}$ and $+3m_{\rm 2nd}/m_{\rm 3rd}$. The dashed line corresoponds to the 2σ contour in a 2HDM type I.

still universal, up to terms proportional to small ratios of fermion masses. Such terms are particularly small for the first generation. Generically, all higher order terms can have order one CP violating phases. Note that in the absence of mixing between the scalar components of the two Higgs doublets ($\alpha = 0$), the 125 GeV Higgs does not couple at all to the first and second generation. For large $\tan\beta$ and away from the decoupling or alignment limit $\cos(\alpha-\beta) = 0$, the couplings can deviate substantially from the SM prediction and can even be significantly enhanced.

Measurements of Higgs production and decay rates can be used to constrain the allowed ranges for the angles α and β. We use the results for the Higgs signal strengths given in [30] to construct a χ^2 function depending on the couplings of the Higgs to vector bosons, top, bottom and charm quarks, as well as taus and muons, including the given correlations of the signal strength uncertainties. The results in [30] consist of 20 combinations of five production mechanisms (gluon

fusion, vector boson fusion, producution in association with W, Z and $t\bar{t}$), and five branching ratios (WW, ZZ, $\gamma\gamma$, $\tau^+\tau^-$, $b\bar{b}$) that combine ATLAS and CMS measurements at 7 and 8 TeV. To construct the signal strengths in our model, we use the SM production cross sections and branching ratios for a 125 GeV Higgs from [137] and reweight them with the appropriate combinations of coupling modifiers. We add to the χ^2 also the 13 TeV bound on the signal strength into muons [138] using the modified inclusive Higgs production cross section at 13 TeV, assuming vanishing correlation with the signal strength measurements from [30].

The derived constraint in the $\cos(\beta-\alpha)$ vs. $\tan\beta$ plane is shown in Fig. 2.1. The dark (light) green region correspond to $\Delta\chi^2 = \chi^2 - \chi^2_{\rm SM} < 1(4)$, allowing the $\mathcal{O}(m_{\rm 2nd}/m_{\rm 3rd})$ terms in the involved Higgs couplings to float between $-3m_{\rm 2nd}/m_{\rm 3rd}$ and $+3m_{\rm 2nd}/m_{\rm 3rd}$. If we set the mass-suppressed corrections to the third generation couplings to zero and we completely neglect the modifications of the charm and muon coupling, the constraint in the $\cos(\beta-\alpha)$ vs. $\tan\beta$ plane coincides with the constraints in a 2HDM type I. The corresponding $\Delta\chi^2 = 4$ contour is shown with a dashed line and qualitatively reproduces the 2HDM type I constraints given in the ATLAS and CMS analyses [139, 140].

We find that the modifications of the charm and muon couplings have an important impact on the fit. For large $\tan\beta$ and away from the decoupling or alignment limit, $\cos(\beta-\alpha) = 0$, the charm and muon couplings can be strongly enhanced, leading to a substantially larger total width of the Higgs and a largely enhanced branching ratio into muons. For moderate and large values of $\tan\beta$, the allowed region therefore differs significantly from the 2HDM type I case. In the remaining parts of this chapter we take into account the constraints coming from the measurments of the 125 GeV Higgs rates by imposing $\Delta\chi^2 < 4$.

In addition to the modified SM couplings of the light Higgs, our framework

also gives rise to the flavor-violating couplings in Eq. (2.13). The corresponding flavor-violating decays of the light Higgs boson have branching ratios of[3]

$$\begin{aligned} \mathrm{BR}(h \to f f') &= \mathrm{BR}(h \to f \bar{f}') + \mathrm{BR}(h \to \bar{f} f') \\ &= \frac{m_h}{8\pi\Gamma_h}\Big(|Y_{ff'}|^2 + |Y_{f'f}|^2\Big) \,, \end{aligned} \tag{2.50}$$

where Γ_h is the total Higgs width and we have neglected tiny phase space effects.

For $h \to \tau\mu$ and $h \to \tau e$ this gives generically branching ratios of the order of

$$\mathrm{BR}(h \to \tau\mu) \sim \mathrm{BR}(h \to \mu^+\mu^-) \sim \frac{m_\mu^2}{3m_b^2} \sim 10^{-3}, \tag{2.51}$$

$$\mathrm{BR}(h \to \tau e) \sim \frac{m_e^2}{m_\mu^2} \times \mathrm{BR}(h \to \tau\mu) \sim 10^{-7} \,. \tag{2.52}$$

This implies that $h \to \tau\mu$ can be at an experimentally accessible level and the model could even explain the observed excess in $h \to \tau\mu$ searches at CMS [108]. The decay $h \to \tau e$, on the other hand, is generically well below the foreseeable experimental sensitivities. The prediction for $h \to \mu e$ is even smaller

$$\mathrm{BR}(h \to \mu e) \sim \frac{m_e^2}{m_\tau^2} \times \mathrm{BR}(h \to \tau\mu) \sim 10^{-10} \,. \tag{2.53}$$

In the quark sector the $h \to bs$ mode has generically the largest branching ratio

$$\mathrm{BR}(h \to bs) \sim |V_{cb}|^2 \times \mathrm{BR}(h \to b\bar{b}) \sim 10^{-3} \,. \tag{2.54}$$

In view of the large $h \to b\bar{b}$ background, this is too small to be seen at the LHC. Other flavor-changing Higgs decays into quarks are even smaller and even more challenging to detect.

[3] Throughout the chapter, we will denote the flavor-changing decays $\bar{f}f' + f\bar{f}'$, simply as ff'.

2.4 Heavy Neutral Higgs Production and Decays

As we saw at the end of Sec. 2.2.2, several of the heavy Higgs couplings depend significantly on the entries of the m' mass matrices, which are free parameters. To simplify our discussion of the heavy Higgs phenomenology we chose a constrained setup with a reduced set of free parameters.

In the λ' Yukawa couplings for the leptons and up-type quarks (see Eq. (2.19)), we set

$$\lambda'^{\ell,u}_{11} = \lambda'^{\ell,u}_{12} = \lambda'^{\ell,u}_{13} = \lambda'^{\ell,u}_{21} = \lambda'^{\ell,u}_{31}\,, \tag{2.55}$$

$$\lambda'^{\ell,u}_{22} = \lambda'^{\ell,u}_{23} = \lambda'^{\ell,u}_{32} = \lambda'^{\ell,u}_{33}\,. \tag{2.56}$$

For any given $\tan\beta$, the values of these parameters are fixed such to reproduce the observed electron, muon, up, and charm masses (we use $\overline{\text{MS}}$ masses at a scale $\mu = 500$ GeV).

For the λ' Yukawa couplings for the down-type quarks, we use the texture in Eq. (2.26) with

$$\lambda'^{d}_{11} = \lambda'^{d}_{21} = \lambda'^{d}_{31}\,, \tag{2.57}$$

$$\lambda'^{d}_{22} = \lambda'^{d}_{32} = \lambda'^{d}_{33}\,. \tag{2.58}$$

The down and strange masses, together with the CKM angles fix all entries of the λ'^{d} matrix for a given value of $\tan\beta$. With the above assumptions, the Higgs mixing angle α and $\tan\beta$ completely determine all Higgs couplings.

All results we will present in the following depend very little on the choice of the λ'_{1i} and λ'_{i1} parameters. However, some results do depend on the chosen

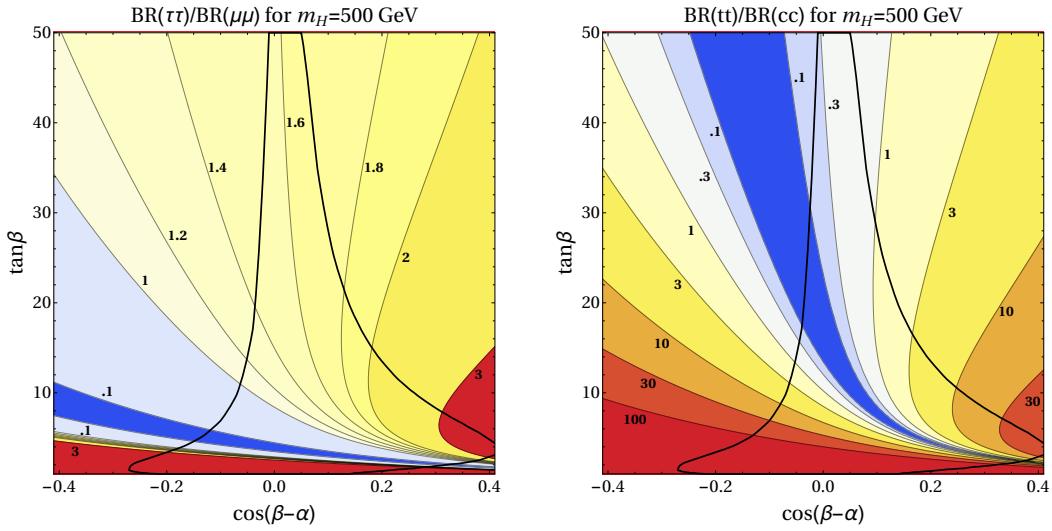

Figure 2.2: Ratio of branching ratios $H \to \tau^+\tau^-$ over $H \to \mu^+\mu^-$ (left) and $H \to t\bar{t}$ over $H \to c\bar{c}$ (right) in the $\tan\beta$ vs. $\cos(\beta-\alpha)$ plane for a heavy Higgs with mass $m_H = 500$ GeV. Outside the black solid contours, the 125 GeV Higgs rates are in conflict with LHC data.

values in the $2-3$ block of the λ' Yukawa couplings. Whenever this dependence is strong, we will comment on the impact a perturbation would have around the described restricted setup.

2.4.1 Branching Ratios

In addition to well-studied heavy Higgs decays $H \to WW/ZZ$, $A \to Zh$, and $A/H \to t\bar{t}, b\bar{b}, \tau^+\tau^-$, we are particularly interested in decays involving lighter fermion flavors like $A/H \to c\bar{c}, \mu^+\mu^-$ and the flavor-violating decays $A/H \to tc, \tau\mu$. We assume that the heavy Higgs sector is approximately degenerate, $m_H \simeq m_A \simeq m_{H^\pm}$, such that no two body decay modes involving heavy Higgses in the final state are kinematically allowed. We also assume that the triple Higgs couplings Hhh and Ahh are sufficiently small such that we can neglect the $H \to hh$ and $A \to hh$ decay modes.[4] For the calculation of the Higgs branching ratios we

[4]The $A \to hh$ decay is automatically zero in the absence of CP violation in the Higgs sector, while, in the almost decoupling or alignment limit and at large values of $\tan\beta$, $H \to hh$ depends

use leading-order expressions for all relevant partial widths.

The characteristic flavor structure of the model can be easily grasped by looking at ratios of branching ratios involving second and third generation fermions. For example, in 2HDMs with natural flavor conservation or flavor alignment one finds

$$\frac{\mathrm{BR}(A \to \tau^+\tau^-)}{\mathrm{BR}(A \to \mu^+\mu^-)} = \frac{\mathrm{BR}(H \to \tau^+\tau^-)}{\mathrm{BR}(H \to \mu^+\mu^-)} = \frac{m_\tau^2}{m_\mu^2} \simeq 300\,, \tag{2.59}$$

$$\frac{\mathrm{BR}(A \to t\bar{t})}{\mathrm{BR}(A \to c\bar{c})} \simeq \frac{\mathrm{BR}(H \to t\bar{t})}{\mathrm{BR}(H \to c\bar{c})} \simeq \frac{m_t^2}{m_c^2} \simeq 7 \times 10^4\,, \tag{2.60}$$

where, for illustration, we used running $\overline{\mathrm{MS}}$ quark masses at the scale $\mu = 500$ GeV and neglected phase space effects that might be relevant in the decay to top quarks. In our setup, the above relations can be strongly violated. For the pseudoscalar A we obtain

$$\frac{\mathrm{BR}(A \to \tau^+\tau^-)}{\mathrm{BR}(A \to \mu^+\mu^-)} \simeq \frac{m_\tau^2}{m_\mu^2}\frac{1}{t_\beta^4}\left(1 - \frac{t_\beta}{s_\beta c_\beta}\frac{m'_{\tau\tau}}{m_\tau}\right)^2\,, \tag{2.61}$$

$$\frac{\mathrm{BR}(A \to t\bar{t})}{\mathrm{BR}(A \to c\bar{c})} \simeq \frac{m_t^2}{m_c^2}\frac{1}{t_\beta^4}\left(1 - \frac{t_\beta}{s_\beta c_\beta}\frac{m'_{tt}}{m_t}\right)^2\,, \tag{2.62}$$

where we neglected respectively $\mathcal{O}(m_\mu/m_\tau)$ and $\mathcal{O}(m_c/m_t)$ corrections. The expressions (2.61) and (2.62) also hold for the heavy scalar H, up to corrections of $\mathcal{O}(v_W^2/m_A^2)$. For moderate t_β we can neglect the terms proportional to $m'_{\tau\tau}$ and m'_{tt} and obtain the ratios $m_\tau^2/(m_\mu^2 t_\beta^4)$ and $m_t^2/(m_c^2 t_\beta^4)$, respectively. For large t_β, the terms proportional to $m'_{\tau\tau}$ and m'_{tt} are dominant and we find the ratios $(m'_{\tau\tau})^2/m_\mu^2$ and $(m'_{tt})^2/m_c^2$. In all cases, the ratios of branching ratios can be of $\mathcal{O}(1)$.

This is illustrated in Fig. 2.2, that shows the ratio of $\tau^+\tau^-$ and $\mu^+\mu^-$ branching

mainly on the λ_7 quartic coupling that is equal to zero if the two doublets have an opposite Z_2 charge (see e.g. [109] for the definition of λ_7).

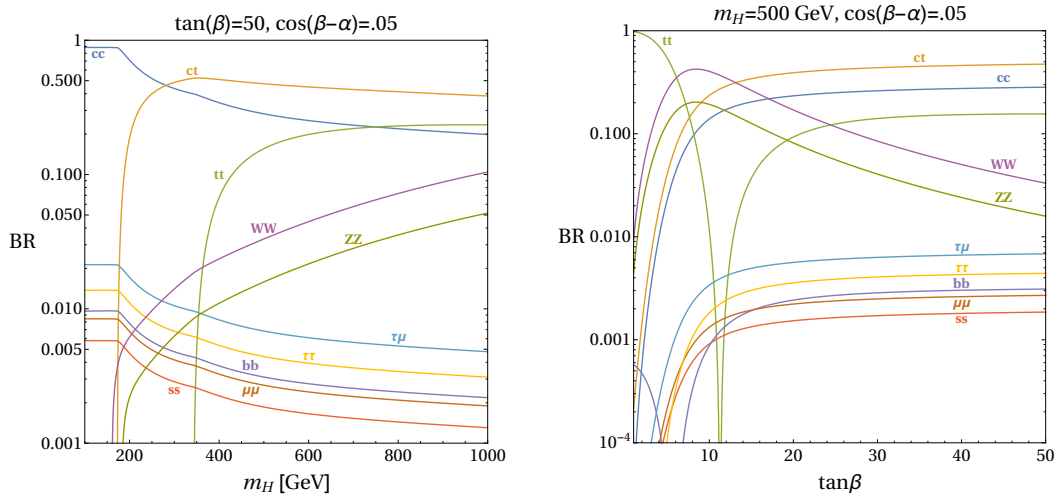

Figure 2.3: Branching ratios of the scalar H as a function of its mass m_H for fixed $\tan\beta = 50$ (left) and as a function of $\tan\beta$ for fixed Higgs mass $m_H = 500$ GeV (right). In both plots we set $\cos(\beta - \alpha) = 0.05$.

ratios (left) as well as of $t\bar{t}$ and $c\bar{c}$ branching ratios (right) of the scalar H in the plane of $\cos(\beta - \alpha)$ vs. $\tan\beta$ for a scalar mass of $m_H = 500$ GeV. The values of the pseudoscalar branching ratios can be obtained from the figure, by fixing $\cos(\beta - \alpha) = 0$. Outside the black solid contours, the 125 GeV Higgs rates are in conflict with LHC data (see Fig. 2.1).

Note that for small and moderate $\tan\beta$, these ratios of branching ratios are not very sensitive to our choice of Yukawa matrices in Eqs. (2.55) and (2.56). For large $\tan\beta$, however, they are determined by m'_{tt} and $m'_{\tau\tau}$ which are in general free parameters. The values shown in Fig. 2.2 in the large $\tan\beta$ regime should therefore be regarded as typical expectations that could be larger or smaller by a factor of few. Overall, we see that the ratios are much smaller than in models with natural flavor conservation, minimal flavor violation or flavor alignment.

Similarly, also the flavor-violating decays into the $\tau\mu$ and tc final states can

have sizable branching ratios. For the pseudoscalar A we have approximately

$$\frac{\mathrm{BR}(A \to \tau\mu)}{\mathrm{BR}(A \to \mu^+\mu^-)} \simeq \frac{1}{s_\beta^4} \frac{(m'_{\mu\tau})^2 + (m'_{\tau\mu})^2}{m_\mu^2}\,, \tag{2.63}$$

$$\frac{\mathrm{BR}(A \to tc)}{\mathrm{BR}(A \to c\bar{c})} \simeq \frac{1}{s_\beta^4} \frac{(m'_{ct})^2 + (m'_{tc})^2}{m_c^2}\,, \tag{2.64}$$

and similar expressions hold for the scalar H. The m' entries which determine (2.63) and (2.64) are in general free parameters. Typically, we expect the flavor-violating branching ratios to be within a factor of few of the flavor-diagonal decays $\mu^+\mu^-$ and $c\bar{c}$, respectively.

The plots in Fig. 2.3 show the branching ratios of the scalar H as a function of m_H for fixed $\tan\beta = 50$ (left) and as a function of $\tan\beta$ for fixed $m_H = 500$ GeV (right). In both plots we set $\cos(\beta - \alpha) = 0.05$ to satisfy constraints from the 125 GeV Higgs coupling measurements as discussed in Sec. 2.3. For low values of $\tan\beta$, the decay into the $t\bar{t}$ final state dominates if kinematically allowed. At large $\tan\beta$, decays into $t\bar{t}$, $c\bar{c}$ and the flavor-violating mode tc have the largest branching ratios. Typically, these decay modes have branching ratios within a factor of few from each other. The sudden and strong suppression of the $t\bar{t}$ branching ratio is due to an accidental cancellation between the two terms entering the coupling of the heavy scalar to tops (cf. Eq. (2.11) and text below). The coupling Y_{tt}^H vanishes at approximately $\tan\beta \simeq 11$. The value of $\tan\beta$ where such a cancellation occurs can shift by a factor of few, depending on the m'_{tt} parameter. For the opposite sign of m'_{tt}, the cancellation does not occur instead. A similar, but less prominent, phenomenon happens for the $b\bar{b}$ branching ratio: for our choices of parameters, the coupling Y_{bb}^H vanishes at $\tan\beta \simeq 5.6$.

For $\cos(\beta - \alpha) = 0.05$, the decay into WW and ZZ can be non-negligible. Typically we find branching ratios of the order of few-10s %. For moderate $\tan\beta$,

these decays can even dominate. Concerning the leptonic decay modes $\tau^+\tau^-$, $\mu^+\mu^-$, and $\tau\mu$, for moderate and large values of $\tan\beta$ we find typical branching ratios at the level of 10^{-3} to 10^{-2}. Branching ratios involving second and third generation down-type quarks (only $b\bar{b}$ and $s\bar{s}$ are shown in the plots) are generically at a comparable level. For moderate and large $\tan\beta$, the values of the flavor-violating partial widths and the partial width to $t\bar{t}$, $b\bar{b}$, and $\tau^+\tau^-$ depend on the m' mass matrices. Therefore, perturbing the m' matrices around the ansatz based on Eqs. (2.55) - (2.58), can increase or suppress the various H branching ratios by a factor of few.

The branching ratios of the pseudoscalar A show qualitatively a very similar behavior and, for this reason, we do not show the corresponding figures. For a mass of A above the $t\bar{t}$ threshold, the $t\bar{t}$ branching ratio is dominant for low $\tan\beta$, while for large $\tan\beta$ also the decay to the $c\bar{c}$ final state and the flavor-violating decay to tc become comparable in size. Decays involving second and third generation leptons are all comparable and typically at a level of few $\times\ 10^{-3}$. In contrast to the heavy scalar, H, the heavy pseudoscalar, A, cannot decay at tree level into a pair of gauge bosons. Instead, the decay $A \to Zh$ is possible. The corresponding partial decay width is proportional to $\cos^2(\beta-\alpha)$. For $\cos(\beta-\alpha) = 0.05$, the $A \to Zh$ branching ratio is around a few %. For heavy pseudoscalar masses and moderate values of $\tan\beta$, this decay mode might dominate.

2.4.2 Production Cross Sections

We consider various production mechanisms of the heavy neutral Higgs bosons, including gluon fusion, vector boson fusion, production in association with weak vector bosons and light quarks, production from a $c\bar{c}$ initial state, and also flavor-violating production in association with a top or a bottom quark. Example dia-

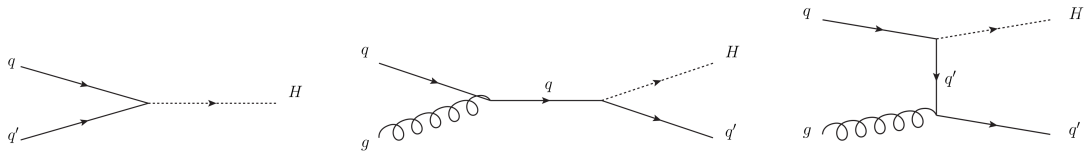

Figure 2.4: Feynman diagrams for the most interesting (and novel) production modes of the heavy neutral Higgs bosons. Left: production from quark quark fusion (mainly coming from $c\bar{c}$); Center and Right: production in association with a top/bottom with the main contributions coming from flavor-changing diagrams where the initial state q is a charm/strange quark.

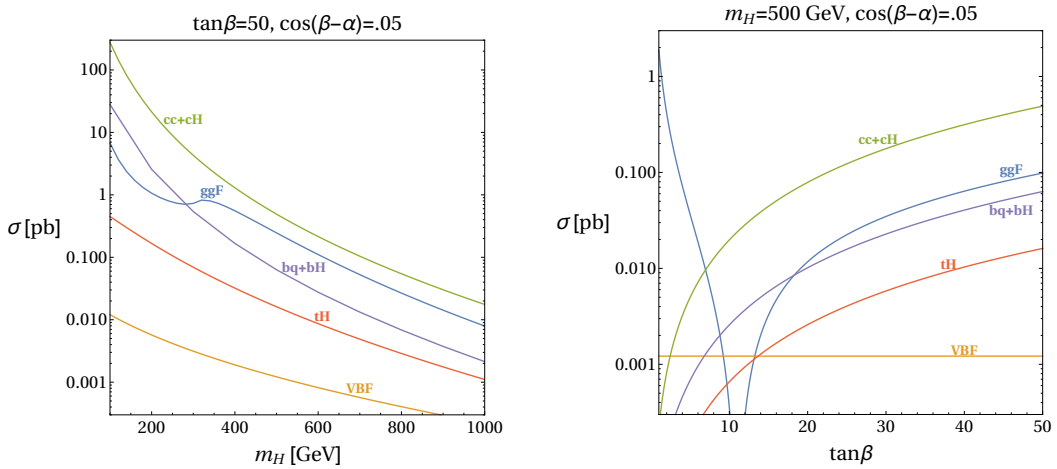

Figure 2.5: Production cross sections of the scalar H at 13 TeV proton proton collisions as a function of the scalar mass m_H for fixed $\tan\beta = 50$ (left) and as a function of $\tan\beta$ for fixed scalar mass $m_H = 500$ GeV (right). The $cc+cH$ curves include both the $c\bar{c}$ and the associated cH and $\bar{c}H$ production cross sections. In both plots we set $\cos(\beta - \alpha) = 0.05$.

grams for the novel processes are shown in Fig. 5.1.

Throughout all regions of parameter space, we find that the gluon fusion production cross section is dominated by the top quark loop. The bottom quark loop gives a % level correction, which is included in the numerics. Also the charm quark loop gives generically only a small correction (approximately 5% in the large $\tan\beta$ regime for a Higgs mass of 500 GeV). In our numerical analysis we use leading-order expressions for the gluon fusion production cross sections that we convolute with MMHT2014 NNLO PDFs [141]. We set the renormalization and

factorization scales to 500 GeV and multiply the cross section with a constant K factor of 2.5 to approximate higher order corrections.

The vector boson fusion production cross section of the heavy scalar H is suppressed by $\cos^2(\beta-\alpha)$, if compared to the corresponding SM Higgs cross section. In the regions of parameter space that are compatible with the observed 125 GeV Higgs rates, vector boson fusion is therefore typically subdominant. The same applies to production of H in association with weak gauge bosons. In our numerical analysis we use the corresponding production cross sections given in [137] rescaled by the appropriate factor $\cos^2(\beta-\alpha)$. The pseuedoscalar A does not couple to weak gauge bosons and thus cannot be produced in vector boson fusion or in association with W or Z bosons. It can be produced in association with the light Higgs: $q\bar{q} \to Z^* \to Ah$. The corresponding cross section is proportional to $\cos^2(\beta-\alpha)$ and therefore small.

Due to the enhanced couplings of the heavy Higgses to second generation quarks, we expect sizable production of H and A from a $c\bar{c}$ initial state. Production in association with a c or $\bar{c}$ from a gluon+charm initial state is also sizable. In such a case the associated charm might escape detection giving rise to collinear logarithms which need a careful analysis. To this end we follow [142] and do not consider production in association with a c or a $\bar{c}$ as a separate production channel but as a NLO correction to $c\bar{c}$. For our calculations we use the corresponding parton level expressions in [142] up to NLO accuracy and convolute them with MMHT2014 NNLO PDFs.

We also consider production of the heavy scalar and pseudoscalar in association with with a top quark and with a bottom quark. These processes are mainly initiated by flavor-violating tc and bs couplings, respectively (see central and right panel of Fig. 5.1). For the production in association with a top quark we use LO

expressions for the parton level cross sections and MMHT2014 NNLO PDFs. For the production in association with a bottom quark we instead perform a LO computation, using MadGraph5 [143].

In Fig. 2.5 we show the production cross sections of the scalar H at 13 TeV proton-proton collisions as a function of m_H for fixed $\tan\beta = 50$ (left) and as a function of $\tan\beta$ for fixed $m_H = 500$ GeV (right). In both plots we set $\cos(\beta - \alpha) = 0.05$. For a heavy Higgs mass of $m_H = 500$ GeV the inclusive production cross section can be few $\times$ 100 fb over a broad range of $\tan\beta$. The most important production modes are gluon fusion (denoted with ggF in the plots) and from processes where the Higgs couples to charm quarks $c\bar{c} \to H$, $gc \to Hc$, and $g\bar{c} \to H\bar{c}$ (the sum of these modes is denoted with $cc + cH$ in the plots). Gluon fusion is dominant for small $\tan\beta$, while charm initiated production can dominate over the gluon fusion cross section for moderate and large values of $\tan\beta$. The strong suppression of the gluon fusion cross section for $\tan\beta \simeq 11$ is due to the same accidental cancellation in Y_{tt}^H which leads to the suppression of $\mathrm{BR}(H \to t\bar{t})$ at this value of $\tan\beta$ (see discussion in the previous subsection).

We find that production from $s\bar{s}$ (not shown in the plots) is suppressed by almost 2 orders of magnitude compared to $c\bar{c}$. The larger strange quark PDF cannot compensate for the much smaller coupling to the heavy Higgs proportional to m_s vs. m_c. For $\cos(\beta - \alpha) = 0.05$, production in vector-boson fusion is very small, with production cross sections ranging from 5.7 fb at a mass of $m_H = 200$ GeV to 0.22 fb at a mass of $m_H = 1$ TeV. Production in association with W or Z (not shown) is even smaller.

The production of the heavy scalar in association with a bottom or a top can have appreciable cross sections at the level of 10s of fb for $m_H = 500$ GeV, over a broad range of $\tan\beta$. In the bottom initiated production we include $bg \to Hb$,

$\bar{b}g \to H\bar{b}$, $b\bar{b} \to H$, $b\bar{s} \to H$, $s\bar{b} \to H$, $sg \to Hb$, and $\bar{s}g \to H\bar{b}$, the latter two processes being the dominant ones, thanks to the strange quark PDF enhancement. For this reason in Fig. 2.5 we label the bottom associated production by $bq + bH$. Overall, the cross section for the bottom associated production is, however, typically smaller than the one predicted in a 2HDM of type II. The Ht associated cross section depends strongly on the free m' parameters and can easily be increased or decreased by a factor of few.

The production modes of the pseudoscalar A show a very similar behavior. Gluon fusion dominates for low $\tan\beta$, charm initiated production dominates for moderate and large values of $\tan\beta$. Production in association with top and bottom can have non-negligible cross sections. Vector boson fusion and production in association with vector bosons is absent for the pseudoscalar.

2.5 Charged Higgs Production and Decays

2.5.1 Branching Ratios

Similarly to the neutral scalars, in addition to the well-studied tb and $\tau\nu$ charged Higgs decay modes, we are interested in the flavor-violating decays, cb and ts, as well as in the decays to second generations, cs and $\mu\nu_\mu$. Particularly, from the charged Higgs couplings in (2.16) - (2.18), we learn that the decay modes tb, ts, cb and cs should be of the same order, as long as they are kinematically open. The same observation holds also for the $\tau\nu_\tau$ and $\mu\nu_\mu$ decay modes, as opposed to the relation $\mathrm{BR}(H^\pm \to \tau\nu_\tau)/\mathrm{BR}(H^\pm \to \mu\nu_\mu) = m_\tau^2/m_\mu^2$, arising in 2HDMs with natural flavor conservation or flavor alignment. Additionally, the ratio of branching ratios between the LHC most searched decay modes tb and $\tau\nu_\tau$

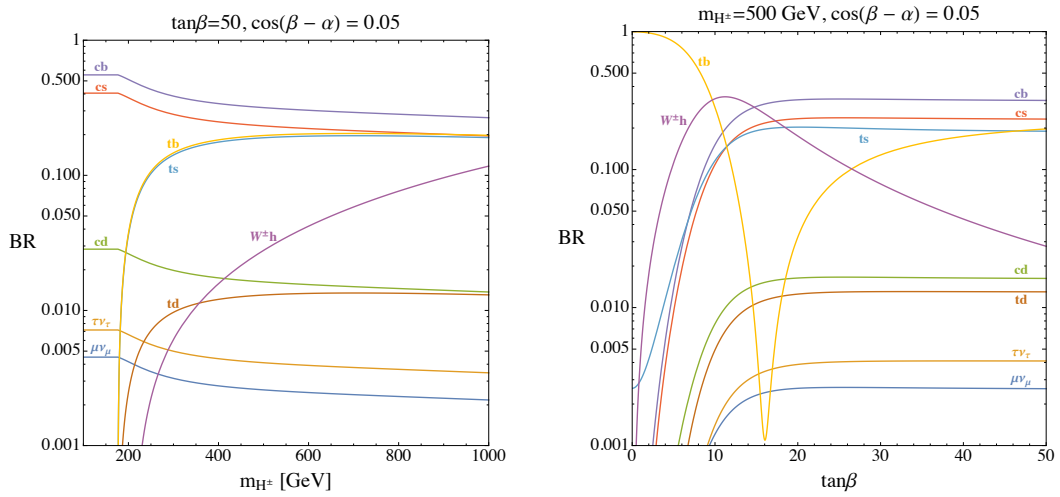

Figure 2.6: Branching ratios of the charged Higgs $H^\pm$ as a function of the charged Higgs mass $m_{H^\pm}$ for fixed $\tan\beta = 50$ (left) and as a function of $\tan\beta$ for fixed Higgs mass $m_{H^\pm} = 500$ GeV (right). For both panels, we fix $\cos(\beta - \alpha) = 0.05$.

obeys the relation

$$\frac{\mathrm{BR}(H^\pm \to tb)}{\mathrm{BR}(H^\pm \to \tau\nu_\tau)} = 3 \times \mathcal{O}\left(\frac{m_c^2}{m_\mu^2}\right) = \mathcal{O}(100), \tag{2.65}$$

valid in the regime of large $\tan\beta$, as opposed to the ratios $3m_t^2/m_\tau^2 \sim 6 \times 10^6$, $3m_b^2/m_\tau^2 \sim 1800$, as arising in type I and type II 2HDM, respectively. For this reason, in our model, we expect the $\tau\nu_\tau$ to be relatively more important than the tb mode, if compared to the most studied type I and II 2HDM. We present the results for the branching ratios of the charged Higgs boson in Fig. 2.6, on the left panel as a function of the charged Higgs mass, having fixed $\tan\beta = 50$, and on the right panel as a function of $\tan\beta$, having fixed the mass of the charged Higgs to 500 GeV. For both panels, we fix $\cos(\beta - \alpha) = 0.05$, in such a way that the Wh charged Higgs partial width is fully determined. Similarly to the neutral heavy Higgs boson, for low values of $\tan\beta$ the largest branching ratios approach the values of a 2HDM of type I, with the tb decay being the dominant one. At large values of $\tan\beta$, instead, the decays to second and third generation quarks have comparable

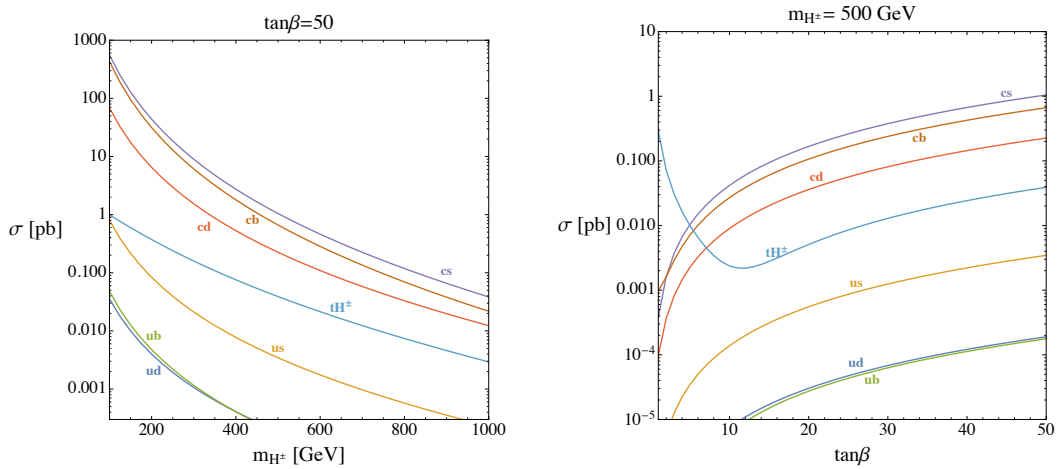

Figure 2.7: Production cross sections of the charged Higgs $H^{\pm}$ at 13 TeV proton proton collisions as a function of the charged Higgs mass $m_{H^{\pm}}$ for fixed $\tan\beta = 50$ (left) and as a function of $\tan\beta$ for fixed mass $m_{H^{\pm}} = 500$ GeV (right). None of these cross sections depend on the value of $\cos(\beta - \alpha)$.

branching ratios, and the decay to leptons ($\mu\nu_{\mu}$ and $\tau\nu_{\tau}$) are comparable and suppressed by roughly two orders of magnitude, as shown in Eq. (2.65). Similarly to the neutral Higgs decaying to WW and ZZ, at intermediate values of $\tan\beta$, the Wh decay mode can be the dominant one, having fixed $\cos(\beta - \alpha) = 0.05$.

2.5.2 Production Cross Sections

In Fig. 2.7, we show the production cross sections of the charged Higgs at 13 TeV proton-proton collisions as a function of its mass ($m_{H^{\pm}} > m_t$) for fixed $\tan\beta = 50$ (left) and as a function of $\tan\beta$ for fixed $m_{H^{\pm}} = 500$ GeV (right). None of these cross sections depend on the value of $\cos(\beta - \alpha)$. For the calculation of these production cross sections, we follow the same procedure as for the neutral Higgs boson. The most interesting features arise at moderate and sizable values of $\tan\beta$, as at small values of $\tan\beta$ the main production cross section comes from the $tH^{\pm}$ associated process, as predicted by the most studied type I and type II 2HDMs. At larger values of $\tan\beta$, the production cross sections from cs, cb, cd

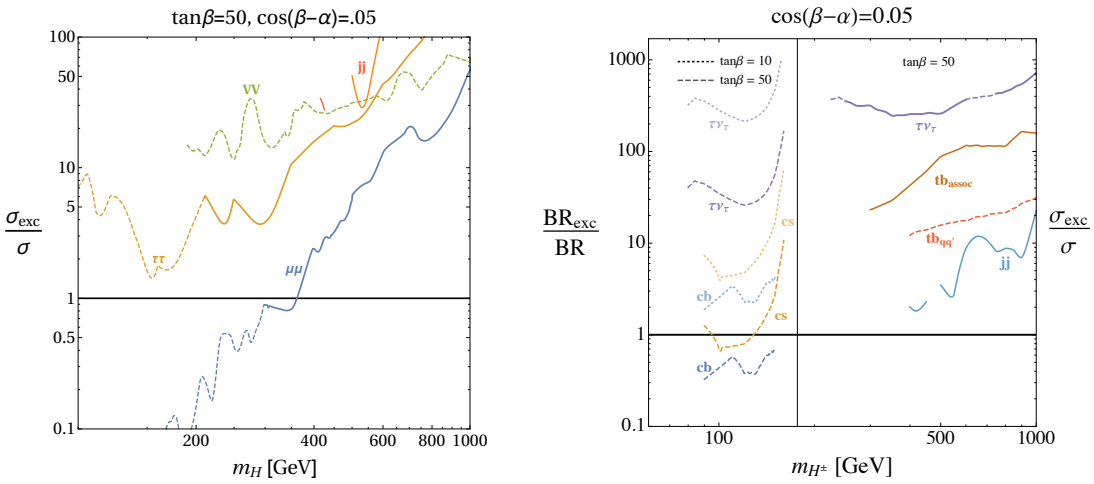

Figure 2.8: Experimental exclusion limits normalized to the predicted cross sections for the heavy scalar boson (left) and for the charged Higgs (right) as a function of the corresponding Higgs mass. We set $\tan\beta = 50$ and $\cos(\beta - \alpha) = 0.05$. Shown are the currently most strigent constraints coming from searches for $\tau^+\tau^-$, ZZ/WW, jj, and $\mu^+\mu^-$ final states (neutral scalar) and cb, cs, $\tau\nu$, tb, and jj final states (charged Higgs). The solid (dashed) curves correspond to 13 (8) TeV analyses.

are also very important and can even dominate over $tH^\pm$. These production cross sections are all of the same order and their exact size depends strongly on the specific values of the m' parameters. Similarly to the neutral Higgs, the inclusive cross section is at the level of few $\times$ 100 fb over a broad range of masses. In the figure, we do not show the cross section for the associated production $pp \to H^\pm h$ since it is typically below the fb level for $\cos(\beta - \alpha) = 0.05$.

For $m_{H^\pm} < m_t$, the charged Higgs is mainly produced from the top decay modes $t \to H^\pm b$ and $t \to H^\pm s$. The branching ratios for these processes are at around few % for $\tan\beta = 50$.

2.6 Experimental Sensitivities and New Signatures

After discussing the branching ratios and production cross sections separately for the neutral and charged Higgs bosons, we confront our model with existing searches for additional Higgs bosons at the LHC. Searches for neutral Higgses have been performed at 8 TeV and 13 TeV in a variety of channels including

(i) $H \to ZZ$ and $H \to WW$ [144–152],

(ii) $A \to Zh$ [153–156],

(iii) $A/H \to \tau^+\tau^-$ [157–161],

(iv) $A/H \to \mu^+\mu^-$ [162],

(v) $A/H \to t\bar{t}$ [163].

Moreover, we also take into account generic searches for

(vi) di-muon resonances [164–169],

(vii) di-jet resonances [170–175],

which, as we will discuss, have interesting sensitivities to our parameter space.

On the left panel of Fig. 2.8 we show the ratio of currently excluded cross section over the cross section predicted in our model as a function of the scalar Higgs mass m_H. A ratio smaller than 1 indicates exclusion. In the plots we set $\tan\beta = 50$ and $\cos(\beta - \alpha) = 0.05$. For a given Higgs mass we show the strongest constraint of a specific category of final states ($\tau^+\tau^-$, ZZ/WW, jj, $\mu^+\mu^-$). The solid (dashed) lines indicate 13 (8) TeV analyses.

The 8 TeV inclusive search for $H \to \mu^+\mu^-$ [162] is the most sensitive at low masses. At higher masses $m_H \gtrsim 300$ GeV, the 13 TeV searches for di-muon resonances turn out to be most sensitive. In comparing the excluded cross sections with our model predictions we add up gluon fusion and production from charm initial states, since we do not expect that the signal efficiencies differ significantly for these production modes. We find that the $H \to \mu^+\mu^-$ searches exclude the heavy scalar with mass $m_H \lesssim 360$ GeV for $\tan\beta = 50$. For lower $\tan\beta$, this constraint becomes weaker, due to the smaller production cross sections, and it does not extend the LEP bound for $\tan\beta \lesssim 12$.

Searches for $H \to \tau^+\tau^-$ give strong constraints on 2HDMs of type II in the large $\tan\beta$ regime. In our model, on the other hand, the small branching ratio of $H \to \tau^+\tau^-$ renders these searches less relevant. Even for $\tan\beta = 50$, we find that current experimental sensitivities do not yet allow to probe the heavy scalar using this channel.

Searches for $H \to ZZ$ currently constrain cross sections that are approximately one order of magnitude larger than those of the benchmark shown in Fig. 2.8. These searches can become relevant for moderate $\tan\beta$ and larger $\cos(\beta - \alpha)$. Searches for $H \to WW$ are generically less sensitive as compared to $H \to ZZ$. The corresponding channel for the pseudo-scalar, which has similar sensitivity, is $A \to Zh$.

Given the large branching ratio $H \to c\bar{c}$ (see Fig. 2.3) also searches for light di-jet resonances might be interesting. The ATLAS di-jet search performed with 3.4 fb^{-1} 13 TeV data [171] using a trigger-object level analysis sets a constraint on the model $\sim$ 1 order of magnitude more stringent than the 8 TeV analyses performed by CMS with data scouting [170, 172], reaching the best sensitivity to our model for masses at around 550 GeV. We also checked the performance of the

analyses [173–175] in testing our model. These CMS and ATLAS searches focus on the production of a (light) di-jet resonance in association with a boosted photon or jet. Due to the very high p_T threshold required for this additional object, these searches are less sensitive to our scenario, if compared to the trigger-object level analysis [171]. the corresponding cross section predicted by our model. As we can see from the left panel of Fig. 2.8, the di-jet constraints are comparable (or even stronger, for some values of m_H) to the constraints from the most studied $H \to \tau^+\tau^-$ searches.

Finally, in the figure we do not show the constraints from $A/H \to t\bar{t}$ [163], as they are very weak. This is due to the interference of the signal with the SM $t\bar{t}$ continuum [125, 176–178].

For the charged Higgs we consider searches for

(i) $(t)H^\pm \to \tau\nu$ [179–182], for both the charged Higgs mass below and above the top mass.

(ii) $H^\pm \to tb$: [183], both for $pp \to tH^\pm$ and $qq' \to H^\pm$ production; [180, 184] for $pp \to (b)tH^\pm$,

(iii) $H^\pm \to cs$ [185], for $m_{H^\pm} < m_t$,

(iv) $H^\pm \to cb$ [186] for $m_{H^\pm} < m_t$,

(v) $H^\pm \to Wh$ [187–191],

(vi) $H^\pm \to \mu\nu_\mu$ [192, 193],

(vii) generic searches for di-jet resonances [170–175].

In the right panel of Fig. 2.8, we only show the bounds from $H^\pm \to \tau\nu$, $H^\pm \to tb$, $H^\pm \to cs$, $H^\pm \to cb$, and searches for di-jet resonances. We do not

show the bound from the Wh decay, as these searches are performed only for very heavy resonances $m_{H^\pm} \gtrsim 800$ GeV and lead only to very weak constraints on the parameter space of our model. Also bounds from $\mu\nu_\mu$ searches are not shown. They do not lead to interesting constraints since the $H^\pm \to \mu\nu_\mu$ branching ratio, despite being enhanced compared to 2HDMs of type I or II, is not large enough in our model.

Below the top mass, the most stringent constraint comes from the cb search [186] performed with the full 8 TeV data set. This is followed by the 8 TeV cs search [185][5]. For $\tan\beta = 50$ charged Higgs masses above the LEP bound and below ~ 160 GeV are fully probed by these searches (see dashed lines in the right panel of Fig. 2.8 for $m_{H^\pm} < m_t$). However, the bound gets significantly weaker for intermediate values of $\tan\beta$, as the charged Higgs production cross section gets smaller: as shown by the dotted lines obtained for $\tan\beta = 10$, the entire mass range below the top mass opens up. For even smaller values of $\tan\beta$ the charged Higgs production increases again, leading to stronger bounds, if compared to $\tan\beta = 10$.

Above the top mass, the most important constraint comes from the search of tb resonances, that are, however, not able to set any bound on our model. Particularly, the process $qq' \to H^\pm \to tb$ [183] (denoted by $tb_{qq'}$ in the figure) is presently probing cross sections up to ~ 10 bigger than the cross sections predicted by our model for $\tan\beta = 50$. The 13 TeV search for $pp \to (b)tH^\pm, H^\pm \to tb$ [184] offers only weaker bounds, due to the production cross section for $tH^\pm$ being more than one order of magnitude smaller than the corresponding $qq' \to H^\pm$ (see right panel of Fig. 2.7). Searches for di-jet resonances have sensitivities that are comparable to the search of tb resonances. To estimate the di-jet signal from the

[5]The bounds we are presenting in the figure for $m_{H^\pm} < m_t$ are a conservative estimates, since they do not keep into account the possible pollution of events coming from the process $t \to sH^\pm$ with a strange quark mis-tagged to be a b-quark.

charged Higgs we take into account the charged Higgs production from cs, cb, and cd initial states and all charged Higgs branching ratios into quarks except those including a top quark. The highest sensitivity comes from the 13 TeV ATLAS search [171] and is shown in the plot by the line denoted by jj.

Our model also predicts a set of novel signatures that can be searched for at the LHC. Interesting signatures include flavor-violating neutral Higgs decays $pp \to H/A \to \tau\mu$ and $pp \to H/A \to tc$ and multi-top final states $pp \to tH/A \to ttc$. Cross sections for the processes involving the scalar, H, are shown in the $m_H - \tan\beta$ plane in the upper and lower left panels of Fig. 2.9, having fixed $\cos(\beta - \alpha) = 0$.

Compared to a 2HDM type II, a much larger region of the $m_H - \tan\beta$ plane is not yet probed by existing searches. In a 2HDM type II, searches for $H/A \to \tau^+\tau^-$ are sensitive to neutral Higgs bosons with masses of 300-400 GeV as long as $\tan\beta \gtrsim 15$ [157–161]. For $\tan\beta \gtrsim 50$, neutral Higgs bosons above 1 TeV can be probed. In our setup, the sensitivity of $H/A \to \tau^+\tau^-$ searches is weak. As discussed above, the most important constraints can be derived from di-muon resonance searches that are sensitive to neutral Higgs bosons of ~ 290 GeV for $\tan\beta \sim 50$. The parameter space that is excluded by current di-muon resonance searches is shaded in gray in the upper and lower left plots of Fig. 2.9.

In the allowed parameter space, the $pp \to H \to \tau\mu$ cross section can be several 10s of fb up to 100 fb. The $pp \to H \to tc$ cross section can be as large as few pb. Finally, the $pp \to tH \to ttc$ cross section can reach ~ 30 fb in the shown scenario. Cross sections that are larger by a factor of few are easily possible by modifying the free parameters m'_{tc} and m'_{ct} that control the size of the Htc coupling. Interestingly enough, generically one half of this cross section corresponds to same sign tops $pp \to tH \to tt\bar{c}$ or $pp \to \bar{t}H \to \bar{t}\bar{t}c$, providing a very distinct signature of this

model.

As shown in the right panel of Fig. 2.8, the parameter space of the charged Higgs above the top mass is completely un-constrained by the current LHC analyses, even at large values of $\tan\beta$ ($= 50$ in the figure). However, notice that there are indirect constraints from the neutral Higgses, because their mass cannot differ too much from the charged Higgs mass. It will be very interesting to design new searches to look for our charged Higgs in the coming years of the LHC. In particular, the cross section for $pp \to tH^{\pm}$ with $H^{\pm} \to cb$ can be at the few hundreds fb - pb level in a large range of parameters for $m_{H^{\pm}} > m_t$ (see lower right panel of Fig. 2.9). Additionally, the cross section for the flavor conserving signature $pp \to tH^{\pm}$ with $H^{\pm} \to cs$ has similar values. This offers a unique opportunity to look for a di-jet resonance (eventually with a b-tag) produced in association with a top quark. Finally, our model also predicts the novel interesting signature $pp \to tH^{\pm}$ with $H^{\pm} \to \mu^{\pm}\nu_{\mu}$, but the cross section is at the fb level even for $\tan\beta = 50$. Therefore, it will be likely more difficult to probe our charged Higgs using this signature.

2.7 Summary

We discussed the distinct collider phenomenology of a class of 2HDMs in which the 125 GeV Higgs is mainly responsible for the masses of the weak gauge bosons and of the third generation fermions, while the second Higgs doublet provides mass for the lighter fermion flavors. This model is particularly well motivated in view of our ignorance concerning the coupling of the 125 GeV Higgs to first two generation quarks and leptons.

The 125 GeV Higgs has modified couplings to SM fermions that qualitatively deviate from the couplings in 2HDMs with natural flavor conservation, minimal

flavor violation, or flavor alignment. While the 125 GeV Higgs couplings to the third generation fermions behave as in a 2HDM type I and are close to their SM values, all couplings to second and first generation fermions can be easily modified by $\mathcal{O}(1)$. We find that the searches for $h \to \mu^+\mu^-$ provide the strongest constraints on deviations from the decoupling limit $\cos(\beta - \alpha) = 0$ for moderate and large values of $\tan\beta$. The framework predicts generically a $\mathcal{O}(0.1\%)$ flavor-violating branching ratio $h \to \tau\mu$.

The heavy neutral Higgs bosons, H and A, have a very distinct phenomenology. They have couplings to second and first generation fermions that are enhanced by $\tan\beta$, while their couplings to the third generation are suppressed. For large $\tan\beta$, we generically find that the dominant decay modes are into $c\bar{c}$, $t\bar{t}$, and ct with branching ratios that are comparable in size. Branching ratios for decays into final states involving gauge bosons ($H \to WW/ZZ$ and $A \to Zh$) can be sizable for moderate values of $\tan\beta$. Decays into $\mu^+\mu^-$, $\tau^+\tau^-$, and $\tau\mu_\tau$ are typically also comparable and the corresponding branching ratios can reach the % level. The most important production modes are gluon fusion and production from charm initial states. For large $\tan\beta$, the cross section from charm can be several hundreds of fb for a Higgs mass of 500 GeV.

The charged Higgs boson is mainly produced by second and third generation quark fusion, as well as in association with a top. Its decays are interestingly different from the decays arising in type I and II 2HDMs, as they are dominated by flavor-violating cb, ts decays and by decays to second generation cs. Also the hierarchy between the decay rate into $\mu\nu_\mu$ and into $\tau\nu_\tau$ is not the same as in 2HDMs with natural flavor conservation or flavor alignment, as the muon decay is parametrically enhanced. This results in weak bounds from the LHC most searched-for signatures, tb and $\tau\nu_\tau$.

Due to the non-standard branching ratios and production modes of H, A, and $H^{\pm}$, the standard searches for heavy Higgs bosons are not necessarily the most sensitive probes of our extended scalar sector. We find that, currently, the searches for low mass di-muon resonances place the most stringent constraints on the model. Also searches for low mass di-jet resonances might probe interesting parameter space in the future. Interesting novel signatures include heavy neutral Higgs bosons decaying in a flavor-violating way, e.g. $pp \to H/A \to \tau\mu$ or $pp \to H/A \to tc$, as well as final states with same sign tops $pp \to tH \to tt\bar{c}$ or $pp \to \bar{t}H \to \overline{t}\overline{t}c$. For the charged Higgs, it will be very interesting to perform searches for cb and cs resonances with mass above the top threshold, produced in association with a top quark.

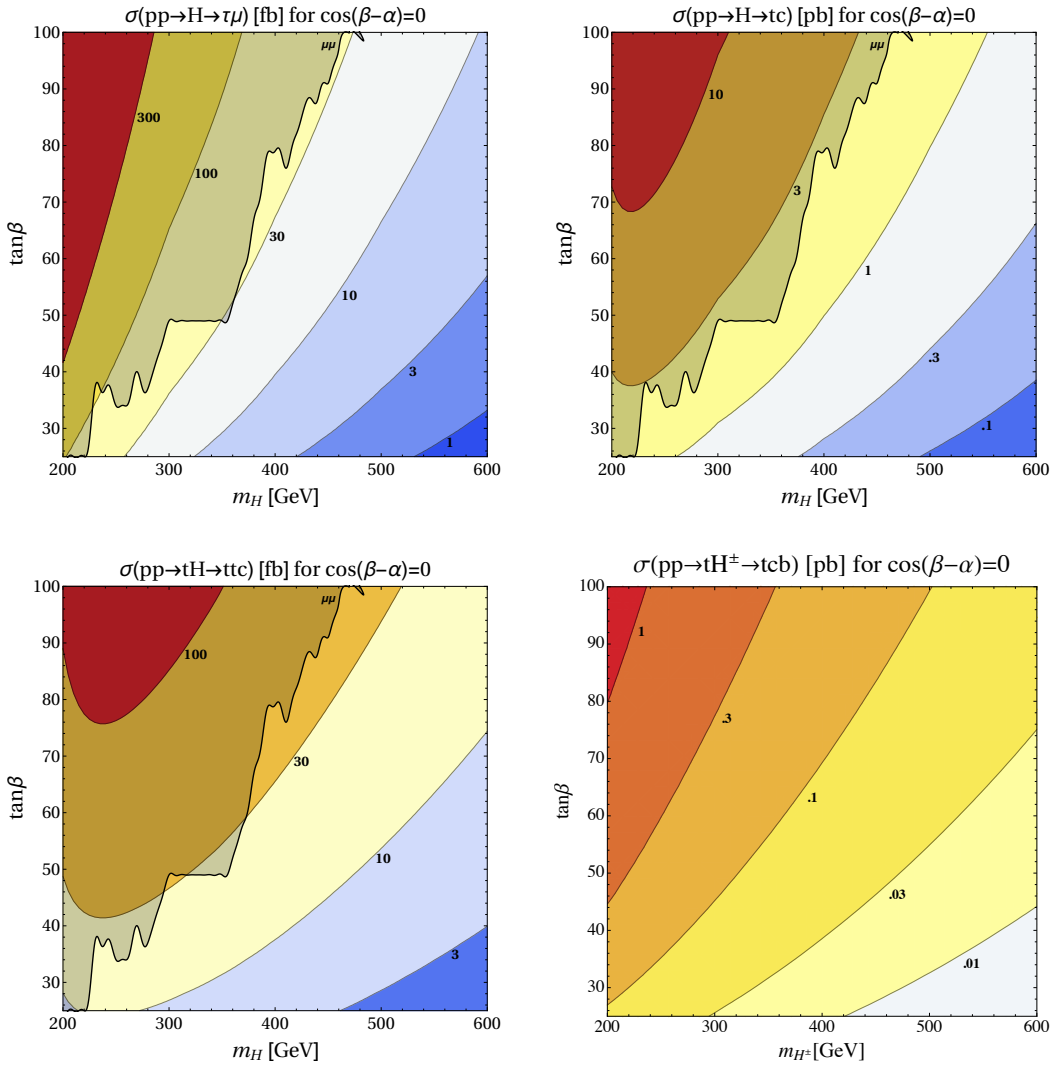

Figure 2.9: Production cross section times branching ratio for the processes $pp \to H \to \tau\mu$ (upper left), $pp \to H \to tc$ (upper right) and $pp \to tH, H \to tc$ (lower left) at 13 TeV in the m_H vs. $\tan\beta$ plane in the decoupling or alignment limit, $\cos(\beta - \alpha) = 0$. The gray shaded region is excluded by existing searches for di-muon resonances. Lower right panel: Production cross section times branching ratio for the process $pp \to tH^\pm, H^\pm cb$ at 13 TeV in the $m_{H^\pm}$ vs. $\tan\beta$ plane in the decoupling or alignment limit.

Chapter 3

The Flavor-Locked Flavorful Two Higgs Doublet Model

3.1 Introduction

In the previous chapter we have presented a dynamical approach to address the SM flavor puzzle in which the first two generations of SM fermions couple exclusively to an additional subleading source of electroweak symmetry breaking, in the form of a second Higgs doublet. Asserting suitable textures for the quark and lepton Yukawa matrices, in order to satisfy flavor constraints, leads to a 'flavorful' two Higgs doublet model (F2HDM). We have seen that the F2HDM includes striking collider signatures for lepton flavor violation, such as $h \to \tau\mu$ or $b \to s\tau\mu$ and large branching ratios for $t \to ch$, as well as heavy Higgs or pseudoscalar decays $H/A \to c\bar{c}$, $t\bar{c}$, $\mu\mu$, $\tau\mu$ and charged Higgs decays $H^{\pm} \to b\bar{c}$, $s\bar{c}$, $\mu\nu$.

A different approach to resolving the SM mass hierarchy puzzle can be achieved with a dynamical alignment mechanism [194] – we refer to it as 'flavor-locking' –

in which the quark (or lepton) Yukawas are generated by the vacuum of a general flavon potential, that introduces a single flavon field and a single 'hierarchon' operator for each quark flavor. (A detailed review follows below; see also Refs. [195,196] for a related, but intrinsically different approach, as well as Refs. [197–200].) In this vacuum, the up- and down-type sets of flavons are dynamically locked into an aligned, rank-1 configuration in the mass basis, so that each SM quark mass is controlled by a unique flavon. Horizontal symmetries between the hierarchon and flavon sectors in turn allow each quark mass to be dynamically set by a unique hierarchon vev. This results in a flavor blind mass generation mechanism – the quarks themselves carry no flavor symmetry beyond the usual $U(3)_{Q,U,D}$ – so that the quark mass hierarchy can be generated independently from the CKM quark mixing hierarchy, by physics that operates at scales generically different to – i.e. lower than – the scale of the flavon effective field theory. In a minimal set up that features only a single SM-type Higgs, however, the CKM mixing matrix is an arbitrary unitary matrix, so that the quark mixing hierarchy itself remains unexplained.

In this chapter we synthesize these two approaches to the flavor puzzle with the following observation: A dynamical realization of an F2HDM-type flavor structure can be generated by applying the flavor-locking mechanism to its Yukawas. Or alternatively: In a flavor-locking scheme for the generation of the quark mass hierarchy, introducing a second Higgs doublet with F2HDM-type couplings generically produces quark mixing hierarchies of the desired size. In particular, we show that in such a setup, the 1–3 and 2–3 quark mixings are automatically produced at the observed order, without the introduction of tunings. The flavor structure of this theory generically leads to tree-level contributions from heavy Higgs exchange to meson mixing observables, that vanish in the heavy Higgs infinite

mass limit. However, for heavy Higgs masses at collider-accessible scales, we show these contributions may be consistent with current data, and in some cases may accommodate the current data mildly better than the SM.

This chapter is structured as follows. In Sec. 4.2 we briefly review the general properties of the F2HDM and its flavor structure. In Sec. 3.3 we develop the flavor-locking mechanism for F2DHM-type theories, including a review of the minimal single Higgs version. We then proceed to explore the generic flavor structure of the flavor-locked F2HDM in Sec. 3.4, discussing both the generation of the CKM mixing hierarchies and constraints from meson mixing. We conclude in Sec. 3.5. Technical details concerning the analysis of the flavon potential are given in Appendices.

3.2 Review of the flavorful 2HDM

The F2HDM, as introduced in Refs. [84, 201], is a 2HDM in which one Higgs doublet predominantly gives mass to the third generation of quarks and leptons, while the second Higgs doublet is responsible for the masses of the first and second generation of SM fermions, as well as for quark mixing. The most general Yukawa Lagrangian of two Higgs doublets with hypercharge $+1/2$ can be written as

$$\begin{aligned}-\mathcal{L}_{\rm Y} =& \sum_{i,J}\left[Y^u_{iJ}(\bar{Q}^i_L\tilde{H}_1U^J_R)+Y'^u_{iJ}(\bar{Q}^i_L\tilde{H}_2U^J_R)\right]+\sum_{i,\widehat{J}}\left[Y^d_{i\widehat{J}}(\bar{Q}^i_LH_1D^{\widehat{J}}_R)+Y'^d_{i\widehat{J}}(\bar{Q}^i_LH_2D^{\widehat{J}}_R)\right]\\ &+\sum_{i,\widehat{J}}\left[Y^\ell_{i\widehat{J}}(\bar{L}^i_LH_1E^{\widehat{J}}_R)+Y'^\ell_{i\widehat{J}}(\bar{L}^i_LH_2E^{\widehat{J}}_R)\right]+\text{h.c.}\,,\end{aligned}\tag{3.1}$$

with two Higgs doublets H_1 and H_2 coupling to the left-handed and right-handed quarks (Q_L, U_R, D_R) and leptons (L_L and E_R), and $\tilde{H}\equiv\epsilon H^*$. The indices $i=1,2,3$ and $J,\widehat{J}=1,2,3$ label the three generations of $SU(2)$ doublet and

singlet fields, respectively. We focus on quark Yukawas hereafter, but the general results of this discussion apply equally to the lepton Yukawas in Eq. (3.1).

The two Higgs doublets decompose in the usual way

$$H_1 = \begin{pmatrix} G^+ \sin\beta - H^+ \cos\beta \\ \frac{1}{\sqrt{2}}(v \sin\beta + h\cos\alpha + H\sin\alpha + iG^0 \sin\beta - iA\cos\beta) \end{pmatrix}, \tag{3.2}$$

$$H_2 = \begin{pmatrix} G^+ \cos\beta + H^+ \sin\beta \\ \frac{1}{\sqrt{2}}(v \cos\beta - h\sin\alpha + H\cos\alpha + iG^0 \cos\beta + iA\sin\beta) \end{pmatrix}, \tag{3.3}$$

where $v = 246$ GeV is the vacuum expectation value of the SM Higgs, G^0 and $G^\pm$ are the Goldstone bosons that provide the longitudinal components for the Z and $W^\pm$ bosons, h and H are physical scalar Higgs bosons, A is a physical pseudoscalar Higgs boson, and $H^\pm$ are physical charged Higgs bosons. The angle α parametrizes diagonalization of the scalar Higgs mass matrix and $\tan\beta$ is the ratio of the vacuum expectation values of H_1 and H_2. The scalar h is identified with the 125 GeV Higgs boson. The overall mass scale of the 'heavy' Higgs bosons $H, A, H^\pm$ is a free parameter. The mass splitting among them is at most of order $O(v^2/m_{H,A,H^\pm})$.

In Refs. [84, 201] the following textures of the two sets of Yukawa couplings Y and Y' were chosen,

$$Y^u \sim \frac{\sqrt{2}}{v\sin\beta}\begin{pmatrix} 0 & & \\ & 0 & \\ & & m_t \end{pmatrix}, \qquad Y'^u \sim \frac{\sqrt{2}}{v\cos\beta}\begin{pmatrix} m_u & m_u & m_u \\ m_u & m_c & m_c \\ m_u & m_c & m_c \end{pmatrix}, \tag{3.4a}$$

$$Y^d \sim \frac{\sqrt{2}}{v\sin\beta}\begin{pmatrix} 0 & & \\ & 0 & \\ & & m_b \end{pmatrix}, \qquad Y'^d \sim \frac{\sqrt{2}}{v\cos\beta}\begin{pmatrix} m_d & \lambda m_s & \lambda^3 m_b \\ m_d & m_s & \lambda^2 m_b \\ m_d & m_s & m_s \end{pmatrix}, \tag{3.4b}$$

where each entry in the Y'^u, Y'^d Yukawas is multiplied by a generic $\mathcal{O}(1)$ coef-

ficient. This structure naturally produces the observed quark masses as well as CKM mixing angles. In this work, we will focus on the dynamical generation of Yukawas of a similar form, with the schematic structure

$$Y^u \sim \frac{\sqrt{2}}{v \sin\beta} \begin{pmatrix} 0 & & \\ & 0 & \\ & & m_t \end{pmatrix}, \qquad Y'^u \sim \frac{\sqrt{2}}{v \cos\beta} U_u \begin{pmatrix} m_u & & \\ & m_c & \\ & & 0 \end{pmatrix} V_u^\dagger, \tag{3.5a}$$

$$Y^d \sim \frac{\sqrt{2}}{v \sin\beta} \begin{pmatrix} 0 & & \\ & 0 & \\ & & m_b \end{pmatrix}, \qquad Y'^d \sim \frac{\sqrt{2}}{v \cos\beta} U_d \begin{pmatrix} m_d & & \\ & m_s & \\ & & 0 \end{pmatrix} V_d^\dagger, \tag{3.5b}$$

in which $U_{u,d}$ and $V_{u,d}$ are unitary matrices. These Yukawas will similarly produce the observed quark mass hierarchies and CKM mixing (see Sec. 3.4 below), and the collider phenomenology of both Yukawa structures is expected to manifest in the same set of signatures.

The F2HDM setup exhibits a very distinct phenomenology, that differs significantly from 2HDMs with natural flavor conservation, flavor alignment, or minimal flavor violation [113, 133–135, 202]. The couplings of the 125 GeV Higgs are modified in a flavor non-universal way. In particular, in regions of parameter space where the couplings of h to the third generation are approximately SM like, the couplings to the first and second generation can still deviate from SM expectations by an $\mathcal{O}(1)$ factor. Also, the heavy Higgs bosons H, A, and $H^\pm$ couple to the SM fermions in a characteristic flavor non-universal way. Their couplings to the third generation are suppressed by $\tan\beta$, while the couplings to first and second generation are enhanced by $\tan\beta$. Therefore, the decays of H, A, and $H^\pm$ to the third generation – t, b quarks and the τ lepton – are not necessarily dominant. For large and moderate $\tan\beta$ we expect sizable branching ratios involving, for example, charm quarks and muons. Similarly, novel non-standard production modes of the heavy Higgs bosons involving second generation quarks can be relevant and

sometimes even dominant [201].

One important aspect of the Yukawa structures in Eqs. (3.4) and Eqs. (3.5) is that they imply tree-level flavor changing neutral Higgs couplings. The flavor-violating couplings of the 125 GeV Higgs vanish in the decoupling/alignment limit, i.e. for $\cos(\beta - \alpha) = 0$. However, flavor-violating couplings of the heavy Higgs bosons persist in this limit and they are proportional to $\tan\beta$. Therefore, for large $\tan\beta$ and heavy Higgs boson masses below the TeV scale, flavor violating processes, such as meson mixing, constrain the F2HDM parameter space. Note that the rank-1 nature of the third generation Yukawas, Y, preserves a $U(2)^5$ flavor symmetry acting on the first and second generation of fermions. This symmetry is only broken by the Y' Yukawa couplings of the second doublet, so that flavor changing transitions from the second to the first generation are protected. Therefore, the constraints from kaon and D-meson oscillation will be less stringent than one might naively expect. We will discuss meson oscillation constraints in detail in Sec. 3.4.

3.3 Flavor-Locking with one and two Higgs bosons

While the distinct phenomenology of the F2HDM alone motivates detailed studies, a mechanism that realizes the flavor structure in Eqs. (3.4) or (3.5) has not been explicitly constructed so far. We now discuss how the flavor structure (3.5) can be dynamically generated by the flavor-locking mechanism, and, conversely, how a F2HDM-type theory permits the flavor-locking mechanism to generate realistic flavor phenomenology. We first review the minimal single Higgs doublet version of the flavor-locking mechanism, followed by the generalization to a theory with two Higgs doublets in Sec. 3.3.4. As we will discuss, while in the presence of only one SM-like Higgs doublet, the predicted quark mixing angles

are generically of $\mathcal{O}(1)$, introducing a second Higgs doublet leads to a theory with suppressed $|V_{cb}|$ and $|V_{ub}|$.

3.3.1 Yukawa portal

The underlying premise of the flavor-locking mechanism [194] is that the Yukawas arise from a three-way portal between the SM fields (the quarks Q_L, U_R, D_R and the Higgs H), a set of 'flavon' fields, λ, and a set of 'hierarchon' operators, s:

$$-\mathcal{L}_{\rm Y} \supset \bar{Q}_L^i \frac{\lambda_{\alpha iJ}}{\Lambda_{\rm F}} \frac{s_\alpha}{\Lambda_{\rm H}} \tilde{H} U_R^J + \bar{Q}_L^i \frac{\lambda_{\widehat{\alpha} i \widehat{J}}}{\Lambda_{\rm F}} \frac{s_{\widehat{\alpha}}}{\Lambda_{\rm H}} H D_R^{\widehat{J}} \,. \tag{3.6}$$

The λ's are bifundamentals of the appropriate $U(3)_Q \times U(3)_{U,D}$ flavor groups for up and down quarks, respectively. The subscripts[1], $\alpha = u, c, t$ and $\widehat{\alpha} = d, s, b$, denote an arbitrary transformation property under a symmetry or set of symmetries, $\mathcal{G}$ and $\widehat{\mathcal{G}}$, that enforces the structure of Eq. (3.6). In the original flavor-locking study [194], $\mathcal{G} \times \widehat{\mathcal{G}}$ was chosen to be a set of discrete $\mathbb{Z}_q^{p_q}$ or $U(1)_q$ 'quark flavor number' symmetries, for $q = d, s, b, u, c, t$. Here, we similarly choose each flavon λ_α ($\lambda_{\widehat{\alpha}}$) to be charged under a gauged $U(1)_\alpha$ ($U(1)_{\widehat{\alpha}}$), but assert a S_3 permutation symmetry among the up (down) flavons and the corresponding $U(1)_\alpha$ ($U(1)_{\widehat{\alpha}}$) gauge bosons, fixing the gauge couplings $g_\alpha = g$ ($g_{\widehat{\alpha}} = \widehat{g}$). Compared to the analysis of Ref. [194] the permutation symmetry produces a convenient, higher symmetry for the flavon potential, such that configurations with the structure of Eqs. (3.5) can be shown to be at its global minimum, as we will discuss in the next subsection. Note that the SM fields are not charged under the $\mathcal{G} \times \widehat{\mathcal{G}}$ symmetry.

The hierarchons s should be thought of as some set of scalar operators that eventually obtain hierarchical vevs, that break the S_3 symmetries in the up and

[1] We always distinguish down-type indices from up-type indices with a hat, and similarly for down-type versus up-type flavon couplings and operators.

down sectors. This hierarchy will be responsible for the quark mass hierarchy, independently from any flavor structure. It should be emphasized that the operators s_α and $s_{\widehat{\alpha}}$ do not carry the quark $U(3)_Q \times U(3)_{U,D}$ flavor symmetries, i.e., they do not carry flavor indices $i, J, \widehat{J}$. Moreover, the hierarchon scale $\Lambda_{\rm H}$ need not be the same as the flavon scale $\Lambda_{\rm F}$, and can generically be much lower. (This could permit, in principle, collider-accessible hierarchon phenomenology, depending on the UV completion of the hierarchon sector, though we shall not consider such possibilities in this work.)

In the remainder of this section, we present the general flavor structures that this type of portal dynamically produces. Details of this analysis, including the identification of global or local minima of the flavon potential, and the algebraic structure of the associated vacua, are presented in Appendix A.1. The spontaneous breaking of continuous symmetries by the flavon vacuum can result in a large number of Goldstone bosons. We assume that mechanisms are at work that remove the Goldstone bosons from the IR.

3.3.2 General flavon potential and vacuum

To generalize beyond the three flavors of the SM, we contemplate a theory of N flavors of up and down type quarks each, $Q_L^i, U_R^J, D_R^{\widehat{J}}$ with $i, J, \widehat{J} = 1, \ldots, N$, charged under the symmetry $U(N)_Q \times U(N)_U \times U(N)_D$. We introduce $n \leq N$ pairs of flavons λ_α, $\lambda_{\widehat{\alpha}}$, with $\alpha, \widehat{\alpha} = 1, \ldots, n$, that generate Yukawa couplings to the quarks as in Eq. (3.6). The flavons for this theory then transform as

$$\lambda_\alpha \sim \boldsymbol{N} \otimes \bar{\boldsymbol{N}} \otimes \boldsymbol{1}\,, \qquad \lambda_{\widehat{\alpha}} \sim \boldsymbol{N} \otimes \boldsymbol{1} \otimes \bar{\boldsymbol{N}}\,. \tag{3.7}$$

We suppress hereafter the $U(N)_Q \times U(N)_{U,D}$ indices, keeping in mind that matrix products only take the form $\lambda_\alpha \lambda_\beta^\dagger$ or $\lambda_\beta^\dagger \lambda_\alpha$, and correspondingly in the down sector.

Up-down matrix products can only take the form $\lambda_\alpha^\dagger \lambda_{\widehat{\alpha}}$ or $\lambda_{\widehat{\alpha}}^\dagger \lambda_\alpha$, but not $\lambda_\alpha \lambda_{\widehat{\alpha}}^\dagger$ nor $\lambda_{\widehat{\alpha}} \lambda_\alpha^\dagger$.

The most general, renormalizable and CP conserving potential for the flavons can then be written in the form

$$V_{\text{fl}} = \sum_\alpha V_{1\text{f}}^\alpha + \sum_{\alpha<\beta} V_{2\text{f}}^{\alpha\beta} + \sum_{\widehat{\alpha}} V_{1\text{f}}^{\widehat{\alpha}} + \sum_{\widehat{\alpha}<\widehat{\beta}} V_{2\text{f}}^{\widehat{\alpha}\widehat{\beta}} + \sum_{\alpha,\widehat{\alpha}} V_{\text{mix}}^{\alpha\widehat{\alpha}} \,. \tag{3.8}$$

Here, the single and pairwise field potentials are

$$V_{1\text{f}}^\alpha = \mu_1 \left| \operatorname{Tr}\left(\lambda_\alpha \lambda_\alpha^\dagger\right) - r^2 \right|^2 + \mu_2 \left[\left| \operatorname{Tr}\left(\lambda_\alpha \lambda_\alpha^\dagger\right) \right|^2 - \operatorname{Tr}\left(\lambda_\alpha \lambda_\alpha^\dagger \lambda_\alpha \lambda_\alpha^\dagger\right) \right], \tag{3.9}$$

$$\begin{aligned} V_{2\text{f}}^{\alpha\beta} = {} & \mu_3 \left| \operatorname{Tr}\left(\lambda_\alpha \lambda_\alpha^\dagger\right) - \operatorname{Tr}\left(\lambda_\beta \lambda_\beta^\dagger\right) \right|^2 + \mu_4 \left| \operatorname{Tr}\left(\lambda_\alpha \lambda_\beta^\dagger\right) \right|^2 \\ & + \mu_{6,1} \operatorname{Tr}\left(\lambda_\alpha^\dagger \lambda_\alpha \lambda_\beta^\dagger \lambda_\beta\right) + \mu_{6,2} \operatorname{Tr}\left(\lambda_\alpha \lambda_\alpha^\dagger \lambda_\beta \lambda_\beta^\dagger\right), \end{aligned} \tag{3.10}$$

and similarly for $V_{1\text{f}}^{\widehat{\alpha}}$ and $V_{2\text{f}}^{\widehat{\alpha}\widehat{\beta}}$, hatting all coefficients (the labeling and notation follows the choices of Ref. [194]). Note that the pairwise potentials respect the $U(1)_\alpha$ and $U(1)_{\widehat{\alpha}}$ symmetries. The mixed potential is

$$\begin{aligned} V_{\text{mix}}^{\alpha\widehat{\alpha}} = {} & \nu_1 r^2 \widehat{r}^2 \left| \operatorname{Tr}\left(\lambda_\alpha \lambda_\alpha^\dagger\right)/r^2 - \operatorname{Tr}\left(\lambda_{\widehat{\alpha}} \lambda_{\widehat{\alpha}}^\dagger\right)/\widehat{r}^2 \right|^2 \\ & - \nu_2 \left[\operatorname{Tr}\left(\lambda_\alpha \lambda_\alpha^\dagger \lambda_{\widehat{\alpha}} \lambda_{\widehat{\alpha}}^\dagger\right) - \frac{1}{n} \operatorname{Tr}\left(\lambda_\alpha \lambda_\alpha^\dagger\right) \operatorname{Tr}\left(\lambda_{\widehat{\alpha}} \lambda_{\widehat{\alpha}}^\dagger\right) \right]. \end{aligned} \tag{3.11}$$

The S_n symmetry ensures that all potential coefficients are the same for all fields $\alpha, \widehat{\alpha}, \beta, \widehat{\beta}$ singly and pairwise. All μ_i and ν_i coefficients, as well as r and $\widehat{r}$, are real and are chosen to be positive.

A detailed analysis of the global minimum of this potential is provided in Appendix A.1. One finds that, provided

$$\mu_{6,2} \geq \nu_2 \widehat{r}^2/r^2 \,, \qquad \widehat{\mu}_{6,2} \geq \nu_2 r^2/\widehat{r}^2 \,, \qquad \text{and} \qquad \nu_1 \geq \nu_2/(2n) \,, \tag{3.12}$$

the potential has a global minimum if and only if the flavons have the vacuum configuration

$$\langle\lambda_1\rangle = U\begin{pmatrix} r & & \\ & 0 & \\ & & \ddots \end{pmatrix}V^\dagger\,, \qquad \langle\lambda_2\rangle = U\begin{pmatrix} 0 & & \\ & r & \\ & & \ddots \end{pmatrix}V^\dagger\,, \qquad \ldots \tag{3.13a}$$

$$\langle\lambda_{\widehat{1}}\rangle = \widehat{U}\begin{pmatrix} \widehat{r} & & \\ & 0 & \\ & & \ddots \end{pmatrix}\widehat{V}^\dagger\,, \qquad \langle\lambda_{\widehat{2}}\rangle = \widehat{U}\begin{pmatrix} 0 & & \\ & \widehat{r} & \\ & & \ddots \end{pmatrix}\widehat{V}^\dagger\,, \qquad \ldots \tag{3.13b}$$

with U, V, $\widehat{U}$, $\widehat{V}$ unitary matrices – crucially, the matrices U, V ($\widehat{U}$, $\widehat{V}$) are the same for all λ_α ($\lambda_{\widehat{\alpha}}$) – and the CKM mixing matrix has the form

$$\mathcal{V}_{\rm ckm} = U^\dagger\widehat{U} = \begin{pmatrix} \mathcal{V}_n & 0 \\ 0 & \mathcal{V}_{N-n} \end{pmatrix}\,, \tag{3.14}$$

with $\mathcal{V}_k$ a $k\times k$ unitary matrix. These n or $N-n$ block CKM rotations are flat directions of the global minimum, and therefore $\mathcal{V}_n$ and $\mathcal{V}_{N-n}$ may be any arbitrary unitary submatrices with generically $\mathcal{O}(1)$ entries. We refer to the configuration in Eqs. (3.13) and (3.14) as being 'flavor-locked'.

3.3.3 Flavor-locked Yukawas

Flavor locking ensures that the Yukawa portal in (3.6) becomes, in the $n = N = 3$ case

$$\bar{Q}_L\frac{r}{\Lambda_{\rm F}}\begin{pmatrix} s_u/\Lambda_{\rm H} & & \\ & s_c/\Lambda_{\rm H} & \\ & & s_t/\Lambda_{\rm H} \end{pmatrix}\tilde{H}U_R + \bar{Q}_L\frac{\widehat{r}}{\Lambda_{\rm F}}\mathcal{V}_{\rm ckm}\begin{pmatrix} s_d/\Lambda_{\rm H} & & \\ & s_s/\Lambda_{\rm H} & \\ & & s_b/\Lambda_{\rm H} \end{pmatrix}HD_R\,, \tag{3.15}$$

under a suitable unitary redefinition of the Q_L, U_R and D_R fields. From these expressions, taking the natural choice $r, \widehat{r} \sim \Lambda_{\rm F}$, it is clear that it is the physics of the hierarchon vev's, $\langle s_\alpha \rangle$, that generates the quark mass hierarchies, i.e. $\langle s_\alpha \rangle / \Lambda_{\rm H} \sim y_\alpha$, the quark Yukawa for flavor α. This physics may operate at scales vastly different to the flavor breaking scale, $\Lambda_{\rm F}$. In Eq. (3.15) the CKM matrix $\mathcal{V}_{\rm ckm}$ is an arbitrary 3×3 unitary matrix.

One might wonder if additional terms in the flavon potential of (3.8) can destabilize the vacuum identified above. In particular, flavon-hierarchon couplings of the form $\mathrm{Tr}\big[\lambda_\alpha^\dagger \lambda_\alpha\big] s_\alpha^\dagger s_\alpha$ ($\mathrm{Tr}\big[\lambda_\alpha^\dagger \lambda_\beta\big] s_\alpha^\dagger s_\beta$) may be present, which can produce (mixed) mass terms that disrupt the $V_{\rm mix}$ ($V_{\rm 2f}$) vacuum once the hierarchons, s_α, obtain vev's. Mixed mass terms may disrupt the alignment between the different $\langle \lambda_\alpha \rangle$, while additional mass terms induce splittings in the radial mode masses, so that the block CKM rotations are no longer flat directions of the vacuum.

In the UV theory, the operator product of two hierarchons with two flavons may, however, be vanishingly small, e.g. if the hierarchons are composite operators in different sectors. Nonetheless, such terms are necessarily generated radiatively by the Yukawa portal (3.6). One may construct UV completions in which this occurs first at the two-loop level, with the (mixed) mass contributions being log-divergent. For example, let us consider a theory containing a flavored fermion $\chi_{\alpha i}$ and a scalar Φ_α, with interactions

$$\lambda_{\alpha i J} \bar{\chi}_{\alpha i} U_R^J + \Phi_\alpha \bar{Q}_L^i \chi_{\alpha i} + \mu \Phi_\alpha^\dagger s_\alpha \tilde{H} \,, \tag{3.16}$$

with $m_\chi \sim \Lambda_{\rm F}$ and $\mu \sim m_\Phi \sim \Lambda_{\rm H}$. This produces the Yukawa portal (3.6) via

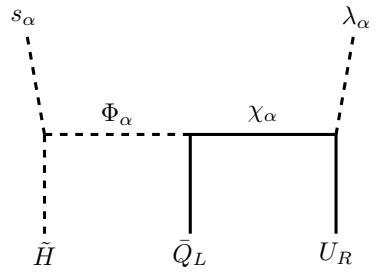

(3.17)

As $\langle s_\alpha \rangle / \Lambda_{\rm H} \sim y_\alpha$, the quark Yukawa for flavor α, the corresponding (mixed) mass term for the flavons is generated at two-loops by mirroring the diagram in (3.17). One finds

$$\delta m^2_{\alpha\beta} \sim \frac{\Lambda_{\rm H}^2}{\Lambda_{\rm F}^2} \frac{y_\alpha y_\beta}{(16\pi^2)^2} \log(\Lambda_{\rm H}/\Lambda_{\rm F})\, r^2 \,, \tag{3.18}$$

once again taking the natural choice $r \sim \Lambda_{\rm F}$. A suitable hierarchy between $\Lambda_{\rm H}$ and $\Lambda_{\rm F}$, combined with the two-loop suppression, renders these terms arbitrarily small. Hence one may safely neglect these terms.

3.3.4 Two-Higgs flavor-locking

Motivated by the flavorful 2HDM, now we turn to consider a Yukawa potential with two Higgs fields: One that couples to the third generation, and one to the first two generations. That is,

$$\bar{Q}_L \left[\frac{\lambda_t}{\Lambda_{\rm F}} \frac{s_t}{\Lambda_{\rm H}} \tilde{H}_1 + \frac{\lambda_{c,u}}{\Lambda_{\rm F}} \frac{s_{c,u}}{\Lambda_{\rm H}} \tilde{H}_2 \right] U_R + \bar{Q}_L \left[\frac{\lambda_b}{\Lambda_{\rm F}} \frac{s_b}{\Lambda_{\rm H}} H_1 + \frac{\lambda_{s,d}}{\Lambda_{\rm F}} \frac{s_{s,d}}{\Lambda_{\rm H}} H_2 \right] D_R \,, \tag{3.19}$$

in which we have suppressed the quark flavor indices. With reference to the UV completion (3.16), one can imagine that this generational structure comes about as a consequence of λ_t, s_t, and H_1 belonging to a different UV sector (or

brane) than $\lambda_{c,u}$, $s_{c,u}$, and H_2, so that terms of the form $\lambda_t s_t \tilde{H}_2$ or $\lambda_{c,u} s_{c,u} \tilde{H}_1$ are heavily suppressed in the effective field theory. Similarly, one can also generate this structure via adding an additional symmetry to $s_{c,u}$, $s_{s,d}$ and H_2 such that $s_{c,u}\tilde{H}_2$ and $s_{d,s}H_2$ are singlets. Such terms (symmetries) will, ultimately, be generated (softly broken) via the $\mu^2 H_1 H_2^\dagger$ term in the Higgs potential, which is necessary to avoid a massless Goldstone boson.

The generational structure implies that cross-terms between the third and first two generations in the flavon potential (3.8) now vanish, and that the S_3 flavon-hierarchon symmetry has been replaced with a $\mathbb{Z}_2$ for just the two light generations. That is, the coefficients of the heavy and light flavon potentials are no longer related, and the heavy-light potentials $V_{\rm 2f}^{t\alpha}$, $V_{\rm 2f}^{b\widehat{\alpha}}$, $V_{\rm mix}^{t\widehat{\alpha}}$, $V_{\rm mix}^{b\alpha}$ vanish, for $\alpha = c, u$ and $\widehat{\alpha} = s, d$ (or they obtain their own, independent, and suppressed coefficients, identical for $\alpha = c, u$ and $\widehat{\alpha} = s, d$). One then also expects the rotation matrices entering in the vacuum configuration of the flavons of the first two generations to be different from those of the third, breaking the heavy-light alignment conditions.

Put a different way, we may write the full potential in the form

$$V_{\rm fl} = V_{\rm fl,h} + V_{\rm fl,l} \tag{3.20}$$

in which the 'h' and 'l' pieces of the potential each have the form of the full potential (3.8), but for one heavy and two light generations, respectively. (With reference to the UV completion (3.16), terms for a heavy-light mixing potential are generated radiatively by the $\mu^2 H_1 H_2^\dagger$ portal combined with the Yukawas (3.19) only at the five-loop level, along with a $\mu^4/\Lambda_{\rm F}^4$ factor.) The potentials $V_{\rm fl,h}$ and $V_{\rm fl,l}$ each have a $N = 3$ flavor-locked vacuum, with generation number $n = 1$ and $n = 2$, respectively. Provided the conditions (3.12) are satisfied for each potential,

this leads to the vacuum structure

$$\langle\lambda_t\rangle = U_t \begin{pmatrix} 0 & & \\ & 0 & \\ & & r \end{pmatrix} V_t^\dagger\,, \quad \langle\lambda_c\rangle = U \begin{pmatrix} 0 & & \\ & r & \\ & & 0 \end{pmatrix} V^\dagger\,, \quad \langle\lambda_u\rangle = U \begin{pmatrix} r & & \\ & 0 & \\ & & 0 \end{pmatrix} V^\dagger\,,$$
$$\langle\lambda_b\rangle = \widehat{U}_b \begin{pmatrix} 0 & & \\ & 0 & \\ & & \widehat{r} \end{pmatrix} \widehat{V}_b^\dagger\,, \quad \langle\lambda_s\rangle = \widehat{U} \begin{pmatrix} 0 & & \\ & \widehat{r} & \\ & & 0 \end{pmatrix} \widehat{V}^\dagger\,, \quad \langle\lambda_d\rangle = \widehat{U} \begin{pmatrix} \widehat{r} & & \\ & 0 & \\ & & 0 \end{pmatrix} \widehat{V}^\dagger\,. \tag{3.21}$$

We call this a '$1+2$' flavor-locked vacuum. Note that the rotation matrices for the third generation quarks $(U_t, V_t, \widehat{U}_b, \widehat{V}_b)$ differ in general from the corresponding rotations for the first and second generation quarks.

For the $1+2$ flavor-locked structure (3.21), the CKM structure of the global minimum in Eq. (3.14) enforces $U^\dagger\widehat{U}$ and $U_t^\dagger\widehat{U}_b$ to each be $2\oplus 1$ block unitary, i.e.

$$U^\dagger\widehat{U} = \begin{pmatrix} \mathcal{V}_2 & \\ & 1 \end{pmatrix}\,, \qquad U_t^\dagger\widehat{U}_b = \begin{pmatrix} \mathcal{W}_2 & \\ & 1 \end{pmatrix}\,, \tag{3.22}$$

where $\mathcal{V}_2$ and $\mathcal{W}_2$ are 2×2 unitary matrices (see App. A.1.3). The $2\oplus 1$ block unitarity permits one to rotate away the tb unitary matrices, so that the Yukawa potential (3.19) attains the form

$$\bar{Q}_L \frac{r}{\Lambda_{\rm F}} \left[\begin{pmatrix} 0 & & \\ & 0 & \\ & & z_t \end{pmatrix} \tilde{H}_1 + U \begin{pmatrix} z_u & & \\ & z_c & \\ & & 0 \end{pmatrix} V^\dagger \tilde{H}_2 \right] U_R$$
$$+ \bar{Q}_L \frac{\widehat{r}}{\Lambda_{\rm F}} \left[\begin{pmatrix} 0 & & \\ & 0 & \\ & & z_b \end{pmatrix} H_1 + U \begin{pmatrix} \mathcal{V}_2 & \\ & 1 \end{pmatrix} \begin{pmatrix} z_d & & \\ & z_s & \\ & & 0 \end{pmatrix} \widehat{V}^\dagger H_2 \right] D_R\,, \tag{3.23}$$

with $z_\alpha = \langle s_\alpha\rangle/\Lambda_{\rm H}$ and $z_{\widehat{\alpha}} = \langle s_{\widehat{\alpha}}\rangle/\Lambda_{\rm H}$. The unitary matrices U, V and $\widehat{V}$ have been redefined to absorb the other unitary matrices, such that Eq. (3.22) is still satisfied, and we have written $\widehat{U} = U\,\mathrm{diag}\{\mathcal{V}_2, 1\}$ accordingly. Matching the structure of Eq. (3.5), Eq. (3.23) is the key result of this section: The dynamical generation of

hierarchical aligned third generation Yukawas, and hierarchical aligned first two generation Yukawas. An additional feature, not present in Eq. (3.5), is that the up- and down-type light Yukawas are aligned up to an overall mixing angle on the left. The mixing angle is a flat direction of the flavon potential and therefore generically of $O(1)$.

3.4 Flavor violation and phenomenology

We now turn to examine the phenomenology of flavor-violating processes generated by the Yukawa structure in Eq. (3.23). If one treats the SM as a UV complete theory, then the quark sector alone naively features multiple tunings towards the infinitesimal: five for the masses of all quarks except the top, and two for the small size of $|V_{cb}|$ and $|V_{ub}|$. In the minimal or F2HDM-type flavor-locking scenarios, the quark mass hierarchies no longer require such tunings, as they can be generated dynamically by $\langle s_\alpha \rangle$. We show below that the structure of Eq. (3.23) also characteristically produces 1–3 and 2–3 quark generation mixing comparable to the observed size of $|V_{cb}|$ and $|V_{ub}|$, without requiring ad hoc suppression of the underlying parameters. In this sense of counting tunings, the flavor-locked F2HDM is a more natural theory of flavor than the SM. Additionally, for the flavor structure (3.23), the heavy Higgs bosons may remain light enough to be accessible to colliders, i.e. with a mass of a few hundred GeV, while not introducing unacceptably large tree-level contributions to meson mixing observables. In some regions of parameter space, these additional contributions better accommodate the current data than the SM. We explore the nature of such contributions below.

3.4.1 Physical parameters

Starting from the general structure of Eq. (3.23), which has already selected the direction of the H_1-generated component of the third generation, the Q, U and D quarks have a maximal $U(2)^3 \times U(1)$ flavor symmetry, which breaks to baryon number. This corresponds to 3 real and 9 imaginary broken generators. The up-type Yukawa in Eq. (3.23) has a total of $3+3+3=9$ real parameters ($z_{t,u,c}$, and the $SO(3)$ rotations of U and V) and $6+6-2-2=8$ imaginary parameters (the phases of U and V, less the phases commuted or annihilated by the rank-2 diagonal matrix). The down-type Yukawa, excluding parameters already contained in U, has $3+1+3=7$ real parameters ($z_{b,d,s}$, and the $SO(2)$ and $SO(3)$ rotations of $\mathcal{V}_2$ and $\widehat{V}$, respectively) and $3+6-2-1=6$ imaginary parameters (the phases of $\mathcal{V}_2$ and $\widehat{V}$, less the phases commuted or annihilated by the rank-2 diagonal matrix). This counting implies that the total number of physical parameters is $9+8+7+6-12=18$, corresponding to 6 masses, 7 angles and 5 phases.

To see this explicitly, we write a general 3×3 unitary matrix in the canonical form

$$U = \begin{pmatrix} e^{i\phi_1} & & \\ & e^{i\phi_2} & \\ & & 1 \end{pmatrix} R_U(\theta_{12}) R_U(\theta_{13},\phi) R_U(\theta_{23}) \begin{pmatrix} e^{i\phi_4} & & \\ & e^{i\phi_5} & \\ & & e^{i\phi_6} \end{pmatrix}, \qquad (3.24)$$

with R_U rotation matrices in the 3×3 flavor space, and $\theta_{12},\theta_{13},\theta_{23}$ and $\phi,\phi_{1,2,4,5,6}$ generic angles and phases, respectively. Here the indices of the angles label the 2×2 rotations. After redefining several phases, we obtain the parametrization

$$\bar{Q}_L \frac{r}{\Lambda_{\rm F}} \left[\begin{pmatrix} 0 & & \\ & 0 & \\ & & z_t \end{pmatrix} \tilde{H}_1 + R_U(\theta_{13},0) R_U(\theta_{23}) \begin{pmatrix} z_u e^{i\psi_u} & & \\ & z_c e^{i\psi_c} & \\ & & 0 \end{pmatrix} R_V^\dagger(\vartheta_{23}) R_V^\dagger(\vartheta_{13},0) \tilde{H}_2 \right] U_R$$

$$+\bar{Q}_L \frac{\widehat{r}}{\Lambda_F}\Bigg[\begin{pmatrix}0 & & \\ & 0 & \\ & & z_b\end{pmatrix} H_1 + R_U(\theta_{13},0)R_U(\theta_{23})\begin{pmatrix}e^{i\psi_m} & & \\ & 1 & \\ & & 0\end{pmatrix}\begin{pmatrix}R(\theta) & \\ & 1\end{pmatrix}$$
$$\times \begin{pmatrix}z_d e^{i\psi_d} & & \\ & z_s e^{i\psi_s} & \\ & & 0\end{pmatrix} R^\dagger_{\widehat{V}}(\widehat{\vartheta}_{23})R^\dagger_{\widehat{V}}(\widehat{\vartheta}_{13},0)H_2\Bigg] D_R\,. \quad (3.25)$$

There is a flavor basis in which the above parametrization reproduces the F2HDM textures shown in (3.4), with coefficients that depend on the several angles $\theta, \vartheta, \widehat{\vartheta}$. In Appendix A.2 we show explicitly how to rotate into this flavor basis.

3.4.2 CKM phenomenology

The unitary $\mathcal{V}_2$ matrix in Eq. (3.23) is a flat direction of the flavon potential, as are U, V and $\widehat{V}$. The quark mixing matrix of the full theory, however, is no longer a flat direction: It is lifted by the $1+2$ flavor-locked structure to an $\mathcal{O}(1)$ $2\oplus 1$ block form with all other entries suppressed by small ratios of quark masses. Diagonalizing the quark mass matrices resulting from (3.25), one finds the following schematic predictions for the CKM matrix elements

$$\mathcal{V}_{\text{ckm}} \sim \begin{pmatrix}1 & \mathcal{O}(\theta) & \mathcal{O}(m_d/m_b)\\ \mathcal{O}(\theta) & 1 & \mathcal{O}(m_s/m_b)\\ \mathcal{O}(m_d/m_b) & \mathcal{O}(m_s/m_b) & 1\end{pmatrix}\,, \quad (3.26)$$

where θ is the rotation angle in the $\mathcal{V}_2$ matrix (see Eq. (3.25)), that is a priori a free parameter of $\mathcal{O}(1)$. This structure suggests that the observed CKM hierarchies can be accommodated: The 1–3 and 2–3 mixing elements are automatically suppressed at a level that resembles the experimental values.

In the decoupling/alignment limit $\cos(\beta-\alpha)=0$, flavor-violating processes from heavy Higgs exchange vanish in the large $m_{H,A}$ limit. However, from Eqs. (3.25) and (3.26) it is not obvious whether the flavor structure of the $1+2$ flavor-locked

configuration reduces to the SM in an appropriate limit. As a demonstration that the $1+2$ flavor-locked configuration is compatible with data, we heuristically identified the following example input parameters,

$$\begin{aligned} &z_t \frac{r}{\Lambda_F}\frac{v_1}{\sqrt{2}} \simeq 173 \text{ GeV}\,, \quad z_c \frac{r}{\Lambda_F}\frac{v_2}{\sqrt{2}} \simeq 1.9 \text{ GeV}\,, \quad z_u \frac{r}{\Lambda_F}\frac{v_2}{\sqrt{2}} \simeq 7 \text{ MeV}\,, \\ &z_b \frac{\widehat{r}}{\Lambda_F}\frac{v_1}{\sqrt{2}} \simeq 4.8 \text{ GeV}\,, \quad z_s \frac{\widehat{r}}{\Lambda_F}\frac{v_2}{\sqrt{2}} \simeq 240 \text{ MeV}\,, \quad z_d \frac{\widehat{r}}{\Lambda_F}\frac{v_2}{\sqrt{2}} \simeq 21 \text{ MeV}\,, \end{aligned} \tag{3.27a}$$

$$\begin{aligned} &\theta_{13} \simeq -0.2\,, \quad \theta_{23} \simeq -0.1\,, \quad \vartheta_{13} \simeq 1.0\,, \quad \vartheta_{23} \simeq 1.0\,, \quad \widehat{\vartheta}_{13} \simeq 0.4\,, \quad \widehat{\vartheta}_{23} \simeq 1.5\,, \\ &\theta \simeq 0.1\,, \qquad \psi_d \simeq -2.1\,, \quad \psi_s \simeq -0.2\,, \end{aligned} \tag{3.27b}$$

and $\psi_u = \psi_c = \psi_m = 0$, where we have defined the two vevs, $v_1 \equiv v\cos\beta$ and $v_2 \equiv v\sin\beta$. The phases ψ_u, ψ_c, ψ_m are set to zero for simplicity, as they have negligible impact on all the observables that we are considering. (The phases ψ_u, ψ_c enter in D^0–$\bar{D}^0$ mixing, but, as we will discuss in Sec. 3.4.3, they are only very weakly constrained.) This parameter set leads to the theoretical predictions shown in Table 3.1 for the six quark masses and a set of five CKM elements.

We compare these predictions to data for the quark masses and CKM parameters, shown in Table 3.1. To be self-consistent, we use data only from processes that are insensitive to heavy Higgs exchange, i.e. processes that are tree-level in the SM. (Since we are ultimately interested in considering the phenomenology of collider-accessible heavy Higgs bosons, loop-level processes in the SM will receive corrections from heavy Higgs exchanges, but measurements of tree-level processes will be insensitive to these effects.) To reproduce the Cabibbo angle $\lambda_C \simeq 0.22506 \pm 0.00050$ [3], θ needs to be constrained accordingly to a narrow $\mathcal{O}(1)$ range. Since we require only a mixing matrix with canonical entries of the

	Mass Data	Benchmark		CKM Data	Benchmark
m_t	173.5 ± 1.5 GeV	$\simeq 173$ GeV	$\lvert V_{us}\rvert$	0.225 ± 0.023	$\simeq 0.23$
m_b	4.8 ± 0.5 GeV	$\simeq 4.8$ GeV	$\lvert V_{cd}\rvert$		
m_c	1.7 ± 0.2 GeV	$\simeq 1.7$ GeV	$\lvert V_{cb}\rvert$	$(40.5 \pm 4.1) \times 10^{-3}$	$\simeq 40 \times 10^{-3}$
m_s	100 ± 10 MeV	$\simeq 100$ MeV	$\lvert V_{ub}\rvert$	$(4.1 \pm 0.4) \times 10^{-3}$	$\simeq 4.1 \times 10^{-3}$
m_u	2.0 ± 2.0 MeV	$\simeq 2$ MeV	γ	$73.2 \pm 7.3^\circ$	$\simeq 71^\circ$
m_d	5.0 ± 5.0 MeV	$\simeq 5$ MeV			

Table 3.1: Data for quark (pole) masses and CKM parameters used in our analysis. The central values correspond to the measured quark masses [3] and CKM parameters [4, 5]. All CKM parameters and the b, c, and s quark masses are assigned 10% uncertainties. In the case of the top mass we use a 1.5 GeV uncertainty, while for the up and down masses we use 100% uncertainties. Also shown are predictions corresponding to the benchmark point (3.27).

same characteristic size as observed in Nature, we do not insist on such a narrow range for θ. Similarly, for comparison of the theoretical predictions to data, instead of using the experimental uncertainties of the observables (which in some cases are measured with remarkable precision), we choose 10% uncertainties for all CKM parameters and the bottom, charm, and strange masses. In the case of the top mass we chose a 1.5 GeV uncertainty, while for the up and down masses we use 100% uncertainties. Using these values, the theoretical predictions for the benchmark point (3.27) are in excellent agreement with the observed quark masses and CKM parameters.

To quantify the "goodness" of the benchmark or other points in the parameter space, we construct a χ^2-like function, X^2_{tree}, for the six quark masses and CKM elements measured from tree-level processes,

$$X^2_{\text{tree}} = \sum_{i=u,c,t,d,s,b} \left[\frac{(m_i^{\text{FL}} - m_i)^2}{(\sigma_{m_i})^2} \right] + \sum_{i=us,cd,cb,ub} \left[\frac{(|V_i|^{\text{FL}} - |V_i|)^2}{(\sigma_{V_i})^2} \right] + \frac{(\gamma^{\text{FL}} - \gamma)^2}{(\sigma_\gamma)^2} \,. \tag{3.28}$$

where the 'FL' superscript denotes the theory prediction at a given point in the

flavor-locked theory parameter space (3.25), and we treat the uncertainties as uncorrelated. While such a X^2 function implies a well-defined p-value for a goodness-of-fit of the quoted data to a given theory point, one cannot construct from X^2 a sense of the probability for a given theory to produce the observed flavor data and hierarchies. Instead, the X^2 function allows us only to understand whether or not the flavor-locked configuration results generically in a flavor structure that agrees with observation at the level of tens of percent.

In Fig. 3.1 we show the X^2_{tree} behavior of the flavor model on various two-dimensional parametric slices in the neighborhood of the benchmark point (3.27), which is denoted by the white circle. That is, in each plot, all the theory parameters are fixed to the benchmark values in Eqs. (3.27), except for the two parameters corresponding to the plot axes. The number of degrees of freedom (dof) in the X^2_{tree} statistic is then $11 - 2 = 9$. The contours show regions of $X^2_{\text{tree}}/\text{dof}$ that lead to an overall good agreement between the observed quark masses and CKM parameters and those predicted in the model.

As can be seen from the plots in Fig. 3.1, there are extended regions of parameter space where there is fairly good agreement between the theory predictions and the measured quark masses and CKM parameters. In particular, $\mathcal{O}(1)$ variations of the mixing angles $\theta_{13}, \theta_{23}, \vartheta_{13}, \vartheta_{23}, \widehat{\vartheta}_{13}, \widehat{\vartheta}_{23}$ around the benchmark point are possible, without worsening the agreement substantially. Only the angle θ that sets the Cabibbo angle is strongly constrained and has to be set to a narrow range by hand. This behavior should be contrasted to the SM, for which two CKM mixing angles – i.e. the suppressed 1–3 and 2–3 mixings – have to be tuned small.

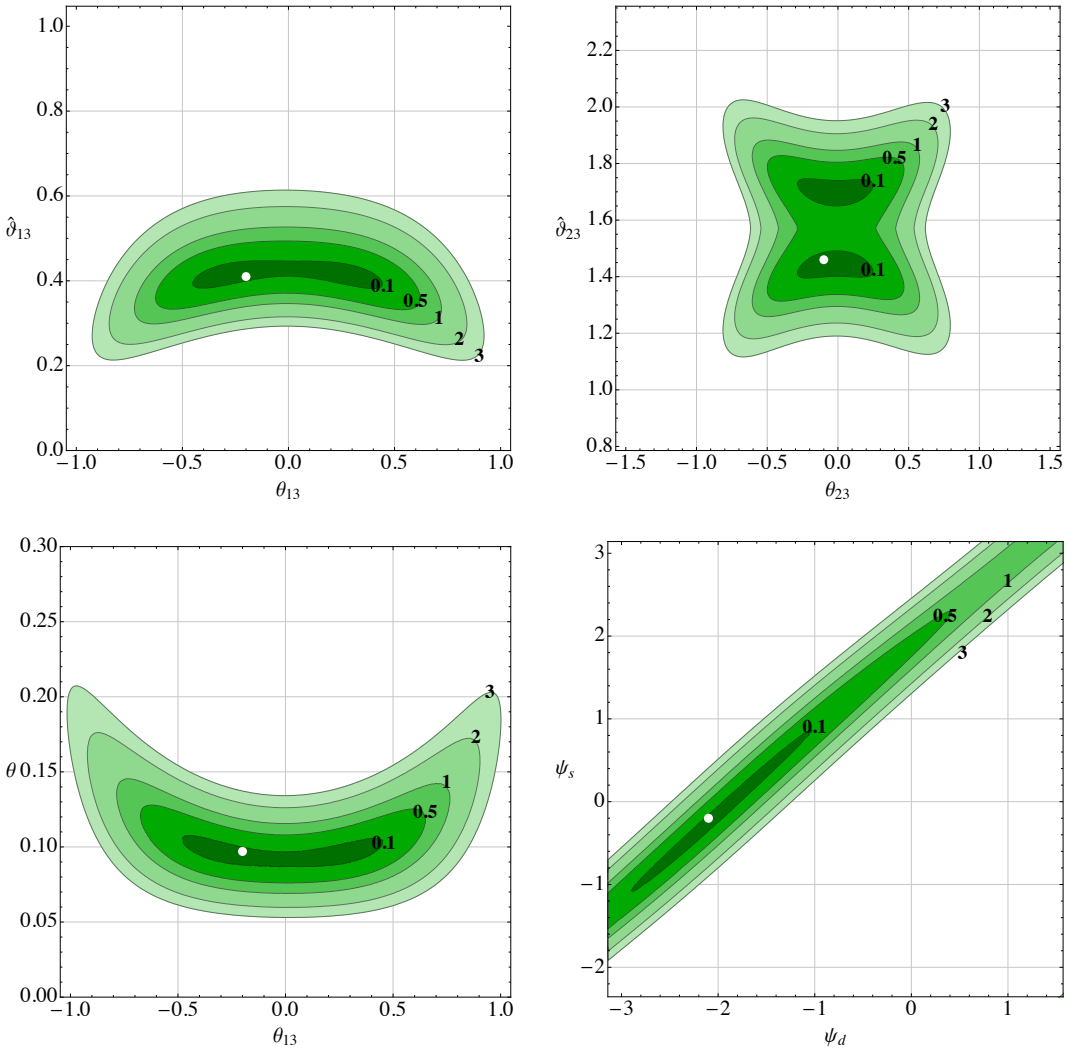

Figure 3.1: $X^2_{\text{tree}}/\text{dof}$ regions on various two-dimensional slices of the 1+2 flavor-locked theory parameter space in the neighborhood of the benchmark point (3.27). Contour values are labeled in black; the benchmark point (3.27) is shown by the white circle.

3.4.3 Constraints from meson mixing

As mentioned above and in Sec. 4.2, the neutral Higgs bosons of the F2HDM setup generically have flavor violating couplings. In particular, their tree-level exchange will contribute to meson oscillations. For kaon oscillations the corre-

sponding new physics (NP) contribution to the mixing amplitude is given by

$$M_{12}^{\rm NP} = m_K^3 \frac{f_K^2}{v^2} \frac{1}{s_\beta^2 c_\beta^2} \left[\frac{1}{4} B_4 \eta_4 \left(\frac{c_{\beta-\alpha}^2}{m_h^2} + \frac{s_{\beta-\alpha}^2}{m_H^2} + \frac{1}{m_A^2} \right) \frac{m'^*_{sd} m'_{ds}}{m_s^2} \right.$$
$$\left. - \left(\frac{5}{48} B_2 \eta_2 - \frac{1}{48} B_3 \eta_3 \right) \left(\frac{c_{\beta-\alpha}^2}{m_h^2} + \frac{s_{\beta-\alpha}^2}{m_H^2} - \frac{1}{m_A^2} \right) \frac{(m'^*_{sd})^2 + (m'_{ds})^2}{m_s^2} \right] .$$

The m' parameters are the off-diagonal entries of the contribution to the down quark mass matrix from the H_2 doublet in the quark mass eigenstate basis, and are fully determined by the parameters entering the 1+2 flavor-locked Yukawas (3.25). The NP mixing amplitude also depends on the heavy Higgs masses m_H and m_A, the ratio of the two Higgs vacuum expectation values $\tan\beta$ and the scalar mixing angle α. As additional parametric input in Eq. (3.29), we have the kaon decay constant $f_K \simeq 155.4$ MeV [203]. The bag parameters $B_2 \simeq 0.46$, $B_3 \simeq 0.79$, $B_4 \simeq 0.78$ are evaluated at the scale $\mu_K = 3$ GeV and are taken from Ref. [204] (see also Refs. [205, 206]). The parameters η_i encode renormalization group running effects. From 1-loop RGEs we find

$$\eta_2 \simeq 0.68 \,, \qquad \eta_3 \simeq -0.03 \,, \qquad \eta_4 = 1 \,. \tag{3.29}$$

The relevant observables that are measured in the neutral kaon system are the mass difference ΔM_K and the CP violating parameter ϵ_K. The experimental results and the corresponding SM predictions and uncertainties are collected in Table 3.2. In terms of the NP mixing amplitude, these observables are given by

$$\Delta M_K = \Delta M_K^{\rm SM} + 2{\rm Re}(M_{12}^{\rm NP}) \,, \qquad \epsilon_K = \epsilon_K^{\rm SM} + \kappa_\epsilon \frac{{\rm Im}(M_{12}^{\rm NP})}{\sqrt{2}\Delta M_K} \,. \tag{3.30}$$

In the expression for ϵ_K we use $\kappa_\epsilon = 0.94$ [207] and the measured value of ΔM_K

	Data	SM Prediction	NP Contribution
ΔM_K	$(5.294 \pm 0.002) \times 10^{-3}$ ps^{-1} [3]	$(4.7 \pm 1.8) \times 10^{-3}$ ps^{-1} [208]	$\simeq -2 \times 10^{-6}$ ps^{-1}
ΔM_{B_d}	0.5055 ± 0.0020 ps^{-1} [209]	0.63 ± 0.07 ps^{-1} [210]	$\simeq 0.01$ ps^{-1}
ΔM_{B_s}	17.757 ± 0.021 ps^{-1} [209]	19.6 ± 1.3 ps^{-1} [210]	$\simeq -1.8$ ps^{-1}
ϵ_K	$(2.288 \pm 0.011) \times 10^{-3}$ [3]	$(1.81 \pm 0.28) \times 10^{-3}$ [208]	$\simeq 0.025 \times 10^{-3}$
ϕ_d	$43.7 \pm 2.4^\circ$ [5]	$47.5 \pm 2.0^\circ$ [5]	$\simeq -2.4^\circ$
ϕ_s	$-1.2 \pm 1.8^\circ$ [209]	$-2.12 \pm 0.04^\circ$ [5]	$\simeq 0.26^\circ$

Table 3.2: Experimental measurements and SM predictions for meson mixing observables. The SM prediction for ΔM_K and its uncertainty refers to the short distance contribution. To account for long distance effects, we use $\Delta M_K^{\rm SM} = \Delta M_K^{\rm exp}(1 \pm 0.5)$ in our numerical analysis. Also shown are the NP contributions corresponding to the benchmark point (3.27).

shown in Table 3.2.

In the case of neutral B meson oscillations, we find it convenient to normalize the NP mixing amplitude directly to the SM amplitude. For B_s mixing we find

$$\frac{M_{12}^{\rm NP}}{M_{12}^{\rm SM}} = \frac{m_{B_s}^2}{s_\beta^2 c_\beta^2}\frac{16\pi^2}{g_2^2}\frac{1}{S_0}\Bigg[2\xi_4\left(\frac{c_{\beta-\alpha}^2}{m_h^2}+\frac{s_{\beta-\alpha}^2}{m_H^2}+\frac{1}{m_A^2}\right)\frac{m'_{bs}{}^* m'_{sb}}{m_b^2 (V_{tb}V_{ts}^*)^2} + (\xi_2+\xi_3)\left(\frac{c_{\beta-\alpha}^2}{m_h^2}+\frac{s_{\beta-\alpha}^2}{m_H^2}-\frac{1}{m_A^2}\right)\frac{(m'_{bs}{}^*)^2+(m'_{sb})^2}{m_b^2 (V_{tb}V_{ts}^*)^2}\Bigg]\,. \quad (3.31)$$

A completely analogous expression holds for B_d oscillations. The SM loop function $S_0 \simeq 2.3$, and the ξ_i factors contain QCD running as well as ratios of hadronic matrix elements. At 1-loop we find

$$\xi_2 \simeq -0.47\ (-0.47)\,, \qquad \xi_3 \simeq -0.005\ (-0.005)\,, \qquad \xi_4 \simeq 0.99\ (1.03)\,, \quad (3.32)$$

where the first (second) value corresponds to B_s (B_d) mixing. To obtain these values

we used bag parameters from Ref. [211] (see also Ref. [210]). The meson oscillation frequencies and the phases of the mixing amplitudes are given by

$$\Delta M_s = \Delta M_s^{\rm SM} \times \left| 1 + \frac{M_{12}^{\rm NP}}{M_{12}^{\rm SM}} \right| , \qquad \phi_s = -2\beta_s + {\rm Arg}\left(1 + \frac{M_{12}^{\rm NP}}{M_{12}^{\rm SM}} \right) , \tag{3.33}$$

$$\Delta M_d = \Delta M_d^{\rm SM} \times \left| 1 + \frac{M_{12}^{\rm NP}}{M_{12}^{\rm SM}} \right| , \qquad \phi_d = 2\beta + {\rm Arg}\left(1 + \frac{M_{12}^{\rm NP}}{M_{12}^{\rm SM}} \right) . \tag{3.34}$$

The experimental results and the corresponding SM predictions and uncertainties for the observables are collected in Table 3.2. Note that the NP contributions to the kaon and B meson mixing amplitudes (3.29) and (3.31) vanish in the decoupling limit $\cos(\beta - \alpha) = 0$, $m_A, m_H \to \infty$. The NP effects in D^0–$\bar{D}^0$ oscillations are suppressed by the tiny up quark mass. We have explicitly checked that D^0–$\bar{D}^0$ oscillations do not lead to relevant constraints.

In the case that the heavy Higgs masses are below the TeV scale, the NP effects in the mixing observables do not vanish, and we proceed to investigate the size of such effects. For the following numerical study, we will set the heavy Higgs masses to a benchmark value, $m_H = m_A = 500$ GeV. We use a moderate value of $\tan\beta = 5$, and work in the alignment limit $\beta - \alpha = \pi/2$. For the benchmark parameters in Eq. (3.27), we show the NP contributions to meson mixing observables in the last column of Table 3.2. For the benchmark point, the NP contributions are in most cases within the combined experimental and SM uncertainties.

Similar to Eq. (3.28), we construct a $X^2_{\rm loop}$ function, that compares the NP contributions to the difference of the data and SM predictions, for the three mass differences ΔM_K, ΔM_d, and ΔM_s, as well as the CP violating observables ϵ_K, ϕ_d, and ϕ_s. That is,

$$X^2_{\rm loop} = \sum_{i=K,d,s} \left[\frac{(\Delta M_i^{\rm NP} - \Delta M_i^{\text{exp-SM}})^2}{(\sigma_{\Delta M_i^{\rm exp}})^2 + (\sigma_{\Delta M_i^{\rm SM}})^2} \right] + \sum_{i=d,s} \left[\frac{(\phi_i^{\rm NP} - \phi_i^{\text{exp-SM}})^2}{(\sigma_{\phi_i^{\rm exp}})^2 + (\sigma_{\phi_i^{\rm SM}})^2} \right] + \frac{(\epsilon_K^{\rm NP} - \epsilon_K^{\text{exp-SM}})^2}{(\sigma_{\epsilon_K^{\rm exp}})^2 + (\sigma_{\epsilon_K^{\rm SM}})^2} , \tag{3.35}$$

where the superscript 'exp-SM' indicates that we are using the difference of the measured

values and the SM predictions given in Table 3.2.

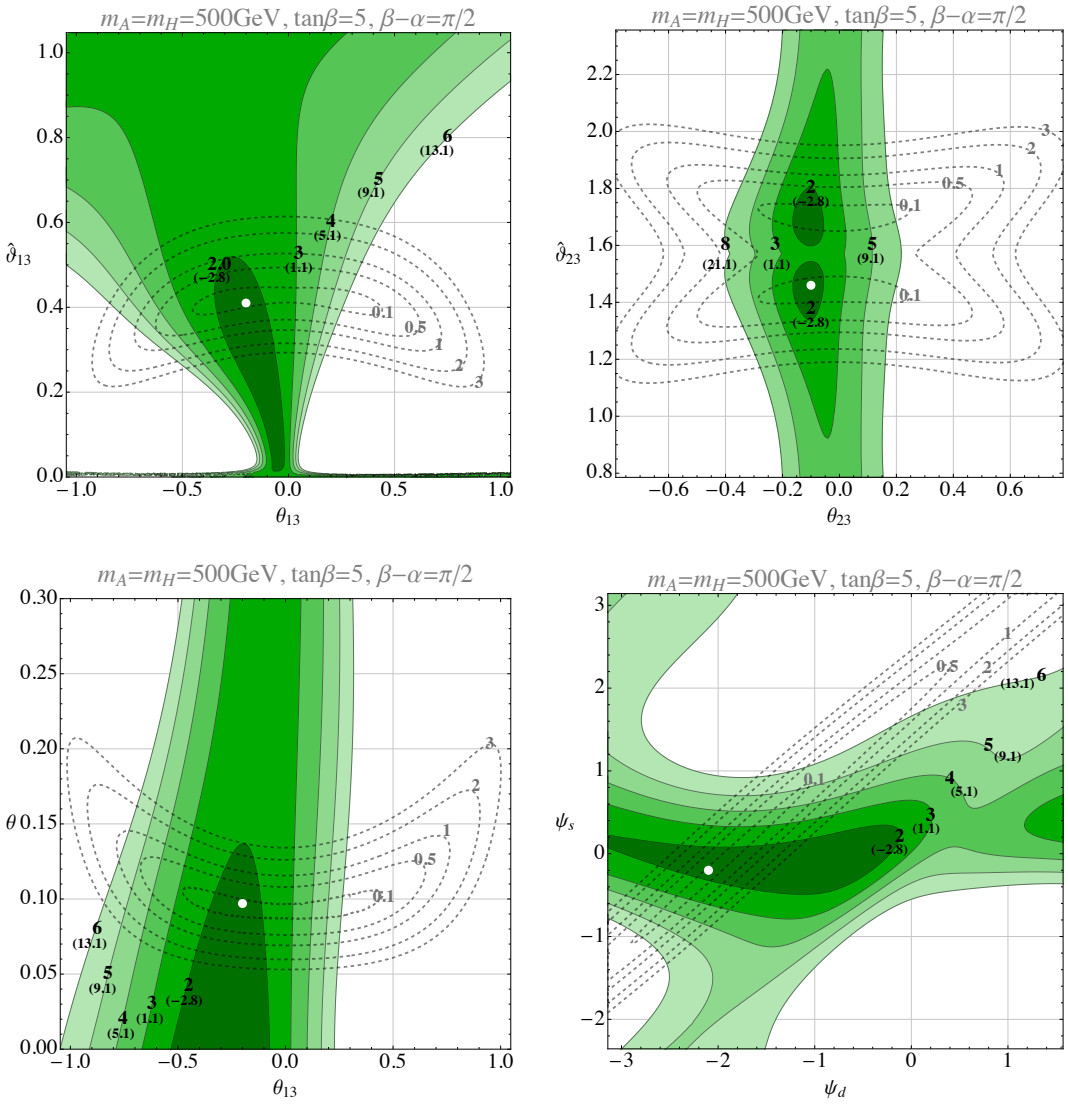

Figure 3.2: $X^2_{\text{loop}}/\text{dof}$ regions on various two-dimensional slices of the 1+2 flavor-locked theory parameter space in the neighborhood of the benchmark point (3.27). Contour values are labeled in black; we also show the values for $X^2_{\text{loop}} - X^2_{\text{loop}}(\text{SM})$ in parentheses. The benchmark point (3.27) is shown by the white circle. The contours from Fig. 3.1 are shown by the dotted lines with the corresponding contours labeled in gray.

Fig. 3.2 shows the $X^2_{\text{loop}}/\text{dof}$ behavior of the flavor model on various two-dimensional parametric slices in the neighborhood of the benchmark point (3.27). As for Fig. 3.1, on each slice all theory parameters are fixed to the benchmark values (3.27), except for the

two parameters corresponding to the plot axes. The number of degrees of freedom in the $X^2_{\rm loop}$ statistic is then $6-2=4$. Note that the SM predictions and experimental results for meson mixing observables from Table 3.2 show slight tensions [210, 212, 213], as indicated by the non-negligible SM contribution to the $X^2_{\rm loop}$ function, $X^2_{\rm loop}({\rm SM}) \simeq 10.8$. We observe that ranges of model parameters exist for which X^2 is mildly better than in the SM: At our benchmark $X^2_{\rm loop} - X^2_{\rm loop}({\rm SM}) \simeq -3.7$. (Identifying all regions of parameter space of our framework that can address existing tensions in meson observables is left for future studies.) Moreover, comparing with the contours obtained from the $X^2_{\rm tree}/{\rm dof}$ function (dotted lines), we find that extended regions of parameter space exist where CKM elements and masses as well as meson mixing observables are described in a satisfactory way.

3.5 Conclusion and outlook

We have presented a new framework to address the SM flavor puzzle, synthesizing the structure of the 'flavorful' 2HDM with the 'flavor-locking' mechanism. This mechanism makes use of distinct flavon and hierarchon sectors to dynamically generate arbitrary quark mass hierarchies, without assigning additional symmetries to the quark fields themselves. In this chapter, we have shown that with suitable symmetry assignments in the flavon and hierarchon sectors, the global minimum of the general renormalizable flavon potential can be identified with a 'flavor-locked' configuration: An aligned, rank-1 configuration for each flavon, and arbitrary (block) unitary misalignment between the up and down quark Yukawas, so that a unique hierarchon vev controls each quark mass.

In the presence of only one SM-like Higgs doublet, this leads to quark mixing angles that are generically $\mathcal{O}(1)$. Introducing instead a flavorful 2HDM Higgs sector – two Higgs doublets, such that one Higgs couples only to the third generation, while the other couples to the first two generations – leads to a $1+2$ flavor-locked theory. We find that quark flavor mixing in this theory is naturally hierarchical too, once one requires

that the dynamically-generated quark masses are themselves hierarchical – the light quark masses need not be tuned in this theory, being generated instead by the flavor-blind flavor-locking portal to the hierarchon sector – and the mixing is generically of the observed size. The collider phenomenology of this theory is quite rich if the additional Higgs bosons are light, with testable signatures at the LHC or HL-LHC.

For an example benchmark point in the theory parameter space, we showed that this 'flavor-locked flavorful 2HDM' model does not require significant tunings in order to reproduce the observed mass, CKM and meson mixing data. In particular, $\mathcal{O}(1)$ variations in model parameters do not substantially or rapidly vary the agreement with the order of the observed CKM matrix, or, in other words, the hierarchical quark mixing is stable over $\mathcal{O}(1)$ variations in the parameters of the theory. By contrast, the SM features naively seven tunings: the five lighter quark masses, and the mixing angles θ_{23} and θ_{13} in the standard CKM parametrization, that produce small $|V_{cb}|$ and $|V_{ub}|$, respectively.

The reduced amount of tuning of the quark masses and CKM mixing in the flavor-locked flavorful 2HDM does not come at the price of large NP contributions to meson mixing, even if the additional neutral Higgs bosons are light: $\mathcal{O}(1)$ variation of the flavor parameters does not lead to a significant deviation in meson mixing observables for heavy Higgs boson masses at around the electro-weak scale (e.g. $m_A \sim m_H \sim 500$ GeV) and moderate $\tan\beta$ (e.g. $\tan\beta \sim 5$), and may in fact better accommodate current meson mixing data than the SM itself. Further exploration of the flavor phenomenology of this theory is left for future studies.

It is straightforward to extend this framework to the charged lepton sector. Possible ways to reproduce a realistic normal or inverted neutrino spectrum and the large neutrino mixing angles will be discussed elsewhere.

Chapter 4

Rare Top Decays as Probes of Flavorful Higgs Bosons

4.1 Introduction

In this chapter, we will explore the effects of the F2HDM on rare top quark decays $t \to hu$ and $t \to hc$, where h is the SM-like Higgs. Flavor-changing neutral current (FCNC) decays of the top quark appear at one-loop in the Standard Model (SM) and are strongly suppressed by the Glashow-Iliopoulos-Maiani (GIM) mechanism [214] and the small mixing of the third generation quarks with the first and second generations. In particular, the branching ratios of the rare decays $t \to hc$ and $t \to hu$ in the SM are predicted to be $\mathcal{O}(10^{-15})$ and $\mathcal{O}(10^{-17})$ [215,216], respectively, which renders these processes unobservable in the foreseeable future [1,217–221]. Observation of such processes at current or planned colliders would be a clear signal of physics beyond the SM.

In the previous two chapters, we considered a setup where the CKM matrix originates in the down quark sector, i.e. the CKM matrix is largely given by the matrix that diagonalizes the down quark Yukawa couplings. Such a setup is a natural choice given the hierarchies in the down quark masses and the CKM matrix elements are comparable,

$V_{us} \sim m_d/m_s$, $V_{cb} \sim m_s/m_b$, $V_{ub} \sim m_d/m_b$. Such setups can lead to enhanced flavor violating couplings of the Higgs bosons to down type quarks, resulting in potentially interesting effects in B meson oscillations and rare B decays. Rare top decays, however, tend to be strongly suppressed. In this work we will instead explore setups in which the CKM matrix is generated in the up quark sector, which can lead to enhanced tree level flavor violating couplings of the Higgs bosons to up type quarks. These couplings can produce branching ratios for the rare top quark decays $t \to hu$ and $t \to hc$ that are orders of magnitudes greater than the SM predictions, and can be within reach of current and future colliders.

Because the mass hierarchies in the up quark sector are rather different than those in the down quark sector, the flavor-locking mechanism [194, 222] is not suitable for generating the CKM matrix in the up sector. Thus, we will consider a scenario where the required up Yukawa textures are dynamically generated by a Froggatt-Nielsen (FN) type mechanism [223].

The chapter is structured as follows. In Sec. 4.2 we discuss F2HDMs with a CKM matrix that originates in the up sector and identify a setup that dynamically generates the required flavor structure of the up Yukawa using the FN mechanism. In Sec. 4.3 we consider the stringent constraints on the model from the rare decay $b \to s\gamma$. In Sec. 4.4 we first update the SM predictions for the branching ratios of the rare decays $t \to hu$ and $t \to hc$. We then study how these decays are affected by the tree-level flavor-changing Higgs couplings htc and htu and compare the F2HDM predictions for the $t \to hu$ and $t \to hc$ branching ratios with existing and expected experimental sensitivities. In Sec. 4.5 we discuss related effects of the model on neutral D meson mixing and the collider phenomenology of the heavy Higgs bosons, identifying features that are different from the down type F2HDMs studied in [201, 224]. We conclude in Sec. 4.6.

4.2 Flavorful 2HDMs with Up Sector CKM

In a generic 2HDM the interactions of the two Higgs doublets, Φ and Φ' (with vevs v and v'), with the SM quarks and leptons are described by the Yukawa Lagrangian

$$-\mathcal{L}_{\text{Yuk}} = \sum_{i,j} \Big(\lambda^u_{ij}(\overline{Q}_i u_j)\tilde{\Phi} + \lambda^d_{ij}(\overline{Q}_i d_j)\Phi + \lambda^e_{ij}(\bar{\ell}_i e_j)\Phi + \lambda'^u_{ij}(\overline{Q}_i u_j)\tilde{\Phi}' + \lambda'^d_{ij}(\overline{Q}_i d_j)\Phi' + \lambda'^e_{ij}(\bar{\ell}_i e_j)\Phi' \Big) + \text{ h.c. }, \tag{4.1}$$

where $\tilde{\Phi}^{(\prime)} = i\sigma_2(\Phi^{(\prime)})^*$, q_i, ℓ_i are the three generations of the left-handed quark and lepton doublets, and u_i, d_i, e_i are the three generations of right-handed up quark, down quark, and charged lepton singlets. Generically, the Yukawa matrices $\lambda^{(\prime)u,d,\ell}$ will contain off-diagonal entries that generate flavor-violating processes at tree-level. In order to avoid tensions with low energy flavor constraints, one often imposes a discrete $\mathbb{Z}_2$ symmetry on the Higgs and quark fields such that the couplings of the Higgs bosons are flavor diagonal, leading to the well studied 2HDMs with natural flavor conservation: type I, type II, flipped, and lepton-specific [133].

A 'flavorful' 2HDM, as introduced in [84, 224], does not impose these discrete symmetries and instead assumes that one set of the Yukawa couplings are rank 1, preserving a $U(2)^5$ symmetry acting on the first two generations that is minimally broken by the second set of Yukawa couplings. In this way, flavor transitions between the first and second generations are protected and appear only at second order as an effective transition. In [224] four such models we identified, that, in analogy to the models with $\mathbb{Z}_2$ symmetry, were denoted by type IB, type IIB, flipped B, and lepton-specific B 2HDMs. In tab. 4.1 we summarize which Higgs boson is primarily responsible for generating the masses of each fermion.

In addition to reproducing the observed quark masses, the F2HDMs also need to accommodate the CKM quark mixing matrix. The CKM matrix arises from the mismatch of rotations of left-handed up and down type quarks when rotating into the

Model	u, c	t	d, s	b	e, μ	τ
Type 1B	Φ'	Φ	Φ'	Φ	Φ'	Φ
Type 2B	Φ'	Φ	Φ	Φ'	Φ	Φ'
Flipped B	Φ'	Φ	Φ	Φ'	Φ'	Φ
Lepton-Specific B	Φ'	Φ	Φ'	Φ	Φ	Φ'

Table 4.1: Dominant source of mass for the SM fermions in F2HDMs.

quark mass eigenstate basis. The CKM matrix can originate dominantly from the rotations in the up quark sector or from those in the down quark sector. In previous studies [84, 201, 222, 224] the CKM matrix was generated in the down quark sector. In this work we will instead generate the CKM matrix in the up quark sector.

Since the hierarchies in the up quark masses are different than those in the CKM matrix, the flavor-locking mechanism is not suitable for generating appropriate Yukawa textures for an "up type" F2HDM. We will therefore use the Froggatt-Nielsen mechanism, which explains the hierarchy of quark masses and mixing by introducing an abelian flavor symmetry – which we will denote by $U(1)_{\rm FN}$ – that distinguishes different fermion flavors. The flavor symmetry is broken by the vev of a SM-singlet scalar field, S, that carries a $U(1)_{\rm FN}$ charge $Q_S = +1$. This breaking is communicated to the SM fermions by higher dimensional operators leading to Yukawa couplings that are suppressed by powers of a small symmetry-breaking parameter $\epsilon = \langle S \rangle / \Lambda_S$, where $\Lambda_S \gg v, v'$ is the scale associated with the breaking of $U(1)_{\rm FN}$. In the resulting effective theory, the Yukawa Lagrangian is given by [1]

$$-\mathcal{L}_{\rm Yuk}^{\rm eff} \supset \sum_{i,j} \left[\left(\frac{\langle S \rangle}{\Lambda_S} \right)^{|x_{ij}^u|} (\overline{Q}_i u_j) \tilde{\Phi} + \left(\frac{\langle S \rangle}{\Lambda_S} \right)^{|x_{ij}'^u|} (\overline{Q}_i u_j) \tilde{\Phi}' \right], \tag{4.2}$$

where the powers $x_{ij}^{(\prime)u}$ are determined from the charge assignments of the Higgs and

[1] Here we only describe the up quark sector, but an analogous discussion applies for down quarks and leptons as well.

quark fields under $U(1)_{\rm FN}$, and we have omitted model dependent prefactors of $O(1)$. In terms of the parameter $\epsilon \approx 0.22$ we aim for the following relations for the quark masses and the CKM matrix elements

$$\begin{aligned} &\frac{m_u}{v_{\rm w}} \sim \epsilon^8 \ , \quad \frac{m_c}{v_{\rm w}} \sim \epsilon^3 \ , \quad \frac{m_t}{v_{\rm w}} \sim \epsilon^0 \ , \quad \frac{m_d}{v_{\rm w}} \sim \epsilon^7 \ , \quad \frac{m_s}{v_{\rm w}} \sim \epsilon^5 \ , \quad \frac{m_b}{v_{\rm w}} \sim \epsilon^3 \ , \\ &|V_{us}| \sim \lambda_c \sim \epsilon \ , \quad |V_{ub}| \sim \lambda_c^3 \sim \epsilon^3 \ , \quad |V_{cb}| \sim \lambda_c^2 \sim \epsilon^2 \ , \end{aligned} \tag{4.3}$$

with the electroweak breaking vev in the SM $v_{\rm w} = \sqrt{v^2 + v'^2} \simeq 246$ GeV and the Cabibbo angle $\lambda_c \simeq 0.22$.

In order to obtain the rank 1 structure of the Yukawa couplings of Φ required by the F2HDM scenario, we introduce an additional $U(1)'$ symmetry. A rank 1 Yukawa coupling λ_u and simultaneous generation of the CKM matrix by λ'_u is possible by charging either the left-handed quark doublet Q_3 or the right-handed top U_3 under the additional symmetry. 2HDMs with a right-handed top that is singled out by a symmetry have been discussed e.g. in [225, 226]. Here we follow the second option and set the $U(1)'$ charges $Q'_\Phi = -Q'_{Q_3} = +1$, while leaving the right-handed top uncharged. We will see that this leads to highly predictive scenarios.

The remaining charge assignments depend on the type of F2HDM under consideration as well as on the value of the parameter $\tan\beta = v/v'$ that can provide part of the fermion mass hierarchies. We restrict the following discussion to the quark sector. The extension to charged leptons is straight forward.

Type IB and Lepton-Specific B: In these types, the coupling of Φ to both up type and down type quarks are rank 1. Given our choice of $U(1)'$ charges discussed above, the charge of the right-handed bottom quark is required to be $Q'_{d_3} = -2$. While all other quarks remain uncharged under the $U(1)'$. For a given value of $\tan\beta$, the scaling in (4.3) fixes all $U(1)_{\rm FN}$ Froggatt-Nielsen charges up a few discrete choices. In Tab. 4.2 we show all inequivalent charge assignments in the cases $\tan\beta \sim 1/\epsilon \sim 5$ and $\tan\beta \sim 1/\epsilon^2 \sim 25$. The charge assignments lead to the following structure for the

	S	Φ	Φ'	$\overline{Q}_1$	$\overline{Q}_2$	$\overline{Q}_3$	u_1	u_2	u_3	d_1	d_2	d_3
$\tan\beta \sim 1/\epsilon$ $U(1)_{\rm FN}$	1	0	0	2	1	0	5 or -9	1	0	4 or -8	3	± 3
$\tan\beta \sim 1/\epsilon^2$ $U(1)_{\rm FN}$	1	0	0	1	0	0	5 or -7	1	0	4 or -6	3	± 3
$U(1)'$	0	1	0	0	0	1	0	0	0	0	0	-2

Table 4.2: Charges of the Froggatt-Nielsen scalar S, the two Higgs doublets Φ and Φ' and quark fields under the $U(1)_{\rm FN}$ and $U(1)'$ symmetries in the type IB and lepton-specific B models for the two choices of $\tan\beta \sim 1/\epsilon$ and $\tan\beta \sim 1/\epsilon^2$.

Yukawa couplings

$$v\lambda_u \sim v_{\rm w} \begin{pmatrix} 0 & 0 & 0 \\ 0 & 0 & 0 \\ \epsilon^{|a|} & \epsilon^1 & 1 \end{pmatrix}, \qquad v'\lambda'_u \sim v_{\rm w} \begin{pmatrix} \epsilon^8 & \epsilon^4 & \epsilon^3 \\ \epsilon^{|b|} & \epsilon^3 & \epsilon^2 \\ 0 & 0 & 0 \end{pmatrix}, \tag{4.4a}$$

$$v\lambda_d \sim v_{\rm w} \begin{pmatrix} 0 & 0 & 0 \\ 0 & 0 & 0 \\ 0 & 0 & \epsilon^3 \end{pmatrix}, \qquad v'\lambda'_d \sim v_{\rm w} \begin{pmatrix} \epsilon^7 & \epsilon^6 & 0 \\ \epsilon^{|c|} & \epsilon^5 & 0 \\ 0 & 0 & 0 \end{pmatrix}, \tag{4.4b}$$

with the powers $|a| = 5$ or 7 or 9, $|b| = 7$ or 9, and $|c| = 6$ or 8, depending on the charge assignments and $\tan\beta$. It is easy to check that the diagonalization of the quark masses that are induced by these Yukawa couplings leads to a CKM matrix with the right texture that is indeed dominantly generated from the up quark rotation. Interestingly, the powers $|a|$, $|b|$, and $|c|$ are not observable in the IR. More importantly, in the quark mass eigenstate basis, the flavor structure of all couplings of the Higgs bosons are entirely determined by the known quark masses and CKM elements. The couplings of

the physical Higgs mass eigenstates $h, H, A, H^\pm$ to the quarks can be parameterized by

$$\begin{aligned} -\mathcal{L}_{\text{Yuk}} \supset & \sum_{i,j} (\bar{d}_i P_R d_j) \Big(h (Y_h^d)_{ij} + H (Y_H^d)_{ij} - iA (Y_A^d)_{ij} \Big) + \text{h.c.} \\ & + \sum_{i,j} (\bar{u}_i P_R u_j) \Big(h (Y_h^u)_{ij} + H (Y_H^u)_{ij} + iA (Y_A^u)_{ij} \Big) + \text{h.c.} \\ & + \sqrt{2} \sum_{i,j} \Big((\bar{d}_i P_R u_j) H^- (Y_\pm^u)_{ij} - (\bar{u}_i P_R d_j) H^+ (Y_\pm^d)_{ij} \Big) + \text{h.c.} \, . \end{aligned} \tag{4.5}$$

For all charge assignments we find for the up quark couplings

$$v_{\text{w}} Y_h^u = \frac{c_\alpha}{s_\beta} \begin{pmatrix} 0 & 0 & 0 \\ 0 & 0 & 0 \\ 0 & 0 & m_t \end{pmatrix} - \frac{s_\alpha}{c_\beta} \begin{pmatrix} m_u & 0 & 0 \\ 0 & m_c & 0 \\ 0 & 0 & 0 \end{pmatrix} + \frac{c_{\beta-\alpha}}{s_\beta c_\beta} \widehat{M}_u \, , \tag{4.6a}$$

$$v_{\text{w}} Y_H^u = \frac{1}{t_\beta} \frac{s_\alpha}{c_\beta} \begin{pmatrix} 0 & 0 & 0 \\ 0 & 0 & 0 \\ 0 & 0 & m_t \end{pmatrix} + t_\beta \frac{c_\alpha}{s_\beta} \begin{pmatrix} m_u & 0 & 0 \\ 0 & m_c & 0 \\ 0 & 0 & 0 \end{pmatrix} - \frac{s_{\beta-\alpha}}{s_\beta c_\beta} \widehat{M}_u \, , \tag{4.6b}$$

$$v_{\text{w}} Y_A^u = -\frac{1}{t_\beta} \begin{pmatrix} 0 & 0 & 0 \\ 0 & 0 & 0 \\ 0 & 0 & m_t \end{pmatrix} + t_\beta \begin{pmatrix} m_u & 0 & 0 \\ 0 & m_c & 0 \\ 0 & 0 & 0 \end{pmatrix} - \frac{1}{s_\beta c_\beta} \widehat{M}_u \, , \tag{4.6c}$$

$$v_{\text{w}} Y_\pm^u = -\frac{1}{t_\beta} \begin{pmatrix} 0 & 0 & 0 \\ 0 & 0 & 0 \\ m_u V_{ub}^* & m_c V_{cb}^* & m_t V_{tb}^* \end{pmatrix} + t_\beta \begin{pmatrix} m_u V_{ud}^* & m_c V_{cd}^* & m_t V_{td}^* \\ m_u V_{us}^* & m_c V_{cs}^* & m_t V_{ts}^* \\ 0 & 0 & 0 \end{pmatrix} , \tag{4.6d}$$

and for the down quark couplings

$$v_{\rm w} Y_h^d = \frac{c_\alpha}{s_\beta}\begin{pmatrix} 0 & 0 & 0 \\ 0 & 0 & 0 \\ 0 & 0 & m_b \end{pmatrix} - \frac{s_\alpha}{c_\beta}\begin{pmatrix} m_d & 0 & 0 \\ 0 & m_s & 0 \\ 0 & 0 & 0 \end{pmatrix}, \tag{4.7a}$$

$$v_{\rm w} Y_H^d = \frac{1}{t_\beta}\frac{s_\alpha}{c_\beta}\begin{pmatrix} 0 & 0 & 0 \\ 0 & 0 & 0 \\ 0 & 0 & m_b \end{pmatrix} + t_\beta \frac{c_\alpha}{s_\beta}\begin{pmatrix} m_d & 0 & 0 \\ 0 & m_s & 0 \\ 0 & 0 & 0 \end{pmatrix}, \tag{4.7b}$$

$$v_{\rm w} Y_A^d = -\frac{1}{t_\beta}\begin{pmatrix} 0 & 0 & 0 \\ 0 & 0 & 0 \\ 0 & 0 & m_b \end{pmatrix} + t_\beta \begin{pmatrix} m_d & 0 & 0 \\ 0 & m_s & 0 \\ 0 & 0 & 0 \end{pmatrix}, \tag{4.7c}$$

$$v_{\rm w} Y_\pm^d = -\frac{1}{t_\beta}\begin{pmatrix} 0 & 0 & V_{ub} m_b \\ 0 & 0 & V_{cb} m_b \\ 0 & 0 & V_{tb} m_b \end{pmatrix} + t_\beta \begin{pmatrix} V_{ud} m_d & V_{us} m_s & 0 \\ V_{cd} m_d & V_{cs} m_s & 0 \\ V_{td} m_d & V_{ts} m_s & 0 \end{pmatrix}, \tag{4.7d}$$

The angle α in the above expressions parameterizes the mixing between the neutral scalar Higgs bosons h and H. The mass matrix $\widehat{M}_u$ that enters the up quark couplings is given by

$$\widehat{M}_u = \begin{pmatrix} m_u |V_{ub}|^2 & m_c V_{ub} V_{cb}^* & m_t V_{ub} V_{tb}^* \\ m_u V_{cb} V_{ub}^* & m_c |V_{cb}|^2 & m_t V_{cb} V_{tb}^* \\ m_u V_{tb} V_{ub}^* & m_c V_{tb} V_{cb}^* & -m_t (|V_{cb}|^2 + |V_{ub}|^2) \end{pmatrix}. \tag{4.8}$$

The proof that the flavor structure of the Higgs couplings in the type IB and lepton-specific B models is indeed entirely determined by known quark masses and CKM elements is given in the appendix B.1. Note that the neutral Higgs couplings are flavor

		S	Φ	Φ'	$\overline{Q}_1$	$\overline{Q}_2$	$\overline{Q}_3$	u_1	u_2	u_3	d_1	d_2	d_3
$\tan\beta \sim 1/\epsilon$	$U(1)_{\rm FN}$	0	0	0	0	+1	+2	-7	-3	-2	-7	-6	-4
	$U(1)'$	0	+1	-1	+1	+1	-1	0	0	0	0	0	0

Table 4.3: Example charges of the Froggatt-Nielsen scalar S, the two Higgs doublets Φ and Φ' and quark fields under the $U(1)_{\rm FN}$ and $U(1)'$ symmetries in the type IIB and lepton-specific B models for $\tan\beta \sim 1/\epsilon$.

diagonal in the down sector. Therefore, there are no tree level contributions to e.g. B and K meson oscillations and rare B meson decays. In the up sector, the neutral Higgs couplings are flavor violating but the amount of flavor violation is controlled by the CKM matrix. Remarkably, the only free parameters in the couplings are $\tan\beta$ and the Higgs mixing angle α, making the type IB and lepton-specific B models with up-sector CKM highly predictive.

Type IIB and Flipped B: In these types, the coupling of Φ to the up type quarks and the coupling of Φ' to the down type quarks are rank 1. We find that with our $U(1)'\times U(1)_{\rm FN}$ setup, it is not possible to construct Yukawa matrices for the down type quarks that exactly mirror the couplings in Eq. (4.4b), but with the role of λ^d and λ'^d exchanged.

However, we find that the λ'^d couplings can still be made rank 1, with a consistent flavor structure as long as $\tan\beta \sim 1/\epsilon \sim 5$. In contrast to the type IB and lepton-specific B setups discussed above, we find that λ^d and λ'^d necessarily contain mixing between the third and the first two generations. One example set of charges is given in Tab. 4.3 which leads to

$$v\lambda_u \sim v_{\rm w}\begin{pmatrix} 0 & 0 & 0 \\ 0 & 0 & 0 \\ \epsilon^5 & \epsilon^1 & \epsilon^0 \end{pmatrix}, \qquad v'\lambda'_u \sim v_{\rm w}\begin{pmatrix} \epsilon^8 & \epsilon^4 & \epsilon^3 \\ \epsilon^7 & \epsilon^3 & \epsilon^2 \\ 0 & 0 & 0 \end{pmatrix}, \tag{4.9a}$$

$$v\lambda_d \sim v_{\rm w} \begin{pmatrix} \epsilon^7 & \epsilon^6 & \epsilon^4 \\ \epsilon^6 & \epsilon^5 & \epsilon^3 \\ 0 & 0 & 0 \end{pmatrix}, \qquad v'\lambda'_d \sim v_{\rm w} \begin{pmatrix} 0 & 0 & 0 \\ 0 & 0 & 0 \\ \epsilon^6 & \epsilon^5 & \epsilon^3 \end{pmatrix}. \tag{4.9b}$$

The more generic structure of the down quark Yukawas implies that the CKM matrix is partly generated also from the rotations in the down sector. Correspondingly, in the type IIB and flipped B models only the generic scaling of the couplings of the physical Higgs bosons can be predicted. The precise values of the physical Higgs couplings depend on unknown $O(1)$ parameters.

As we will see in Sec. 4.3, constraints from the rare decay $B \to X_s\gamma$ push the masses of the additional Higgs bosons to uninterestingly large values in the type IIB and flipped B models. We therefore forgo an in-depth discussion of constructing the mass matrices and couplings in those types.

4.3 Constraints from Rare B Decays

As discussed in the previous section, in the type IB and lepton-specific B models the neutral Higgs bosons couple to down type quarks in a flavor diagonal way. Many constraints from FCNCs in the down quark sector are therefore automatically avoided. There is one important exception: the $b \to s\gamma$ decay. We find that 1-loop contributions from charged Higgs bosons can lead to sizable NP effects in the $b \to s\gamma$ transition.[2] Both the SM prediction [227] and the experimental measurements of the $B \to X_s\gamma$ rate [209] have uncertainties of less than 10% and are in good agreement with each other, resulting in strong constraints on non-standard effects.

The new physics effects induced by charged Higgs loops can be described by modi-

[2]We also checked 1-loop charged Higgs contributions to the $B_s \to \mu^+\mu^-$ decay and tree level charged Higgs contributions to the $B \to \tau\nu$ and $B \to D^{(*)}\tau\nu$ decays and found that they are negligible in regions of parameter space that are allowed by $b \to s\gamma$.

fications of the Wilson coefficients C_7 and C_8 of an effective Hamiltonian

$$\mathcal{H}_{\text{eff}}^{\text{NP}} = -\frac{4G_F}{\sqrt{2}} V_{tb} V_{ts}^* \frac{e^2}{16\pi^2} \left(\Delta C_7 Q_7 + \Delta C_8 Q_8\right) \ , \tag{4.10}$$

with the dipole operators

$$Q_7 = \frac{1}{e} m_b (\bar{s}\sigma_{\mu\nu} P_R b) F^{\mu\nu} \ , \quad Q_8 = \frac{g_s}{e^2} (\bar{s}\sigma_{\mu\nu} T^a P_R b) G_a^{\mu\nu} \ , \tag{4.11}$$

Using the results from [228] we find for the charged Higgs contribution in the type IB and lepton-specific B scenarios

$$\Delta C_7 = \frac{m_t^2}{m_{H^\pm}^2} f_7\left(\frac{m_t^2}{m_{H^\pm}^2}\right) \ , \tag{4.12a}$$

$$\Delta C_8 = \frac{m_t^2}{m_{H^\pm}^2} f_8\left(\frac{m_t^2}{m_{H^\pm}^2}\right) \ . \tag{4.12b}$$

In the type IIB and flipped B scenarios the Wilson coefficients are only determined up to model dependent $O(1)$ factors

$$\Delta C_7 = O(1) \times \left(\frac{m_t^2}{m_{H^\pm}^2} g_7\left(\frac{m_t^2}{m_{H^\pm}^2}\right) + \tan^2\beta \frac{m_t^2}{m_{H^\pm}^2} h_7\left(\frac{m_t^2}{m_{H^\pm}^2}\right)\right) \ , \tag{4.13a}$$

$$\Delta C_8 = O(1) \times \left(\frac{m_t^2}{m_{H^\pm}^2} g_8\left(\frac{m_t^2}{m_{H^\pm}^2}\right) + \tan^2\beta \frac{m_t^2}{m_{H^\pm}^2} h_8\left(\frac{m_t^2}{m_{H^\pm}^2}\right)\right) \ . \tag{4.13b}$$

The loop functions $f_{7,8}$, $g_{7,8}$, and $h_{7,8}$ are given in appendix B.2. Note that in our type IB and lepton-specific B scenarios the contributions are independent of $\tan\beta$, while the contributions in the type IIB and flipped B scenarios contain terms that are proportional to $\tan^2\beta$ and can become extremely large in regions of parameter space with large $\tan\beta$. This is in contrast to 2HDMs with natural flavor conservation, where the contributions are proportional to $1/\tan^2\beta$ (type I and lepton-specific) and independent of $\tan\beta$ (type II and flipped).

Using the constraints on the Wilson coefficients from $b \to s\gamma$ transitions derived in [229] and taking into account 1-loop renormalization group running between the

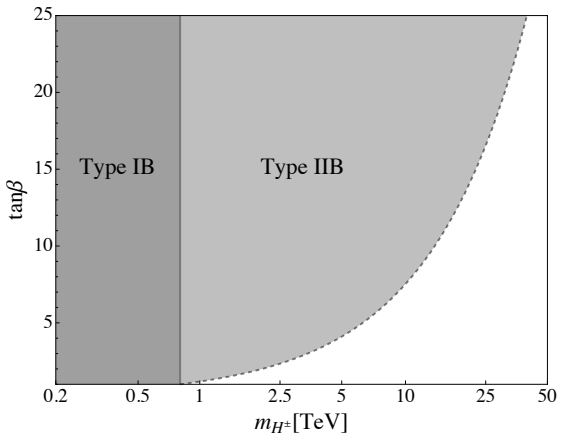

Figure 4.1: Constraints from the $b \to s\gamma$ transition in the charged Higgs mass $m_{H^\pm}$ vs. $\tan\beta$ plane. The dark gray region is excluded in the type IB and lepton-specific B scenarios at the 95% C.L. The light gray region is excluded in the type IIB and flipped B scenarios at the 95% C.L.

electroweak scale and the b scale, we find at the 95% C.L.

$$-0.032 < \eta^{\frac{16}{23}} \Delta C_7 + \frac{8}{3}\left(\eta^{\frac{14}{23}} - \eta^{\frac{16}{23}}\right) \Delta C_8 < 0.027 \ , \tag{4.14}$$

with $\eta = \alpha_s(m_t)/\alpha_s(m_b) \simeq 0.52$.

The corresponding constraints are shown in the plots of Fig. 4.1 in the charged Higgs mass $m_{H^\pm}$ vs. $\tan\beta$ plane. In the case of the type IB and lepton-specific B models, we find a $\tan\beta$ independent bound on the charged Higgs mass of $m_{H^\pm} \gtrsim 800$ GeV. In the type IIB and flipped B models, we show as illustration the case where the free $O(1)$ parameters are set to exactly 1. In these types of models, the $b \to s\gamma$ constraint is highly dependent on $\tan\beta$, e.g. $m_{H^\pm} \gtrsim 800$ GeV for $\tan\beta = 1$, but $m_{H^\pm} \gtrsim 15$ TeV for $\tan\beta = 10$. Varying the $O(1)$ coefficients shifts the exclusion line up or down by an order one factor.

Note that because of the $SU(2)_L$ gauge symmetry, the masses of the heavy scalar and pseudoscalar Higgs differ from the charged Higgs mass only by a small amount: $m_H \simeq m_A \simeq m_{H^\pm}$ with splittings of the order of $v^2/m^2_{H^\pm} \lesssim 10\%$. The bounds on the

charged Higgs mass from $b \to s\gamma$ therefore hold approximately for the masses of the heavy scalar and pseudoscalar Higgs as well.

As discussed in Sec. 4.2, for the purpose of generating the fermion mass hierarchy we have in mind values of $\tan\beta \sim 1/\lambda_c \sim 5$ or $\tan\beta \sim 1/\lambda_c^2 \sim 25$. In the type IIB and flipped B models, we see that the $b \to s\gamma$ constraints therefore strongly disfavor Higgs bosons with masses at the TeV scale. This remains true even if we take into account generous choices of the free $O(1)$ parameters. With this in mind we focus our remaining analysis on the type IB and lepton-specific B models.

4.4 Rare Top Decays

In the SM, flavor-changing top quark decays $t \to hq$ are both loop and GIM suppressed, and are predicted to have very small branching ratios. Using the results from [230, 231] for the partial widths $\Gamma(t \to hq)$ and normalizing to the $t \to Wb$ decay width which dominates the total top width, we derive the following compact expression for the branching ratios

$$\mathrm{BR}(t \to hq)_{\mathrm{SM}} = \frac{G_F^2 m_b^4}{4\pi^4}|V_{qb}|^2 \frac{\left(1 - m_h^2/m_{t,\,\mathrm{pole}}^2\right)^2}{\left(1 - m_W^2/m_{t,\,\mathrm{pole}}^2\right)^2\left(1 + 2m_W^2/m_{t,\,\mathrm{pole}}^2\right)} \mathcal{F}\left(\frac{m_t^2}{m_W^2}, \frac{m_h^2}{m_W^2}\right) . \tag{4.15}$$

The branching ratio is suppressed by four powers of the bottom mass, as expected from GIM. We use the bottom $\overline{\mathrm{MS}}$ mass at the scale of the top $m_b(m_t) = 2.73\,\mathrm{GeV}$. Note that we are using the top pole mass in the phase space factors, but the top $\overline{\mathrm{MS}}$ mass in the loop function $\mathcal{F}$. The explicit expression for $\mathcal{F}$ is given in the appendix B.3. For central values of the Higgs mass $m_h = 125.18\,\mathrm{GeV}$ [26] and the top $\overline{\mathrm{MS}}$ mass $m_t(m_t) = 163.4\,\mathrm{GeV}$ (corresponding to a top pole mass of $m_{t,\,\mathrm{pole}} = 173.0\,\mathrm{GeV}$ [26]) we find $\mathcal{F} \simeq 0.48$. By far the largest uncertainties in the rare top branching ratios are due to the CKM factors $|V_{cb}| = (42.2 \pm 0.8) \times 10^{-3}$ [26] and $|V_{ub}| = (3.94 \pm 0.36) \times 10^{-3}$ [26] and due to higher order QCD effects that we estimate by varying the renormalization

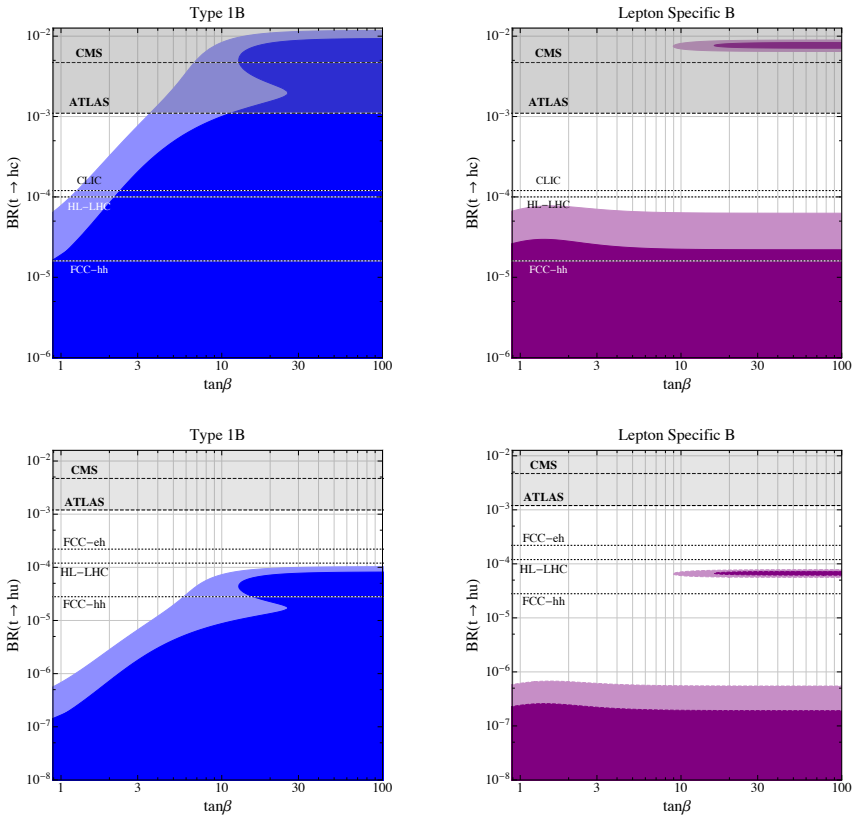

Figure 4.2: The branching ratios $t \to hc$ (top) and $t \to hu$ (bottom) as a function of $\tan\beta$ in the type IB model (left) and lepton-specific B model (right). The blue and purple shaded regions are consistent with Higgs signal strength measurements. The dashed horizontal lines labeled "ATLAS" are the current best upper bounds on the branching ratios [1]. The dotted horizontal lines are the future projections from the HL-LHC, the FCC, and CLIC.

scale of the bottom $\overline{\text{MS}}$ mass $m_b(\mu)$ in the range $m_t/2 < \mu < 2m_t$. We obtain

$$\text{BR}(t \to hu)_{\text{SM}} = (3.66^{+0.94}_{-0.70} \pm 0.67) \times 10^{-17}\,, \tag{4.16a}$$

$$\text{BR}(t \to hc)_{\text{SM}} = (4.19^{+1.08}_{-0.80} \pm 0.16) \times 10^{-15}\,, \tag{4.16b}$$

where the first uncertainty is due to the variation of the renormalization scale and the second is due to the CKM matrix elements. The current strongest experimental bounds on these decays are obtained by the ATLAS experiment, using an integrated luminosity

of 36 fb^{-1} of pp collision data with $\sqrt{s} = 13$ TeV in multi-lepton final state searches [1], and read

$$\mathrm{BR}(t \to hu) < 0.12\% \tag{4.17a}$$

$$\mathrm{BR}(t \to hc) < 0.11\%, \tag{4.17b}$$

The predicted values for these processes in the SM are far below the current sensitivities shown above. The projected sensitivities for the rare top decays at the high luminosity LHC (HL-LHC) for an integrated luminosity of 3 ab^{-1} at 14 TeV are $\mathcal{O}(10^{-4})$ [218,220]. The projections for the Future Circular Collider (FCC) indicate sensitivities comparable to the HL-LHC for the $t \to hu$ decay and about an order of magnitude stronger for the $t \to hc$ decay [221]. The Compact Linear Collider (CLIC) could also place a limit comparable to the HL-LHC for the $t \to hc$ decay [219].

The Yukawa textures in Sec. 4.2 generate flavor-changing couplings for the SM-like Higgs boson, allowing for the rare top decays to appear at tree-level. Approximating the total width of the top quark by its dominant partial decay width to a W boson and a b quark, the branching ratios of the rare decays can be written as

$$\begin{aligned}\mathrm{BR}(t \to hq) &\simeq 2|V_{qb}|^2 \frac{\cos^2(\beta-\alpha)}{\sin^2\beta\cos^2\beta} \frac{\left(1 - m_h^2/m_{t,\,\mathrm{pole}}^2\right)^2}{\left(1 - m_W^2/m_{t,\,\mathrm{pole}}^2\right)^2 \left(1 + 2m_W^2/m_{t,\,\mathrm{pole}}^2\right)} \\ &\simeq \frac{\cos^2(\beta-\alpha)}{\sin^2\beta\cos^2\beta} \times \begin{cases} 9.2 \times 10^{-4} & \text{for} \quad t \to hc\ , \\ 8.0 \times 10^{-6} & \text{for} \quad t \to hu\ . \end{cases}\end{aligned} \tag{4.18}$$

As long as $\cos(\beta - \alpha) \neq 0$, the rare top decay branching ratios can be many orders of magnitude larger than the SM values, making these processes in our model accessible to current and future colliders. If $\cos(\beta - \alpha) = 0$ (the so called alignment limit) the couplings of the 125 GeV Higgs are exactly SM-like. Deviations of $\cos(\beta - \alpha)$ from 0 are constrained by measurements of Higgs production and decays at the LHC. The constraints depend strongly on $\tan\beta$. In the appendix B.4 we show the allowed regions

in the $\cos(\beta-\alpha)$ vs. $\tan\beta$ plane, taking into account all relevant LHC results on Higgs signal strength measurements.

In Fig. 4.2 we use these allowed regions to give predictions for the rare top branching ratios as a function of $\tan\beta$ in the type IB model (left) and lepton-specific B model (right). The region in gray is excluded by the current ATLAS limits, while the dotted horizontal lines correspond to projected sensitives from the HL-LHC [220], the FCC [221], and CLIC [219].

In the lepton-specific B model, we observe two disjoint regions of parameter space. The upper region opens up for $\tan\beta \gtrsim 10$ and corresponds to a scenario where some of the Higgs couplings differ from the SM prediction by a sign, but are otherwise equal in magnitude. Such a scenario predicts $\mathrm{BR}(t \to hu) \simeq 6\times10^{-5}$ and $\mathrm{BR}(t \to hc) \simeq 7\times10^{-3}$ and is already excluded by the existing LHC constraints from [1].

In general our models can give values for $\mathrm{BR}(t \to hu)$ and $\mathrm{BR}(t \to hc)$ that are much larger than the SM prediction, and can be in reach of current or future experimental sensitivities. In the case of $t \to hu$, the current LHC constraint from [1] does not probe the parameter space of our model. Also future projections from the the HL-LHC are unlikely to probe our model as they barely touch the region of predicted branching ratio values. The FCC-hh will start to cut into interesting parameter space of $t \to hu$ with a projected sensitivity of the order 10^{-5}.

For the $t \to hc$ decay channel, the current LHC constraints already probe part of our model parameter space for moderate to large values of $\tan\beta \gtrsim 10$. Projections from the HL-LHC and CLIC will be also sensitive to parameter space with much lower choices of $\tan\beta$.

4.5 Related Signatures

Although the primary motivation for this model is to explore enhanced $t \to hq$ decays, the flavor structure of the up Yukawa couplings leads to other interesting features

and signatures. We examine possible effects on D meson mixing that arise from tree-level exchange of neutral Higgs bosons. We also consider the collider phenomenology of the heavy neutral and charged Higgs bosons (H, A, $H^{\pm}$), identifying the most prominent production and decay modes.

4.5.1 Enhanced D Meson Mixing from Flavorful Higgs Bosons

In the SM, $D^0 - \bar{D}^0$ mixing proceeds through loop diagrams and is parameterized by the absolute values of the dispersive and absorptive part of the mixing amplitude, $x_{12} = 2|M_{12}^D|\tau_D$, $y_{12} = |\Gamma_{12}^D|\tau_D$, and their relative phase $\phi_{12} = \text{Arg}(M_{12}^D/\Gamma_{12}^D)$, where τ_D is the lifetime of the D^0 meson.

The current world averages for the mixing parameters are [209]

$$x_{12}^{\text{exp}} = (0.43^{+0.10}_{-0.11})\% \ , \quad y_{12}^{\text{exp}} = (0.63 \pm 0.06)\% \ , \quad \phi_{12}^{\text{exp}} = (-0.25^{+0.96}_{-0.99})^\circ \ . \tag{4.19}$$

In our model, we generically predict tree level Higgs contributions to $D^0 - \bar{D}^0$ mixing. The corresponding effect on the dispersive part of the mixing amplitude is given by

$$M_{12}^D = m_D^3 \frac{f_D^2}{v_{\text{w}}^2} \frac{(V_{cb}V_{ub}^*)^2}{s_\beta^2 c_\beta^2} \Big[\frac{1}{4} B_4 \eta_4 \Big(\frac{c_{\beta-\alpha}^2}{m_h^2} + \frac{s_{\beta-\alpha}^2}{m_H^2} + \frac{1}{m_A^2} \Big) \frac{m_u}{m_c} \\ - \Big(\frac{5}{24} B_2 \eta_2 - \frac{1}{48} B_3 \eta_3 \Big) \Big(\frac{c_{\beta-\alpha}^2}{m_h^2} + \frac{s_{\beta-\alpha}^2}{m_H^2} - \frac{1}{m_A^2} \Big) \Big] \ , \tag{4.20}$$

where the decay constant of the D^0 meson is $f_D \simeq 212\,\text{MeV}$ [232], the bag parameters are $B_2 \simeq 0.65$, $B_3 \simeq 0.96$, $B_4 \simeq 0.91$ [204], and the 1-loop renormalization group factors are $\eta_2 \simeq 0.68$, $\eta_3 \simeq -0.03$, $\eta_4 = 1$ [224]. The absorptive part Γ_{12} is unaffected in the model. The results for the mixing amplitude are independent of the type of F2HDM, they hold both in type IB and in the lepton-specific B model.

Despite the fact that the neutral Higgs bosons contribute to $D^0 - \bar{D}^0$ mixing at tree level, the approximate $SU(2)^5$ flavor symmetry of the F2HDMs ensures that their

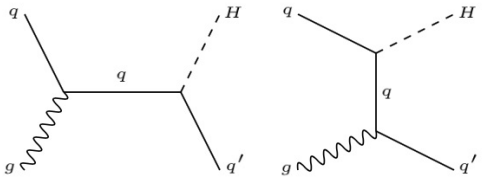

Figure 4.3: The Feynman diagrams for quark associated production of the heavy and charged Higgs bosons. In the context of F2HDMs this production mode can have a sizeable cross section due to the tree level flavor-changing neutral currents.

contributions are very small, suppressed by small quark masses and CKM matrix elements. For Higgs boson masses around 1 TeV and values of $\tan\beta$ as large as 100, we find that the NP contribution to $D^0 - \bar{D}^0$ mixing is much smaller than the uncertainties in Eq. 4.19. Improvements in precision by more than two orders of magnitude would be required to become sensitive to the predicted non-standard effects in our models.

4.5.2 Collider Phenomenology of Heavy Higgs Bosons

The F2HDMs considered here offer a rich set of phenomenological consequences. Not only do these models predict additional Higgs bosons that could be within reach of the LHC but the introduction of tree-level FCNCs means that we anticipate distinct signatures coming from the new Higgs bosons that set this model apart from more traditional 2HDMs.

Heavy Higgs Production and Decays

There are several production modes via which the heavy Higgs bosons can be produced at the LHC. Due to the enhanced off-diagonal couplings in the up quark sector we expect top associated production, see Fig. 4.3, to contribute with a sizable cross section.

In order to evaluate the production cross sections, we follow the steps described in [201, 224]. The results for the production cross sections are identical for the type IB

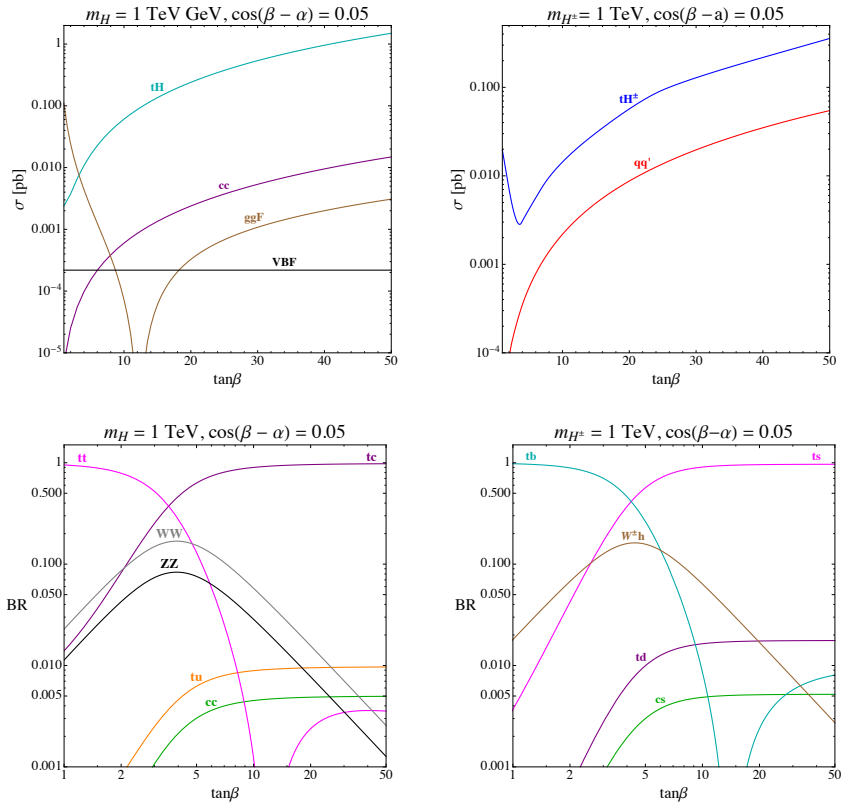

Figure 4.4: Production cross sections (top) and branching ratios (bottom) of the heavy neutral Higgs H (left) and the charged Higgs $H^\pm$ (right) in the flavorful 2HDM of type IB as a function of $\tan\beta$ with the masses m_H and $m_{H^\pm}$ fixed to 1 TeV and $\cos(\beta - \alpha) = 0.05$.

and lepton-specific B models. The cross sections of the heavy neutral Higgs H and the charged Higgs $H^\pm$ at 13 TeV proton-proton collisions as a function of $\tan\beta$ for fixed Higgs masses of 1 TeV and $\cos(\beta - \alpha) = 0.05$ are shown in the upper plots of Fig. 4.4. Small values of $\cos(\beta - \alpha) \ll 1$ are motivated by the constraints from Higgs signal strength measurements (see appendix B.4).

For the neutral scalar H, associated production with a top and gluon-gluon fusion are the dominant production modes. At low $\tan\beta$ gluon-gluon fusion is largest because the coupling to tops is unsuppressed. As $\tan\beta$ increases the gluon-gluon fusion rate drops and is overtaken by top associated production which is enhanced for large $\tan\beta$. The dominant production cross sections for the heavy pseudoscalar A are almost identical

to those of the heavy Higgs. For the charged Higgs, top associated production is the largest production mechanism over the full range of $\tan\beta$ values.

The branching ratios of the heavy neutral Higgs H and the charged Higgs $H^{\pm}$ are shown in the lower plots Fig. 4.4 in the type IB model. Results in the lepton-specific B model are almost identical. The main difference in the lepton-specific B model is the presence of a $\tau\tau$ branching ratio at the level of few percent, which is strongly suppressed in the type IB model.

As expected, for moderate to large $\tan\beta$ the dominant decay mode of H is the flavor-changing $H \to ct$. The branching ratio to $t\bar{t}$ can be substantial, however this decay mode primarily plays a role for small $\tan\beta$ which is less motivated by the quark mass hierarchy. For moderate $\tan\beta$ we also notice that the gauge bosons can contribute at a level between $1 - 10\%$. The branching ratios of the charged Higgs tend to be dominated by ts and tb decays. In particular, for low $\tan\beta$ tb dominates. Once $\tan\beta$ becomes larger than about 5 we see ts dominates for the rest of the parameter space. In addition to the most dominant decays, we see that at the level of a few percent or lower we can expect decays to $W^{\pm}h$.

Collider Signatures

The constraints on this model from existing searches for heavy Higgs boson are very weak due to the unique flavor structure. The overwhelming decay of the neutral Higgses to ct means the branching ratio to other modes is highly suppressed as seen in Fig. 4.4. Typical search channels at the LHC are through these suppressed channels, such as $\mu\mu$, $\tau\tau$, VV, and jj, making the prospects of discovering a heavy Higgs through these channels very weak. Also, the standard searches for charged Higgs bosons in the $\tau\nu$ channel hardly constrain our parameter space, due to the strongly reduced branching ratios $H^{\pm} \to \tau\nu$. Unique signatures that are relevant to collider searches of our model are driven by the large non-standard decay modes $H, A \to tc$, and $H^{\pm} \to ts$.

The charged Higgs produced via top associated production and subsequent decay

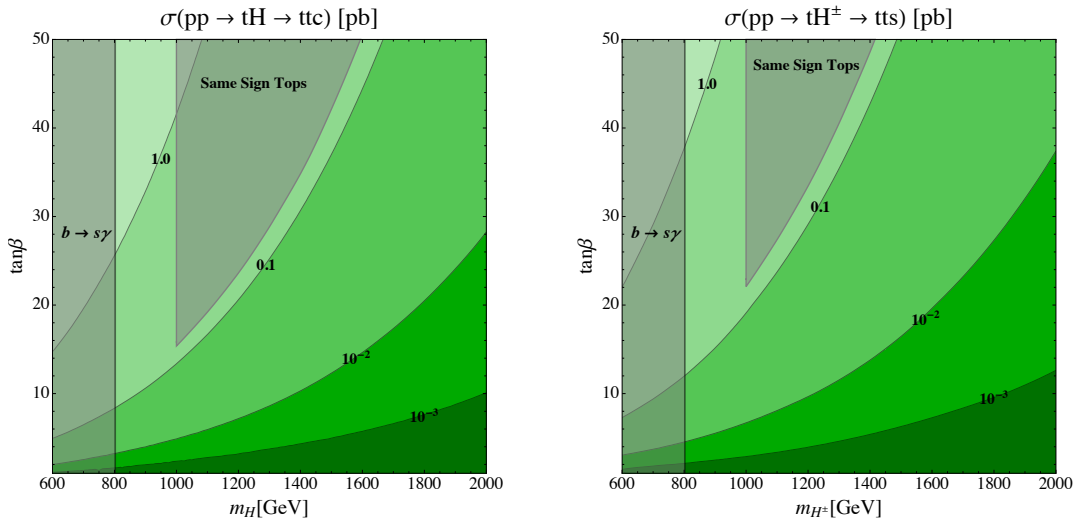

Figure 4.5: Cross section of same-sign tops plus jet from the production and decay of a neutral heavy Higgs H (left) as well as opposite-sign tops plus jet from the production and decay of a charged Higgs (right) in the considered flavorful 2HDM of type IB in the plane of Higgs mass vs. $\tan\beta$. The gray shaded regions for light Higgs masses are excluded by $b \to s\gamma$ constraints (see Sec. 4.3). The triangle shaped gray region for large $\tan\beta$ is excluded by existing searches for same-sign tops [2]. Throughout the plots we set $\cos(\beta - \alpha) = 0.05$.

to ts leads to opposite-sign tops that do not reconstruct a resonance. This is similar to charged Higgs bosons in 2HDMs with natural flavor conservation. The unique feature with respect to 2HDMs with natural flavor conservation is that the accompanying jet of the $t\bar{t}$ system is not a b-jet but a strange jet. The cross section for the $t\bar{t}$ + jet signature as a function of $\tan\beta$ and charged Higgs mass is shown in the right plot of Fig. 4.5. We find cross sections that can easily exceed 100 fb for Higgs masses of $O(1\,\text{TeV})$ and sizable $\tan\beta$. The shaded region to the left of the vertical line at Higgs masses of around 800 GeV is excluded by the constraint from $b \to s\gamma$. Existing searches for charged Higgs bosons that decay to tb [233,234] make heavy use of b-tagging and are therefore not directly applicable in our scenario. Our work motivates dedicated studies of the $pp \to tH^- \to t\bar{t}s$ signature.

The heavy neutral Higgs being produced through top associated production along

with a decay into tc leads also to a final state with di-tops that do not reconstruct a resonance. In our flavorful 2HDMs, 50% of the time the final state will be *same-sign* tops, in contrast to 2HDMs with natural flavor conservation that only produce opposite sign tops. Same-sign tops have been identified as important probes in a number of new physics scenarios, including RPV SUSY [235], 2HDMs [226, 236, 237], additional scalars [238, 239], colored vectors [240], and effective field theories [241]. The cross section of same-sign tops in our scenario is shown in the left plot of Fig. 4.5 in the plane of Higgs mass vs. $\tan\beta$. For Higgs masses of $O(1\,\text{TeV})$ we find cross sections up to 1 pb. The shaded region to the left of the vertical line at Higgs masses of around 800 GeV is excluded by the constraint from $b \to s\gamma$ assuming that $m_H \simeq m_{H^\pm}$.

In [2] searches for same-sign leptons are interpreted in a benchmark model in which same-sign tops are created by a neutral spin-1 mediator. Assuming that the acceptances and efficiencies are comparable in our scenario with a scalar mediator, we find that the large $\tan\beta$ region is already partly probed by the existing search. We show the region that is excluded by the same-sign top search also in the charged Higgs plot, assuming that $m_H \simeq m_{H^\pm}$. Keeping in mind that our $pp \to Ht \to tt\bar{c}$ cross section approximately scales as $\tan^2\beta$, we expect that parameter space with $\tan\beta$ as low as ~ 10 might be probed by same-sign top searches at the high luminosity LHC.

4.6 Conclusions

Rare top decays are strongly suppressed in the SM and their observation at existing or planned colliders would be a clear indication of new physics. One new physics framework that can lead to branching ratios of $t \to hc$ and $t \to hu$ in reach of current or future colliders are flavorful 2HDMs.

In this chapter we explored a version of flavorful 2HDM where quark mixing dominantly resides in the up quark sector, leading to FCNCs in the up quark sector at tree level. We constructed a flavor model based on $U(1)$ flavor symmetries which successfully

reproduces the measured quark masses and CKM mixing angles. We find that our model is highly predictive as the flavor structure of all Higgs couplings is fully determined by the quark masses and CKM matrix elements.

We give predictions for $t \to hc$ and $t \to hu$ rates in our model and show that the branching ratios can reach values of $\mathrm{BR}(t \to hc) \sim 10^{-2}$ and $\mathrm{BR}(t \to hu) \sim 10^{-4}$ (see Fig. 4.2) without violating constraints from Higgs signal strength measurements at the LHC. Existing bounds on $\mathrm{BR}(t \to hc)$ from the LHC already start to constrain model parameter space. Expected sensitivities at the high-luminosity LHC or future colliders will be able to probe broad regions of parameter space. In passing we also provide updated predictions for the $t \to hc$ and $t \to hu$ branching ratios in the SM (see Eq. 4.15).

We explored additional effects of the up quark FCNCs in low energy flavor violating processes. In particular, we find that 1 loop effects in the rare B decay $b \to s\gamma$ lead to strong constraints on the masses of the additional Higgs bosons of at least $\sim 800\,\mathrm{GeV}$. On the other hand, constraints from D meson mixing are weak in our setup.

Finally, we explored the phenomenology of the heavy neutral and charged Higgs bosons of the F2HDM. We find that both neutral and charged Higgses are mainly produced in association with top quarks. The by far dominant decay modes are tc and ts, respectively. These final states are not typical search channels of Higgs bosons in traditional 2HDMs. Therefore, current constraints from colliders are weak. The most prominent signatures of the models are $pp \to tH^- \to t\bar{t}s$, i.e. opposite sign tops + jet, and in particular $pp \to tH \to tt\bar{c}$, i.e. same-sign tops + jet. Cross sections of these signatures can be of the order of 100 fb for Higgs masses around 1 TeV (see Fig. 4.5). Our results in the F2HDM framework motivate continued searches for same-sign tops and provides an additional benchmark model in which future same-sign top searches can be interpreted.

Part III

Anomalies in Low Energy Physics

Chapter 5

Electric dipole moments in a leptoquark scenario for the B-physics anomalies

5.1 Introduction

Over the past several years, multiple B-physics experiments, including BaBar, LHCb, and Belle, have reported anomalies in decays associated with the $b \to c\ell\nu$ and $b \to s\ell\ell$ transitions. Violations of lepton flavor universality (LFU), known to be theoretically clean probes of New Physics (NP), are of particular interest. In the Standard Model (SM) LFU is only broken by the lepton masses. Hints for additional sources of LFU violation have been observed in the ratios of branching ratios of flavor-changing charged current and neutral current decays of B mesons, R_D, R_{D^*}, R_K, and R_{K^*},

$$R_{D^{(*)}} = \frac{\mathrm{BR}(B \to D^{(*)}\tau\nu)}{\mathrm{BR}(B \to D^{(*)}\ell\nu)}\,, \qquad R_{K^{(*)}} = \frac{\mathrm{BR}(B \to K^{(*)}\mu^+\mu^-)}{\mathrm{BR}(B \to K^{(*)}e^+e^-)}\,. \tag{5.1}$$

The experimental world averages of R_D and R_{D^*} from the heavy flavor averaging group (HFLAV) are based on measurements from BaBar [60], Belle [61–63], and LHCb [64,65],

and read [66]

$$R_D = 0.340 \pm 0.027 \pm 0.013\,, \qquad R_{D^*} = 0.295 \pm 0.011 \pm 0.008\,, \tag{5.2}$$

with an error correlation of $\rho = -38\%$. The corresponding SM predictions are known with high precision [67–69]. The values adopted by HFLAV are [66]

$$R_D^{\rm SM} = 0.299 \pm 0.003\,, \qquad R_{D^*}^{\rm SM} = 0.258 \pm 0.005\,. \tag{5.3}$$

The combined discrepancy between the SM prediction and experimental world averages of R_D and R_{D^*} is at the 3.1σ level.

The most precise measurement to date of the LFU ratio R_K has been performed by LHCb [70]

$$R_K = 0.846^{+0.060+0.016}_{-0.054-0.014}\,, \qquad \text{for} \quad 1.1\,\text{GeV}^2 < q^2 < 6\,\text{GeV}^2\,, \tag{5.4}$$

with q^2 being the dilepton invariant mass squared. The SM predicts $R_K^{\rm SM} \simeq 1$ with theoretical uncertainties well below the current experimental ones [71]. The above experimental value is closer to the SM prediction than the Run-1 result [72]. However, the reduced experimental uncertainties still imply a tension between theory and experiment of 2.5σ.

The most precise measurement of R_{K^*} is from a Run-1 LHCb analysis [73] that finds

$$R_{K^*} = \begin{cases} 0.66^{+0.11}_{-0.07} \pm 0.03\,, & \text{for } 0.045\,\text{GeV}^2 < q^2 < 1.1\,\text{GeV}^2\,, \\ 0.69^{+0.11}_{-0.07} \pm 0.05\,, & \text{for } 1.1\,\text{GeV}^2 < q^2 < 6\,\text{GeV}^2\,. \end{cases} \tag{5.5}$$

The result for both q^2 bins are in tension with the SM prediction [71], $R_{K^*}^{\rm SM} \simeq 1$, by

$\sim 2.5\sigma$ each. Recent measurements of R_{K^*} and R_K by Belle [74, 75][1]

$$R_{K^*} = \begin{cases} 0.90^{+0.27}_{-0.21} \pm 0.10\,, & \text{for } 0.1\,\text{GeV}^2 < q^2 < 8\,\text{GeV}^2\,, \\ 1.18^{+0.52}_{-0.32} \pm 0.10\,, & \text{for } 15\,\text{GeV}^2 < q^2 < 19\,\text{GeV}^2\,, \end{cases} \tag{5.6}$$

$$R_K = \begin{cases} 0.98^{+0.27}_{-0.23} \pm 0.06\,, & \text{for } 1\,\text{GeV}^2 < q^2 < 6\,\text{GeV}^2\,, \\ 1.11^{+0.29}_{-0.26} \pm 0.07\,, & \text{for } 14.18\,\text{GeV}^2 < q^2\,, \end{cases} \tag{5.7}$$

are compatible with both the SM prediction and the LHCb results. Several papers have re-analyzed the status of the B anomalies in light of the latest experimental updates, and found preference for new physics with high significance [76–82].

While the anomalies detailed upon above persist, the question of the origin of the observed baryon asymmetry [242] also remains a long standing problem in cosmology. Any dynamical explanation requires sizable C- and CP-violating interactions in the early universe [243]. In light of upcoming low-energy experiments with much greater sensitivity to electric and magnetic dipole moments of elementary particles, it is interesting to ask whether solutions to the flavor anomalies may also be associated with sizable CP violating complex phases that may be probed by these experiments.

The only known viable, single-mediator explanation of all flavor anomalies is a U_1 vector leptoquark [244–250]. This leptoquark generically introduces new sources of CP violation in the Lagrangian in the form of complex parameters [251]. The scope of the present study is to explore, for the first time, the prospects of observing electric dipole moments (EDMs) induced by a U_1 vector leptoquark that could explain the flavor anomalies reviewed above. We additionally explore collider constraints, as well as constraints from measurements of the magnetic moments, and other flavor observables. Implications for EDMs and other CPV observables in scalar leptoquark scenarios have recently been discussed in [252–258].

This chapter is organized as follows: In Sec. 5.2, we introduce the CP violating U_1

[1] Here we quote the isospin average of $B^0 \to K^{(*)0}\ell^+\ell^-$ and $B^\pm \to K^{(*)\pm}\ell^+\ell^-$ decays.

model and discuss its effects on the B-physics anomalies. In Sec. 5.3, we give an overview of the effects of the CP violating leptoquark on EDMs of quarks, leptons, and neutrons. We also include a discussion of the present status of the experimental searches and the prospects for future measurements. In Sec. 5.4, we report the main results, showing the leptoquark parameter space that can be probed by B-physics and EDM measurements. In Sec. 5.5, we discuss the LHC bounds on our leptoquark model. Finally, we reserve Sec. 5.6 for our conclusions.

5.2 The CP violating U_1 Vector Leptoquark Model

We consider the vector leptoquark $U_1 = (\mathbf{3},\mathbf{1})_{2/3}$ (triplet under $SU(3)_c$, singlet under $SU(2)_L$, and with hypercharge $+2/3$). This model may be viewed as the low energy limit of Pati-Salam models described in Ref. [259, 260] (see also [261–268]). The most general dimension-4 Lagrangian describing the vector leptoquark of mass M_{U_1} is (see e.g. [269] for a recent review)

$$\begin{aligned}\mathcal{L}_{U_1} \;=\; & -\frac{1}{2}U^\dagger_{\mu\nu}U^{\mu\nu} + M^2_{U_1}U^\dagger_\mu U^\mu \\ & + ig_s U^\dagger_\mu T_a U_\nu \left(\kappa_s G^{\mu\nu}_a + \tilde{\kappa}_s \tilde{G}^{\mu\nu}_a\right) + ig'\frac{2}{3}U^\dagger_\mu U_\nu \left(\kappa_Y B^{\mu\nu} + \tilde{\kappa}_Y \tilde{B}^{\mu\nu}\right), \\ & + \sum_{i,j}\left(\lambda^q_{ij}(\bar{Q}_i\gamma_\mu P_L L_j)U^\mu + \lambda^d_{ij}(\bar{D}_i\gamma_\mu P_R E_j)U^\mu\right) + \text{h.c.}\,, \end{aligned} \tag{5.8}$$

where $U^{\mu\nu} = D^\mu U^\nu - D^\nu U^\mu$ is the leptoquark field strength tensor in terms of its vector potential U^μ and gauge covariant derivative $D^\mu = \partial^\mu + ig_s T_a G^\mu_a + ig'\frac{2}{3}B^\mu$. G^μ_a and B^μ, and $G^{\mu\nu}_a$ and $B^{\mu\nu}$ are the gluon and hypercharge vector potentials and field strengths, respectively. The dual field strength tensors are $\tilde{G}^{\mu\nu}_a = \frac{1}{2}\epsilon^{\mu\nu\rho\sigma}G_{a\,\rho\sigma}$ and $\tilde{B}^{\mu\nu} = \frac{1}{2}\epsilon^{\mu\nu\rho\sigma}B_{\rho\sigma}$.

The third line in Eq. (5.8) contains couplings of U_1 with the SM quarks and leptons. Specifically, Q_i and L_i are the left-handed quark and lepton doublets, while D_j and E_j are the right-handed down quark and charged lepton singlets. We assume that the

model does not contain light right-handed neutrinos. (If right-handed neutrinos are introduced, additional couplings of U_1 with right-handed neutrinos and right-handed up quarks are possible [270].) The couplings λ^q_{ij} and λ^d_{ij} are in general complex and are therefore a potential source of CP violation of the model. We work in the fermion mass eigenstate basis and define the leptoquark couplings λ^q_{ij} and λ^d_{ij} in a way such that

$$\mathcal{L}_{U_1} \supset \sum_{ijk}(V_{ik}\lambda^q_{kj})(\bar{u}_i\gamma_\mu P_L\nu_j)U^\mu + \sum_{ij}\lambda^q_{ij}(\bar{d}_i\gamma_\mu P_L\ell_j)U^\mu + \sum_{ij}\lambda^d_{ij}(\bar{d}_i\gamma_\mu P_R\ell_j)U^\mu + \text{h.c.}\,, \tag{5.9}$$

where V is the CKM matrix.

The second line in Eq. (5.8) encodes the chromo- and hypercharge- magnetic and electric dipole moments of the U_1 leptoquark.

If the leptoquark arises from the spontaneous breakdown of a gauge symmetry, gauge invariance requires these couplings to be fixed to $\kappa_s = \kappa_Y = 1$, $\tilde{\kappa}_s = \tilde{\kappa}_Y = 0$. In more generic scenarios where U_1 is composite, the values of κ_s, $\tilde{\kappa}_s$, κ_Y, $\tilde{\kappa}_Y$ are free parameters. Non-zero values for $\tilde{\kappa}_s$ and $\tilde{\kappa}_Y$ are an additional potential source of CP violation. However, since they do not directly influence flavor physics, we will focus our attention to CP-violation contained in λ^q_{ij} and λ^d_{ij} (even though in Sec. 5.3 we will present fully generic expressions for the EDMs, including their dependence on $\tilde{\kappa}_s$ and $\tilde{\kappa}_Y$).

5.2.1 Leptoquark Effects in B-meson Decays

The U_1 leptoquark can simultaneously address the hints for LFU violation in charged current decays $R_{D^{(*)}}$ and in neutral current decays $R_{K^{(*)}}$[2]. Here we will use the results of a recent study [80] that identified a benchmark point in the leptoquark parameter space that gives a remarkably consistent new physics explanation of these hints. We will explore the parameter space around this benchmark point (supplemented by a few

[2]Note that the small anomaly in the low q^2 bin of R^*_K in (5.5) cannot be fully addressed by the U_1 leptoquark, but it requires the presence of light NP [271–274].

more points), focusing on the implications for dipole moments. As we discuss below, not all leptoquark couplings in (5.8) are required to address the anomalies.

Explaining the observed values of $R_{D^{(*)}}$ by non-standard effects in the $b \to c\tau\nu$ transition is possible if the leptoquark has sizable couplings to the left-handed tau. Avoiding strong constraints from leptonic tau decays $\tau \to \nu_\tau \ell \bar{\nu}_\ell$ and the $B \to X_s\gamma$ decay is possible in a well defined parameter space around the benchmark point with $\lambda^q_{33} \simeq 0.7$, $\lambda^q_{23} \simeq 0.6$ with a leptoquark mass of $M_{U_1} = 2\,\text{TeV}$ [80]. This corresponds to the following non-standard value for $R_{D^{(*)}}$

$$\frac{R_{D^{(*)}}}{R^{\text{SM}}_{D^{(*)}}} = \left| 1 + \frac{v^2}{2M^2_{U_1}} \frac{\lambda^{q*}_{33}\lambda^q_{23}}{V_{cs}V_{cb}} \right|^2 \simeq 1.2\,, \tag{5.10}$$

which is in good agreement with observations (in this equation we normalize $v = 246$ GeV).

The results for $R_{K^{(*)}}$ can be accommodated by a non-standard effect in the $b \to s\mu\mu$ transition if the couplings to the left-handed muon obey $\text{Re}(\lambda^q_{22} \times \lambda^q_{32}) \simeq -2.5 \times 10^{-3}$ for $M_{U_1} = 2\,\text{TeV}$ [80]. The leptoquark effects for this choice of couplings are described by a shift in the Wilson coefficients of the effective Hamiltonian relevant for $b \to s\ell\ell$ transitions (see e.g. [80] for the precise definition)

$$C_9^{bs\mu\mu} = -C_{10}^{bs\mu\mu} = -\frac{4\pi^2}{e^2} \frac{v^2}{M^2_{U_1}} \frac{\lambda^q_{32}\lambda^{q*}_{22}}{V^*_{ts}V_{tb}} \simeq -0.4\,. \tag{5.11}$$

This agrees well with the best fit value for the Wilson coefficients found in [80].

The muonic couplings $\lambda^q_{22}, \lambda^q_{32}$ (that can explain the $R_{K^{(*)}}$ anomalies) in combination with the tauonic couplings $\lambda^q_{23}, \lambda^q_{33}$ (that are required to explain the $R_{D^{(*)}}$ anomalies) lead to lepton flavor violating decays. The strongest constraints arise from the decays $\tau \to \phi\mu$ and $B \to K\tau\mu$. For the λ^q_{33}, λ^q_{23} benchmark mentioned above, existing limits on those decay modes result in the bounds on the leptoquark couplings $|\lambda^q_{22}| \lesssim 0.16$ and $|\lambda^q_{32}| \lesssim 0.40$ for $M_{U_1} = 2\,\text{TeV}$ [80].

The experimental values of $R_{K^{(*)}}$ may also be explained by new physics in the

$b \to see$ transition as opposed to modifying the $b \to s\mu\mu$ transition. Focusing on left-handed couplings, the required shifts in the relevant Wilson coefficients is [80]

$$C_9^{bsee} = -C_{10}^{bsee} = -\frac{4\pi^2}{e^2}\frac{v^2}{M_{U_1}^2}\frac{\lambda_{31}^q \lambda_{21}^{q*}}{V_{ts}^* V_{tb}} \simeq +0.4\,, \tag{5.12}$$

corresponding to the couplings $\mathrm{Re}(\lambda_{21}^q \times \lambda_{31}^q) \simeq +2.5 \times 10^{-3}$ for $M_{U_1} = 2\,\mathrm{TeV}$. The experimental bounds on the lepton flavor violating processes $\tau \to \phi e$ and $B \to K\tau e$ are comparable to those of $\tau \to \phi\mu$ and $B \to K\tau\mu$ [275–277]. We therefore expect that the constraints on the left-handed electron couplings $|\lambda_{21}^q|$ and $|\lambda_{31}^q|$ are similar to the muon couplings mentioned above, i.e. $|\lambda_{21}^q| \lesssim 0.16$ and $|\lambda_{31}^q| \lesssim 0.40$ for $M_{U_1} = 2\,\mathrm{TeV}$.

Motivated by this discussion, in the next sections we will explore the leptoquark parameter space in the neighborhood of four benchmark scenarios:

$$\text{BM1:}\quad \lambda_{33}^q = 0.7\,,\ \lambda_{23}^q = 0.6\,,\quad \lambda_{32}^q = -0.25\,,\ \lambda_{22}^q = 0.01\,,\quad \lambda_{31}^q = \lambda_{21}^q = 0\,, \tag{5.13a}$$

$$\text{BM2:}\quad \lambda_{33}^q = 0.7\,,\ \lambda_{23}^q = 0.6\,,\quad \lambda_{32}^q = \lambda_{22}^q = 0\,,\quad \lambda_{31}^q = 0.05\,, \lambda_{21}^q = 0.05\,, \tag{5.13b}$$

$$\text{BM3:}\quad \lambda_{33}^q = \lambda_{23}^q = 0\,,\quad \lambda_{32}^q = -1.4\,,\ \lambda_{22}^q = 10^{-3}\,,\quad \lambda_{31}^q = \lambda_{21}^q = 0\,, \tag{5.13c}$$

$$\text{BM4:}\quad \lambda_{33}^q = \lambda_{23}^q = 0\,,\quad \lambda_{32}^q = \lambda_{22}^q = 0\,,\quad \lambda_{31}^q = 0.5\,,\ \lambda_{21}^q = 5.0 \times 10^{-3}\,, \tag{5.13d}$$

$$M_{U_1} = 2\ \mathrm{TeV},\ \ \kappa_{Y,s} = 1,\ \ \tilde{\kappa}_{Y,s} = 0 \text{ for all benchmarks}$$

with all the other fermionic couplings of the leptoquark in Eq. (5.8) set to zero. In BM1 and BM2 both the $R_{D^{(*)}}$ and $R_{K^{(*)}}$ anomalies are addressed. The $R_{K^{(*)}}$ explanations involve new physics in the $b \to s\mu\mu$ transition (BM1) or in the $b \to see$ transition (BM2). For benchmark points BM3 and BM4 we forgo an explanation of $R_{D^{(*)}}$. This allows us to increase the couplings to muons/electrons while avoiding the strong constraints from lepton flavor violating tau decays. Note that in benchmark BM3, the $R_{K^{(*)}}$ anomalies are only partially addressed. For BM3 we have $R_K \simeq R_K^* \simeq 0.88$ which is in good agreement with the latest R_K measurement, but $\sim 2\sigma$ away from the measured R_{K^*} value. As we discuss below in Sec. 5.4.2 benchmark BM3 is motivated because it can

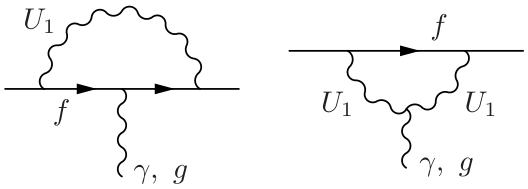

Figure 5.1: Feynman diagrams contributing to the dipole moments of quarks and leptons from leptoquark exchange.

accommodate the longstanding discrepancy in the anomalous magnetic moment of the muon.

For all benchmark scenarios we explicitly checked compatibility with the measurements of the di-lepton [278] and di-tau [279] invariant mass distributions at the LHC and searches for electron-quark contact interactions at LEP [58]. In the case of the di-lepton invariant mass distributions at the LHC, the value of λ^q_{32} in BM3 is close to the exclusion bound.

Starting with these benchmark points, in the following sections we turn on couplings to right-handed taus λ^d_{33}, muons λ^d_{32}, and electrons λ^d_{31} and determine the expected size of electric and magnetic dipole moments of the leptons as function of the real and imaginary part of the new couplings. In principle, the couplings λ^d_{23}, λ^d_{22} and λ^d_{21} will also influence the dipole moments; we comment on λ^d_{22} and λ^d_{21} in Secs. 5.4.2 and 5.4.3, but we do not consider λ^d_{23} since it does not play any role in explaining the flavor anomalies. The couplings λ^d_{3i} mentioned above do modify the new physics contributions to the flavor anomalies. However, as we will discuss below in Sec. 5.4, once the existing constraints on those couplings from other flavor observables are taken into account, the effect on the flavor anomalies turns out to be small.

5.3 Dipole Moments of Quarks and Leptons

In this section, we calculate and present new and original formulae for shifts in the electric and magnetic dipole moments of leptons and quarks induced by the leptoquark.

We then estimate the size of the neutron electric dipole. Finally, we review experimental limits on the dipole moments.

The leptoquark radiatively induces dipole moments starting at one loop order as shown in Fig. 5.1. After integrating out the leptoquark, effective interactions encoding the dipole moments are given by the effective Lagrangian

$$\mathcal{L}_{\text{eff}} = \sum_f \left(a_f \frac{eQ_f}{4m_f} (\bar{f}\sigma^{\mu\nu} f) F_{\mu\nu} - \frac{id_f}{2} (\bar{f}\sigma^{\mu\nu}\gamma_5 f) F_{\mu\nu} \right) , \tag{5.14}$$

where a_f is the anomalous magnetic dipole moment, and d_f is the electric dipole moment of SM fermion f. In the absence of right-handed neutrinos, the U_1 leptoquark does not generate dipole moments for neutrinos.

Through its coupling with the gluons, the leptoquark induces chromomagnetic, $\widehat{a}_q$, and chromoelectric, $\widehat{d}_q$, dipole moments of quarks

$$\mathcal{L}_{\text{eff}} = \sum_q \left(\frac{\widehat{a}_q}{4m_q} (\bar{q}\sigma^{\mu\nu} T^a q) G^a_{\mu\nu} - \frac{i\widehat{d}_q}{2} (\bar{q}\sigma^{\mu\nu} T^a \gamma_5 q) G^a_{\mu\nu} \right) . \tag{5.15}$$

5.3.1 Leptoquark Contribution to Dipole Moments of SM Leptons and Quarks

In the large M_{U_1} limit, the leptoquark contribution to the anomalous magnetic moment of the muon is

$$\begin{aligned} a_\mu = \frac{N_C}{16\pi^2} \sum_i \Big[& 2\text{Re}(\lambda^q_{i2}\lambda^{d*}_{i2}) \frac{m_{d_i} m_\mu}{M^2_{U_1}} \Big(2Q_d + Q_U \big((1-\kappa_Y) \ln\left(\frac{\Lambda^2_{\text{UV}}}{M^2_{U_1}}\right) + \frac{1-5\kappa_Y}{2} \big) \Big) \\ & + 2Q_U \tilde{\kappa}_Y \text{Im}(\lambda^q_{i2}\lambda^{d*}_{i2}) \frac{m_{d_i} m_\mu}{M^2_{U_1}} \Big(\ln\left(\frac{\Lambda^2_{\text{UV}}}{M^2_{U_1}}\right) + \frac{5}{2} \Big) \\ & - (|\lambda^q_{i2}|^2 + |\lambda^d_{i2}|^2) \frac{m^2_\mu}{M^2_{U_1}} \Big(\frac{4}{3} Q_d + Q_U \big((1-\kappa_Y) \ln\left(\frac{\Lambda^2_{\text{UV}}}{M^2_{U_1}}\right) - \frac{1+9\kappa_Y}{6} \big) \Big) \Big] , \end{aligned} \tag{5.16}$$

where $Q_d = -1/3$, $Q_U = +2/3$ is the leptoquark electric charge, and $N_C = 3$. Our formula is in agreement with [280,281] when specialized to the vector leptoquark model

with $\kappa_Y = 1$ and $\tilde{\kappa}_Y = 0$. Note that if $\kappa_Y \neq 1$ or $\tilde{\kappa}_Y \neq 0$, relevant for scenarios in which the leptoquark is not a gauge boson, the dipole moment exhibits logarithmic dependence on the cut-off scale Λ_{UV} not far above the leptoquark mass. This cut-off dependence signals the presence of additional contributions in UV complete scenarios (e.g. from other resonances in a strongly coupled model.) Even in the case that the leptoquark is a gauge boson, and the expressions that we derive are thus formally UV finite, we would like to remark that UV models will likely contain additional contributions to EDMs e.g. from an extended Higgs sector.

Similarly, the muon electric dipole moment is

$$\begin{aligned} d_\mu = \frac{eN_C}{16\pi^2}\sum_i \Big[&\mathrm{Im}(\lambda^q_{i2}\lambda^{d*}_{i2})\frac{m_{d_i}}{M^2_{U_1}}\Big(2Q_d + Q_U\big((1-\kappa_Y)\ln\left(\frac{\Lambda^2_{\mathrm{UV}}}{M^2_{U_1}}\right) + \frac{1-5\kappa_Y}{2}\big)\Big) \\ &+ Q_U\tilde{\kappa}_Y \mathrm{Re}(\lambda^q_{i2}\lambda^{d*}_{i2})\frac{m_{d_i}}{M^2_{U_1}}\big(\ln\left(\frac{\Lambda^2_{\mathrm{UV}}}{M^2_{U_1}}\right) + \frac{5}{2}\big) \\ &+ Q_U\tilde{\kappa}_Y(|\lambda^q_{i2}|^2 + |\lambda^d_{i2}|^2)\frac{m_\mu}{M^2_{U_1}}\big(\frac{1}{2}\ln\left(\frac{\Lambda^2_{\mathrm{UV}}}{M^2_{U_1}}\right) + \frac{3}{4}\big)\Big]. \end{aligned} \quad (5.17)$$

CP violation is provided either by the imaginary part of the fermion coupling combination $\lambda^q_{i2}\lambda^{d*}_{i2}$, or by the CP violating hypercharge coupling $\tilde{\kappa}_Y$. Dipole moments of other charged leptons are obtained by the appropriate replacement of the muon mass, m_μ, and leptoquark couplings to muons, λ_{i2}.

The bottom quark electric dipole moment induced by the leptoquark is

$$\begin{aligned} d_b = \frac{e}{16\pi^2}\sum_i \Big[&\mathrm{Im}(\lambda^q_{3i}\lambda^{d*}_{3i})\frac{m_{\ell_i}}{M^2_{U_1}}\Big(2Q_\ell + Q_U\big((1-\kappa_Y)\ln\left(\frac{\Lambda^2_{\mathrm{UV}}}{M^2_{U_1}}\right) + \frac{1-5\kappa_Y}{2}\big)\Big) \\ &+ Q_U\tilde{\kappa}_Y \mathrm{Re}(\lambda^q_{3i}\lambda^{d*}_{3i})\frac{m_{\ell_i}}{M^2_{U_1}}\big(\ln\left(\frac{\Lambda^2_{\mathrm{UV}}}{M^2_{U_1}}\right) + \frac{5}{2}\big) \\ &- Q_U\tilde{\kappa}_Y(|\lambda^q_{3i}|^2 + |\lambda^d_{3i}|^2)\frac{m_b}{M^2_{U_1}}\big(\frac{1}{2}\ln\left(\frac{\Lambda^2_{\mathrm{UV}}}{M^2_{U_1}}\right) + \frac{3}{4}\big)\Big], \end{aligned} \quad (5.18)$$

and the chromoelectric dipole moment (cEDM) is

$$\widehat{d}_b = \frac{g_s}{16\pi^2}\sum_i \Big[\mathrm{Im}(\lambda^q_{3i}\lambda^{d*}_{3i})\frac{m_{\ell_i}}{M^2_{U_1}}\Big((1-\kappa_Y)\ln\left(\frac{\Lambda^2_{\rm UV}}{M^2_{U_1}}\right)+\frac{1-5\kappa_Y}{2}\Big) + \tilde{\kappa}_Y \mathrm{Re}(\lambda^q_{3i}\lambda^{d*}_{3i})\frac{m_{\ell_i}}{M^2_{U_1}}\big(\ln\left(\frac{\Lambda^2_{\rm UV}}{M^2_{U_1}}\right)+\frac{5}{2}\big) - \tilde{\kappa}_Y(|\lambda^q_{3i}|^2+|\lambda^d_{3i}|^2)\frac{m_b}{M^2_{U_1}}\big(\frac{1}{2}\ln\left(\frac{\Lambda^2_{\rm UV}}{M^2_{U_1}}\right)+\frac{3}{4}\big)\Big]. \quad (5.19)$$

The other down-type quark (chromo-)electric dipole moments can be obtained by appropriate replacements of flavor indices.

Analogously, up-type quark (chromo-)electric dipole moments are obtained from the bottom quark result by the replacement $\lambda^q_{ij} \to V_{ik}\lambda^q_{kj}$, $\lambda^d_{ij} \to 0$, $m_\ell \to m_\nu = 0$, $m_b \to m_u$ yielding

$$d_u = -\frac{e}{16\pi^2}Q_U\tilde{\kappa}_Y\sum_i |(V\lambda^q)_{1i}|^2\frac{m_u}{M^2_{U_1}}\Big(\frac{1}{2}\ln\left(\frac{\Lambda^2_{\rm UV}}{M^2_{U_1}}\right)+\frac{3}{4}\Big), \quad (5.20)$$

and

$$\widehat{d}_u = -\frac{g_s}{16\pi^2}\tilde{\kappa}_Y\sum_i |(V\lambda^q)_{1i}|^2\frac{m_u}{M^2_{U_1}}\Big(\frac{1}{2}\ln\left(\frac{\Lambda^2_{\rm UV}}{M^2_{U_1}}\right)+\frac{3}{4}\Big). \quad (5.21)$$

We do not consider anomalous (chromo-)magnetic moments of the quarks as they are hardly constrained by experiment. Note that the anomalous magnetic moments of the top quark is constrained by measurements of $t\bar{t}$ production at the LHC. Current bounds of $\widehat{a}_t \sim 0.1$ [282] are, however, not sensitive to the effects induced by heavy leptoquark loops in our scenario.

5.3.2 Connecting Quark Dipole Moments to the Neutron EDM

In the following, we determine the neutron electric dipole moment due to quark-level dipole moments. We neglect the running of quark dipole moments from the leptoquark scale to the hadronic scale, since the neglected logarithm of order $\alpha_s \ln\Big(M^2_{U_1}/M^2_n\Big) \approx 1.6$ leads to corrections which are small compared to the relevant hadronic uncertainties discussed below.

The dominant contributions to the neutron EDM are from the short range QCD interactions involving quark EDMs, d_i, and cEDMs, $\widehat{d}_i$, given by

$$d_n \sim -\frac{v}{\sqrt{2}}\left[\beta_n^{uG}\widehat{d}_u + \beta_n^{dG}\widehat{d}_d + \beta_n^{sG}\widehat{d}_s + \beta_n^{u\gamma}d_u + \beta_n^{d\gamma}d_d + \beta_n^{s\gamma}d_s\right], \tag{5.22}$$

where the $\beta_i^{(k)}$ are the hadronic matrix elements. Estimates from quark cEDM are given by $\beta_n^{uG} \approx 4^{+6}_{-3} \times 10^{-4}\, e$ fm and $\beta_n^{dG} \approx 8^{+10}_{-6} \times 10^{-4}\, e$ fm [283]. The most recent lattice evaluations of the matrix elements involving the electromagnetic EDMs are [284, 285] $-\frac{v}{\sqrt{2}}\beta_n^{u\gamma} \approx -0.233(28)$, $-\frac{v}{\sqrt{2}}\beta_n^{d\gamma} \approx 0.776(66)$ and $-\frac{v}{\sqrt{2}}\beta_n^{s\gamma} \approx 0.008(9)$.

Contributions from heavy quark cEDM are estimated by integrating out the heavy quark, $Q = c, b$, to generate the three gluon Weinberg (gluon cEDM) operator,

$$\mathcal{L} = \frac{c_{\tilde{\mathrm{G}}}}{m_Q^2}\frac{g_s f^{abc}}{3}\tilde{G}^a_{\mu\nu}G^b_{\nu\rho}G^{c\,\mu}_{\rho}\,, \tag{5.23}$$

where the Wilson coefficient is given by [286–288]

$$c_{\tilde{\mathrm{G}}} = \frac{g_s^2}{32\pi^2}m_Q\widehat{d}_Q\,. \tag{5.24}$$

Contributions to $c_{\tilde{\mathrm{G}}}$ from CP-violating leptoquark gluon interactions proportional to $\tilde{\kappa}_s$ are also present, but we do not consider them since they are unrelated to flavor anomalies. In terms of $c_{\tilde{\mathrm{G}}}$, the neutron EDM is given by [283]

$$d_n = \frac{v^2}{m_Q^2}\beta_n^{\tilde{G}}c_{\tilde{\mathrm{G}}} \tag{5.25}$$

where $\beta_n^{\tilde{G}} \approx [2,\, 40] \times 10^{-20}$ e cm is the nucleon matrix element estimated using QCD sum rules and chiral perturbation theory [289, 290].

To compare the relative sizes of contributions from light and heavy quark to the neutron EDM, we take the strange and bottom quark contributions, and assume for simplicity that $\kappa_Y = 1$, $\tilde{\kappa}_Y = 0$. We also assume $M_{U_1} \sim 2$ TeV for the leptoquark scale.

Putting together Eqs. (5.18) and (5.19) with Eq. (5.22), we find that the strange

quark EDM contribution to the neutron EDM is

$$\begin{aligned} d_n^{\text{strange}} &\approx -\frac{5}{24\pi^2 M_{U_1}^2 \text{ cm}} \left[m_\tau \text{Im}(\lambda_{23}^q \lambda_{23}^{d*}) + m_\mu \text{Im}(\lambda_{22}^q \lambda_{22}^{d*}) \right] \times 0.008 \ e \text{ cm} \\ &\sim -\left(\text{Im}(\lambda_{23}^q \lambda_{23}^{d*}) + 0.06 \ \text{Im}(\lambda_{22}^q \lambda_{22}^{d*}) \right) \times 1.5 \times 10^{-24} \ e \text{ cm} \,. \end{aligned} \tag{5.26}$$

The bottom quark cEDM contribution to the neutron EDM is instead given by

$$\begin{aligned} d_n^{\text{bottom}} &\approx -\frac{g_s^3 v^2}{(16\pi^2)^2 m_b M_{U_1}^2} \left[m_\tau \text{Im}(\lambda_{33}^q \lambda_{33}^{d*}) + m_\mu \text{Im}(\lambda_{32}^q \lambda_{32}^{d*}) \right] \times [2, 40] \times 10^{-20} \\ &\sim -\left(\text{Im}(\lambda_{33}^q \lambda_{33}^{d*}) + 0.06 \ \text{Im}(\lambda_{32}^q \lambda_{32}^{d*}) \right) \times [2, 40] \times 5 \times 10^{-27} \ e \text{ cm} \,. \end{aligned} \tag{5.27}$$

For generic $\mathcal{O}(1)$ sized leptoquark couplings λ_{ik}^q and λ_{ik}^d the strange quark contribution (5.26) to the neutron EDM is much larger than the bottom quark contribution (5.27). However, in the region of parameter space we are exploring, the bottom quark contribution is typically bigger than the strange quark contribution.

5.3.3 Experimental Status and Prospects

We review here the current experimental status of dipole moments of Standard Model fermions. The anomalous magnetic moments of the electron, a_e, and the muon, a_μ, are measured extremely precisely [25, 291], and are predicted to similarly high precision within the SM, with new physics contributions constrained to lie within the range [292, 293] (see also [294–296])

$$\Delta a_\mu = (28.0 \pm 6.3_{\text{exp}} \pm 3.8_{\text{th}}) \times 10^{-10} \,, \qquad \Delta a_e = (-8.9 \pm 3.6_{\text{exp}} \pm 2.3_{\text{th}}) \times 10^{-13} \,, \tag{5.28}$$

In addition to the long standing discrepancy in the muon magnetic moment with a significance of more than 3σ, a discrepancy in the electron magnetic moment arose after

a recent precision measurement of the fine structure constant [297] with a significance of $\sim 2.4\sigma$. Combining the expected sensitivity from the running $g-2$ experiment at Fermilab [298] with expected progress on the SM prediction (see [299–304] for recent lattice efforts and [305–309] for recent efforts using the framework of dispersion relations) the uncertainty on Δa_μ will be reduced by a factor of a few in the coming years. Similarly, for Δa_e we expect an order of magnitude improvement in the sensitivity [310].

The anomalous magnetic moment of the tau, a_τ, is currently only very weakly constrained. The strongest constraint comes from LEP and reads at 95% C.L. [311]

$$-0.055 < a_\tau < 0.013\,. \tag{5.29}$$

Improvements in sensitivity by an order of magnitude or more might be achieved at Belle II or future electron positron colliders (see [312] for a review).

Strong experimental constraints exist for the EDM of the electron. The strongest bound is inferred from the bound on the EDM of ThO obtained by the ACME collaboration which gives at 90% C.L. [313]

$$|d_e| < 1.1 \times 10^{-29}\, e\,\mathrm{cm}\,. \tag{5.30}$$

Significant improvements by an order of magnitude or more can be expected from ACME in the future [313].

Only weak constraints exist for the EDMs of the muon and the tau, d_μ and d_τ. Analyses by the Muon g-2 collaboration [314] and the Belle collaboration [315] give the following bounds at 95% C.L.

$$|d_\mu| < 1.9 \times 10^{-19}\, e\,\mathrm{cm}\,, \qquad -2.2 \times 10^{-17}\, e\,\mathrm{cm} < d_\tau < 4.5 \times 10^{-17}\, e\,\mathrm{cm}\,. \tag{5.31}$$

The proposed muon EDM experiment at PSI aims at improving the sensitivity to the muon EDM by 4 orders of magnitude, $d_\mu \lesssim 5 \times 10^{-23} e\,\mathrm{cm}$ [316]. Improving the sensi-

observable	SM theory	current exp.	projected sens.
$a_e - a_e^{\rm SM}$	$\pm 2.3 \times 10^{-13}$ [292, 297]	$(-8.9 \pm 3.6) \times 10^{-13}$ [25]	$\sim 10^{-14}$ [310]
$a_\mu - a_\mu^{\rm SM}$	$\pm 3.8 \times 10^{-10}$ [292]	$(28.0 \pm 6.3) \times 10^{-10}$ [291]	1.6×10^{-10} [298]
$a_\tau - a_\tau^{\rm SM}$	$\pm 3.9 \times 10^{-8}$ [292]	$(-2.1 \pm 1.7) \times 10^{-2}$ [311]	
d_e	$< 10^{-44}$ e cm [320, 321]	$< 1.1 \times 10^{-29}\, e\,$cm [313]	$\sim 10^{-30}\, e\,$cm [313]
d_μ	$< 10^{-42}$ e cm [321]	$< 1.9 \times 10^{-19}\, e\,$cm [314]	$\sim 10^{-23}\, e\,$cm [316]
d_τ	$< 10^{-41}$ e cm [321]	$(1.15 \pm 1.70) \times 10^{-17}\, e\,$cm [315]	$\sim 10^{-19}\, e\,$cm [317]
d_n	$\sim 10^{-32}$ e cm [322]	$< 1.8 \times 10^{-26}\, e\,$cm [318]	few$\times 10^{-28} e\,$cm [319]

Table 5.1: Summary of Standard Model theory errors/bounds (first column), current experimental measurements/limits (second column) and projected precision of next-generation experiments (third column) of magnetic moment anomalies and electric dipole moments of the charged leptons and the neutron. For clarity, for the anomalous magnetic moments, the Standard Model central values have been subtracted. We are not aware of any experimental analysis for the projected sensitivity of the tau magnetic moment.

tivity to the tau EDM by roughly two orders of magnitude ($d_\tau < 2 \times 10^{-19}\ e\,$cm) might be possible at Belle II or at future e^+e^- colliders [317].

Turning to quarks, we note that the magnetic and chromo-magnetic dipole moments of quarks, a_q and $\widehat{a}_q$, are very weakly constrained and we therefore do not consider them in this work. As discussed in the previous section, the EDMs and cEDMs of quarks, d_q and $\widehat{d}_q$, lead to EDMs of hadronic systems like the neutron and are therefore strongly constrained. In the following we will focus on the neutron EDM which is bounded at 90% C.L. by [318]

$$|d_n| < 1.8 \times 10^{-26}\, e\,\text{cm}\,. \tag{5.32}$$

Experimental sensitivities should improve by two orders of magnitude to a few $10^{-28} e\,$cm in the next decade [319].

We collect the SM predictions, the current experimental results, and expected future experimental sensitivities to the dipole moments in Table 5.1.

5.4 Flavor Anomalies and Electric Dipole Moments

In this section, we study the impact of leptoquarks on (c)EDMs and B-physics measurements at the benchmark points presented in Sec. 5.2.1.

5.4.1 Probing the Parameter Space Using Tau Measurements

Given the BM1 and BM2 benchmarks for the leptoquark couplings to left-handed taus, $\lambda^q_{33} \simeq 0.7$, $\lambda^q_{23} \simeq 0.6$, we begin by turning on the coupling to right-handed taus λ^d_{33} while setting the right-handed couplings to muons and electrons (λ^d_{32} and λ^d_{31}, respectively) to zero. The coupling λ^d_{33} will induce the dipole moments of the tau as in Eqs. (5.16) and (5.17), as well as transition dipole moments leading to the lepton flavor violating decay modes $\tau \to \mu\gamma$ and $\tau \to e\gamma$. In the limit $m_e, m_\mu \ll m_\tau \ll m_b$, the partial width for the U_1 contribution to $\tau \to \mu\gamma$ is given by

$$\Gamma_{\tau\to\mu\gamma} = \frac{\alpha m_\tau^3 N_C^2}{256\pi^4 M_{U_1}^4} m_b^2 |\lambda^q_{32}\lambda^{d*}_{33}|^2 \left[\left(2Q_b - Q_U\Big((1-\kappa_Y)\ln\left(\frac{\Lambda^2_{\rm UV}}{M^2_{U_1}}\right) + \frac{1-5\kappa_Y}{2}\Big)\right)^2 + Q_U^2\tilde{\kappa}_Y^2\Big(\ln\left(\frac{\Lambda^2_{\rm UV}}{M^2_{U_1}}\right) + \frac{5}{2}\Big)^2 \right]. \quad (5.33)$$

This expression is in agreement with [250], when specialized to the vector leptoquark model with $\kappa_Y = 1$ and $\tilde{\kappa}_Y = 0$. The expression for the decay mode $\tau \to e\gamma$ is obtained by an appropriate replacement of the lepton flavor index. The experimental upper limits on the branching ratios of the $\tau \to \mu\gamma$ and $\tau \to e\gamma$ decays are 5.0×10^{-8} and 5.4×10^{-8}, respectively [66].

In addition to inducing lepton flavor violating tau decays, the λ^d_{33} coupling will modify the new physics contributions to charged current decays based on the $b \to c\tau\nu$ and $b \to u\tau\nu$ transitions and neutral current decays based on $b \to s\tau\tau$. The decay modes that are particularly sensitive to right-handed currents are the helicity suppressed two body decays $B_c \to \tau\nu$ [323, 324], $B^\pm \to \tau\nu$, and $B_s \to \tau^+\tau^-$. We find

$$\frac{\mathrm{BR}(B_c \to \tau\nu)}{\mathrm{BR}(B_c \to \tau\nu)_{\mathrm{SM}}} = \left|1 - \frac{\sum_j V_{cj}\lambda^q_{j3}}{V_{cb}} \frac{v^2}{M^2_{U_1}} \left(\frac{\lambda^{q*}_{33}}{2} + \frac{\lambda^{d*}_{33} m^2_{B_c}}{m_\tau(m_b + m_c)}\right)\right|^2 , \quad (5.34)$$

$$\frac{\mathrm{BR}(B^\pm \to \tau\nu)}{\mathrm{BR}(B^\pm \to \tau\nu)_{\mathrm{SM}}} = \left|1 - \frac{\sum_j V_{uj}\lambda^q_{j3}}{V_{ub}} \frac{v^2}{M^2_{U_1}} \left(\frac{\lambda^{q*}_{33}}{2} + \frac{\lambda^{d*}_{33} m^2_{B^\pm}}{m_\tau m_b}\right)\right|^2 , \quad (5.35)$$

Using the expression for the branching ratio in terms of the Wilson coefficients from [325], we find

$$\begin{aligned}\frac{\mathrm{BR}(B_s \to \tau^+\tau^-)}{\mathrm{BR}(B_s \to \tau^+\tau^-)_{\mathrm{SM}}} = & \\ & \left|1 + \frac{4\pi^2}{e^2 C^{\mathrm{SM}}_{10}} \frac{v^2}{M^2_{U_1}} \left(\frac{\lambda^{q*}_{33}\lambda^q_{23} + \lambda^{d*}_{33}\lambda^d_{23}}{V^*_{ts}V_{tb}} - \frac{m^2_{B_s}}{m_\tau m_b} \frac{\lambda^{q*}_{33}\lambda^d_{23} + \lambda^{d*}_{33}\lambda^q_{23}}{V^*_{ts}V_{tb}}\right)\right|^2 \\ & + \frac{16\pi^4}{e^4 (C^{\mathrm{SM}}_{10})^2} \frac{v^4}{M^4_{U_1}} \frac{m^4_{B_s}}{m^2_\tau m^2_b} \left|\frac{\lambda^{q*}_{33}\lambda^d_{23} - \lambda^{d*}_{33}\lambda^q_{23}}{V^*_{ts}V_{tb}}\right|^2 \left(1 - \frac{4m^2_\tau}{m^2_{B_s}}\right)\end{aligned} \quad (5.36)$$

where we neglected the finite life time difference in the B_s system. We use a normalization such that the SM value for the Wilson coefficient is $C^{\mathrm{SM}}_{10} \simeq -4.1$ [326]. Renormalization group running from the leptoquark scale down to the b-scale can be incorporated by evaluating the quark masses in Eqs. (5.34)-(5.36) at the scale $\mu \simeq 2\,\mathrm{TeV}$. Note that the terms containing both left-handed and right-handed couplings enjoy a mild chiral enhancement by factors $m^2_{B_c}/(m_\tau(m_b+m_c))$, $m^2_{B^\pm}/(m_\tau m_b)$, and $m^2_{B_s}/(m_\tau m_b)$, respectively.

The measured $\mathrm{BR}(B^\pm \to \tau\nu) = (1.09 \pm 0.24) \times 10^{-4}$ [26] agrees well with the SM prediction $\mathrm{BR}(B^\pm \to \tau\nu)_{\mathrm{SM}} = (0.838^{+0.039}_{-0.029}) \times 10^{-4}$ [5], yielding

$$\frac{\mathrm{BR}(B^\pm \to \tau\nu)}{\mathrm{BR}(B^\pm \to \tau\nu)_{\mathrm{SM}}} = 1.30 \pm 0.29\,. \tag{5.37}$$

So far no direct measurement of the $B_c \to \tau\nu$ branching ratio has been performed. We impose the bound $\mathrm{BR}(B_c \to \tau\nu) < 30\%$ [324]. The SM branching ratio is

$$\mathrm{BR}(B_c \to \tau\nu)_{\mathrm{SM}} = \tau_{B_c} m_{B_c} \frac{f_{B_c}^2 G_F^2}{8\pi} |V_{cb}|^2 m_\tau^2 \left(1 - \frac{m_\tau^2}{m_{B_c}^2}\right)^2 = (2.21 \pm 0.09) \times 10^{-2}\,, \tag{5.38}$$

with the lifetime of the B_c meson $\tau_{B_c} = (0.507 \pm 0.009) \times 10^{-12}$ s [26], the B_c decay constant $f_{B_c} = (0.427 \pm 0.006)$ GeV [327] and we used $|V_{cb}| = (41.6 \pm 0.56) \times 10^{-3}$ [5].

Similarly, the $B_s \to \tau^+\tau^-$ decay has not been observed so far. The first direct limit on the branching ratio was placed by LHCb [328] and is $\mathrm{BR}(B_s \to \tau^+\tau^-) < 6.8 \times 10^{-3}$, while the SM branching ratio is $\mathrm{BR}(B_s \to \tau^+\tau^-)_{\mathrm{SM}} = (7.73 \pm 0.49) \times 10^{-7}$ [329]. The projected sensitivity $\mathrm{BR}(B_s \to \tau^+\tau^-) \sim 5 \times 10^{-4}$ from LHCb with 50 fb^{-1} [330].

In Fig. 5.2, we show current and projected constraints on the U_1 leptoquark in the plane of the complex λ_{33}^d coupling divided by the leptoquark mass for BM1 and BM2 benchmark points. The figure represents both BM1 and BM2, since the shown constraints are independent of the muon couplings $\lambda_{32}^q, \lambda_{22}^q$ and electron couplings $\lambda_{31}^q, \lambda_{21}^q$ and changing from BM1 to BM2 does not affect our results. The most stringent constraint comes from $B_s \to \tau^+\tau^-$ and is depicted by the gray shaded region in the figure. The projected sensitivity of LHCb to $B_s \to \tau^+\tau^-$ is indicated by the dashed gray curve. Constraints from $B^\pm \to \tau\nu$, $B_c \to \tau\nu$, and lepton flavor violating tau decays ($\tau \to \mu\gamma$ for benchmark BM1 and $\tau \to e\gamma$

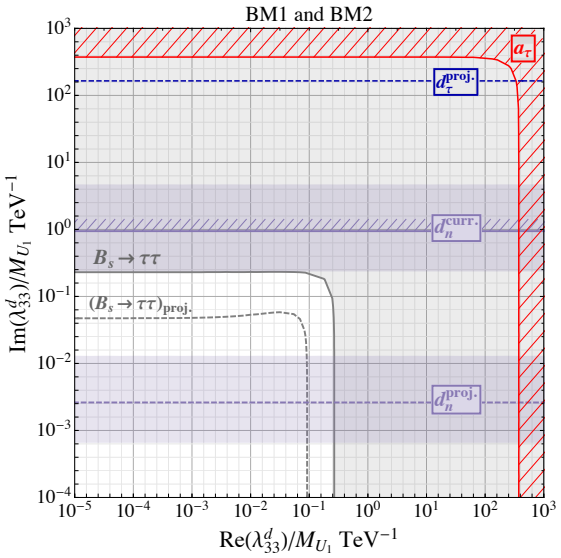

Figure 5.2: Constraints on the U_1 leptoquark parameter space in the plane of the complex coupling λ_{33}^d divided by the leptoquark mass, M_{U_1}, and all other parameters fixed as in BM1 (5.13a) or BM2 (5.13b). The gray region enclosed by the solid gray curve represents parameter space that is excluded by $B_s \to \tau^+\tau^-$, while the dashed gray curve is the projected sensitivity of LHCb to $B_s \to \tau^+\tau^-$. The red hatched region is excluded by the bound on the tau lepton anomalous magnetic moment. The dashed blue line is the projected sensitivity of future experiments to the tau EDM. The region above the solid purple line is excluded by bounds on the neutron EDM, and the dashed purple line is the projected sensitivity of future neutron EDM experiments. The surrounding purple bands reflect the theoretical uncertainty in the nucleon matrix element $\beta_n^{\tilde{G}}$. Note that the observables shown in the figure are independent of $\lambda_{32}^q, \lambda_{22}^q$ and $\lambda_{31}^q, \lambda_{21}^q$, and the change from benchmark BM1 to BM2 has no effect on the exclusion curves.

for BM2) are slightly weaker and exclude values of λ_{33}^d that are a factor of a few larger than those excluded by $B_s \to \tau^+\tau^-$. (In Fig. 5.2 we show only the strongest constraint coming from $B_s \to \tau^+\tau^-$.) Once the bounds are imposed, the allowed values of the right-handed coupling λ_{33}^d are sufficiently small such that they do not affect $R_{D^{(*)}}$, $R_{K^{(*)}}$ in a significant way. Therefore, in all the allowed region in Fig. 5.2, the anomalies are satisfied.

From the figure, we observe that the current experimental bounds on d_τ and a_τ do not constraint the parameter space in a relevant way. The constraint from a_τ is depicted by the red hatched region in Fig. 5.2, while the experimental bound on d_τ constrains values of $\mathrm{Im}(\lambda_{33}^d)/M_{U_1}$ that are $\mathcal{O}(10^5)$ TeV^{-1}, and, therefore, beyond the range of the plot. Projected sensitivities of next-generation experiments to the tau EDM [317] (shown by the dashed blue line) are still far from being able to probe the viable new physics parameter space.

In addition to the tau electric and anomalous magnetic dipole moments, the U_1 leptoquark coupling, λ_{33}^d, will contribute to the neutron EDM, d_n. The constraint from the current bound on the neutron EDM is shown by the solid purple line in Fig. 5.2, where the region above this line is excluded due to the leptoquark generating a contribution to the neutron EDM that is too large. The surrounding purple bands reflect the theoretical uncertainty in the nucleon matrix element $\beta_n^{\tilde{G}}$. We observe that the currend bound on the neutron EDM leads to a constraint that is weaker than $B_s \to \tau^+\tau^-$ and is not yet probing the allowed parameter space. On the other hand, the projected sensitivity of future neutron EDM experiments [319] (shown by the dashed purple line) will begin probing the new physics parameter space and can lead to stronger constraints on the amount of CP violation present in the right-handed couplings of U_1 to tau leptons.

5.4.2 Probing the Parameter Space Using Muon Measurements

Next we focus on the BM1 and BM3 benchmarks, and investigate the impact of the leptoquark couplings to right-handed muons, λ^d_{32}, while setting the right-handed tau and electron couplings (λ^d_{33} and λ^d_{31}, respectively) to zero. The coupling λ^d_{32} will lead to a shift in the anomalous magnetic moment of the muon, Δa_μ, in the muon EDM, d_μ, and in the EDM of the bottom quark given in Eqs. (5.16), (5.17), and (5.18), as well as the lepton flavor violating decay mode $\tau \to \mu\gamma$ given in Eq. (5.33) with $|\lambda^q_{32}\lambda^{d*}_{33}|^2 \to |\lambda^d_{32}\lambda^{q*}_{33}|^2$. In the presence of the coupling λ^d_{32}, the muon dipole moment enjoys a sizable chiral enhancement by m_b/m_μ.

In addition, the coupling λ^d_{32} can also give sizable non-standard effects in the $B_s \to \mu^+\mu^-$ decay. The corresponding expression is analogous to the one for the $B_s \to \tau^+\tau^-$ decay given in Eq. (5.36)

$$\frac{\text{BR}(B_s \to \mu^+\mu^-)}{\text{BR}(B_s \to \mu^+\mu^-)_{\text{SM}}} = \left|1 + \frac{4\pi^2}{e^2 C_{10}^{\text{SM}}} \frac{v^2}{M_{U_1}^2}\left(\frac{\lambda^{q*}_{32}\lambda^q_{22} + \lambda^{d*}_{32}\lambda^d_{22}}{V^*_{ts}V_{tb}} - \frac{m^2_{B_s}}{m_\mu m_b}\frac{\lambda^{q*}_{32}\lambda^d_{22} + \lambda^{d*}_{32}\lambda^q_{22}}{V^*_{ts}V_{tb}}\right)\right|^2 + \frac{16\pi^4}{e^4 (C_{10}^{\text{SM}})^2}\frac{v^4}{M^4_{U_1}}\frac{m^4_{B_s}}{m^2_\mu m^2_b}\left|\frac{\lambda^{q*}_{32}\lambda^d_{22} - \lambda^{d*}_{32}\lambda^q_{22}}{V^*_{ts}V_{tb}}\right|^2 . \tag{5.39}$$

The terms that contain both left-handed and right-handed couplings are chirally enchanced by a factor $m^2_{B_s}/(m_\mu m_b)$.

The branching ratio $\text{BR}(B_s \to \mu^+\mu^-)$ has been measured at LHCb, CMS and ATLAS [331–334]. We use the average of these results from [80], that, combined

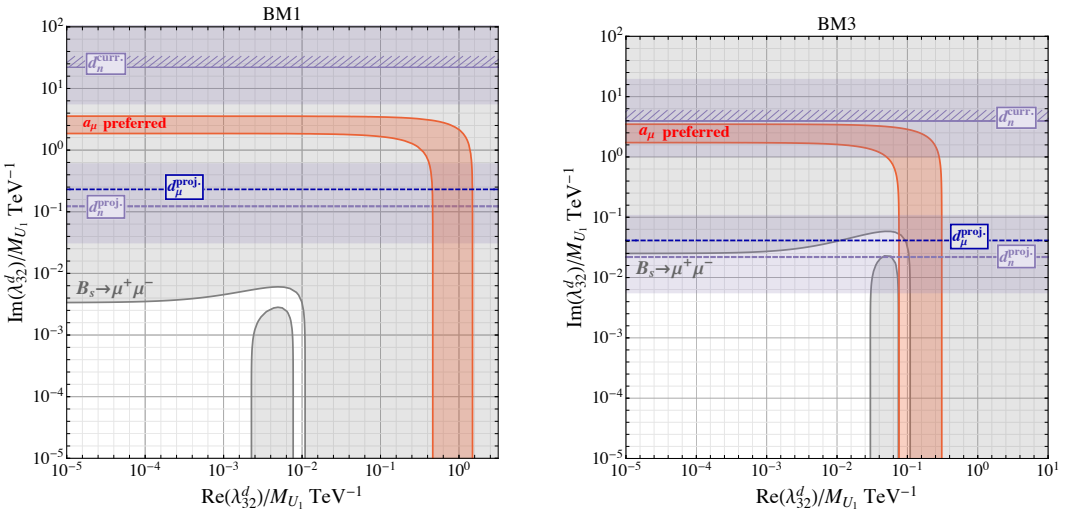

Figure 5.3: Constraints on the U_1 leptoquark parameter space in the plane of the complex λ_{32}^d coupling divided by the leptoquark mass for the benchmark points BM1 (left panel) and BM3 (right panel). The gray region is excluded by $B_s \to \mu^+\mu^-$ at the 95% C.L.. The dashed blue line is the projected sensitivity of future experiments to the muon EDM. The red shaded region corresponds to the parameter space the can address the anomaly in the anomalous magnetic moment of the muon. The solid (dashed) purple lines represent the current constraint (projected sensitivity) from the neutron EDM, with the purple bands reflecting the uncertainty in the nucleon matrix element $\beta_n^{\tilde{G}}$.

with the SM prediction [329, 335], reads

$$\frac{\text{BR}(B_s \to \mu^+\mu^-)}{\text{BR}(B_s \to \mu^+\mu^-)_{\text{SM}}} = 0.73^{+0.13}_{-0.10}\,, \tag{5.40}$$

which is in slight tension ($\sim 2\sigma$) with the SM prediction. Interestingly enough, in the region of parameter space where the couplings to left-handed muons λ_{22}^q, λ_{32}^q provide an explanation of $R_{K^{(*)}}$, the tension in $B_s \to \mu^+\mu^-$ is largely lifted.

In Fig. 5.3 we show the current and projected constraints on the U_1 leptoquark for BM1 (left) and BM3 (right) in the plane of the complex coupling λ_{32}^d divided by the leptoquark mass. For both benchmarks, the most stringent constraint arises from $B_s \to \mu^+\mu^-$. The region that is excluded at the 95% C.L. is shaded in gray. Once the constraints from $B_s \to \mu^+\mu^-$ are imposed, the allowed values

of λ^d_{32} are sufficiently small that they do not affect $R_{K^{(*)}}$ in a significant way. The region that is shaded in red is the region of parameter space that is able to address the anomaly in the anomalous magnetic moment of the muon, while the blue dashed lines are the projected sensitivities of future experiments to the muon EDM. Similar to Fig. 5.2, the solid (dashed) purple line is the current constraint (projected sensitivity) of the neutron EDM. The current bound on the muon EDM, d_μ, is very weak and constrains values of $\mathrm{Im}(\lambda^d_{32})/M_{U_1}$ outside from the range of the plot ($\mathrm{Im}(\lambda^d_{32})/M_{U_1} \sim \mathcal{O}(10^3)$ TeV^{-1} for BM1 and $\mathrm{Im}(\lambda^d_{32})/M_{U_1} \sim \mathcal{O}(10^2)$ TeV^{-1} for BM3).

In the left plot of Fig. 5.3 we observe that, once the constraints from $B_s \to \mu^+\mu^-$ is imposed, the BM1 benchmark cannot address the a_μ anomaly. We conclude that the U_1 leptoquark can not explain the B anomalies and the $(g-2)_\mu$ anomaly simultaneously with the parameters fixed to those of BM1. This is mainly due to limits on lepton flavor violating decays $\tau \to \phi\mu$ and $B \to K\tau\mu$ that impose stringent constraints on the size of the left-handed muonic couplings λ^q_{32} and λ^q_{22} (see discussion in Sec. 5.2.1).

In order to avoid these constraints, we can instead set the U_1 couplings to left-handed tau leptons, λ^q_{33} and λ^q_{23}, to zero as in BM3 in (5.13c). The decay rates $\tau \to \phi\mu$, $B \to K\tau\mu$, and $\tau \to \mu\gamma$ mediated by U_1 then go to zero, allowing the muonic couplings λ^q_{32} and λ^q_{22} to have larger values. However, by switching off λ^q_{33} and λ^q_{23} we forgo an explanation of $R_{D^{(*)}}$.

In the right plot of Fig. 5.3 we show that, for BM3, the region of parameter space that can address the a_μ anomaly (the red shaded region) overlaps with the region of parameter space that is allowed by $B_s \to \mu^+\mu^-$, and the U_1 leptoquark can therefore address both the $(g-2)_\mu$ anomaly and (at least partially, cf. discussion in Sec. 5.2.1) the $R_{K^{(*)}}$ anomalies. Finally, we notice that, for this

benchmark, projected sensitivities to the neutron EDM might start to probe the viable parameter space.

We also explored the region of parameter space with nonzero λ^d_{22} instead of λ^d_{32}. In this case, for BM1 and BM3, the neutron EDM is dominated by the strange quark contribution (5.26), so its projected sensitivity covers larger region of parameter space. However in this case, we did not find any viable region of parameter space explaining the anomaly in a_μ.

5.4.3 Probing the parameter space using electron measurements

Instead of muon specific couplings that address the discrepancies in the LFU ratios $R_{K^{(*)}}$ by new physics that suppresses the $b \to s\mu\mu$ transitions, one can also entertain the possibility that new physics addresses the anomaly by enhancing the $b \to see$ transitions. This can be achieved with the leptoquark couplings λ^d_{31}, λ^d_{21} as given in Eq. (5.12) and by our benchmark points BM2 and BM4.

These couplings will also lead to shifts in the anomalous magnetic moment of the electron, Δa_e, and, in the presence of CP violation, induce an electron EDM, d_e, (see Eqs. (5.16) and (5.17), respectively), and the lepton flavor violating mode $\tau \to e\gamma$ (see Eq. (5.33) with $|\lambda^q_{32}\lambda^{d*}_{33}|^2 \to |\lambda^d_{31}\lambda^{q*}_{33}|^2$). Note that the chiral enhancement of the dipole moments m_b/m_e can be particularly pronounced in the case of the electron.

In this scenario, potentially important constraints arise from the $B_s \to e^+e^-$ decay. The effect of the leptoquark is given by an expression analogous to Eq. (5.39) with $m_\mu \to m_e$ and $\lambda^f_{32}, \lambda^f_{22} \to \lambda^f_{31}, \lambda^f_{21}$, with the SM prediction given by $\mathrm{BR}(B_s \to e^+e^-) = (8.54 \pm 0.55) \times 10^{-14}$ [329]. Experimentally, the $B_s \to e^+e^-$ branching

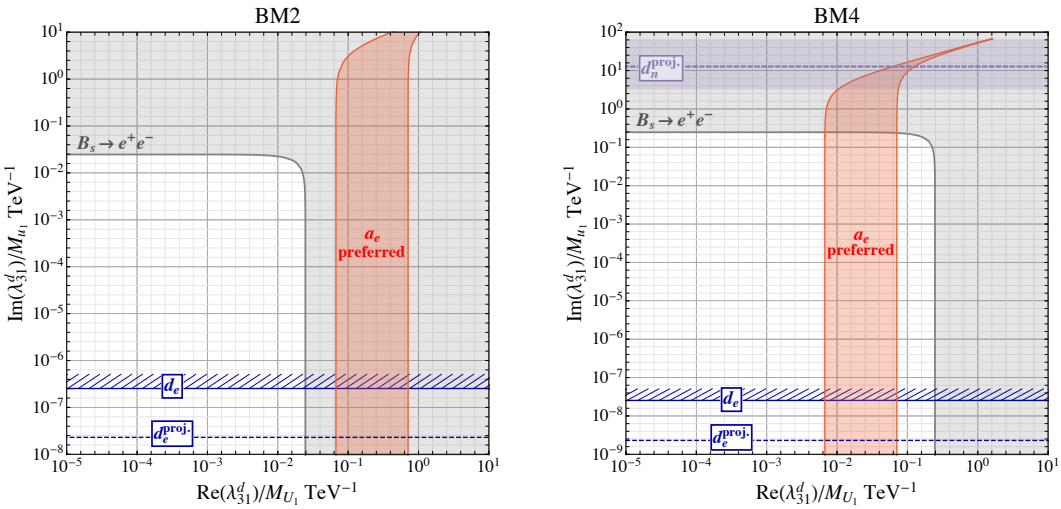

Figure 5.4: Constraints on the U_1 leptoquark parameter space in the plane of the complex coupling λ_{31}^d divided by the leptoquark mass for the benchmark points BM2 and BM4, left and right panel, respectively). The gray region is excluded by $B_s \to e^+e^-$ at the 95% C.L.. The red shaded region corresponds to the parameter space the can address the anomaly in the anomalous magnetic moment of the electron. The solid (dashed) blue lines represent the current constraint (projected sensitivity) from the electron EDM. In the right panel, the dashed purple line represents the projected sensitivity from the neutron EDM, with the purple band reflecting the uncertainty in the nucleon matrix element $\beta_n^{\tilde{G}}$.

ratio is bounded at the 90% C.L. by [336]

$$\text{BR}(B_s \to e^+e^-) < 2.8 \times 10^{-7} \ . \tag{5.41}$$

The plots in Fig. 5.4 show the current and projected constraints on the U_1 leptoquark in the plane of the complex coupling λ_{31}^d divided by the leptoquark mass for BM2 (left) and BM4 (right). In both panels the gray region is excluded by the bound from $B_s \to e^+e^-$, while the red shaded region is the region of parameter space that can address the 2.4σ anomaly in the electron magnetic moment, a_e. The blue solid (dashed) lines are the current constraint (projected sensitivity) of the electron electric dipole moment, d_e. In the right panel, the dashed purple line and the surrounding purple band is the projected sensitivity of the neutron EDM,

d_n.

For BM2 (left plot of Fig. 5.4) we observe that the region of parameter space that is able to address the anomaly in a_e is excluded by constraints from $B_s \to e^+e^-$ and a simultaneous explanation of all the B anomalies and a_e is not possible. This is due to stringent constraints on the size of λ^q_{31} from the lepton flavor violating decays $\tau \to \phi e$ and $B \to K\tau e$ (see discussion in Sec. 5.2.1). Constrains from the $\tau \to e\gamma$ are slightly weaker.

To avoid the stringent constraints from lepton flavor violating decays, we can set all the U_1 couplings to tau leptons to zero. Then, the $\tau \to \phi e$ and $B \to K\tau e$ rates as well as the $\tau \to e\gamma$ rate go to zero, and the left-handed couplings to electrons can be larger. However, by setting λ^q_{33} and λ^q_{23} to zero, we forgo an explanation of $R_{D^{(*)}}$. This scenario is given by BM4, and the resulting constraints are shown in the right plot of Fig. 5.4. We observe that the smaller value of $\lambda^q_{21} = 0.005$ in BM4 leads to weaker constraints on λ^d_{31} from $B_s \to e^+e^-$. In addition, the larger value of $\lambda^q_{31} = 0.5$ generates a larger contribution to the electron magnetic moment necessary to explain the slight tension in a_e. In moving from BM2 to BM4 the bound from $B_s \to e^+e^-$ opens up a wide region in parameter space favorable for the electron magnetic moment, a_e. We conclude that BM4 can address the anomalies in both $R_{K^{(*)}}$ and a_e.

We also investigated the region of parameter space with nonzero λ^d_{21} instead of λ^d_{31}. We find in BM2 and BM4 that sensitivity to d_e is reduced because it is chirally enhanced by m_s rather than m_b in Eq. (5.17). We also find no region of parameter space where the U_1 leptoquark explains the tension of the measured a_e with theory.

LHC Bounds on Scalar Leptoquarks		
Channel	Experiment	Limit
First Generation Leptoquarks		
$eejj$ ($\beta = 1$)	ATLAS [337]	1400 GeV
	CMS [338]	1435 GeV
$e\nu jj$ ($\beta = 0.5$)	ATLAS [337]	1290 GeV
	CMS [338]	1270 GeV
Second Generation Leptoquarks		
$\mu\mu jj$ ($\beta = 1$)	ATLAS [337]	1560 GeV
	CMS [339]	1530 GeV
$\mu\nu jj$ ($\beta = 0.5$)	ATLAS [337]	1230 GeV
	CMS [339]	1285 GeV
Third Generation Leptoquarks		
$b\tau b\tau$	ATLAS [340]	1030 GeV
	CMS [341]	1020 GeV
Reinterpreted SUSY searches		
$q\nu q\nu$	CMS [342]	980 GeV
$t\nu t\nu$	ATLAS [340]	1000 GeV
	CMS [342]	1020 GeV
LHC Bounds on Vector Leptoquarks		
Channel	Experiment	Limit
Reinterpreted SUSY searches		
$q\nu q\nu$	CMS [342]	1410 GeV ($\kappa_s = 0$) 1790 GeV ($\kappa_s = 1$)
$t\nu t\nu$	CMS [342]	1460 GeV ($\kappa_s = 0$) 1780 GeV ($\kappa_s = 1$)

Table 5.2: LHC bounds on pair-production of scalar and vector leptoquarks. For scalar leptoquarks, the first three sections correspond to bounds from dedicated leptoquark searches, while the last section corresponds to bounds derived from the reinterpretation of squark pair production searches. For vector leptoquarks, only reintepreted SUSY searches exist. The parameter β denotes the branching ratio of the leptoquark to a quark and a charged lepton. We do not report the bounds on the decays of the LQ to down-type quarks and a neutrino since these decays do not exist in our model.

5.5 LHC Bounds on the Leptoquark

Low-energy flavor observables like those discussed in the previous sections provide an indirect probe of the U_1 leptoquark. A complementary approach to probe the existence of U_1 is direct production at high energy colliders and looking for signatures of their decay products. The goal of this section is to compute the lower bound on the leptoquark mass in the allowed regions of parameter space in Figs. 5.2 -5.4.

The two main production mechanisms are single production in association with a lepton ($gq \to \ell\, U_1$), and pair production ($gg, q\bar{q} \to U_1\, \overline{U_1}$). For a recent review see [343, 344]. Once produced, the leptoquark will decay into a pair of SM fermions. The interactions of the U_1 leptoquark with SM quarks and leptons in Eq. (5.9) generate the decays of U_1 into an up-type quark and a neutrino, or a down-type quark and a charged lepton. In the limit where M_{U_1} is much larger than the masses of the decay products, the partial widths of U_1 are given by

$$\Gamma(U_1 \to u_i \nu_j) = \frac{M_{U_1}}{24\pi} \left| \sum_{k=1,2,3} V_{ik} \lambda^q_{kj} \right|^2 , \tag{5.42a}$$

$$\Gamma(U_1 \to d_i \ell_j) = \frac{M_{U_1}}{24\pi} \left(\left|\lambda^q_{ij}\right|^2 + \left|\lambda^d_{ij}\right|^2 \right) , \tag{5.42b}$$

where $i, j = 1, 2, 3$ label the three generations.

Several dedicated searches for singly and pair produced scalar leptoquarks have been performed by the LHC, and are classified according to whether the leptoquark decays to first, second, or third generation fermions. The strongest bounds on leptoquark pair-production from ATLAS and CMS have been compiled in Tab. 5.2, where the searches are organized according to whether the branching ratio into a quark and a charged lepton (denoted by β) is 100% or 50%, with the remaining 50% to a quark and a neutrino. In addition, in the table we also report

the CMS reinterpretation of the squark pair production searches to place constraints on pair produced vector leptoquarks decaying to a quark and a neutrino, $t\nu$, or $q\nu$ ($q = u, c, d, s$) [342]. Similarly, ATLAS have presented reinterpretations of squark searches [340], although they only consider the decay of a leptoquark into 3rd generation quarks. We note that the ATLAS and CMS searches also consider leptoquark decays into down-type quarks and a neutrino (e.g $b\nu b\nu$ final states), but the corresponding couplings do not exist in our model and, therefore, we do not consider them here.

Singly produced scalar leptoquarks have been searched in ej, μj, and $b\tau$ final states. The bounds on the leptoquark mass from single production depends on the coupling of the leptoquark to quarks and leptons. For unit couplings, 8 TeV searches for single production of first and second generation scalar leptoquarks constrain the leptoquark mass to be above $\sim$ 1700 GeV and $\sim$ 700 GeV, respectively [345], while the 13 TeV search for third generation scalar leptoquarks constrains the mass to be above 740 GeV [346]. In our benchmark models, the leptoquarks are mainly coupled to bottom or strange quarks. For this reason, the searches for singly produced leptoquarks are less sensitive to our benchmark models than the searches for pair produced leptoquarks. In the following, we will discuss in some details the bounds from searches of pair produced leptoquarks in all benchmarks.

For BM1 and BM2, the dominant non-zero couplings of U_1 are couplings involving tau leptons ($\lambda^q_{33}, \lambda^q_{23}$) and the dominant decay modes are $U_1 \to b\tau, s\tau, t\nu_\tau, c\nu_\tau$. At small values of λ^d_{33} (see Fig. 5.2), the branching ratios of the $b\tau$ and $\tau\nu_\tau$ decay modes are similar in value ($\sim$ 0.25) and dominate over the $s\tau$ and $c\nu_\tau$ decays modes, which themselves have similar branching ratios ($\sim$ 0.18). For values of λ^d_{33} near the border of the region allowed by $B_s \to \tau^+\tau^-$ (see Fig. 5.2), the decay into

$b\tau$ becomes the dominant decay mode with $\mathrm{BR}(U_1 \to b\tau) \sim 0.4$.

The reinterpreted SUSY search for pair production of vector leptoquarks decaying to $t\nu$ [342] and the CMS search for leptoquarks decaying to $b\tau$ [341] are the most sensitive searches. We find that these searches yield a similar lower bound on the mass of U_1 at around 1.2 TeV in the region of parameter space with small λ^d_{33}. The exact bound varies by at most ∼100 GeV in the region allowed by $B_s \to \tau^+\tau^-$.

In BM3, U_1 couples dominantly to 2nd generation leptons and the main decay modes are $U_1 \to b\mu, s\mu, t\nu_\mu, c\nu_\mu$, with the $b\mu$ and $t\nu_\mu$ decays modes being the dominant ones since $\lambda^q_{32} \gg \lambda^q_{22}$, $\mathrm{BR}(U_1 \to t\nu_\mu) \sim \mathrm{BR}(U_1 \to b\mu) \sim 0.5$. The most stringent LHC constraint on this benchmark comes from the search for pair produced leptoquarks in final states with two muons and two jets in [339][3]. This search leads to the bound $m_{U_1} \gtrsim 1.9$ TeV. This bound is valid in the entire parameter space shown in the right panel Fig. 5.3, since λ^d_{32} is constrained to be very small, and therefore does not affect the leptoquark branching ratios.

Finally, in BM4, U_1 couples dominantly to 1st generation leptons and the main decay modes are $U_1 \to be$ and $U_1 \to t\nu_e$. In particular, at small values of λ^d_{31} (see Fig. 5.4), the branching ratios of these decay modes are very similar in value (~ 0.5). At larger values of λ^d_{31}, the branching ratio into be becomes the dominant one, with $\mathrm{BR}(U_1 \to be) \sim 0.7$ at the border of the allowed region for λ^d_{31}, as shown in the right plot of Fig. 5.4. The search for pair produced leptoquarks decaying in an electron and a jet in [338] provides the strongest constraint on the mass of U_1 and gives a lower bound of ~ 1.8 TeV at small values of λ^d_{31}. The exact bound varies by at most ∼100 GeV in the region allowed by $B_s \to e^+e^-$.

[3]The search does not require any anti-b tagging, and, therefore, we can simply apply it to our benchmark.

5.6 Conclusions

In this study, we focused on the possible, and quite likely, existence of new sources of CP violation if the flavor anomalies in $b \to c$ and $b \to s$ decays are due to new physics, specifically in the case where the new physics consists of a U_1 vector leptoquark. The underpinning of our study is that the U_1 vector leptoquark is one of the only (if not the only) new physics scenarios known to us that can provide a simultaneous explanation of the anomalies observed in lepton flavor universality ratios in $b \to c\ell\nu$ and $b \to s\ell\ell$ decays, $R_{D^{(*)}}$ and $R_{K^{(*)}}$. Since the couplings of the U_1 to quarks and leptons are generically CP violating, they are expected just as generically to produce potentially observable electric dipole moments (EDMs) in leptonic and hadronic systems. Here, we have first provided new, original, and complete formulae for the calculation of the relevant EDMs, and carried out a phenomenological study of a few benchmark cases of how EDMs can constrain the U_1 leptoquark interpretation of the anomalies.

We note that the expressions we provided are the most general expressions for dipole moments induced by vector leptoquarks at one loop level, accounting for the most generic set of leptoquark couplings, which can accomodate scenarios for which the leptoquark may be composite.

We explored the parameter space of the U_1 leptoquark in the vicinity of 4 benchmark points that explain the $R_{D^{(*)}}$ and $R_{K^{(*)}}$ anomalies (or a subset of them). We identified viable regions of parameter space where the existing discrepancies in the anomalous magnetic dipole moments of the electron a_e and the muon a_μ can be explained in addition to $R_K^{(*)}$. However, we concluded that a simultaneous explanation of all three classes of discrepancies ($R_{D^{(*)}}$, $R_{K^{(*)}}$, $a_{e,\mu}$) is not possible.

We found that, in the presence of non-zero CP-violating phases in the lepto-

quark couplings, EDMs play an important role in probing the parameter space of the model. Existing bounds on the electron EDM already exclude large parts of parameter space with CP violating leptoquark couplings to electrons. The expected sensitivities to the neutron EDM can probe into motivated parameter space and probe imaginary parts of leptoquark couplings to taus and muons.

Chapter 6

Conclusion and Outlook

It is an exciting time for particle physics. The advent of the LHC has shown that the SM is the most successful theoretical description of fundamental particles and their interactions, with the discovery of the Higgs boson being perhaps the greatest achievement of experimental and theoretical efforts. However, the SM faces many theoretical and experimental issues and it was hoped that the LHC would elucidate many, if not all, of them. Unfortunately, no new fundamental particles have been observed at the LHC since the discovery of the Higgs boson, raising doubt on many of ideas that have motivated searches for BSM physics (e.g. weak scale supersymmetry). Now more than ever it is important to begin exploring many BSM models that predict phenomenology that are very different from the standard searches at the LHC, and to motivate experimental collaborations to begin searching for these unique signatures.

In this thesis we have attempted to address two problems: the SM flavor puzzle and experimental anomalies in low energy flavor observables. The SM flavor puzzle is a question about the large hierarchies observed in the fermion masses, but can be rephrased into our lack of knowledge of the 125 GeV Higgs couplings to light fermions. From an experimental perspective, it is unknown if the VEV of the

Higgs is responsible for generating mass for the first and second generations of fermions. While there is experimental evidence that the 125 GeV couplings to the weak gauge bosons and the third generations fermions are SM-like, much less is known about its couplings to the light fermions.

In Part II we have attempted to answer the question: does the 125 GeV Higgs give mass to all SM fermions? The traditional approach to answering this question is to say "Yes! The 125 GeV Higgs give mass to all particle", and to then try to measure all the Higgs couplings very precisely at high-energy colliders. While the muon and the charm quark coupling are expected to be measured with great precision in the future [347], other techniques must be used to measure the Higgs couplings to the up, down, and strange quarks such as rare Higgs decays $h \to M\gamma$ to mesons M made up of light quarks, di-Higgs production, and deviations of the Higgs transverse momentum distribution . Even if in the far future the Higgs couplings to all fermions are measured, the situation is still unsatisfactory: the question of why there is large hierarchy in the SM Higgs couplings to fermions has not been answered.

A complimentary approach to answering this question was presented in Ch. 2. We have investigated a potential solution to the SM flavor puzzle by introducing an additional source of EWSB that couples exclusively to the first and second generations. In such a scenario, the SM Higgs generates mass only for the third generation fermions while a second Higgs doublet generates mass for the light fermions. In this way, the hierarchy in the couplings of the SM Higgs boson to quarks and leptons can be reduced to a hierarchy in the VEVs of the two Higgs doublets. In Ch. 2 we presented the first iteration of so-called 'Flavorful 2HDMs' where a suitable choice for the Yukawa matrices of the two Higgs doublets gives the observed values of the fermion masses and CKM quark mixing matrix. Such a

scenario has very distinct collider phenomenology compared to standard 2HDMs (e.g. Type I, II). Among the most interesting signatures are flavor changing decays of the heavy Higgs bosons involving second generation quarks and leptons (such as $H/ \to tc, \tau\nu$ and $H^\pm \to cb, cs, \mu\nu_\mu$), and decays to second (third) generation fermions that are enhanced (suppressed) compared to standard 2HDMs. In particular we found that the decay $H \to \mu\mu$ in the flavorul 2HDM is many orders of magnitude larger than, for example, a Type I 2HDM, and that the decay $H \to \tau\tau$ is highly suppressed. These collider signatures are very different than what is traditional searched for at the LHC, and the current searches are not sensitive probes of our model. We have discussed some of the signatures that are the most promising in constraining the parameter space of our model, such as signatures with same-sign top quarks in association with a light jet from processes like $pp \to tH \to ttc$ or $pp \to tH^\pm \to tts$. In Ch. 3 we presented a UV completion of the flavorful 2HDM via the flavor-locking mechanism, and we also explored the effects of tree-level flavor violating Higgs couplings on quark flavor observables.

In Ch. 4 we presented a few variations on the flavorful 2HDM theme. The flavorful 2HDM discussed above is a variation of the Type I 2HDM where the first and second generation fermions couple to a different Higgs double than the third generation; the third generation couples to the same Higgs doublet as in the Type I 2HDM. This idea can be extended to the other types of 2HDMs so that we have flavorful Type II, Flipped, and Lepton Specific 2HDMs. The phenomenology of these other flavorful 2HDMs with the CKM matrix generated in the down quark sector has been studied in [224], to which we point the reader for further reading. In this work we have presented flavorful 2HDMs with an additional variation: generating the CKM matrix in the up quark sector. The main result presented here is that this leads to enhanced flavor violating couplings of the SM-like Higgs boson

and we have studied the effect of this on rare top quark decays $t \to hq$. These decays can be enhanced compared to the SM values by many order of magnitude. We have shown that this prediction of our model is accessible at future collider such as the HL-LHC and the FCC. We have also presented a UV completion of this scenario. The flavor-locking mechanism is not suitable for generating the CKM matrix in the up quark sector and we instead used the Froggatt-Nielsen mechanism to generate the Yukawa textures presented in Ch. 4.

In Ch. 5 we studied the effects of a CP-violating leptoquark solution the anomalies observed in B meson decays. The U_1 leptoquark scenario generically introduces new sources of CP violation and we have explored, for the first time, their effects on electromagnetic dipole moments. We found that in certain regions of parameter space the U_1 leptoquark can can explain the experimental anomalies observed in the anomalous magnetic moment of the electron a_e and the muon a_μ, together with the anomalies seen in R_K and R_{K^*}. However, we concluded that all the anomalies $R_{K^{(*)}}, R_{D^{(*)}}, a_{e,\mu}$ can not be simultaneously explained by this leptoquark scenario. We additionally found that CP violation is constrained by electric dipole moments. In particular, the current bound on the value of the electron EDM imposes severe constraints on the amount of CP violation in leptoquarks that couple dominantly to electrons. On the other hand, the current and projected bounds on the EDMs of the muon and tau are not yet probing the parameter space leptoquarks that couple to dominantly to muons and taus, respectively. On the other hand, the U_1 leptquark will contribute the neutron EDM and future project on d_n are beginning to probe the parameter space of our model.

Appendix A

The General Flavon Potential and the Flavor Basis of the Flavor-Locked F2HDM

A.1 Analysis of the general flavon potential

In this appendix we determine the global minimum of the flavon potential (3.8).

A.1.1 General flavon potential

The single and pairwise field potentials (3.9), (3.10) are manifestly positive semidefinite. Noting that the μ_6 terms can be written in the form $\mathrm{Tr}\Big([\lambda_\alpha \lambda_\beta^\dagger]^\dagger \lambda_\alpha \lambda_\beta^\dagger\Big)$ and $\mathrm{Tr}\Big([\lambda_\alpha^\dagger \lambda_\beta]^\dagger \lambda_\alpha^\dagger \lambda_\beta\Big)$ and moreover that $\mathrm{Tr}\Big[A^\dagger A\Big] = \sum_{ij} |A_{ij}|^2 = 0$ if and only if

$A = 0$, the global minimum – zero – of $V_{1\mathrm{f}}, V_{2\mathrm{f}}$ is attained if and only if

$$\begin{aligned} &1.\ \mathrm{Tr}\Big[\langle\lambda_\alpha\rangle\langle\lambda_\alpha^\dagger\rangle\Big] = r^2, \\ &2.\ \langle\lambda_\alpha\rangle \text{ is rank-1}, \\ &3.\ \langle\lambda_\alpha^\dagger\rangle\langle\lambda_\beta\rangle = 0 \text{ and } \langle\lambda_\alpha\rangle\langle\lambda_\beta^\dagger\rangle = 0 \text{ for all } \alpha \neq \beta. \end{aligned} \tag{A.1}$$

These algebraic conditions are equivalent to the set $\langle\lambda_\alpha\rangle$ being simultaneously real diagonalizable with disjoint unit rank spectra. That is,

$$\langle\lambda_1\rangle = U\,\mathrm{diag}\{r,0,0,\ldots\}\,V^\dagger\,, \qquad \langle\lambda_2\rangle = U\,\mathrm{diag}\{0,r,0,\ldots\}\,V^\dagger\,,\ldots\,, \tag{A.2}$$

with U, V generic unitary matrices, the same for all λ_α, that are flat directions of the global minimum, and r real. A similar analysis follows immediately for the down-type potentials, so that

$$\langle\lambda_{\widehat{1}}\rangle = \widehat{U}\,\mathrm{diag}\{\widehat{r},0,0,\ldots\}\,\widehat{V}^\dagger\,, \qquad \langle\lambda_{\widehat{2}}\rangle = \widehat{U}\,\mathrm{diag}\{0,\widehat{r},0,\ldots\}\,\widehat{V}^\dagger\,,\ldots\,. \tag{A.3}$$

We refer to this type of aligned structure as 'flavor-locked'. (It is possible to switch the rank-1 structure for degeneracy by setting $\mu_2 < 0$ [194], though we do not consider this possibility in this work.)

A.1.2 Mixing terms: single flavon generation

The first, ν_1, term of the mixed potential (3.11) manifestly respects the vacuum of $V_{1\mathrm{f}}$ and $V_{2\mathrm{f}}$. It follows from the Cauchy-Schwarz inequality and positive

semidefiniteness of $\lambda_\alpha \lambda_\alpha^\dagger$, that

$$\mathrm{Tr}\left(\lambda_\alpha \lambda_\alpha^\dagger\right) \mathrm{Tr}\left(\lambda_{\widehat{\alpha}} \lambda_{\widehat{\alpha}}^\dagger\right) \geq \mathrm{Tr}\left(\lambda_\alpha \lambda_\alpha^\dagger \lambda_{\widehat{\alpha}} \lambda_{\widehat{\alpha}}^\dagger\right). \tag{A.4}$$

Hence for the case of $n = 1$ generations of flavons, the ν_2 term and full potential is immediately positive semidefinite, with global minimum at $V_{\mathrm{fl}} = 0$. Based on the flavor-locked configurations in Eqs. (A.2) and (A.3),

$$[\langle \lambda_\alpha^\dagger \rangle \langle \lambda_{\widehat{\alpha}} \rangle]_{I\widehat{J}} = \mathcal{V}_{\mathrm{ckm}}^{\alpha\widehat{\alpha}} r\widehat{r}\ [V]_{IJ} \delta_{\alpha J} \delta_{\widehat{\alpha}\widehat{I}} [\widehat{V}]^\dagger_{\widehat{I}\widehat{J}}, \tag{A.5}$$

in which we have momentarily restored the $U(N)_U \times U(N)_D$ indices and $\mathcal{V}_{\mathrm{ckm}} = U^\dagger \widehat{U}$ is the unitary CKM matrix. Without loss of generality, we can choose the non-zero eigenvalues of the single up and down flavon being in the first diagonal entry, at the flavor-locked configuration. One then obtains for the $n = 1$ mixed potential

$$V_{\mathrm{mix}} = -\nu_2 r^2 \widehat{r}^2 \left[\left| \mathcal{V}_{\mathrm{ckm}}^{1\widehat{1}} \right|^2 - 1 \right]. \tag{A.6}$$

This vanishes if and only if $\mathcal{V}_{\mathrm{ckm}}$ is $1 \oplus (N-1)$ block unitary, i.e.

$$\mathcal{V}_{\mathrm{ckm}} = \begin{pmatrix} 1 & 0 \\ 0 & \mathcal{V}_{N-1} \end{pmatrix}, \tag{A.7}$$

in which $\mathcal{V}_{N-1}$ is an $N-1 \times N-1$ unitary submatrix (as in Eq. (3.14)). Therefore, the potential has a global minimum if and only if the flavons lie in the flavor-locked configuration, with a block-unitary mixing matrix.

A.1.3 Mixing terms: arbitrary flavon generations

For the general case that $N \geq n \geq 1$, the ν_2 term is not positive definite by itself. The full potential may, however, be reorganized into the form

$$V_{\rm fl} = \sum_{\alpha} U_{\rm 1f}^{\alpha} + \sum_{\alpha<\beta} U_{\rm 2f}^{\alpha\beta} + \sum_{\widehat{\alpha}} U_{\rm 1f}^{\widehat{\alpha}} + \sum_{\widehat{\alpha}<\widehat{\beta}} U_{\rm 2f}^{\widehat{\alpha}\widehat{\beta}} + U_{\rm mix}^{0} + \sum_{\alpha,\widehat{\alpha}} U_{\rm mix}^{\alpha\widehat{\alpha}} \,. \tag{A.8}$$

in which the pure up-type potentials

$$\begin{aligned} U_{\rm 1f}^{\alpha} &= \mu_1 \left| \mathrm{Tr}\left(\lambda_\alpha^\dagger \lambda_\alpha\right) - r^2 \right|^2 + \left(\mu_2 + \frac{\nu_2}{2}\frac{\widehat{r}^2}{r^2}\right)\left[\left| \mathrm{Tr}\left(\lambda_\alpha^\dagger \lambda_\alpha\right)\right|^2 - \mathrm{Tr}\left(\lambda_\alpha \lambda_\alpha^\dagger \lambda_\alpha \lambda_\alpha^\dagger\right)\right], \\ U_{\rm 2f}^{\alpha\beta} &= \mu_3 \left| \mathrm{Tr}\left(\lambda_\alpha^\dagger \lambda_\alpha\right) - \mathrm{Tr}\left(\lambda_\beta^\dagger \lambda_\beta\right)\right|^2 + \mu_4 \left| \mathrm{Tr}\left(\lambda_\alpha^\dagger \lambda_\beta\right)\right|^2 \\ &\quad + \mu_{6,1}\,\mathrm{Tr}\left(\lambda_\alpha^\dagger \lambda_\alpha \lambda_\beta^\dagger \lambda_\beta\right) + \left(\mu_{6,2} - \frac{\nu_2 \widehat{r}^2}{r^2}\right)\mathrm{Tr}\left(\lambda_\alpha \lambda_\alpha^\dagger \lambda_\beta \lambda_\beta^\dagger\right), \end{aligned} \tag{A.9}$$

and similarly for the down-type potentials, exchanging all unhatted and hatted couplings. The two mixed potentials

$$U_{\rm mix}^{0} = \frac{\nu_2 r^2 \widehat{r}^2}{2}\,\mathrm{Tr}\left[\left(\sum_{\alpha}\frac{\lambda_\alpha \lambda_\alpha^\dagger}{r^2} - \sum_{\widehat{\alpha}}\frac{\lambda_{\widehat{\alpha}} \lambda_{\widehat{\alpha}}^\dagger}{\widehat{r}^2}\right)^2\right], \tag{A.10}$$

$$U_{\rm mix}^{\alpha\widehat{\alpha}} = \left(\nu_1 - \frac{\nu_2}{2n}\right) r^2 \widehat{r}^2 \left| \mathrm{Tr}\left(\lambda_\alpha \lambda_\alpha^\dagger\right)/r^2 - \mathrm{Tr}\left(\lambda_{\widehat{\alpha}} \lambda_{\widehat{\alpha}}^\dagger\right)/\widehat{r}^2 \right|^2 . \tag{A.11}$$

Hence each term of the full potential is now positive semidefinite, provided

$$\mu_{6,2} \geq \nu_2 \widehat{r}^2/r^2 \,, \qquad \widehat{\mu}_{6,2} \geq \nu_2 r^2/\widehat{r}^2 \,, \qquad \text{and} \qquad \nu_1 \geq \nu_2/(2n) \,. \tag{A.12}$$

We write the flavor-locked configuration in the ordered form of Eqs. (A.2) and (A.3), so that the first n eigenvalues of $\langle \lambda_\alpha \rangle$ are non-zero. At the flavor-locked

configuration, the mixed potential becomes

$$\sum_{\alpha,\widehat{\alpha}} V_{\rm mix}^{\alpha\widehat{\alpha}} = -\nu_2 r^2 \widehat{r}^2 \sum_{\alpha,\widehat{\alpha}} \left[\left| \mathcal{V}_{\rm ckm}^{\alpha\widehat{\alpha}} \right|^2 - 1/n \right] = 0\,. \tag{A.13}$$

Unitarity ensures that

$$\sum_{\alpha,\widehat{\alpha}=1}^{n} \left| \mathcal{V}_{\rm ckm}^{\alpha\widehat{\alpha}} \right|^2 \leq n\,, \tag{A.14}$$

so that on the flavor-locked contour the mixing terms and hence full potential is minimized, with $V_{\rm fl} = 0$, if and only if $\mathcal{V}_{\rm ckm}$ is $n \oplus (N-n)$ block unitary. I.e.

$$\mathcal{V}_{\rm ckm} = U^\dagger \widehat{U} = \begin{pmatrix} \mathcal{V}_n & 0 \\ 0 & \mathcal{V}_{N-n} \end{pmatrix}, \tag{A.15}$$

with $\mathcal{V}_k$ a $k \times k$ unitary matrix. Note that the n or $N-n$ block CKM rotations are flat directions of the global minimum, and therefore $\mathcal{V}_n$ and $\mathcal{V}_{N-n}$ may be any arbitrary unitary submatrices with generically $\mathcal{O}(1)$ entries. We often refer to Eq. (A.15) in combination with Eqs. (A.2) and (A.3) as the 'flavor-locked' configuration, too.

A.1.4 Local minimum analysis

So far we have shown that under the conditions (A.12) the global minimum of the potential is $V_{\rm fl} = 0$ and it is realized if and only if the flavons are in the flavor-locked configuration. One may also explore the weaker condition that the flavor-locked configuration is only a local minimum of the potential, by applying the general perturbations

$$\langle \lambda_\alpha \rangle \to \langle \lambda_\alpha \rangle + \epsilon X_\alpha\,, \qquad \text{and} \qquad \langle \lambda_{\widehat{\alpha}} \rangle \to \langle \lambda_{\widehat{\alpha}} \rangle + \epsilon X_{\widehat{\alpha}}\,. \tag{A.16}$$

To this end, it is convenient to define

$$H_\alpha = \frac{1}{r^2}\Big[\langle\lambda_\alpha\rangle X_\alpha^\dagger + X_\alpha\langle\lambda_\alpha^\dagger\rangle\Big]\,, \qquad P = \frac{1}{r^2}\sum_\alpha \langle\lambda_\alpha\rangle\langle\lambda_\alpha^\dagger\rangle\,, \qquad \widehat{P} = \frac{1}{\widehat{r}^2}\sum_{\widehat{\alpha}}\langle\lambda_{\widehat{\alpha}}\rangle\langle\lambda_{\widehat{\alpha}}^\dagger\rangle\,, \tag{A.17}$$

Observe H_α is Hermitian and $\mathrm{Tr}[P] = n$. One may show that $\mathrm{Tr}[PH_\alpha] = \mathrm{Tr}[H_\alpha]$, and, as a consequence of the block unitarity (A.15), that further $\mathrm{Tr}\Big[\widehat{P}H_\alpha\Big] = \mathrm{Tr}[H_\alpha]$. Under perturbation of the mixing terms, one finds to $\mathcal{O}(\epsilon^2)$,

$$\begin{aligned}\delta[U^0_{\rm mix} + \sum_{\alpha,\widehat{\alpha}} U^{\alpha\widehat{\alpha}}_{\rm mix}] = \epsilon^2\frac{\nu_2 r^2\widehat{r}^2}{2}\,\mathrm{Tr}\left[\Big(\sum_\alpha H_\alpha - \sum_{\widehat{\alpha}} H_{\widehat{\alpha}}\Big)^2\right] \\ + \epsilon^2\left(\nu_1 - \frac{\nu_2}{2n}\right)r^2\widehat{r}^2\sum_{\alpha,\widehat{\alpha}}\Big|\,\mathrm{Tr}\,H_\alpha - \mathrm{Tr}\,H_{\widehat{\alpha}}\Big|^2\,,\end{aligned} \tag{A.18}$$

which is positive semidefinite, provided the condition

$$\nu_1 \geq \nu_2/(2n)\,, \tag{A.19}$$

holds (cf. (A.12)). The vacuum configuration in (3.13) is then a local minimum of the flavon potential.

More generically, one may also re-organize the potential, such that

$$V_{\rm fl} = \bar{U}^0_{\rm 1f} + \sum_\alpha \bar{U}^\alpha_{\rm 1f} + \sum_{\alpha<\beta}\bar{U}^{\alpha\beta}_{\rm 2f} + \sum_{\widehat{\alpha}}\bar{U}^{\widehat{\alpha}}_{\rm 1f} + \sum_{\widehat{\alpha}<\widehat{\beta}}\bar{U}^{\widehat{\alpha}\widehat{\beta}}_{\rm 2f} + \bar{U}^0_{\rm mix} + \sum_{\alpha,\,\widehat{\alpha}}\bar{U}^{\alpha\widehat{\alpha}}_{\rm mix}\,. \tag{A.20}$$

in which we have defined, for an arbitrary real coefficient, ω,

$$\begin{aligned}\bar{U}^0_{\rm 1f} &= \omega\frac{\nu_2}{2n}\frac{\widehat{r}^2}{r^2}\Big|\sum_\alpha\Big[\,\mathrm{Tr}\left(\lambda_\alpha^\dagger\lambda_\alpha\right) - r^2\Big]\Big|^2 \\ \bar{U}^\alpha_{\rm 1f} &= \left(\mu_1 - \omega\frac{\nu_2}{2}\frac{\widehat{r}^2}{r^2}\right)\Big|\,\mathrm{Tr}\left(\lambda_\alpha^\dagger\lambda_\alpha\right) - r^2\Big|^2\end{aligned}$$

$$+\left(\mu_2+\frac{\nu_2}{2}\frac{\widehat{r}^2}{r^2}\right)\left[\left|\operatorname{Tr}\left(\lambda_\alpha^\dagger\lambda_\alpha\right)\right|^2-\operatorname{Tr}\left(\lambda_\alpha\lambda_\alpha^\dagger\lambda_\alpha\lambda_\alpha^\dagger\right)\right],$$

$$\bar{U}_{2\mathrm{f}}^{\alpha\beta}=\left(\mu_3-(1-\omega)\frac{\nu_2}{2n}\frac{\widehat{r}^2}{r^2}\right)\left|\operatorname{Tr}\left(\lambda_\alpha^\dagger\lambda_\alpha\right)-\operatorname{Tr}\left(\lambda_\beta^\dagger\lambda_\beta\right)\right|^2+\mu_4\left|\operatorname{Tr}\left(\lambda_\alpha^\dagger\lambda_\beta\right)\right|^2$$
$$+\mu_{6,1}\operatorname{Tr}\left(\lambda_\alpha^\dagger\lambda_\alpha\lambda_\beta^\dagger\lambda_\beta\right)+\left(\mu_{6,2}-\frac{\nu_2\widehat{r}^2}{r^2}\right)\operatorname{Tr}\left(\lambda_\alpha\lambda_\alpha^\dagger\lambda_\beta\lambda_\beta^\dagger\right), \tag{A.21}$$

and analogously in the down sector for the $\widehat{\alpha}$ and $\widehat{\beta}$ pieces. The mixing terms are given by

$$\bar{U}_{\mathrm{mix}}^{0}=\frac{\nu_2 r^2\widehat{r}^2}{2}\left\{\operatorname{Tr}\left[\left(\sum_\alpha\frac{\lambda_\alpha\lambda_\alpha^\dagger}{r^2}-\sum_{\widehat{\alpha}}\frac{\lambda_{\widehat{\alpha}}\lambda_{\widehat{\alpha}}^\dagger}{\widehat{r}^2}\right)^2\right]-\frac{1}{n}\left|\operatorname{Tr}\left(\sum_\alpha\frac{\lambda_\alpha\lambda_\alpha^\dagger}{r^2}-\sum_{\widehat{\alpha}}\frac{\lambda_{\widehat{\alpha}}\lambda_{\widehat{\alpha}}^\dagger}{\widehat{r}^2}\right)\right|^2\right\},$$
$$\bar{U}_{\mathrm{mix}}^{\alpha\widehat{\alpha}}=\nu_1 r^2\widehat{r}^2\left|\operatorname{Tr}\left(\lambda_\alpha\lambda_\alpha^\dagger\right)/r^2-\operatorname{Tr}\left(\lambda_{\widehat{\alpha}}\lambda_{\widehat{\alpha}}^\dagger\right)/\widehat{r}^2\right|^2. \tag{A.22}$$

This time, under perturbations of the flavor-locked configuration, one finds

$$\delta\bar{U}_{\mathrm{mix}}^{0}=\epsilon^2\frac{\nu_2 r^2\widehat{r}^2}{2}\operatorname{Tr}\left[\left(\sum_\alpha H_\alpha-\sum_{\widehat{\alpha}}H_{\widehat{\alpha}}-\frac{P}{n}\operatorname{Tr}\left[\sum_\alpha H_\alpha-\sum_{\widehat{\alpha}}H_{\widehat{\alpha}}\right]\right)^2\right], \tag{A.23}$$

which is positive semidefinite. Hence, no matter the form of the ν_1 term, a local minimum can also be achieved for the case that

$$\mu_1\geq\omega\frac{\nu_2}{2}\frac{\widehat{r}^2}{r^2}, \qquad \mu_3\geq(1-\omega)\frac{\nu_2}{2n}\frac{\widehat{r}^2}{r^2}, \qquad \omega\geq 0, \qquad \mu_{6,2}\geq\frac{\nu_2\widehat{r}^2}{r^2}, \tag{A.24}$$

and similarly for the hatted couplings.

A.1.5 Two-Higgs alignment conditions

The Two-Higgs potential (3.20) is equivalent to the general potential (3.8), but with the t–c, t–u and b–d, b–s cross-terms effectively vanishing. The vacuum for

$V_{1\text{f}} + V_{2\text{f}}$ then has the structure

$$\begin{aligned}
&1.\ \mathrm{Tr}\Big[\langle\lambda_\alpha^\dagger\rangle\langle\lambda_\alpha\rangle\Big] = r^2, \\
&2.\ \langle\lambda_\alpha\rangle \text{ is rank-1}, \\
&3.\ \langle\lambda_c^\dagger\rangle\langle\lambda_u\rangle = 0 \text{ and } \langle\lambda_c\rangle\langle\lambda_u^\dagger\rangle = 0
\end{aligned} \tag{A.25}$$

but neither $\langle\lambda_t^\dagger\rangle\langle\lambda_{c,u}\rangle$ nor $\langle\lambda_t\rangle\langle\lambda_{c,u}^\dagger\rangle$ need to vanish, and similarly for the down-type flavons. The potentials $V_{\text{fl,h}}$ and $V_{\text{fl,l}}$ then each have a $N = 3$ flavor-locked vacuum, with generation number $n = 1$ and $n = 2$, respectively. This leads immediately to the vacuum in Eqs (3.21) and (3.22).

A.2 Flavor basis for the F2HDM Yukawa texture

Starting from the general parametrization of the flavor-locked Yukawas in (3.25) we perform the following quark field rotations in flavor space

$$U_L \to \mathcal{U}_{U_L} U_L\ ,\quad D_L \to \mathcal{U}_{D_L} D_L\ ,\quad U_R \to \mathcal{U}_{U_R} U_R\ ,\quad D_R \to \mathcal{U}_{D_R} D_R\ , \tag{A.26}$$

where the $\mathcal{U}_i$ are $2 \oplus 1$ block unitary matrices

$$\begin{aligned}
\mathcal{U}_{U_L} &= \begin{pmatrix} \cos\theta_{U_L} & \sin\theta_{U_L} & 0 \\ -\sin\theta_{U_L} & \cos\theta_{U_L} & 0 \\ 0 & 0 & 1 \end{pmatrix}\ ,\quad \mathcal{U}_{D_L} = \begin{pmatrix} \cos\theta_{D_L} e^{i\psi_{D_L}} & \sin\theta_{D_L} & 0 \\ -\sin\theta_{D_L} e^{i\psi_{D_L}} & \cos\theta_{D_L} & 0 \\ 0 & 0 & 1 \end{pmatrix}\ , \\
\mathcal{U}_{U_R} &= \begin{pmatrix} \cos\theta_{U_R} & \sin\theta_{U_R} & 0 \\ -\sin\theta_{U_R} & \cos\theta_{U_R} & 0 \\ 0 & 0 & 1 \end{pmatrix}\ ,\quad \mathcal{U}_{D_R} = \begin{pmatrix} \cos\theta_{D_R} & \sin\theta_{D_R} & 0 \\ -\sin\theta_{D_R} & \cos\theta_{D_R} & 0 \\ 0 & 0 & 1 \end{pmatrix}\ .
\end{aligned} \tag{A.27}$$

The rotation angels and the phase are chosen such that

$$\tan\theta_{U_L} = \sin\theta_{13}\tan\theta_{23}\ , \tag{A.28}$$

$$\tan\theta_{U_R} = \sin\vartheta_{13}\tan\vartheta_{23}\ , \tag{A.29}$$

$$\tan\theta_{D_R} = \sin\widehat{\vartheta}_{13}\tan\widehat{\vartheta}_{23}\ , \tag{A.30}$$

$$\tan\theta_{D_L} = \sin\theta_{13}\tan\theta_{23}\cos\psi_{D_L} - \tan\theta\frac{\cos\theta_{13}}{\cos\theta_{23}}\cos(\psi_m+\psi_{D_L})\ , \tag{A.31}$$

$$\tan\psi_{D_L} = \frac{\tan\theta\sin\psi_m}{\sin\theta_{23}\tan\theta_{13}-\tan\theta\cos\psi_m}\ . \tag{A.32}$$

In this flavor basis the Yukawas in (3.25) reproduce the F2HDM textures from Eq. (3.4) with coefficients that depend on the several angles $\theta_{13},\theta_{23},\vartheta_{13},\vartheta_{23}$, $\widehat{\vartheta}_{13},\widehat{\vartheta}_{23},\theta$ and phases $\psi_d,\psi_s,\psi_u,\psi_c,\psi_m$.

Appendix B

Yukawa Couplings, Loop Functions, and Higgs Constraints on the F2HDM with Up Quark Sector CKM

B.1 Yukawa Couplings in the Quark Mass Eigenstate Basis

In this appendix we show that in the considered type IB and lepton-specific B models, the couplings of the Higgs bosons to the quarks in the quark mass eigenstate basis are entirely determined by the known quark masses and CKM elements.

The starting point are the Yukawa couplings λ^q and λ'^q in Eq. (5.9) that need to be rotated into the quark mass eigenstate basis. We perform unitary rotations on the left-handed and right-handed quark fields $q_{L/R} \to U_{q_{L/R}} q_{L/R}$ such that $U_{u_L}^\dagger (v\lambda^u + v'\lambda'^u) U_{u_R} = \mathrm{diag}(m_u, m_c, m_t) \equiv m_u^{\mathrm{diag}}$ and analogous for the down

quarks. Given the structure of λ^u and λ'^u in Eq. (4.4a) we can introduce the matrix $\Pi = \mathrm{diag}(0,0,1)$ that leaves λ^u invariant and that annihilates λ'^u: $\Pi\,\lambda^u = \lambda^u$ and $\Pi\,\lambda'^u = 0$. Using this matrix, we can express λ^u in the mass eigenstate basis directly in terms of quark masses and the CKM matrix

$$U_{u_L}^\dagger \lambda^u U_{u_R} = U_{u_L}^\dagger \Pi(\lambda^u + \frac{v'}{v}\lambda'^u) U_{u_R} = \frac{\sqrt{2}}{v} U_{u_L}^\dagger \Pi\, U_{u_L} m_u^{\mathrm{diag}} = \frac{\sqrt{2}}{v} V_{\mathrm{CKM}} \Pi\, V_{\mathrm{CKM}}^\dagger m_u^{\mathrm{diag}} \,. \tag{B.1}$$

In the last step we used the definition of the CKM matrix $V_{\mathrm{CKM}} = U_{u_L}^\dagger U_{d_L}$ and the fact that U_{d_L} and Π commute due to the structure of λ^d and λ'^d in Eq. (4.4b). Analogously, we can use the matrix $\Pi' = \mathrm{diag}(1,1,0)$ to get an expression for λ'^u in the mass eigenstate basis

$$U_{u_L}^\dagger \lambda'^u U_{u_R} = U_{u_L}^\dagger \Pi'(\frac{v}{v'}\lambda^u + \lambda'^u) U_{u_R} = \frac{\sqrt{2}}{v'} U_{u_L}^\dagger \Pi'\, U_{u_L} m_u^{\mathrm{diag}} = \frac{\sqrt{2}}{v'} V_{\mathrm{CKM}} \Pi'\, V_{\mathrm{CKM}}^\dagger m_u^{\mathrm{diag}} \,. \tag{B.2}$$

In the down quark sector we instead get

$$U_{d_L}^\dagger \lambda^d U_{d_R} = U_{d_L}^\dagger \Pi(\lambda^d + \frac{v'}{v}\lambda'^d) U_{d_R} = \frac{\sqrt{2}}{v} U_{d_L}^\dagger \Pi\, U_{d_L} m_d^{\mathrm{diag}} = \frac{\sqrt{2}}{v} \Pi\, m_d^{\mathrm{diag}} \,, \tag{B.3}$$

$$U_{d_L}^\dagger \lambda'^d U_{d_R} = U_{d_L}^\dagger \Pi'(\frac{v}{v'}\lambda^d + \lambda'^d) U_{d_R} = \frac{\sqrt{21}}{v'} U_{d_L}^\dagger \Pi'\, U_{d_L} m_d^{\mathrm{diag}} = \frac{\sqrt{2}}{v'} \Pi'\, m_d^{\mathrm{diag}} \tag{B.4}$$

B.2 Loop Functions for $b \to s\gamma$

In this appendix we give the explicit expressions for the loop functions that enter the results for the charged Higgs contributions to the $b \to s\gamma$ decay in section 4.3.

$$f_7(x) = \frac{(2-3x)^2 \log x}{12(1-x)^4} + \frac{11 - 43x + 38x^2}{72(1-x)^3} \,, \quad \lim_{x\to 0} f_7(x) = \frac{1}{3}\log(x) + \frac{11}{72} \,, \tag{B.5}$$

$$f_8(x) = \frac{(2-3x)\log x}{4(1-x)^4} + \frac{16-29x+7x^2}{24(1-x)^3} \ , \qquad \lim_{x\to 0} f_8(x) = \frac{1}{2}\log(x) + \frac{2}{3} \ , \quad \text{(B.6)}$$

$$g_7(x) = -\frac{x(2-3x)\log x}{12(1-x)^4} - \frac{7-5x-8x^2}{72(1-x)^3} \ , \qquad \lim_{x\to 0} g_7(x) = -\frac{7}{72} \ , \quad \text{(B.7)}$$

$$g_8(x) = -\frac{x\log x}{4(1-x)^4} - \frac{2+5x-x^2}{24(1-x)^3} \ , \qquad \lim_{x\to 0} g_8(x) = -\frac{1}{12} \ , \quad \text{(B.8)}$$

$$h_7(x) = \frac{(2-3x)\log x}{6(1-x)^3} + \frac{3-5x}{12(1-x)^2} \ , \qquad \lim_{x\to 0} h_7(x) = \frac{1}{3}\log(x) + \frac{1}{4} \ , \quad \text{(B.9)}$$

$$h_8(x) = \frac{\log x}{2(1-x)^3} + \frac{3-x}{4(1-x)^2} \ , \qquad \lim_{x\to 0} h_8(x) = \frac{1}{2}\log(x) + \frac{3}{4} \ . \quad \text{(B.10)}$$

B.3 Loop Function for $t \to hq$

The loop function $\mathcal{F}$ that enters our SM expression of the rare top branching ratios Eq. (4.15) can be written as

$$\begin{aligned}\mathcal{F}(x,y) =& \frac{1}{16(x-y)^2}\Big| x\Big(B_0(0,0,1) - B_0(x,0,1)\Big) + y\Big(B_0(y,0,0) - B_0(0,0,1)\Big) \\ & 4\Big(B_0(x,0,1) - B_0(y,0,0)\Big) + (2+y)\Big(B_0(y,1,1) - B_0(x,1,0)\Big) \\ & - (4-2x+y)C_0(y,x,0,0,0,1) \\ & + (2-y+y^2-x(2+y))C_0(y,x,0,1,1,0) + 2(y-x)B_0'(0,1,0) \\ & + 2(x-2)B_0'(x,1,0) + 2(x^2+y-xy-2)C_0'(y,x,0,1,1,0)\Big|^2 \ , \end{aligned} \quad \text{(B.11)}$$

with the following definitions of the Passarino-Veltman functions

$$\frac{i}{16\pi^2} B_0(p^2, m_1^2, m_2^2) = \bar{\mu}^{4-D} \int \frac{\mathrm{d}^D q}{(2\pi)^D} \frac{1}{(q^2-m_1^2)((q+p)^2-m_2^2)} \ , \quad \text{(B.12)}$$

$$\begin{aligned}&\frac{i}{16\pi^2} C_0(p^2, k^2, (p+k)^2, m_1^2, m_2^2, m_3^2) \\ &\qquad = \int \frac{\mathrm{d}^4 q}{(2\pi)^4} \frac{1}{(q^2-m_1^2)((q+p)^2-m_2^2)((q+p+k)^2-m_3^2)} \ . \end{aligned} \quad \text{(B.13)}$$

The derivatives in Eq. (B.11) act on the last argument of the functions, i.e.

$$B_0'(a,b,c) = \frac{\partial}{\partial c} B_0(a,b,c) \ , \tag{B.14}$$

$$C_0'(a,b,c,d,e,f) = \frac{\partial}{\partial f} C_0(a,b,c,d,e,f) \ . \tag{B.15}$$

B.4 Higgs Signal Strength Fit

Away from the alignment limit $\cos(\beta-\alpha)=0$, the couplings of the 125 GeV Higgs boson differ from their SM predictions. Therefore, signal strength measurements from ATLAS and CMS can be used to constrain the parameter space of our 2HDMs. With respect to our previous signal strength analysis in [224], we include LHC Run 2 updates of $h \to WW$ [348–350], $h \to \tau\tau$ [32, 351], $h \to \mu\mu$ [352], the recent $h \to bb$ observations [33, 34] and the results for tth production [35, 36].

In Fig. B.1 we show the allowed ranges in the $\cos(\beta-\alpha)$ vs. $\tan\beta$ plane in the type IB model (top left), type IIB model (top right), lepton-specific B model (bottom left), and flipped B model (bottom right) at 1σ (dark green) and 2σ (light green). The dotted lines indicate the 2σ constraint in the corresponding 2HDMs with natural flavor conservation.

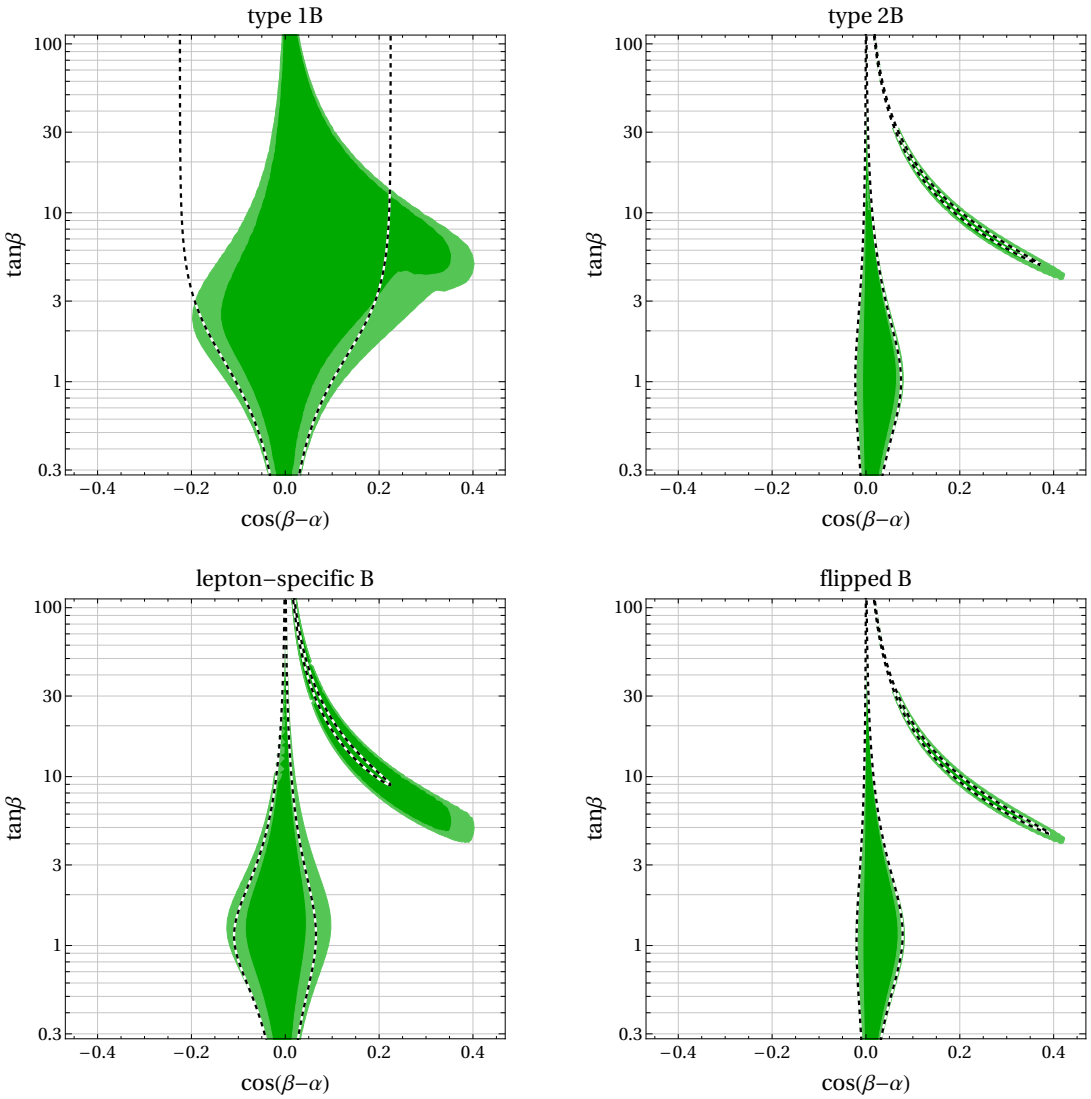

Figure B.1: Constraints in the $\cos(\beta - \alpha)$ vs. $\tan\beta$ plane based on LHC measurements of the 125 GeV Higgs signal strengths. Parameter space of the flavorful 2HDMs that is compatible with the data at the 1σ and 2σ level is shown in green. For comparison, the 2σ regions in the corresponding 2HDMs with natural flavor conservation are shown by dashed contours.

Bibliography

[1] ATLAS Collaboration, M. Aaboud et al., Search for top-quark decays $t \to Hq$ with 36 fb^{-1} of pp collision data at $\sqrt{s} = 13$ TeV with the ATLAS detector, JHEP **05** (2019) 123, arXiv:1812.11568 [hep-ex].

[2] ATLAS Collaboration, M. Aaboud et al., Search for new phenomena in events with same-charge leptons and b-jets in pp collisions at $\sqrt{s} = 13$ TeV with the ATLAS detector, JHEP **12** (2018) 039, arXiv:1807.11883 [hep-ex].

[3] Particle Data Group Collaboration, C. Patrignani et al., Review of Particle Physics, Chin. Phys. **C40** (2016) 100001.

[4] A. Hocker, H. Lacker, S. Laplace, and F. Le Diberder, A New approach to a global fit of the CKM matrix, Eur. Phys. J. C **21** (2001) 225–259, arXiv:hep-ph/0104062.

[5] CKMfitter Group Collaboration, J. Charles et al., CP violation and the CKM matrix: Assessing the impact of the asymmetric B factories, Eur. Phys. J. **C41** (2005) 1–131, arXiv:hep-ph/0406184 [hep-ph], and updates at http://ckmfitter.in2p3.fr/.

[6] ATLAS Collaboration, G. Aad et al., Observation of a new particle in the search for the Standard Model Higgs boson with the ATLAS detector at the LHC, Phys. Lett. B **716** (2012) 1–29, arXiv:1207.7214 [hep-ex].

[7] CMS Collaboration, S. Chatrchyan et al., Observation of a New Boson at a Mass of 125 GeV with the CMS Experiment at the LHC, Phys. Lett. B **716** (2012) 30–61, arXiv:1207.7235 [hep-ex].

[8] F. Englert and R. Brout, Broken Symmetry and the Mass of Gauge Vector Mesons, Phys. Rev. Lett. **13** (1964) 321–323.

[9] P. W. Higgs, Broken Symmetries and the Masses of Gauge Bosons, Phys. Rev. Lett. **13** (1964) 508–509.

[10] G. Guralnik, C. Hagen, and T. Kibble, Global Conservation Laws and Massless Particles, Phys. Rev. Lett. **13** (1964) 585–587.

[11] UA1 Collaboration, G. Arnison et al., Experimental Observation of Isolated Large Transverse Energy Electrons with Associated Missing Energy at $\sqrt{s}$ = 540-GeV, Phys. Lett. B **122** (1983) 103–116.

[12] UA2 Collaboration, M. Banner et al., Observation of Single Isolated Electrons of High Transverse Momentum in Events with Missing Transverse Energy at the CERN $p\bar{p}$ Collider, Phys. Lett. B **122** (1983) 476–485.

[13] UA1 Collaboration, G. Arnison et al., Experimental Observation of Lepton Pairs of Invariant Mass Around 95-GeV/c**2 at the CERN SPS Collider, Phys. Lett. B **126** (1983) 398–410.

[14] CDF Collaboration, F. Abe et al., Observation of top quark production in $\bar{p}p$ collisions, Phys. Rev. Lett. **74** (1995) 2626–2631, arXiv:hep-ex/9503002.

[15] D0 Collaboration, S. Abachi et al., Observation of the top quark, Phys. Rev. Lett. **74** (1995) 2632–2637, arXiv:hep-ex/9503003.

[16] SLAC-SP-017 Collaboration, J. Augustin et al., Discovery of a Narrow Resonance in e^+e^- Annihilation, Phys. Rev. Lett. **33** (1974) 1406–1408.

[17] E598 Collaboration, J. Aubert et al., Experimental Observation of a Heavy Particle J, Phys. Rev. Lett. **33** (1974) 1404–1406.

[18] TASSO Collaboration, R. Brandelik et al., Evidence for Planar Events in e+ e- Annihilation at High-Energies, Phys. Lett. B **86** (1979) 243–249.

[19] D. Barber et al., Discovery of Three Jet Events and a Test of Quantum Chromodynamics at PETRA Energies, Phys. Rev. Lett. **43** (1979) 830.

[20] PLUTO Collaboration, C. Berger et al., Evidence for Gluon Bremsstrahlung in e+ e- Annihilations at High-Energies, Phys. Lett. B **86** (1979) 418–425.

[21] JADE Collaboration, W. Bartel et al., Observation of Planar Three Jet Events in e+ e- Annihilation and Evidence for Gluon Bremsstrahlung, Phys. Lett. B **91** (1980) 142–147.

[22] DONUT Collaboration, K. Kodama et al., Observation of tau neutrino interactions, Phys. Lett. B **504** (2001) 218–224, arXiv:hep-ex/0012035.

[23] T. Aoyama, M. Hayakawa, T. Kinoshita, and M. Nio, Tenth-Order QED Contribution to the Electron g-2 and an Improved Value of the Fine Structure Constant, Phys. Rev. Lett. **109** (2012) 111807, arXiv:1205.5368 [hep-ph].

[24] T. Aoyama, T. Kinoshita, and M. Nio, Revised and Improved Value of the QED Tenth-Order Electron Anomalous Magnetic Moment, Phys. Rev. D **97** (2018) 036001, arXiv:1712.06060 [hep-ph].

[25] D. Hanneke, S. Fogwell, and G. Gabrielse, New Measurement of the Electron Magnetic Moment and the Fine Structure Constant, Phys. Rev. Lett. **100** (2008) 120801, arXiv:0801.1134 [physics.atom-ph].

[26] Particle Data Group Collaboration, M. Tanabashi et al., Review of Particle Physics, Phys. Rev. D **98** (2018) 030001.

[27] UTfit Collaboration, M. Bona et al., The Unitarity Triangle Fit in the Standard Model and Hadronic Parameters from Lattice QCD: A Reappraisal after the Measurements of Delta m(s) and BR(B —> tau nu(tau)), JHEP **10** (2006) 081, arXiv:hep-ph/0606167.

[28] CMS Collaboration, V. Khachatryan et al., Precise determination of the mass of the Higgs boson and tests of compatibility of its couplings with the standard model predictions using proton collisions at 7 and 8 TeV, Eur. Phys. J. C **75** (2015) 212, arXiv:1412.8662 [hep-ex].

[29] ATLAS Collaboration, G. Aad et al., Measurements of the Higgs boson production and decay rates and coupling strengths using pp collision data at $\sqrt{s} = 7$ and 8 TeV in the ATLAS experiment, Eur. Phys. J. C **76** (2016) 6, arXiv:1507.04548 [hep-ex].

[30] ATLAS, CMS Collaboration, G. Aad et al., Measurements of the Higgs boson production and decay rates and constraints on its couplings from a combined ATLAS and CMS analysis of the LHC pp collision data at $\sqrt{s} = 7$ and 8 TeV, JHEP **08** (2016) 045, arXiv:1606.02266 [hep-ex].

[31] CMS Collaboration, A. M. Sirunyan et al., Observation of the Higgs boson decay to a pair of τ leptons with the CMS detector, Phys. Lett. B **779** (2018) 283–316, arXiv:1708.00373 [hep-ex].

[32] ATLAS Collaboration, M. Aaboud et al., Cross-section measurements of the Higgs boson decaying into a pair of τ-leptons in proton-proton collisions at $\sqrt{s} = 13$ TeV with the ATLAS detector, Phys. Rev. D **99** (2019) 072001, arXiv:1811.08856 [hep-ex].

[33] CMS Collaboration, A. M. Sirunyan et al., Observation of Higgs boson decay to bottom quarks, Phys. Rev. Lett. **121** (2018) 121801, arXiv:1808.08242 [hep-ex].

[34] ATLAS Collaboration, M. Aaboud et al., Observation of $H \to b\bar{b}$ decays and VH production with the ATLAS detector, Phys. Lett. B **786** (2018) 59–86, arXiv:1808.08238 [hep-ex].

[35] CMS Collaboration, A. M. Sirunyan et al., Observation of $t\bar{t}H$ production, Phys. Rev. Lett. **120** (2018) 231801, arXiv:1804.02610 [hep-ex].

[36] ATLAS Collaboration, M. Aaboud et al., Observation of Higgs boson production in association with a top quark pair at the LHC with the ATLAS detector, Phys. Lett. B **784** (2018) 173–191, arXiv:1806.00425 [hep-ex].

[37] ATLAS Collaboration, G. Aad et al., A search for the dimuon decay of the Standard Model Higgs boson with the ATLAS detector, arXiv:2007.07830 [hep-ex].

[38] CMS Collaboration„ Measurement of Higgs boson decay to a pair of muons in proton-proton collisions at $\sqrt{s} = 13\,\text{TeV}$,.

[39] W. Altmannshofer, J. Brod, and M. Schmaltz, Experimental constraints on the coupling of the Higgs boson to electrons, JHEP **05** (2015) 125, arXiv:1503.04830 [hep-ph].

[40] D. d'Enterria, Physics at the FCC-ee, pp. , 182–191. 2017. arXiv:1602.05043 [hep-ex].

[41] G. T. Bodwin, F. Petriello, S. Stoynev, and M. Velasco, Higgs boson decays to quarkonia and the $H\bar{c}c$ coupling, Phys. Rev. D **88** (2013) 053003, arXiv:1306.5770 [hep-ph].

[42] ATLAS Collaboration, G. Aad et al., Search for Higgs and Z Boson Decays to J/$\psi\gamma$ and ?(nS)γ with the ATLAS Detector, Phys. Rev. Lett. **114** (2015) 121801, arXiv:1501.03276 [hep-ex].

[43] G. Perez, Y. Soreq, E. Stamou, and K. Tobioka, Prospects for measuring the Higgs boson coupling to light quarks, Phys. Rev. D **93** (2016) 013001, arXiv:1505.06689 [hep-ph].

[44] M. König and M. Neubert, Exclusive Radiative Higgs Decays as Probes of Light-Quark Yukawa Couplings, JHEP **08** (2015) 012, arXiv:1505.03870 [hep-ph].

[45] C. Delaunay, T. Golling, G. Perez, and Y. Soreq, Enhanced Higgs boson coupling to charm pairs, Phys. Rev. D **89** (2014) 033014, arXiv:1310.7029 [hep-ph].

[46] G. Perez, Y. Soreq, E. Stamou, and K. Tobioka, Constraining the charm Yukawa and Higgs-quark coupling universality, Phys. Rev. D **92** (2015) 033016, arXiv:1503.00290 [hep-ph].

[47] I. Brivio, F. Goertz, and G. Isidori, Probing the Charm Quark Yukawa Coupling in Higgs+Charm Production, Phys. Rev. Lett. **115** (2015) 211801, arXiv:1507.02916 [hep-ph].

[48] A. L. Kagan, G. Perez, F. Petriello, Y. Soreq, S. Stoynev, and J. Zupan, Exclusive Window onto Higgs Yukawa Couplings, Phys. Rev. Lett. **114** (2015) 101802, arXiv:1406.1722 [hep-ph].

[49] ATLAS Collaboration, M. Aaboud et al., Search for Higgs and Z Boson Decays to $\phi\gamma$ with the ATLAS Detector, Phys. Rev. Lett. **117** (2016) 111802, arXiv:1607.03400 [hep-ex].

[50] F. Bishara, U. Haisch, P. F. Monni, and E. Re, Constraining Light-Quark Yukawa Couplings from Higgs Distributions, Phys. Rev. Lett. **118** (2017) 121801, arXiv:1606.09253 [hep-ph].

[51] Y. Soreq, H. X. Zhu, and J. Zupan, Light quark Yukawa couplings from Higgs kinematics, JHEP **12** (2016) 045, arXiv:1606.09621 [hep-ph].

[52] G. Bonner and H. E. Logan, Constraining the Higgs couplings to up and down quarks using production kinematics at the CERN Large Hadron Collider, arXiv:1608.04376 [hep-ph].

[53] F. Yu, Phenomenology of Enhanced Light Quark Yukawa Couplings and the $W^{\pm}h$ Charge Asymmetry, JHEP **02** (2017) 083, arXiv:1609.06592 [hep-ph].

[54] D. Asner et al., ILC Higgs White Paper, in Community Summer Study 2013: Snowmass on the Mississippi. 10, 2013. arXiv:1310.0763 [hep-ph].

[55] ALEPH, DELPHI, L3, OPAL, SLD, LEP Electroweak Working Group, SLD Electroweak Group, SLD Heavy Flavour Group Collaboration, S. Schael et al., Precision electroweak measurements on the Z resonance, Phys. Rept. **427** (2006) 257–454, arXiv:hep-ex/0509008.

[56] ATLAS Collaboration, M. Aaboud et al., Precision measurement and interpretation of inclusive W^+ , W^- and Z/γ^* production cross sections with the ATLAS detector, Eur. Phys. J. C **77** (2017) 367, arXiv:1612.03016 [hep-ex].

[57] CDF Collaboration, A. Abulencia et al., Measurements of inclusive W and Z cross sections in p anti-p collisions at s**(1/2) = 1.96-TeV, J. Phys. G **34** (2007) 2457–2544, arXiv:hep-ex/0508029.

[58] ALEPH, DELPHI, L3, OPAL, LEP Electroweak Collaboration, S. Schael et al., Electroweak Measurements in Electron-Positron Collisions at W-Boson-Pair Energies at LEP, Phys. Rept. **532** (2013) 119–244, arXiv:1302.3415 [hep-ex].

[59] LHCb Collaboration, R. Aaij et al., Measurement of forward $W \to e\nu$ production in pp collisions at $\sqrt{s} = 8\,\text{TeV}$, JHEP **10** (2016) 030, arXiv:1608.01484 [hep-ex].

[60] BaBar Collaboration, J. P. Lees et al., Evidence for an excess of $\bar{B} \to D^{(*)}\tau^-\bar{\nu}_\tau$ decays, Phys. Rev. Lett. **109** (2012) 101802, arXiv:1205.5442 [hep-ex].

[61] Belle Collaboration, M. Huschle et al., Measurement of the branching ratio of $\bar{B} \to D^{(*)}\tau^-\bar{\nu}_\tau$ relative to $\bar{B} \to D^{(*)}\ell^-\bar{\nu}_\ell$ decays with hadronic tagging at Belle, Phys. Rev. **D92** (2015) 072014, arXiv:1507.03233 [hep-ex].

[62] Belle Collaboration, S. Hirose et al., Measurement of the τ lepton polarization and $R(D^*)$ in the decay $\bar{B} \to D^*\tau^-\bar{\nu}_\tau$, Phys. Rev. Lett. **118** (2017) 211801, arXiv:1612.00529 [hep-ex].

[63] Belle Collaboration, G. Caria et al., Measurement of $\mathcal{R}(D)$ and $\mathcal{R}(D^*)$ with a semileptonic tagging method, arXiv:1910.05864 [hep-ex].

[64] LHCb Collaboration, R. Aaij et al., Measurement of the ratio of branching fractions $\mathcal{B}(\bar{B}^0 \to D^{*+}\tau^-\bar{\nu}_\tau)/\mathcal{B}(\bar{B}^0 \to D^{*+}\mu^-\bar{\nu}_\mu)$, Phys. Rev. Lett. **115** (2015) 111803, arXiv:1506.08614 [hep-ex], [Erratum: Phys. Rev. Lett.115,no.15,159901(2015)].

[65] LHCb Collaboration, R. Aaij et al., Measurement of the ratio of the $B^0 \to D^{*-}\tau^+\nu_\tau$ and $B^0 \to D^{*-}\mu^+\nu_\mu$ branching fractions using three-prong τ-lepton decays, Phys. Rev. Lett. **120** (2018) 171802, arXiv:1708.08856 [hep-ex].

[66] HFLAV Collaboration, Y. S. Amhis et al., Averages of b-hadron, c-hadron, and τ-lepton properties as of 2018, arXiv:1909.12524 [hep-ex].

[67] F. U. Bernlochner, Z. Ligeti, M. Papucci, and D. J. Robinson, Combined analysis of semileptonic B decays to D and D^*: $R(D^{(*)})$, $|V_{cb}|$, and new physics, Phys. Rev. **D95** (2017) 115008, arXiv:1703.05330 [hep-ph], [erratum: Phys. Rev.D97,no.5,059902(2018)].

[68] D. Bigi, P. Gambino, and S. Schacht, $R(D^*)$, $|V_{cb}|$, and the Heavy Quark Symmetry relations between form factors, JHEP **11** (2017) 061, arXiv:1707.09509 [hep-ph].

[69] S. Jaiswal, S. Nandi, and S. K. Patra, Extraction of $|V_{cb}|$ from $B \to D^{(*)}\ell\nu_\ell$ and the Standard Model predictions of $R(D^{(*)})$, JHEP **12** (2017) 060, arXiv:1707.09977 [hep-ph].

[70] LHCb Collaboration, R. Aaij et al., Search for lepton-universality violation in $B^+ \to K^+\ell^+\ell^-$ decays, Phys. Rev. Lett. **122** (2019) 191801, arXiv:1903.09252 [hep-ex].

[71] M. Bordone, G. Isidori, and A. Pattori, On the Standard Model predictions for R_K and R_{K^*}, Eur. Phys. J. **C76** (2016) 440, arXiv:1605.07633 [hep-ph].

[72] LHCb Collaboration, R. Aaij et al., Test of lepton universality using $B^+ \to K^+\ell^+\ell^-$ decays, Phys. Rev. Lett. **113** (2014) 151601, arXiv:1406.6482 [hep-ex].

[73] LHCb Collaboration, R. Aaij et al., Test of lepton universality with $B^0 \to K^{*0}\ell^+\ell^-$ decays, JHEP **08** (2017) 055, arXiv:1705.05802 [hep-ex].

[74] Belle Collaboration, A. Abdesselam et al., Test of lepton flavor universality in $B \to K^*\ell^+\ell^-$ decays at Belle, arXiv:1904.02440 [hep-ex].

[75] Belle Collaboration, A. Abdesselam et al., Test of lepton flavor universality in $B \to K\ell^+\ell^-$ decays, arXiv:1908.01848 [hep-ex].

[76] M. AlguerÃş, B. Capdevila, A. Crivellin, S. Descotes-Genon, P. Masjuan, J. Matias, and J. Virto, Emerging patterns of New Physics with and without Lepton Flavour Universal contributions, Eur. Phys. J. **C79** (2019) 714, arXiv:1903.09578 [hep-ph].

[77] A. K. Alok, A. Dighe, S. Gangal, and D. Kumar, Continuing search for new physics in $b \to s\mu\mu$ decays: two operators at a time, JHEP **06** (2019) 089, arXiv:1903.09617 [hep-ph].

[78] M. Ciuchini, A. M. Coutinho, M. Fedele, E. Franco, A. Paul, L. Silvestrini, and M. Valli, New Physics in $b \to s\ell^+\ell^-$ confronts new data on Lepton Universality, Eur. Phys. J. **C79** (2019) 719, arXiv:1903.09632 [hep-ph].

[79] A. Datta, J. Kumar, and D. London, The B Anomalies and New Physics in $b \to s e^+ e^-$, Phys. Lett. **B797** (2019) 134858, arXiv:1903.10086 [hep-ph].

[80] J. Aebischer, W. Altmannshofer, D. Guadagnoli, M. Reboud, P. Stangl, and D. M. Straub, B-decay discrepancies after Moriond 2019, arXiv:1903.10434 [hep-ph].

[81] K. Kowalska, D. Kumar, and E. M. Sessolo, Implications for new physics in $b \to s\mu\mu$ transitions after recent measurements by Belle and LHCb, Eur. Phys. J. **C79** (2019) 840, arXiv:1903.10932 [hep-ph].

[82] A. Arbey, T. Hurth, F. Mahmoudi, D. M. Santos, and S. Neshatpour, Update on the $b \to s$ anomalies, Phys. Rev. **D100** (2019) 015045, arXiv:1904.08399 [hep-ph].

[83] S. Bifani, S. Descotes-Genon, A. Romero Vidal, and M.-H. Schune, Review of Lepton Universality tests in B decays, J. Phys. G **46** (2019) 023001, arXiv:1809.06229 [hep-ex].

[84] W. Altmannshofer, S. Gori, A. L. Kagan, L. Silvestrini, and J. Zupan, Uncovering Mass Generation Through Higgs Flavor Violation, Phys. Rev. D **93** (2016) 031301, arXiv:1507.07927 [hep-ph].

[85] D. Ghosh, R. S. Gupta, and G. Perez, Is the Higgs Mechanism of Fermion Mass Generation a Fact? A Yukawa-less First-Two-Generation Model, Phys. Lett. B **755** (2016) 504–508, arXiv:1508.01501 [hep-ph].

[86] F. Botella, G. Branco, M. Rebelo, and J. Silva-Marcos, What if the masses of the first two quark families are not generated by the standard model Higgs boson?, Phys. Rev. D **94** (2016) 115031, arXiv:1602.08011 [hep-ph].

[87] A. K. Das and C. Kao, A Two Higgs doublet model for the top quark, Phys. Lett. B **372** (1996) 106–112, arXiv:hep-ph/9511329.

[88] A. E. Blechman, A. A. Petrov, and G. Yeghiyan, The Flavor puzzle in multi-Higgs models, JHEP **11** (2010) 075, arXiv:1009.1612 [hep-ph].

[89] ATLAS Collaboration, M. Aaboud et al., Evidence for the $H \to b\bar{b}$ decay with the ATLAS detector, arXiv:1708.03299 [hep-ex].

[90] CMS Collaboration, A. M. Sirunyan et al., Evidence for the Higgs boson decay to a bottom quark-antiquark pair, arXiv:1709.07497 [hep-ex].

[91] CMS Collaboration„ Search for the standard model Higgs boson decaying into two muons in pp collisions at sqrt(s)=13TeV, Tech. Rep. CMS-PAS-HIG-17-019, CERN, Geneva, 2017. http://cds.cern.ch/record/2292159.

[92] ATLAS Collaboration, M. Aaboud et al., Search for the dimuon decay of the Higgs boson in pp collisions at $\sqrt{s} = 13$ TeV with the ATLAS detector, Phys. Rev. Lett. **119** (2017) 051802, arXiv:1705.04582 [hep-ex].

[93] CMS Collaboration„ Projected Performance of an Upgraded CMS Detector at the LHC and HL-LHC: Contribution to the Snowmass Process, in Proceedings, 2013 Community Summer Study on the Future of U.S. Particle Physics: Snowmass on the Mississippi (CSS2013): Minneapolis, MN, USA, July 29-August 6, 2013. 2013. arXiv:1307.7135 [hep-ex]. https://inspirehep.net/record/1244669/files/arXiv:1307.7135.pdf.

[94] Projections for measurements of Higgs boson cross sections, branching ratios and coupling parameters with the ATLAS detector at a HL-LHC,.

[95] M. Testa, Prospects on Higgs Physics at the HL-LHC for ATLAS, Talk at Workshop on the physics of HL-LHC, and perspectives at HE-LHC (2017), https://indico.cern.ch/event/647676.

[96] ATLAS Collaboration„ Search for the decay of the Higgs boson to charm quarks with the ATLAS experiment,.

[97] LHCb Collaboration„ Search for $H^0 \to b\bar{b}$ or $c\bar{c}$ in association with a W or Z boson in the forward region of pp collisions,.

[98] K. Fujii et al., Physics Case for the 250 GeV Stage of the International Linear Collider, arXiv:1710.07621 [hep-ex].

[99] B. Mellado, The status of the LHeC project and its impact on Higgs Physics, pp. , 235–240. 2015.

[100] J. Gao, Probing light-quark Yukawa couplings via hadronic event shapes at lepton colliders, arXiv:1608.01746 [hep-ph].

[101] L. M. Carpenter, T. Han, K. Hendricks, Z. Qian, and N. Zhou, Higgs Boson Decay to Light Jets at the LHC, Phys. Rev. **D95** (2017) 053003, arXiv:1611.05463 [hep-ph].

[102] D. d'Enterria, Higgs physics at the Future Circular Collider, PoS **ICHEP2016** (2017) 434, arXiv:1701.02663 [hep-ex].

[103] J. Cohen, S. Bar-Shalom, G. Eilam, and A. Soni, Light-quarks Yukawa and new physics in exclusive high-p_T Higgs + jet(b-jet) events, arXiv:1705.09295 [hep-ph].

[104] CMS Collaboration„ Search for lepton flavour violating decays of the Higgs boson to $\mu\tau$ and eτ in proton-proton collisions at $\sqrt{s} = 13$ TeV,.

[105] ATLAS Collaboration, G. Aad et al., Search for lepton-flavour-violating decays of the Higgs and Z bosons with the ATLAS detector, Eur. Phys. J. **C77** (2017) 70, arXiv:1604.07730 [hep-ex].

[106] ATLAS Collaboration, M. Aaboud et al., Search for top quark decays $t \to qH$, with $H \to \gamma\gamma$, in $\sqrt{s} = 13$ TeV pp collisions using the ATLAS detector, JHEP **10** (2017) 129, arXiv:1707.01404 [hep-ex].

[107] CMS Collaboration„ Search for the flavor-changing interactions of the top quark with the Higgs boson in $H \to b\bar{b}$ channel at $\sqrt{s} = 13$ TeV, Tech. Rep. CMS-PAS-TOP-17-003, 2017.

[108] CMS Collaboration, V. Khachatryan et al., Search for Lepton-Flavour-Violating Decays of the Higgs Boson, Phys. Lett. B **749** (2015) 337–362, arXiv:1502.07400 [hep-ex].

[109] G. Branco, P. Ferreira, L. Lavoura, M. Rebelo, M. Sher, and J. P. Silva, Theory and phenomenology of two-Higgs-doublet models, Phys. Rept. **516** (2012) 1–102, arXiv:1106.0034 [hep-ph].

[110] A. Crivellin, A. Kokulu, and C. Greub, Flavor-phenomenology of two-Higgs-doublet models with generic Yukawa structure, Phys. Rev. D **87** (2013) 094031, arXiv:1303.5877 [hep-ph].

[111] D. S. Alves, P. J. Fox, and N. J. Weiner, Higgs Signals in a Type I 2HDM or with a Sister Higgs, arXiv:1207.5499 [hep-ph].

[112] N. Craig and S. Thomas, Exclusive Signals of an Extended Higgs Sector, JHEP **11** (2012) 083, arXiv:1207.4835 [hep-ph].

[113] W. Altmannshofer, S. Gori, and G. D. Kribs, A Minimal Flavor Violating 2HDM at the LHC, Phys. Rev. D **86** (2012) 115009, arXiv:1210.2465 [hep-ph].

[114] Y. Bai, V. Barger, L. L. Everett, and G. Shaughnessy, General two Higgs doublet model (2HDM-G) and Large Hadron Collider data, Phys. Rev. D **87** (2013) 115013, arXiv:1210.4922 [hep-ph].

[115] B. Grinstein and P. Uttayarat, Carving Out Parameter Space in Type-II Two Higgs Doublets Model, JHEP **06** (2013) 094, arXiv:1304.0028 [hep-ph], [Erratum: JHEP 09, 110 (2013)].

[116] C.-Y. Chen, S. Dawson, and M. Sher, Heavy Higgs Searches and Constraints on Two Higgs Doublet Models, Phys. Rev. D **88** (2013) 015018, arXiv:1305.1624 [hep-ph], [Erratum: Phys.Rev.D 88, 039901 (2013)].

[117] N. Craig, J. Galloway, and S. Thomas, Searching for Signs of the Second Higgs Doublet, arXiv:1305.2424 [hep-ph].

[118] V. Barger, L. L. Everett, H. E. Logan, and G. Shaughnessy, Scrutinizing the 125 GeV Higgs boson in two Higgs doublet models at the LHC, ILC, and Muon Collider, Phys. Rev. D **88** (2013) 115003, arXiv:1308.0052 [hep-ph].

[119] M. Carena, I. Low, N. R. Shah, and C. E. Wagner, Impersonating the Standard Model Higgs Boson: Alignment without Decoupling, JHEP **04** (2014) 015, arXiv:1310.2248 [hep-ph].

[120] S. Chang, S. K. Kang, J.-P. Lee, K. Y. Lee, S. C. Park, and J. Song, Two Higgs doublet models for the LHC Higgs boson data at $\sqrt{s} = 7$ and 8 TeV, JHEP **09** (2014) 101, arXiv:1310.3374 [hep-ph].

[121] K. Cheung, J. S. Lee, and P.-Y. Tseng, Higgcision in the Two-Higgs Doublet Models, JHEP **01** (2014) 085, arXiv:1310.3937 [hep-ph].

[122] A. Celis, V. Ilisie, and A. Pich, Towards a general analysis of LHC data within two-Higgs-doublet models, JHEP **12** (2013) 095, arXiv:1310.7941 [hep-ph].

[123] P. Ferreira, J. F. Gunion, H. E. Haber, and R. Santos, Probing wrong-sign Yukawa couplings at the LHC and a future linear collider, Phys. Rev. D **89** (2014) 115003, arXiv:1403.4736 [hep-ph].

[124] S. Kanemura, K. Tsumura, K. Yagyu, and H. Yokoya, Fingerprinting nonminimal Higgs sectors, Phys. Rev. D **90** (2014) 075001, arXiv:1406.3294 [hep-ph].

[125] N. Craig, F. D'Eramo, P. Draper, S. Thomas, and H. Zhang, The Hunt for the Rest of the Higgs Bosons, JHEP **06** (2015) 137, arXiv:1504.04630 [hep-ph].

[126] F. Botella, G. Branco, M. Nebot, and M. Rebelo, Flavour Changing Higgs Couplings in a Class of Two Higgs Doublet Models, Eur. Phys. J. C **76** (2016) 161, arXiv:1508.05101 [hep-ph].

[127] M. Buschmann, J. Kopp, J. Liu, and X.-P. Wang, New Signatures of Flavor Violating Higgs Couplings, JHEP **06** (2016) 149, arXiv:1601.02616 [hep-ph].

[128] M. Sher and K. Thrasher, Flavor Changing Leptonic Decays of Heavy Higgs Bosons, Phys. Rev. D **93** (2016) 055021, arXiv:1601.03973 [hep-ph].

[129] G. Cvetic, S. Hwang, and C. Kim, One loop renormalization group equations of the general framework with two Higgs doublets, Int. J. Mod. Phys. A **14** (1999) 769–798, arXiv:hep-ph/9706323.

[130] G. Cvetic, C. Kim, and S. Hwang, Higgs mediated flavor changing neutral currents in the general framework with two Higgs doublets: An RGE analysis, Phys. Rev. D **58** (1998) 116003, arXiv:hep-ph/9806282.

[131] M. Bauer, M. Carena, and K. Gemmler, Creating the fermion mass hierarchies with multiple Higgs bosons, Phys. Rev. D **94** (2016) 115030, arXiv:1512.03458 [hep-ph].

[132] M. Bauer, M. Carena, and K. Gemmler, Flavor from the Electroweak Scale, JHEP **11** (2015) 016, arXiv:1506.01719 [hep-ph].

[133] S. L. Glashow and S. Weinberg, Natural Conservation Laws for Neutral Currents, Phys. Rev. D **15** (1977) 1958.

[134] A. Pich and P. Tuzon, Yukawa Alignment in the Two-Higgs-Doublet Model, Phys. Rev. D **80** (2009) 091702, arXiv:0908.1554 [hep-ph].

[135] G. D'Ambrosio, G. Giudice, G. Isidori, and A. Strumia, Minimal flavor violation: An Effective field theory approach, Nucl. Phys. B **645** (2002) 155–187, arXiv:hep-ph/0207036.

[136] A. J. Buras, M. V. Carlucci, S. Gori, and G. Isidori, Higgs-mediated FCNCs: Natural Flavour Conservation vs. Minimal Flavour Violation, JHEP **10** (2010) 009, arXiv:1005.5310 [hep-ph].

[137] LHC Higgs Cross Section Working Group Collaboration, J. R. Andersen et al., Handbook of LHC Higgs Cross Sections: 3. Higgs Properties, arXiv:1307.1347 [hep-ph].

[138] ATLAS Collaboration,, Search for Higgs bosons decaying into di-muon in pp collisions at $\sqrt{s} = 13$ TeV with the ATLAS detector,.

[139] ATLAS Collaboration, G. Aad et al., Constraints on new phenomena via Higgs boson couplings and invisible decays with the ATLAS detector, JHEP **11** (2015) 206, arXiv:1509.00672 [hep-ex].

[140] CMS Collaboration,, Summary results of high mass BSM Higgs searches using CMS run-I data,.

[141] L. Harland-Lang, A. Martin, P. Motylinski, and R. Thorne, Parton distributions in the LHC era: MMHT 2014 PDFs, Eur. Phys. J. C **75** (2015) 204, arXiv:1412.3989 [hep-ph].

[142] R. V. Harlander and W. B. Kilgore, Higgs boson production in bottom quark fusion at next-to-next-to leading order, Phys. Rev. D **68** (2003) 013001, arXiv:hep-ph/0304035.

[143] J. Alwall, R. Frederix, S. Frixione, V. Hirschi, F. Maltoni, O. Mattelaer, H. S. Shao, T. Stelzer, P. Torrielli, and M. Zaro, The automated computation of tree-level and next-to-leading order differential cross sections, and their matching to parton shower simulations, JHEP **07** (2014) 079, arXiv:1405.0301 [hep-ph].

[144] CMS Collaboration, V. Khachatryan et al., Search for a Higgs boson in the mass range from 145 to 1000 GeV decaying to a pair of W or Z bosons, JHEP **10** (2015) 144, arXiv:1504.00936 [hep-ex].

[145] ATLAS Collaboration, G. Aad et al., Search for an additional, heavy Higgs boson in the $H \to ZZ$ decay channel at $\sqrt{s} = 8$ TeV in pp collision data with the ATLAS detector, Eur. Phys. J. C **76** (2016) 45, arXiv:1507.05930 [hep-ex].

[146] ATLAS Collaboration, G. Aad et al., Search for a high-mass Higgs boson decaying to a W boson pair in pp collisions at $\sqrt{s} = 8$ TeV with the ATLAS detector, JHEP **01** (2016) 032, arXiv:1509.00389 [hep-ex].

[147] CMS Collaboration,, Studies of Higgs boson production in the four-lepton final state at $\sqrt{s} = 13$ TeV, http://cds.cern.ch/record/2139978.

[148] Search for a high-mass Higgs boson decaying to a pair of W bosons in pp collisions at sqrt(s)=13 TeV with the ATLAS detector,.

[149] CMS Collaboration,, Search for high mass Higgs to WW with fully leptonic decays using 2015 data,.

[150] ATLAS Collaboration,, Search for a high-mass Higgs boson decaying to a pair of W bosons in pp collisions at $\sqrt{s}$=13 TeV with the ATLAS detector,.

[151] CMS Collaboration,, Measurements of properties of the Higgs boson and search for an additional resonance in the four-lepton final state at sqrt(s) = 13 TeV,.

[152] ATLAS Collaboration,, Study of the Higgs boson properties and search for high-mass scalar resonances in the $H \to ZZ^* \to 4\ell$ decay channel at $\sqrt{s} =$ 13 TeV with the ATLAS detector,.

[153] ATLAS Collaboration, G. Aad et al., Search for a CP-odd Higgs boson decaying to Zh in pp collisions at $\sqrt{s} = 8$ TeV with the ATLAS detector, Phys. Lett. B **744** (2015) 163–183, arXiv:1502.04478 [hep-ex].

[154] Search for a CP-odd Higgs boson decaying to Zh in pp collisions at $\sqrt{s} =$ 13 TeV with the ATLAS detector,.

[155] CMS Collaboration, V. Khachatryan et al., Search for a pseudoscalar boson decaying into a Z boson and the 125 GeV Higgs boson in $?^+?^?b\bar{b}$ final states, Phys. Lett. B **748** (2015) 221–243, arXiv:1504.04710 [hep-ex].

[156] CMS Collaboration, V. Khachatryan et al., Searches for a heavy scalar boson H decaying to a pair of 125 GeV Higgs bosons hh or for a heavy pseudoscalar boson A decaying to Zh, in the final states with $h \to \tau\tau$, Phys. Lett. B **755** (2016) 217–244, arXiv:1510.01181 [hep-ex].

[157] CMS Collaboration, V. Khachatryan et al., Search for neutral MSSM Higgs bosons decaying to a pair of tau leptons in pp collisions, JHEP **10** (2014) 160, arXiv:1408.3316 [hep-ex].

[158] ATLAS Collaboration, G. Aad et al., Search for neutral Higgs bosons of the minimal supersymmetric standard model in pp collisions at $\sqrt{s} = 8$ TeV with the ATLAS detector, JHEP **11** (2014) 056, arXiv:1409.6064 [hep-ex].

[159] Search for Neutral Minimal Supersymmetric Standard Model Higgs Bosons $H/A \to \tau\tau$ produced in pp collisions at $\sqrt{s} = 13$ TeV with the ATLAS Detector,.

[160] CMS Collaboration,, Search for a neutral MSSM Higgs boson decaying into $\tau\tau$ at 13 TeV,.

[161] ATLAS Collaboration,, Search for Minimal Supersymmetric Standard Model Higgs Bosons H/A in the $\tau\tau$ final state in up to 13.3 $\text{fb}^{?1}$ of pp collisions at $\sqrt{s}$= 13 TeV with the ATLAS Detector,.

[162] CMS Collaboration, V. Khachatryan et al., Search for neutral MSSM Higgs bosons decaying to $\mu^+\mu^-$ in pp collisions at $\sqrt{s} = 7$ and 8 TeV, Phys. Lett. B **752** (2016) 221–246, arXiv:1508.01437 [hep-ex].

[163] ATLAS Collaboration,, Search for heavy Higgs bosons A/H decaying to a top-quark pair in pp collisions at $\sqrt{s} = 8$ TeV with the ATLAS detector,.

[164] ATLAS Collaboration, G. Aad et al., Search for high-mass dilepton resonances in pp collisions at $\sqrt{s} = 8$ TeV with the ATLAS detector, Phys. Rev. D **90** (2014) 052005, arXiv:1405.4123 [hep-ex].

[165] CMS Collaboration, V. Khachatryan et al., Search for physics beyond the standard model in dilepton mass spectra in proton-proton collisions at $\sqrt{s} = 8$ TeV, JHEP **04** (2015) 025, arXiv:1412.6302 [hep-ex].

[166] Search for new phenomena in the dilepton final state using proton-proton collisions at $\sqrt{}$ s = 13 TeV with the ATLAS detector,.

[167] CMS Collaboration,, Search for a Narrow Resonance Produced in 13 TeV pp Collisions Decaying to Electron Pair or Muon Pair Final States,.

[168] CMS Collaboration,, Search for a high-mass resonance decaying into a dilepton final state in 13 fb^{-1} of pp collisions at $\sqrt{s} = 13$ TeV,.

[169] ATLAS Collaboration,, Search for new high-mass resonances in the dilepton final state using proton-proton collisions at $\sqrt{s} = 13$ TeV with the ATLAS detector,.

[170] CMS Collaboration,, Search for Resonances Decaying to Dijet Final States at $\sqrt{s} = 8$ TeV with Scouting Data,.

[171] ATLAS Collaboration,, Search for light dijet resonances with the ATLAS detector using a Trigger-Level Analysis in LHC pp collisions at $\sqrt{s} = 13$~TeV,.

[172] CMS Collaboration, V. Khachatryan et al., Search for narrow resonances in dijet final states at $\sqrt{(s)} = 8$ TeV with the novel CMS technique of data scouting, Phys. Rev. Lett. **117** (2016) 031802, arXiv:1604.08907 [hep-ex].

[173] ATLAS Collaboration,, Search for new light resonances decaying to jet pairs and produced in association with a photon or a jet in proton-proton collisions at $\sqrt{s} = 13$~TeV with the ATLAS detector,.

[174] ATLAS Collaboration,, Search for new light resonances decaying to jet pairs and produced in association with a photon in proton-proton collisions at $\sqrt{s} = 13$~TeV with the ATLAS detector,.

[175] CMS Collaboration,, Search for light vector resonances decaying to quarks at 13 TeV,.

[176] S. Jung, J. Song, and Y. W. Yoon, Dip or nothingness of a Higgs resonance from the interference with a complex phase, Phys. Rev. D **92** (2015) 055009, arXiv:1505.00291 [hep-ph].

[177] S. Gori, I.-W. Kim, N. R. Shah, and K. M. Zurek, Closing the Wedge: Search Strategies for Extended Higgs Sectors with Heavy Flavor Final States, Phys. Rev. D **93** (2016) 075038, arXiv:1602.02782 [hep-ph].

[178] M. Carena and Z. Liu, Challenges and opportunities for heavy scalar searches in the $t\bar{t}$ channel at the LHC, JHEP **11** (2016) 159, arXiv:1608.07282 [hep-ph].

[179] ATLAS Collaboration, M. Aaboud et al., Search for charged Higgs bosons produced in association with a top quark and decaying via $H^{\pm} \to \tau\nu$ using pp collision data recorded at $\sqrt{s} = 13$ TeV by the ATLAS detector, Phys. Lett. B **759** (2016) 555–574, arXiv:1603.09203 [hep-ex].

[180] CMS Collaboration, V. Khachatryan et al., Search for a charged Higgs boson in pp collisions at $\sqrt{s} = 8$ TeV, JHEP **11** (2015) 018, arXiv:1508.07774 [hep-ex].

[181] ATLAS Collaboration,, Search for charged Higgs bosons in the τ+jets final state using 14.7 fb−1 of pp collision data recorded at s$\sqrt{}$=13 TeV with the ATLAS experiment,.

[182] ATLAS Collaboration, G. Aad et al., Search for charged Higgs bosons decaying via $H^{\pm} \to \tau^{\pm}\nu$ in fully hadronic final states using pp collision data at $\sqrt{s} = 8$ TeV with the ATLAS detector, JHEP **03** (2015) 088, arXiv:1412.6663 [hep-ex].

[183] ATLAS Collaboration, G. Aad et al., Search for charged Higgs bosons in the $H^{\pm} \to tb$ decay channel in pp collisions at $\sqrt{s} = 8$ TeV using the ATLAS detector, JHEP **03** (2016) 127, arXiv:1512.03704 [hep-ex].

[184] ATLAS Collaboration,, Search for charged Higgs bosons in the $H^{\pm} \to tb$ decay channel in pp collisions at $\sqrt{s} = 13$ TeV using the ATLAS detector,.

[185] CMS Collaboration, V. Khachatryan et al., Search for a light charged Higgs boson decaying to c$\bar{\text{s}}$ in pp collisions at $\sqrt{s} = 8$ TeV, JHEP **12** (2015) 178, arXiv:1510.04252 [hep-ex].

[186] CMS Collaboration,, Search for Charged Higgs boson to c$\bar{\text{b}}$ in lepton+jets channel using top quark pair events,.

[187] CMS Collaboration, V. Khachatryan et al., Search for a massive resonance decaying into a Higgs boson and a W or Z boson in hadronic final states in proton-proton collisions at $\sqrt{s} = 8$ TeV, JHEP **02** (2016) 145, arXiv:1506.01443 [hep-ex].

[188] CMS Collaboration, V. Khachatryan et al., Search for massive WH resonances decaying into the $\ell\nu b\bar{b}$ final state at $\sqrt{s} = 8$ TeV, Eur. Phys. J. C **76** (2016) 237, arXiv:1601.06431 [hep-ex].

[189] CMS Collaboration,, Search for heavy resonances decaying into a vector boson and a Higgs boson in the (ll, lnu, nunu) bb final state,.

[190] Search for new resonances decaying to a W or Z boson and a Higgs boson in the $\ell\ell b\bar{b}$, $\ell\nu b\bar{b}$, and $\nu\nu b\bar{b}$ channels in pp collisions at $\sqrt{s} = 13$~TeV with the ATLAS detector,.

[191] ATLAS Collaboration, M. Aaboud et al., Search for new resonances decaying to a W or Z boson and a Higgs boson in the $\ell^+\ell^- b\bar{b}$, $\ell\nu b\bar{b}$, and $\nu\bar{\nu}b\bar{b}$ channels with pp collisions at $\sqrt{s} = 13$ TeV with the ATLAS detector, Phys. Lett. B **765** (2017) 32–52, arXiv:1607.05621 [hep-ex].

[192] ATLAS Collaboration,, Search for new resonances decaying to a charged lepton and a neutrino in pp collisions at $\sqrt{s} = 13$ TeV with the ATLAS detector,.

[193] CMS Collaboration,, Search for SSM W' production, in the lepton+MET final state at a center-of-mass energy of 13 TeV,.

[194] S. Knapen and D. J. Robinson, Disentangling Mass and Mixing Hierarchies, Phys. Rev. Lett. **115** (2015) 161803, arXiv:1507.00009 [hep-ph].

[195] N. Cabibbo and L. Maiani, Weak interactions and the breaking of hadron symmetries, pp. , 50–80. 1970.

[196] L. Michel and L. A. Radicati, Properties of the breaking of hadronic internal symmetry, Annals Phys. **66** (1971) 758–783.

[197] R. Alonso, M. Gavela, L. Merlo, and S. Rigolin, On the scalar potential of minimal flavour violation, JHEP **07** (2011) 012, arXiv:1103.2915 [hep-ph].

[198] R. Alonso, M. B. Gavela, G. Isidori, and L. Maiani, Neutrino Mixing and Masses from a Minimum Principle, JHEP **11** (2013) 187, arXiv:1306.5927 [hep-ph].

[199] R. Alonso, M. Gavela, D. Hernández, L. Merlo, and S. Rigolin, Leptonic Dynamical Yukawa Couplings, JHEP **08** (2013) 069, arXiv:1306.5922 [hep-ph].

[200] A. Crivellin, J. Fuentes-Martin, A. Greljo, and G. Isidori, Lepton Flavor Non-Universality in B decays from Dynamical Yukawas, Phys. Lett. **B766** (2017) 77–85, arXiv:1611.02703 [hep-ph].

[201] W. Altmannshofer, J. Eby, S. Gori, M. Lotito, M. Martone, and D. Tuckler, Collider Signatures of Flavorful Higgs Bosons, Phys. Rev. **D94** (2016) 115032, arXiv:1610.02398 [hep-ph].

[202] S. Gori, H. E. Haber, and E. Santos, High scale flavor alignment in two-Higgs doublet models and its phenomenology, JHEP **06** (2017) 110, arXiv:1703.05873 [hep-ph].

[203] R. J. Dowdall, C. T. H. Davies, G. P. Lepage, and C. McNeile, Vus from pi and K decay constants in full lattice QCD with physical u, d, s and c quarks, Phys. Rev. **D88** (2013) 074504, arXiv:1303.1670 [hep-lat].

[204] ETM Collaboration, N. Carrasco, P. Dimopoulos, R. Frezzotti, V. Lubicz, G. C. Rossi, S. Simula, and C. Tarantino, ÎT̆S=2 and ÎT̆C=2 bag parameters in the standard model and beyond from N_f=2+1+1 twisted-mass lattice QCD, Phys. Rev. **D92** (2015) 034516, arXiv:1505.06639 [hep-lat].

[205] SWME Collaboration, B. J. Choi et al., Kaon BSM B-parameters using improved staggered fermions from $N_f = 2 + 1$ unquenched QCD, Phys. Rev. D **93** (2016) 014511, arXiv:1509.00592 [hep-lat].

[206] RBC/UKQCD Collaboration, N. Garron, R. J. Hudspith, and A. T. Lytle, Neutral Kaon Mixing Beyond the Standard Model with $n_f = 2 + 1$ Chiral Fermions Part 1: Bare Matrix Elements and Physical Results, JHEP **11** (2016) 001, arXiv:1609.03334 [hep-lat].

[207] A. J. Buras, D. Guadagnoli, and G. Isidori, On ϵ_K Beyond Lowest Order in the Operator Product Expansion, Phys. Lett. B **688** (2010) 309–313, arXiv:1002.3612 [hep-ph].

[208] J. Brod and M. Gorbahn, Next-to-Next-to-Leading-Order Charm-Quark Contribution to the CP Violation Parameter ϵ_K and ΔM_K, Phys. Rev. Lett. **108** (2012) 121801, arXiv:1108.2036 [hep-ph].

[209] HFLAV Collaboration, Y. Amhis et al., Averages of b-hadron, c-hadron, and τ-lepton properties as of summer 2016, Eur. Phys. J. C **77** (2017) 895, arXiv:1612.07233 [hep-ex].

[210] Fermilab Lattice, MILC Collaboration, A. Bazavov et al., $B^0_{(s)}$-mixing matrix elements from lattice QCD for the Standard Model and beyond, Phys. Rev. D **93** (2016) 113016, arXiv:1602.03560 [hep-lat].

[211] ETM Collaboration, N. Carrasco et al., B-physics from $N_f = 2$ tmQCD: the Standard Model and beyond, JHEP **03** (2014) 016, arXiv:1308.1851 [hep-lat].

[212] M. Blanke and A. J. Buras, Universal Unitarity Triangle 2016 and the tension between $\Delta M_{s,d}$ and ε_K in CMFV models, Eur. Phys. J. C **76** (2016) 197, arXiv:1602.04020 [hep-ph].

[213] A. J. Buras and F. De Fazio, 331 Models Facing the Tensions in $\Delta F = 2$ Processes with the Impact on ε'/ε, $B_s \to \mu^+\mu^-$ and $B \to K^*\mu^+\mu^-$, JHEP **08** (2016) 115, arXiv:1604.02344 [hep-ph].

[214] S. Glashow, J. Iliopoulos, and L. Maiani, Weak Interactions with Lepton-Hadron Symmetry, Phys. Rev. D **2** (1970) 1285–1292.

[215] B. Mele, S. Petrarca, and A. Soddu, A New evaluation of the t —> cH decay width in the standard model, Phys. Lett. B **435** (1998) 401–406, arXiv:hep-ph/9805498.

[216] J. Aguilar-Saavedra, Top flavor-changing neutral interactions: Theoretical expectations and experimental detection, Acta Phys. Polon. B **35** (2004) 2695–2710, arXiv:hep-ph/0409342.

[217] CMS Collaboration, A. M. Sirunyan et al., Search for the flavor-changing neutral current interactions of the top quark and the Higgs boson which decays into a pair of b quarks at $\sqrt{s} = 13$ TeV, JHEP **06** (2018) 102, arXiv:1712.02399 [hep-ex].

[218] ATLAS Collaboration,, Expected sensitivity of ATLAS to FCNC top quark decays $t \to Zu$ and $t \to Hq$ at the High Luminosity LHC,.

[219] R. Franceschini et al., The CLIC Potential for New Physics, arXiv:1812.02093 [hep-ph].

[220] A. Cerri et al.

[221] FCC Collaboration, A. Abada et al.

[222] W. Altmannshofer, S. Gori, D. J. Robinson, and D. Tuckler, The Flavor-locked Flavorful Two Higgs Doublet Model, JHEP **03** (2018) 129, arXiv:1712.01847 [hep-ph].

[223] C. Froggatt and H. B. Nielsen, Hierarchy of Quark Masses, Cabibbo Angles and CP Violation, Nucl. Phys. B **147** (1979) 277–298.

[224] W. Altmannshofer and B. Maddock, Flavorful Two Higgs Doublet Models with a Twist, Phys. Rev. D **98** (2018) 075005, arXiv:1805.08659 [hep-ph].

[225] C.-W. Chiang, H. Fukuda, M. Takeuchi, and T. T. Yanagida, Flavor-Changing Neutral-Current Decays in Top-Specific Variant Axion Model, JHEP **11** (2015) 057, arXiv:1507.04354 [hep-ph].

[226] S. Gori, C. Grojean, A. Juste, and A. Paul, Heavy Higgs Searches: Flavour Matters, JHEP **01** (2018) 108, arXiv:1710.03752 [hep-ph].

[227] M. Misiak et al., Updated NNLO QCD predictions for the weak radiative B-meson decays, Phys. Rev. Lett. **114** (2015) 221801, arXiv:1503.01789 [hep-ph].

[228] C. Bobeth, M. Misiak, and J. Urban, Matching conditions for $b \to s\gamma$ and $b \to sgluon$ in extensions of the standard model, Nucl. Phys. B **567** (2000) 153–185, arXiv:hep-ph/9904413.

[229] A. Paul and D. M. Straub, Constraints on new physics from radiative B decays, JHEP **04** (2017) 027, arXiv:1608.02556 [hep-ph].

[230] G. Eilam, B. Haeri, and A. Soni, FLAVOR CHANGING HIGGS TRANSITIONS, Phys. Rev. D **41** (1990) 875.

[231] G. Abbas, A. Celis, X.-Q. Li, J. Lu, and A. Pich, Flavour-changing top decays in the aligned two-Higgs-doublet model, JHEP **06** (2015) 005, arXiv:1503.06423 [hep-ph].

[232] Flavour Lattice Averaging Group Collaboration, S. Aoki et al., FLAG Review 2019: Flavour Lattice Averaging Group (FLAG), Eur. Phys. J. C **80** (2020) 113, arXiv:1902.08191 [hep-lat].

[233] ATLAS Collaboration, M. Aaboud et al., Search for charged Higgs bosons decaying into top and bottom quarks at $\sqrt{s} = 13$ TeV with the ATLAS detector, JHEP **11** (2018) 085, arXiv:1808.03599 [hep-ex].

[234] CMS Collaboration,, Search for a charged Higgs boson decaying into top and bottom quarks in proton-proton collisions at 13TeV in events with electrons or muons,.

[235] G. Durieux and C. Smith, The same-sign top signature of R-parity violation, JHEP **10** (2013) 068, arXiv:1307.1355 [hep-ph].

[236] C. Kim, Y. W. Yoon, and X.-B. Yuan, Exploring top quark FCNC within 2HDM type III in association with flavor physics, JHEP **12** (2015) 038, arXiv:1509.00491 [hep-ph].

[237] W.-S. Hou, M. Kohda, and T. Modak, Constraining a Lighter Exotic Scalar via Same-sign Top, Phys. Lett. B **786** (2018) 212–216, arXiv:1808.00333 [hep-ph].

[238] S. Bar-Shalom, A. Rajaraman, D. Whiteson, and F. Yu, Collider Signals of Maximal Flavor Violation: Same-Sign Leptons from Same-Sign Tops at the Tevatron, Phys. Rev. D **78** (2008) 033003, arXiv:0803.3795 [hep-ph].

[239] R. S. Chivukula, E. H. Simmons, and N. Vignaroli, Same-Sign Dileptons from Colored Scalars in the Flavorful Top-Coloron Model, Phys. Rev. D **88** (2013) 034006, arXiv:1306.2248 [hep-ph].

[240] H. Zhang, E. L. Berger, Q.-H. Cao, C.-R. Chen, and G. Shaughnessy, Color Sextet Vector Bosons and Same-Sign Top Quark Pairs at the LHC, Phys. Lett. B **696** (2011) 68–73, arXiv:1009.5379 [hep-ph].

[241] D. Atwood, S. K. Gupta, and A. Soni, Same-sign Tops: A Powerful Diagnostic Test for Models of New Physics, JHEP **04** (2013) 035, arXiv:1301.2250 [hep-ph].

[242] Planck Collaboration, P. A. R. Ade et al., Planck 2015 results. XIII. Cosmological parameters, Astron. Astrophys. **594** (2016) A13, arXiv:1502.01589 [astro-ph.CO].

[243] A. D. Sakharov, Violation of CP Invariance, C asymmetry, and baryon asymmetry of the universe, Pisma Zh. Eksp. Teor. Fiz. **5** (1967) 32–35, [Usp. Fiz. Nauk161,no.5,61(1991)].

[244] R. Alonso, B. Grinstein, and J. Martin Camalich, Lepton universality violation and lepton flavor conservation in B-meson decays, JHEP **10** (2015) 184, arXiv:1505.05164 [hep-ph].

[245] B. Bhattacharya, A. Datta, J.-P. GuÃĪvin, D. London, and R. Watanabe, Simultaneous Explanation of the R_K and $R_{D^{(*)}}$ Puzzles: a Model Analysis, JHEP **01** (2017) 015, arXiv:1609.09078 [hep-ph].

[246] D. Buttazzo, A. Greljo, G. Isidori, and D. Marzocca, B-physics anomalies: a guide to combined explanations, JHEP **11** (2017) 044, arXiv:1706.07808 [hep-ph].

[247] L. Calibbi, A. Crivellin, and T. Li, Model of vector leptoquarks in view of the B-physics anomalies, Phys. Rev. **D98** (2018) 115002, arXiv:1709.00692 [hep-ph].

[248] A. Crivellin, C. Greub, D. Müller, and F. Saturnino, Importance of Loop Effects in Explaining the Accumulated Evidence for New Physics in B Decays with a Vector Leptoquark, Phys. Rev. Lett. **122** (2019) 011805, arXiv:1807.02068 [hep-ph].

[249] A. Angelescu, D. BeÄĐireviÄĞ, D. A. Faroughy, and O. Sumensari, Closing the window on single leptoquark solutions to the B-physics anomalies, JHEP **10** (2018) 183, arXiv:1808.08179 [hep-ph].

[250] C. Cornella, J. Fuentes-Martin, and G. Isidori, Revisiting the vector leptoquark explanation of the B-physics anomalies, JHEP **07** (2019) 168, arXiv:1903.11517 [hep-ph].

[251] G. Panico, A. Pomarol, and M. Riembau, EFT approach to the electron Electric Dipole Moment at the two-loop level, JHEP **04** (2019) 090, arXiv:1810.09413 [hep-ph].

[252] P. Herczeg, CP violating electron-nucleon interactions from leptoquark exchange, Phys. Rev. **D68** (2003) 116004, [Erratum: Phys. Rev.D69,039901(2004)].

[253] N. Yamanaka, B. K. Sahoo, N. Yoshinaga, T. Sato, K. Asahi, and B. P. Das, Probing exotic phenomena at the interface of nuclear and particle physics with the electric dipole moments of diamagnetic atoms: A unique window to hadronic and semi-leptonic CP violation, Eur. Phys. J. **A53** (2017) 54, arXiv:1703.01570 [hep-ph].

[254] C. Bobeth and A. J. Buras, Leptoquarks meet ε'/ε and rare Kaon processes, JHEP **02** (2018) 101, arXiv:1712.01295 [hep-ph].

[255] K. Fuyuto, M. Ramsey-Musolf, and T. Shen, Electric Dipole Moments from CP-Violating Scalar Leptoquark Interactions, Phys. Lett. **B788** (2019) 52–57, arXiv:1804.01137 [hep-ph].

[256] K. Yanase, N. Yoshinaga, K. Higashiyama, and N. Yamanaka, Electric dipole moment of ^{199}Hg atom from P, CP-odd electron-nucleon interaction, Phys. Rev. **D99** (2019) 075021, arXiv:1805.00419 [nucl-th].

[257] W. Dekens, J. de Vries, M. Jung, and K. K. Vos, The phenomenology of electric dipole moments in models of scalar leptoquarks, JHEP **01** (2019) 069, arXiv:1809.09114 [hep-ph].

[258] A. Crivellin and F. Saturnino, Correlating tauonic B decays with the neutron electric dipole moment via a scalar leptoquark, Phys. Rev. **D100** (2019) 115014, arXiv:1905.08257 [hep-ph].

[259] M. Bordone, C. Cornella, J. Fuentes-Martin, and G. Isidori, A three-site gauge model for flavor hierarchies and flavor anomalies, Phys. Lett. **B779** (2018) 317–323, arXiv:1712.01368 [hep-ph].

[260] M. Bordone, C. Cornella, J. Fuentes-Martin, and G. Isidori, Low-energy signatures of the PS^3 model: from B-physics anomalies to LFV, JHEP **10** (2018) 148, arXiv:1805.09328 [hep-ph].

[261] N. Assad, B. Fornal, and B. Grinstein, Baryon Number and Lepton Universality Violation in Leptoquark and Diquark Models, Phys. Lett. **B777** (2018) 324–331, arXiv:1708.06350 [hep-ph].

[262] L. Di Luzio, A. Greljo, and M. Nardecchia, Gauge leptoquark as the origin of B-physics anomalies, Phys. Rev. **D96** (2017) 115011, arXiv:1708.08450 [hep-ph].

[263] R. Barbieri and A. Tesi, B-decay anomalies in Pati-Salam SU(4), Eur. Phys. J. **C78** (2018) 193, arXiv:1712.06844 [hep-ph].

[264] M. Blanke and A. Crivellin, B Meson Anomalies in a Pati-Salam Model within the Randall-Sundrum Background, Phys. Rev. Lett. **121** (2018) 011801, arXiv:1801.07256 [hep-ph].

[265] A. Greljo and B. A. Stefanek, Third family quarkâĂŞlepton unification at the TeV scale, Phys. Lett. **B782** (2018) 131–138, arXiv:1802.04274 [hep-ph].

[266] J. Heeck and D. Teresi, Pati-Salam explanations of the B-meson anomalies, JHEP **12** (2018) 103, arXiv:1808.07492 [hep-ph].

[267] S. Balaji, R. Foot, and M. A. Schmidt, Chiral SU(4) explanation of the $b \to s$ anomalies, Phys. Rev. **D99** (2019) 015029, arXiv:1809.07562 [hep-ph].

[268] B. Fornal, S. A. Gadam, and B. Grinstein, Left-Right SU(4) Vector Leptoquark Model for Flavor Anomalies, Phys. Rev. **D99** (2019) 055025, arXiv:1812.01603 [hep-ph].

[269] I. Dorsner, S. Fajfer, A. Greljo, J. F. Kamenik, and N. Kosnik, Physics of leptoquarks in precision experiments and at particle colliders, Phys. Rept. **641** (2016) 1–68, arXiv:1603.04993 [hep-ph].

[270] D. J. Robinson, B. Shakya, and J. Zupan, Right-handed neutrinos and R(D*), JHEP **02** (2019) 119, arXiv:1807.04753 [hep-ph].

[271] F. Sala and D. M. Straub, A New Light Particle in B Decays?, Phys. Lett. **B774** (2017) 205–209, arXiv:1704.06188 [hep-ph].

[272] D. Ghosh, Explaining the R_K and R_{K^*} anomalies, Eur. Phys. J. **C77** (2017) 694, arXiv:1704.06240 [hep-ph].

[273] A. Datta, J. Kumar, J. Liao, and D. Marfatia, New light mediators for the R_K and R_{K^*} puzzles, Phys. Rev. **D97** (2018) 115038, arXiv:1705.08423 [hep-ph].

[274] W. Altmannshofer, M. J. Baker, S. Gori, R. Harnik, M. Pospelov, E. Stamou, and A. Thamm, Light resonances and the low-q^2 bin of R_{K^*}, JHEP **03** (2018) 188, arXiv:1711.07494 [hep-ph].

[275] BaBar Collaboration, B. Aubert et al., Improved limits on lepton flavor violating tau decays to $\ell\phi$, $\ell\rho$, ℓK^* and $\ell\bar{K}^*$, Phys. Rev. Lett. **103** (2009) 021801, arXiv:0904.0339 [hep-ex].

[276] Belle Collaboration, Y. Miyazaki et al., Search for Lepton-Flavor-Violating tau Decays into a Lepton and a Vector Meson, Phys. Lett. **B699** (2011) 251–257, arXiv:1101.0755 [hep-ex].

[277] BaBar Collaboration, J. P. Lees et al., A search for the decay modes $B^\pm \to h^\pm\tau\ell$, Phys. Rev. **D86** (2012) 012004, arXiv:1204.2852 [hep-ex].

[278] A. Greljo and D. Marzocca, High-p_T dilepton tails and flavor physics, Eur. Phys. J. **C77** (2017) 548, arXiv:1704.09015 [hep-ph].

[279] D. A. Faroughy, A. Greljo, and J. F. Kamenik, Confronting lepton flavor universality violation in B decays with high-p_T tau lepton searches at LHC, Phys. Lett. **B764** (2017) 126–134, arXiv:1609.07138 [hep-ph].

[280] F. S. Queiroz and W. Shepherd, New Physics Contributions to the Muon Anomalous Magnetic Moment: A Numerical Code, Phys. Rev. **D89** (2014) 095024, arXiv:1403.2309 [hep-ph].

[281] K. Kowalska, E. M. Sessolo, and Y. Yamamoto, Constraints on charmphilic solutions to the muon g-2 with leptoquarks, Phys. Rev. **D99** (2019) 055007, arXiv:1812.06851 [hep-ph].

[282] CMS Collaboration, C. Collaboration, Search for Anomalous Top Chromomagnetic Dipole Moments from angular distributions in $t\bar{t}$ Dileptonic events at $\sqrt{s} = 7$ TeV with the CMS detector.,.

[283] J. Engel, M. J. Ramsey-Musolf, and U. van Kolck, Electric Dipole Moments of Nucleons, Nuclei, and Atoms: The Standard Model and Beyond, Prog. Part. Nucl. Phys. **71** (2013) 21–74, arXiv:1303.2371 [nucl-th].

[284] T. Bhattacharya, V. Cirigliano, R. Gupta, H.-W. Lin, and B. Yoon, Neutron Electric Dipole Moment and Tensor Charges from Lattice QCD, Phys. Rev. Lett. **115** (2015) 212002, arXiv:1506.04196 [hep-lat].

[285] T. Bhattacharya, V. Cirigliano, S. Cohen, R. Gupta, H.-W. Lin, and B. Yoon, Axial, Scalar and Tensor Charges of the Nucleon from 2+1+1-flavor Lattice QCD, Phys. Rev. **D94** (2016) 054508, arXiv:1606.07049 [hep-lat].

[286] D. Chang, W.-Y. Keung, C. S. Li, and T. C. Yuan, QCD Corrections to CP Violation From Color Electric Dipole Moment of b Quark, Phys. Lett. **B241** (1990) 589–592.

[287] G. Boyd, A. K. Gupta, S. P. Trivedi, and M. B. Wise, Effective Hamiltonian for the Electric Dipole Moment of the Neutron, Phys. Lett. **B241** (1990) 584–588.

[288] M. Dine and W. Fischler, Constraints on New Physics From Weinberg's Analysis of the Neutron Electric Dipole Moment, Phys. Lett. **B242** (1990) 239–244.

[289] D. A. Demir, M. Pospelov, and A. Ritz, Hadronic EDMs, the Weinberg operator, and light gluinos, Phys. Rev. **D67** (2003) 015007, arXiv:hep-ph/0208257 [hep-ph].

[290] U. Haisch and A. Hala, Sum rules for CP-violating operators of Weinberg type, JHEP **11** (2019) 154, arXiv:1909.08955 [hep-ph].

[291] Muon g-2 Collaboration, G. W. Bennett et al., Final Report of the Muon E821 Anomalous Magnetic Moment Measurement at BNL, Phys. Rev. **D73** (2006) 072003, arXiv:hep-ex/0602035 [hep-ex].

[292] A. Keshavarzi, D. Nomura, and T. Teubner, The $g-2$ of charged leptons, $\alpha(M_Z^2)$ and the hyperfine splitting of muonium, arXiv:1911.00367 [hep-ph].

[293] H. Davoudiasl and W. J. Marciano, Tale of two anomalies, Phys. Rev. **D98** (2018) 075011, arXiv:1806.10252 [hep-ph].

[294] M. Davier, A. Hoecker, B. Malaescu, and Z. Zhang, A new evaluation of the hadronic vacuum polarisation contributions to the muon anomalous magnetic moment and to $\boldsymbol{\alpha(m_Z^2)}$, arXiv:1908.00921 [hep-ph].

[295] A. Crivellin, M. Hoferichter, and P. Schmidt-Wellenburg, Combined explanations of $(g-2)_{\mu,e}$ and implications for a large muon EDM, Phys. Rev. **D98** (2018) 113002, arXiv:1807.11484 [hep-ph].

[296] F. Jegerlehner, Muon g - 2 theory: The hadronic part, EPJ Web Conf. **166** (2018) 00022, arXiv:1705.00263 [hep-ph].

[297] R. H. Parker, C. Yu, W. Zhong, B. Estey, and H. MÃijller, Measurement of the fine-structure constant as a test of the Standard Model, Science **360** (2018) 191, arXiv:1812.04130 [physics.atom-ph].

[298] Muon g-2 Collaboration, J. Grange et al., Muon (g-2) Technical Design Report, arXiv:1501.06858 [physics.ins-det].

[299] T. Blum, N. Christ, M. Hayakawa, T. Izubuchi, L. Jin, C. Jung, and C. Lehner, Connected and Leading Disconnected Hadronic Light-by-Light Contribution to the Muon Anomalous Magnetic Moment with a Physical Pion Mass, Phys. Rev. Lett. **118** (2017) 022005, arXiv:1610.04603 [hep-lat].

[300] RBC, UKQCD Collaboration, T. Blum, P. A. Boyle, V. GÃijlpers, T. Izubuchi, L. Jin, C. Jung, A. JÃijttner, C. Lehner, A. Portelli, and J. T. Tsang, Calculation of the hadronic vacuum polarization contribution to the muon anomalous magnetic moment, Phys. Rev. Lett. **121** (2018) 022003, arXiv:1801.07224 [hep-lat].

[301] Fermilab Lattice, LATTICE-HPQCD, MILC Collaboration, C. T. H. Davies et al., Hadronic-Vacuum-Polarization Contribution to the Muon's Anomalous Magnetic Moment from Four-Flavor Lattice QCD, arXiv:1902.04223 [hep-lat].

[302] PACS Collaboration, E. Shintani and Y. Kuramashi, Hadronic vacuum polarization contribution to the muon $g-2$ with 2+1 flavor lattice QCD on a larger than $(10\ \mathrm{fm})^4$ lattice at the physical point, Phys. Rev. **D100** (2019) 034517, arXiv:1902.00885 [hep-lat].

[303] A. GÃľrardin, M. CÃĺ, G. von Hippel, B. HÃűrz, H. B. Meyer, D. Mohler, K. Ottnad, J. Wilhelm, and H. Wittig, The leading hadronic contribution to $(g-2)_\mu$ from lattice QCD with $N_\mathrm{f} = 2+1$ flavours of O(a) improved Wilson quarks, Phys. Rev. **D100** (2019) 014510, arXiv:1904.03120 [hep-lat].

[304] T. Blum, N. Christ, M. Hayakawa, T. Izubuchi, L. Jin, C. Jung, and C. Lehner, The hadronic light-by-light scattering contribution to the muon anomalous magnetic moment from lattice QCD, arXiv:1911.08123 [hep-lat].

[305] G. Colangelo, M. Hoferichter, M. Procura, and P. Stoffer, Dispersion relation for hadronic light-by-light scattering: theoretical foundations, JHEP **09** (2015) 074, arXiv:1506.01386 [hep-ph].

[306] G. Colangelo, M. Hoferichter, M. Procura, and P. Stoffer, Rescattering effects in the hadronic-light-by-light contribution to the anomalous magnetic moment of the muon, Phys. Rev. Lett. **118** (2017) 232001, arXiv:1701.06554 [hep-ph].

[307] M. Hoferichter, B.-L. Hoid, B. Kubis, S. Leupold, and S. P. Schneider, Pion-pole contribution to hadronic light-by-light scattering in the anomalous magnetic moment of the muon, Phys. Rev. Lett. **121** (2018) 112002, arXiv:1805.01471 [hep-ph].

[308] G. Colangelo, M. Hoferichter, and P. Stoffer, Two-pion contribution to hadronic vacuum polarization, JHEP **02** (2019) 006, arXiv:1810.00007 [hep-ph].

[309] M. Hoferichter, B.-L. Hoid, and B. Kubis, Three-pion contribution to hadronic vacuum polarization, JHEP **08** (2019) 137, arXiv:1907.01556 [hep-ph].

[310] G. Gabrielse, S. E. Fayer, T. G. Myers, and X. Fan, Towards an Improved Test of the Standard Model's Most Precise Prediction, Atoms **7** (2019) 45, arXiv:1904.06174 [quant-ph].

[311] DELPHI Collaboration, J. Abdallah et al., Study of tau-pair production in photon-photon collisions at LEP and limits on the anomalous electromagnetic moments of the tau lepton, Eur. Phys. J. **C35** (2004) 159–170, arXiv:hep-ex/0406010 [hep-ex].

[312] A. Pich, Precision Tau Physics, Prog. Part. Nucl. Phys. **75** (2014) 41–85, arXiv:1310.7922 [hep-ph].

[313] ACME Collaboration, V. Andreev et al., Improved limit on the electric dipole moment of the electron, Nature **562** (2018) 355–360.

[314] Muon (g-2) Collaboration, G. W. Bennett et al., An Improved Limit on the Muon Electric Dipole Moment, Phys. Rev. **D80** (2009) 052008, arXiv:0811.1207 [hep-ex].

[315] Belle Collaboration, K. Inami et al., Search for the electric dipole moment of the tau lepton, Phys. Lett. **B551** (2003) 16–26, arXiv:hep-ex/0210066 [hep-ex].

[316] A. Adelmann, K. Kirch, C. J. G. Onderwater, and T. Schietinger, Compact storage ring to search for the muon electric dipole moment, J. Phys. **G37** (2010) 085001.

[317] Belle-II Collaboration, W. Altmannshofer et al., The Belle II Physics Book, arXiv:1808.10567 [hep-ex].

[318] nEDM Collaboration, C. Abel et al., Measurement of the permanent electric dipole moment of the neutron, Phys. Rev. Lett. **124** (2020) 081803, arXiv:2001.11966 [hep-ex].

[319] R. K. Ellis et al., Physics Briefing Book, arXiv:1910.11775 [hep-ex].

[320] M. Pospelov and A. Ritz, CKM benchmarks for electron electric dipole moment experiments, Phys. Rev. **D89** (2014) 056006, arXiv:1311.5537 [hep-ph].

[321] C. Smith and S. Touati, Electric dipole moments with and beyond flavor invariants, Nucl. Phys. **B924** (2017) 417–452, arXiv:1707.06805 [hep-ph].

[322] S. Dar, The Neutron EDM in the SM: A Review, arXiv:hep-ph/0008248 [hep-ph].

[323] X.-Q. Li, Y.-D. Yang, and X. Zhang, Revisiting the one leptoquark solution to the R(D*) anomalies and its phenomenological implications, JHEP **08** (2016) 054, arXiv:1605.09308 [hep-ph].

[324] R. Alonso, B. Grinstein, and J. Martin Camalich, Lifetime of B_c^- Constrains Explanations for Anomalies in $B \to D^{(*)}\tau\nu$, Phys. Rev. Lett. **118** (2017) 081802, arXiv:1611.06676 [hep-ph].

[325] W. Altmannshofer, C. Niehoff, and D. M. Straub, $B_s \to \mu^+\mu^-$ as current and future probe of new physics, JHEP **05** (2017) 076, arXiv:1702.05498 [hep-ph].

[326] W. Altmannshofer, P. Ball, A. Bharucha, A. J. Buras, D. M. Straub, and M. Wick, Symmetries and Asymmetries of $B \to K^*\mu^+\mu^-$ Decays in the Standard Model and Beyond, JHEP **01** (2009) 019, arXiv:0811.1214 [hep-ph].

[327] C. McNeile, C. T. H. Davies, E. Follana, K. Hornbostel, and G. P. Lepage, Heavy meson masses and decay constants from relativistic heavy quarks in full lattice QCD, Phys. Rev. **D86** (2012) 074503, arXiv:1207.0994 [hep-lat].

[328] LHCb Collaboration, R. Aaij et al., Search for the decays $B_s^0 \to \tau^+\tau^-$ and $B^0 \to \tau^+\tau^-$, Phys. Rev. Lett. **118** (2017) 251802, arXiv:1703.02508 [hep-ex].

[329] C. Bobeth, M. Gorbahn, T. Hermann, M. Misiak, E. Stamou, and M. Steinhauser, $B_{s,d} \to l^+ l^-$ in the Standard Model with Reduced Theoretical Uncertainty, Phys. Rev. Lett. **112** (2014) 101801, arXiv:1311.0903 [hep-ph].

[330] J. Albrecht, F. Bernlochner, M. Kenzie, S. Reichert, D. Straub, and A. Tully, Future prospects for exploring present day anomalies in flavour physics measurements with Belle II and LHCb, arXiv:1709.10308 [hep-ph].

[331] CMS Collaboration, S. Chatrchyan et al., Measurement of the $B_s^0 \to \mu^+\mu^-$ Branching Fraction and Search for $B^0 \to \mu^+\mu^-$ with the CMS Experiment, Phys. Rev. Lett. **111** (2013) 101804, arXiv:1307.5025 [hep-ex].

[332] CMS, LHCb Collaboration, V. Khachatryan et al., Observation of the rare $B_s^0 \to \mu^+\mu^-$ decay from the combined analysis of CMS and LHCb data, Nature **522** (2015) 68–72, arXiv:1411.4413 [hep-ex].

[333] LHCb Collaboration, R. Aaij et al., Measurement of the $B_s^0 \to \mu^+\mu^-$ branching fraction and effective lifetime and search for $B^0 \to \mu^+\mu^-$ decays, Phys. Rev. Lett. **118** (2017) 191801, arXiv:1703.05747 [hep-ex].

[334] ATLAS Collaboration, M. Aaboud et al., Study of the rare decays of B_s^0 and B^0 mesons into muon pairs using data collected during 2015 and 2016 with the ATLAS detector, JHEP **04** (2019) 098, arXiv:1812.03017 [hep-ex].

[335] M. Beneke, C. Bobeth, and R. Szafron, Enhanced electromagnetic correction to the rare B-meson decay $B_{s,d} \to \mu^+\mu^-$, Phys. Rev. Lett. **120** (2018) 011801, arXiv:1708.09152 [hep-ph].

[336] CDF Collaboration, T. Aaltonen et al., Search for the Decays $B_s^0 \to e^+\mu^-$ and $B_s^0 \to e^+e^-$ in CDF Run II, Phys. Rev. Lett. **102** (2009) 201801, arXiv:0901.3803 [hep-ex].

[337] ATLAS Collaboration, M. Aaboud et al., Searches for scalar leptoquarks and differential cross-section measurements in dilepton-dijet events in proton-proton collisions at a centre-of-mass energy of $\sqrt{s} = 13$ TeV with the ATLAS experiment, Eur. Phys. J. **C79** (2019) 733, arXiv:1902.00377 [hep-ex].

[338] CMS Collaboration, A. M. Sirunyan et al., Search for pair production of first-generation scalar leptoquarks at $\sqrt{s} = 13$ TeV, Phys. Rev. **D99** (2019) 052002, arXiv:1811.01197 [hep-ex].

[339] CMS Collaboration, A. M. Sirunyan et al., Search for pair production of second-generation leptoquarks at $\sqrt{s} = 13$ TeV, Phys. Rev. **D99** (2019) 032014, arXiv:1808.05082 [hep-ex].

[340] ATLAS Collaboration, M. Aaboud et al., Searches for third-generation scalar leptoquarks in $\sqrt{s} = 13$ TeV pp collisions with the ATLAS detector, JHEP **06** (2019) 144, arXiv:1902.08103 [hep-ex].

[341] CMS Collaboration, A. M. Sirunyan et al., Search for heavy neutrinos and third-generation leptoquarks in hadronic states of two τ leptons and two jets in proton-proton collisions at $\sqrt{s} = 13$ TeV, JHEP **03** (2019) 170, arXiv:1811.00806 [hep-ex].

[342] CMS Collaboration, A. M. Sirunyan et al., Constraints on models of scalar and vector leptoquarks decaying to a quark and a neutrino at $\sqrt{s} = 13$ TeV, Phys. Rev. **D98** (2018) 032005, arXiv:1805.10228 [hep-ex].

[343] B. Diaz, M. Schmaltz, and Y.-M. Zhong, The leptoquark HunterâĂŹs guide: Pair production, JHEP **10** (2017) 097, arXiv:1706.05033 [hep-ph].

[344] I. Dorsner and A. Greljo, Leptoquark toolbox for precision collider studies, JHEP **05** (2018) 126, arXiv:1801.07641 [hep-ph].

[345] CMS Collaboration, V. Khachatryan et al., Search for single production of scalar leptoquarks in proton-proton collisions at $\sqrt{s} = 8\ TeV$, Phys. Rev. **D93** (2016) 032005, arXiv:1509.03750 [hep-ex], [Erratum: Phys. Rev.D95,no.3,039906(2017)].

[346] CMS Collaboration, A. M. Sirunyan et al., Search for a singly produced third-generation scalar leptoquark decaying to a τ lepton and a bottom quark in proton-proton collisions at $\sqrt{s} = 13$ TeV, JHEP **07** (2018) 115, arXiv:1806.03472 [hep-ex].

[347] J. de Blas et al., Higgs Boson Studies at Future Particle Colliders, JHEP **01** (2020) 139, arXiv:1905.03764 [hep-ph].

[348] ATLAS Collaboration, M. Aaboud et al., Measurements of gluon-gluon fusion and vector-boson fusion Higgs boson production cross-sections in the $H \to WW^* \to e\nu\mu\nu$ decay channel in pp collisions at $\sqrt{s} = 13$ TeV with the ATLAS detector, Phys. Lett. B **789** (2019) 508–529, arXiv:1808.09054 [hep-ex].

[349] CMS Collaboration, A. M. Sirunyan et al., Measurements of properties of the Higgs boson decaying to a W boson pair in pp collisions at $\sqrt{s} = 13$ TeV, Phys. Lett. B **791** (2019) 96, arXiv:1806.05246 [hep-ex].

[350] ATLAS Collaboration, G. Aad et al., Measurement of the production cross section for a Higgs boson in association with a vector boson in the $H \to WW^* \to \ell\nu\ell\nu$ channel in pp collisions at $\sqrt{s} = 13$ TeV with the ATLAS detector, Phys. Lett. B **798** (2019) 134949, arXiv:1903.10052 [hep-ex].

[351] CMS Collaboration, A. M. Sirunyan et al., Search for the associated production of the Higgs boson and a vector boson in proton-proton collisions at $\sqrt{s} = 13$ TeV via Higgs boson decays to τ leptons, JHEP **06** (2019) 093, arXiv:1809.03590 [hep-ex].

[352] CMS Collaboration, A. M. Sirunyan et al., Search for the Higgs boson decaying to two muons in proton-proton collisions at $\sqrt{s} = 13$ TeV, Phys. Rev. Lett. **122** (2019) 021801, arXiv:1807.06325 [hep-ex].